SYNTHESIS, CHARACTERIZATION, BIOASSAY AND DENSITY FUNCTIONAL THEORY STUDIES OF CATIONIC IRON HALF SANDWICH COMPLEXES OF SELECTED HETEROFUNCTIONAL ACTIVE PHARMACEUTICAL AGENTS

KATANA CHENGO (MSc.)

I84/32248/2015

A THESIS SUBMITTED IN FULFILMENT OF THE REQUIREMENTS FOR THE AWARD OF THE OF DOCTOR OF PHILOSOPHY DEGREE (IN APPLIED CHEMISTRY) IN THE SCHOOL OF PURE AND APPLIED SCIENCES OF KENYATTA UNIVERSITY

FEBRUARY, 2020

DECLARATION

This thesis is my original work and has not been presented for degree or other awards in any other university

Signature……Date……

Katana Chengo

I84/32248/2015

Department of Chemistry

This thesis has been submitted with our approval as university supervisors

Dr Evans Changamu Signature……. Date……
Department of Chemistry
Kenyatta University

Dr Lucy Kiruri Signature……. Date……
Department of Chemistry
Kenyatta University

Dr John Maingi Signature……. Date……
Department of Biochemistry, Microbiology and Biotechnology
Kenyatta University

DEDICATION

To Lawrence, Felistas and to the memory of my beloved parents Bahati Chengo and Chengo Tinga Nyale

ACKNOWLEDGEMENTS

During the years of research and development of this thesis, I have had the privilege of being guided into the wonderland research by my supervisors, Dr Evans Changamu, Dr Lucy Kiruri and Dr John Maingi. My sincere thanks are due to them for their constant guidance and their valuable contribution. To Rosemary Osok, George Omollo, Isaac Odhiambo, Jackson Kilonzo and Adamu Abdulhameed thank you for being there whenever I needed you. I want to thank Daniel Ng'ang'a for his considerable help in the biological tests. I am also indebted to the entire technical staff in the Department of Chemistry Kenyatta University in particular Jane, Kariuki, Njagi, Catherine, John and Esther. You deserve my warmest gratitude for your patience and helpfulness.

It would not have been possible to evolve into what I am, where I am without the essential contributions of the academic staff of Department Chemistry Kenyatta University and their friends wherever they are. The support, the help, the analyses, the smiles and most importantly the words of encouragement are all worth mentioning. I hope that these special people could find in these words my heartfelt gratitude. To the African Development Bank (ADB) and the National Research Foundation (NRF) thank you so much for the generous offer of funding my studies and making my dream come true. I also deeply appreciate the CHPC facility in South Africa and the Chemistry programme administrator Dr Krishna Govinder for the use of the Cluster for my theoretical studies. I would also want to thank Kenyatta University for acquiring computers and allocating us a dedicated room for molecular modelling. Finally, glory is to the Almighty God for everything that has happened in my life.

TABLE OF CONTENTS

LIST OF TABLES

LIST OF FIGURES

LIST OF ABBREVIATIONS AND ACRONYMS

4-ASA	4-Aminosalicylic Acid
APA	Active pharmaceutical agent
API	Active Pharmaceutical Ingredient
ADB	African Development Bank
ATR	Attenuated Total Reflection
B3LYP	Becke 3-Parameter (Exchange), Lee, Yang And Parr (Correlation; Density Functional Theory)
CO	Carbonyl
CHPC	Centre For High Computing
C-PCM	Conductor-Like Polarizable Continuum Model
CAM-B3LYP	Coulomb-Attenuating Method - Becke 3-Parameter (Exchange), Lee, Yang and Parr (Correlation; Density Functional Theory)
Cp	Cyclopentadienyl
Fp	Cyclopentadienyl Iron(II) Dicarbonyl
FpI	CyclopentadienylIron(II)Dicarbonyl Iodide
CS	Cycloserine
DFT	Density Functional Theory
DNA	Deoxyribonucleic Acid
DCM	Dichloromethane
Et_2O	Diethyl Ether
DMSO	Dimethyl Sulfoxide
EA	Electron Affinity
ETH	Ethionamide
XDR-TB	Extensively Drug Resistant Tuberculosis
FD	Finite Difference
FTIR	Fourier Transform Infra-Red
FMO	Frontier Molecular Orbital
G09	Gaussian 09
HOMO	Highest Occupied Molecular Orbital

HIV	Human Immunodeficiency Virus
IR	Infra-Red
IP	Ionisation Potential
INH	Isoniazid
L	Ligand
LZD	Linezolid
LUMO	Lowest Unoccupied Molecular Orbital
MIC	Minimum Inhibitory Concentration
MDR-TB	Multi-Drug Resistant Tuberculosis
NRF	National Research Foundation
NBO	Natural Bond Orbital
NMR	Nuclear Magnetic Resonance
PAS	Para-Aminosalicylic Acid
Fp*	Pentamethyl Cyclopentadienyl Iron(II) Dicarbonyl
PBEPBE	Perdew, Burke & Ernzerhof; Perdew, Burke & Ernzerhof
PTH	Prothionamide
PZA	Pyrazinamide
SERMs	Selective Estrogen Receptor Modulators
SA	South Africa
TZD	Terizidone
TCE	Tetracyanoethylene
THF	Tetrahydrofuran
TB	Tuberculosis
USA	United States Of Ameica
WHO	World Health Organisation

ABSTRACT

The molecular modification of purely organic drugs by the incorporation of a metal atom is an active area of research. However, there is paucity of data in the use of half sandwich organometallic fragments and in particular the cationic iron half sandwich, $[\eta^5\text{-}C_5H_5(CO)_2Fe]^+$, in structural modification of drug molecules. The cationic iron half sandwich organometallic fragment provides a metal centre that could participate in biochemical reactions with potentially the desirable benefit of conferring new or modified modes of action of the drug molecules. Therefore, the objective of this study was to modify the molecular structures of the active pharmaceutical agents (APAs); 3-aminosalicylic acid (3-ASA), 4-aminosalicylic acid (4-ASA), 5-aminosalicylic acid (5-ASA), terizidone (TZD), ethionamide (ETH), prothionamide (PTH) and linezolid (LZD) by the incorporation of the cationic iron half sandwich organometallic fragment. A two pronged approach involving molecular modelling and organometallic synthesis was employed. In molecular modelling, the molecular geometries of the seven selected drug molecules were optimized and their local and global reactivity indices calculated in order to predict their ligation behaviours towards the iron half sandwich. The most stable molecular geometries and spectroscopic properties of the seven active pharmaceutical agents and their organometallic complex salts were predicted computationally using the DFT functionals; B3LYP, CAM-B3LYP and PBEPBE and 6-311g(d,p), 6-311g(2d,p) and LANL2DZ basis sets in Gaussian 09 and 16. Experimentally, the iron half sandwich organometallic salts of the APAs were synthesized, purified and characterized by FT-IR spectroscopy, ^1H and ^{13}C NMR spectroscopy, and elemental analysis. Antibacterial susceptibility tests of the new compounds against selected gram-positive and gram-negative bacteria showed that the LZD and TZD complexes had good abilities to inhibit the growth of the tested bacteria with comparable or better growth inhibition ability than their corresponding free ligands. Furthermore, the incorporation of the cationic iron half sandwich organometallic moiety to 3-ASA, 4-ASA, 5-ASA, ETH and PTH conferred antibacterial activity against the selected bacterial strains hence broadening the drugs spectra of activity. Therefore, the structural modification of APAs by the incorporation of the iron half sandwich can be pursued as a means of enhancing the usefulness of drugs.

CHAPTER ONE

INTRODUCTION

1.1 Background to the Study

In the quest to overcome the drug resistance problem two broad approaches are currently in use. The first strategy involves the molecular modification of drugs currently in clinical use, to produce structural analogs by purely organic means or by the introduction of a metal atom to the purely organic molecule to produce metal-based chemotherapeutic compounds (Coordination or organometallic). The second approach involves coming up with completely new classes of compounds that the microbes have never encountered (Theuretzbacher, 2011).

Conventionally, the drug discovery process has concentrated on the development of organic molecules as pharmacophores. However, the limited structural diversity of these purely organic molecules makes it difficult for them to access other scaffolds that span the whole spectrum of the biologically relevant chemical space, some of which may contain potential drug candidates (Dobson, 2004; Lipinski and Hopkins, 2004; Koch *et al*., 2005). This has left large areas of the chemical space containing structurally and chemically unique motifs unexplored. In order to tap into this substantial, potentially valuable and largely unexplored chemical space, scaffolds which are not readily accessible with organic chemistry need to be explored (Chow *et al*., 2014).

Transition-metal scaffolds are uniquely suited for the development of potential drug candidates. This can be attributed to several factors. Transition-metal complexes can

readily accommodate higher coordination numbers and hence access different molecular geometries not possible with purely organic molecules. Transition-metal complexes are also bestowed with tunable properties, such as multiple oxidation states that are stable under normal conditions. Furthermore, these complexes also have predictable reactivities based on metal-ligand bonding interactions (Meggers, 2009). Hence, metal-based compounds offer opportunities for the design of chemotherapeutic agents not readily available to organic compounds. The extensive range of coordination numbers and geometries, accessible redox states, thermodynamic and kinetic characteristics, and the intrinsic properties of the cationic metal ion and the ligand itself provide the medicinal inorganic chemist a broad spectrum of reactivities that can be exploited (Bruijnincx and Sadler, 2008).

Traditionally, metals ions have been incorporated in anticancer agents to exploit their reactivity and have been particularly attractive due to the exceptionally wide range of reactivities available. However, metals can also be used as building blocks for well-defined, three-dimensional constructs. In this fashion, the availability of numerous and diverse coordination geometries allows for the synthesis of structures with unique stereochemistry and orientation of organic ligands and structures which are not available through purely organic molecules. The kinetic inertness of the coordination/organometallic bonds make transition-metal complexes in principle behave like organic compounds. This approach greatly increases the ability to map biologically relevant chemical space (Meggers *et al*., 2007). Hence, the development of

novel metal-based drugs is increasingly becoming a major new theme in drug development (Regiel-Futyra *et al*., 2017).

Coordination complexes of active pharmaceutical agents (APA) of virtually all the transition metals in the Periodic Table of elements have been reported,as can be attested to by the numerous monographs, major reviews, and dedicated volumes on this aspect of chemistry (Obaleye *et al*., 2001; Zupanicic *et al*., 2001; Pilar *et al*., 2003; Bourque *et al*., 2005; Chohan and Supuran, 2006; Quintal *et al*., 2006; Upadhyay *et al*., 2006; El-Wahed *et al*., 2008; Marzano *et al*., 2009; Obaleye *et al*., 2009; Obaleye *et al*., 2011; Refat and Mohamed, 2011; Muthumariappan, 2013; Soliman and Mohamed, 2013; Krivosudský *et al*., 2014; Thakkar *et al*., 2014; Samuel and Justice, 2016; Basit Wani, *et al*., 2017; Ciol *et al*., 2018; Cuprys *et al*., 2018; De Oliveira *et al*., 2018; Lachowicz *et al*., 2018). From an organometallic perspective the coupling of APAs compounds with ferrocene to produce Ferrocenyl organometallic derivatives of antimalarials, antibiotics, anticancer agents and other chemotherapeutic agents is an active area of research (Patra *et al*., 2011 Patra *et al*., 2012a; Ong, *et al*., 2019). The ferrocifens and ferroquines are currently the most advanced ferrocene based drug candidates (Biot *et al*., 1997; Biot *et al*., 1999a, b; Biot *et al*., 2000; Top *et al*., 2001; Ogunniran *et al*., 2007; Dubar *et al*., 2008; Gasser *et al*., 2009; Patra *et al*., 2009; Dubar *et al*., 2011; Gasser, and Metzler-Nolte, 2011; Biot *et al*., 2011; Wani *et al*., 2015; Kumar *et al*., 2019b).

Some of these metal derivatives are more biologically active than their parent compounds, against both susceptible and drug resistant microbes, hence making them promising candidates as metallo-drugs (Sanchez-Delgado *et al*., 1993; Turel *et al*., 1999; Navarro *et al*., 2001; Zupanici *et al*., 2001; Dive and Biot, 2008; Martínez *et al*., 2008; Martínez *et al*., 2009; Gibaud and Jaouen, 2010; Martínez *et al*., 2010; Turel *et al*., 2010; Martínez *et al*., 2011; Demoro *et al*., 2012; Martínez *et al*., 2012; Gasser, 2015; Held *et al*., 2015).

Despite the evident success of metal derivatives in general and the ferrocene and/or metallocene derivatives of APAs in particular as chemotherapeutic agents, the potential of the cationic iron half sandwich organometallic complexes of APAs as antimicrobials in general and specifically as antibacterial agents so far has seen little exploration. It was, therefore, important to carry out a systematic study of the ligation behaviour of the selected APAs with a view of modifying their structures with the cationic iron half sandwich organometallic fragment. The introduction of the iron half sandwich organometallic fragment into these purely organic APAs modifies the two and three dimensional profiles of the selected APAs, and also introduces or enhances some aromaticity via the cyclopentadienyl ligand, both of which are important to druglikness of molecules.

1.2 Statement of Problem and Justification

The development of bacterial resistance to commercial antibiotics is a significant global problem. There is, therefore, an urgent need for the development of new types of

antibacterial agents, reengineered or repositioned drugs to tackle the ever growing drug resistance menace. One approach of combating drug resistance or restoring the activity of organic therapeutic agents for which resistance has developed is structure modification involving introduction of a metal fragment leading either to metal coordination complexes or their organometallic derivatives. The coordination and organometallic complexes of the active pharmaceutical agent (APAs) are likely to exhibit different modes action from that of the purely organic drug. This approach is premised on the knowledge that ferrocenyl organometallic derivatives of antimalarials and anticancer agents have shown impressive results. There is, however, a paucity of data on the cationic iron half sandwich complexes of APAs in the literature. To gain greater insight into the effect of introducing the cationic iron half sandwich organometallic fragment into the molecular structure of active drug molecules on their activity, the cationic iron half-sandwich organometallic fragment $[\eta^5\text{-}C_5H_5(CO)_2Fe]^+$ was incorporated into the molecular structures of selected APAs as mixed donor ligands and activity of the resultant complexes was determined against selected gram-negative and gram-positive bacteria.

1.3 Hypothesis

The iron half sandwich organometallic fragment $[\eta^5\text{-}C_5H_5(CO)_2Fe]^+$ will coordinate to the APA forming organometallic salts of the form $[[\eta^5\text{-}C_5H_5(CO)_2Fe(L)]BF_4$ (where L = ethionamide (ETH), prothionamide (PTH),3-aminosalicylic acid (3-ASA), p-aminosalicylic acid (PAS) {or 4-aminosalicylic acid (4-ASA)}, 5-aminosalicylic acid

(5-ASA), linezolid (LZD) or terizidone (TZD)) that are likely to be more bioactive than the parent organic ligands.

1.4 Objectives

1.4.1 General Objective

To modify the structures of the selected known active pharmaceutical agents using the cationic iron half sandwich organometallic fragment to form iron half sandwich organometallic salts as potential therapeutic agents.

1.4.2 Specific Objectives

i. To determine the ligation properties of the selected APAs based on the global molecular and regional reactivity descriptors
ii. To determine the thermodynamic, global molecular and spectroscopic properties of the selected APAs and their corresponding Fp complex salts.
iii. To synthesize and characterize the cationic iron half sandwich complexes of the selected APAs
iv. To determine the antibacterial activity of the synthesized Fp complexes against selected Gram (+) and Gram (-) bacterial strains

1.5 Significance of the Study

New cationic iron half sandwich complex salts of active pharmaceutical agents as potential therapeutics have been successful synthesized, characterized and their

bioactivities assessed. The study forms part of a contribution to the fight against bacterial drug resistance.

1.6 Scope and Limitations of the Study

Only complexes of the organometallic Lewis acid $[\eta^5\text{-}C_5R_5(CO)_2Fe]^+$(R= H) were studied. Only seven ligands, namely, 3 aminosalicylic acid (3-ASA), 4-aminosalicylic acid (4-ASA), 5-aminosalicylic acid (5-ASA), ethionamide (ETH), prothionamide (PTH), linezolid (LZD) and terizidone (TZD) were selected for the study. The level of theory used was DFT with three functionals (CAM-B3LYP, B3LYP and PBEPBE) as implemented in the code G09 and G16. The counter ion used was only tetrafluoroborate. Only six bacterial strains namely; the gram negative strains: bacteria *Staphylococcus aureus, Bacillus subtilis* and *Enterococcus faecalis*, and the gram positive strains: *Escherichia coli, Salmonella typhi* and *Pseudomonas aeruginosa* were used for the antibacterial activity tests.

CHAPTER TWO

LITERATURE REVIEW

2.1 Drug Resistance

A survey of literature reveals that, virtually every drug in the market today more so the purely organic drugs whether for the treatment of protozoal, viral, malaria, cancer, bacterial or fungal infections has met some form of resistance (Parker and Jevons, 1964; Parker ,1970; Harnett ***et*** *al.*, 1991; Cohen,1992; Ullman, 1995; Doern *et al*., 1998; Moellering, 1998; Loeffler, and Stevens, 2003; Meka and Gold, 2004; Ellner , 2008; Ellner , 2009; Locke *et al*., 2010;Strasfeld and Chou, 2010; Long and Vester, 2011;Yang *et al*., 2011; Tazi *et al*., 2013; Kurz *et al*., 2016; Kuo *et al*., 2018). As soon as the resistance to a particular antimicrobial drug has reached a critical prevalence, the utility of such a therapeutic agent becomes severely compromised. Most often, an alternative therapy will have to be prescribed. Antimicrobial resistance in general and antibacterial resistance in particular is of grave concern not only in patient care centres where antibiotics are in great clinical use, but also in adjacent communities due to sharing of resistant genes between bacteria (Cohen,1992; Neu, 1992; Panlilio *et al*., 1992; Sievert *et al*., 2008).

Consequently, this has led to the emergence of tough-to-treat infections caused by the so called “superbugs”, The most horrible ones are the strains of bacteria that cannot be treated by any of the existing antibiotic drugs (Raviglione, 2008; Spellberg 2008). Multidrug-resistant bacteria are currently considered as an emergent and major global public health problem (Shenoi and Friedland, 2009; Roca *et al*., 2015). Multidrug

resistance (MDR) is defined as insensitivity or resistance of a microbe to the administered antimicrobial drugs (which are structurally unrelated and have different molecular targets) despite previous susceptibility to the medicines (Nikaido, 2009; WHO, 2014; WHO, 2018). These resistant microorganisms (bacteria, fungi, viruses, and parasites) are able to fight attack by the antimicrobial agents, which eventually leads to ineffective treatment resulting in persistence and spreading of infections (WHO, 2014; WHO, 2018). It should be noted that the development of MDR is a natural phenomenon, however this phenomenon is exacerbated by the extensive rise in the number of immunocompromised conditions in an individual, such as HIV-infection, diabetes, organ transplantation, and severe burns, makes the body an easy target for hospital acquired infectious diseases, thereby contributing to further spread of MDR. Therefore**,** there is an urgent need for the search of novel classes of antimicrobial agents in general and in particular antibacterial agents having completely new modes of action to control the virulence of both the drug susceptible and multidrug-resistant bacteria (Norrby *et al*., 2005; Talbot *et al*., 2006; Theuretzbacher, 2011).

2.2 Bacterial Drug Resistance

Antibiotics are the ‘wonder drugs’ in the fight against bacterial infections. For decades a variety of antibiotics have been used both for therapeutic and prophylactic purposes in humans, for veterinary and agricultural purposes. These drugs have proved to be remarkably effective in controlling bacterial infections. Antibiotics, either are cytotoxic or cytostatic to the pathogens, allowing the body’s natural defences, such as the immune system, to eradicate them (Leeb, 2004).

Bacterial resistance to the antibiotics currently in clinical use is increasing rapidly and has become a global human threat (Neu, 1992; Nathan, 2004; Finch and Hunter, 2006; Ellner , 2008; Rice *et al*., 2008; Spellberg *et al*., 2008; Ellner , 2009 ; Ferguson and Rhoads, 2009; Nikaido, 2009; WHO, 2014; Roca *et al*., 2015 WHO, 2018). Although there is a vast number of antibacterial agents currently in the market for clinical use, they still cannot meet the challenges posed by the rapid increase in drug resistance by the pathogens (Nathan, 2004; Lee, 2008; Ferguson and Rhoads, 2009; Davies and Davies, 2010). Bacterial resistance to almost all of the available antibacterial agents have been isolated (Nathan, 2004; Paterson and Doi, 2007).

For instance, in the report "Bad Bugs, No Drugs: No ESKAPE" the Infectious Diseases Society of America (IDSA) declared drug resistance by the pathogens, ***E****nterococcus faecium*, ***S****taphylococcus aureus*, ***K****lebsiella pneumoniae*, ***A****cinetobacter baumanii*, ***P****seudomonas aeruginosa* and the **E**nterobacter species a global concern (Boucher *et al*., 2009). Over the years Methicillin-resistant ***S****taphylococcus aureus* (MRSA), fluoroquinolone-resistant ***P****seudomonas aeruginosa* and vancomycin-resistant Enterococcus (VRE) have shown increasing rates of infection (Parker and Jevons, 1964; Parker, 1970; Moellering, 1998; Giske *et al*., 2007; Sievert *et al*., 2008).

The existing therapeutic options for these pathogens are extremely limited (Bradford *et al*., 2004; NNIS, 2004; Falagas *et al*., 2005; Norrby *et al*., 2005; Falagas and Bliziotis, 2007; Paterson and Doi, 2007; Lee, 2008; Urban, 2008). The number of antibacterials in advanced development also remains disappointing. The unavailability of particular

agents designed to treat infections due to resistant gram-negative bacilli places patients with these infections in grave danger (Roca *et al*., 2015). Currently, there are no systemically administered antibiotics in advanced pipeline of development that have activity against either a purely gram-negative spectrum or bacteria already resistant to all currently available antibacterial drugs (Talbot *et al*., 2006; Boucher *et al*., 2009**).** There is, therefore, an urgent need to develop new classes of antibacterial agents and/or reengineered or repositioned drugs that may elude the mechanisms of resistance developed by the bacteria against the chemotherapeutic agents currently in clinical use.

2.3 Combating Drug Resistance

There are a number of solutions to the problem of bacterial resistance. Fruitful strategies comprise of; the combination of existing antibacterial agents with other drugs, the development of enhanced diagnostic procedures leading to the rapid identification of the causative pathogens and thus permitting the use of antibiotics with a narrow spectrum of activity. Another strategy that is actively explored by medicinal chemists is the discovery of novel classes of antibacterial agents with new mechanisms of action. However, the most popular and promising approach, is the molecular modification of existing classes of antibacterial agents to produce new analogs with enhanced activities. This can be attested by the vast reports on this aspect of chemistry (Weaver *et al*., 1978; Selvakumar *et al*., 2002; Weidner-Wells *et al*., 2002; Einsiedel *et al*., 2003; Selvakumar *et al*., 2006; Zhai *et al*., 2006; Dolezal *et al*., 2008; Srivastava *et al*., 2008; Rieder, 2009; Yan *et al*., 2010; Palumbo Piccionello *et al*., 2012; Fortuna *et al*., 2013; Kamal *et*

al., 2013a,b; Suzuki *et al*., 2013;Fortuna *et al*., 2014; Naresh *et al*., 2014; Srivastava and Lee, 2015; Volkova *et al*., 2016; War *et al*., 2017; Zhang *et al*., 2018)

2.3.1 Molecular Modification

Molecular modification is a chemical change in a molecule which could be a lead compound or an active pharmaceutical agent with the aim of aiming enhancing the drug's pharmacokinetic, or pharmacodynamics, or pharmaceutical properties (Jean *et al*., 2012). This strategy has been used by medicinal chemists for several years allowing the discovery of many available drugs present in the market today (Silva *et al*., 2005; Jean *et al*., 2012). This strategy has been taunted as a classical short-term approach to combat drug resistance of existing drugs or to improve their potency and/or spectrum. This approach has shown to be quite promising given the number active pharmaceutical agents in the market developed using this strategy. Molecular modification strategies can be classified into three, the prodrug approach, molecular hybridization and biosisoterism (Jean *et al*., 2012). The long term goal of this study is to design and develop new drugs or formulations from the currently existing active pharmaceutical agents (APA) from a prodrug approach. Therefore, a brief discussion on the prodrug approach highlighting its application to drug discovery is given.

By definition a prodrug is a compound that undergoes biotransformation prior to the display of its pharmacological effects (Albert, 1958; Jean *et al*., 2012). The term drug latentiation is also used in close relation to the term prodrug. Drug latentiation is used to mean the chemical modification of a biologically active substance to form a new

compound that, upon *in vivo* enzymatic attack, releases the parent compound (Haper, 1959; Jean *et al*., 2012).

Generally, prodrugs can be classified into two: bioprecursors and carrier prodrugs. Bioprecursors are new compounds arising from the molecular modification strategy. These new compounds provide a substrate for the metabolizing enzymes that after biotransformation demonstrate biological activity. Examples of drugs available in the market to date arising from this approach include; sulindac, acyclovir, and losartan (Silva *et al*., 2005). On the other hand, carriers' prodrugs are designed using labile linkage between a carrier group and an active compound. This prodrug after chemical or biological biotransformation releases the parental drug responsible for the biological activity**.** The carrier selection could explore two strategies; the first one is use an inactive carrier (non-toxic) and the second one uses active compounds so as to obtain synergistic effect. In the later strategy the compounds can be termed as mutual prodrugs or codrugs. This prodrug approach has been used by several workers in the discovery of new antitubercular compounds. For instance, the list of bioprecursor prodrugs includes the most familiar antituberculars' pyrazinamide (PZA), isoniazid (INH), prothionamide (PTH), para-aminosalicylic acid (PAS) and ethionamide (ETH). In both the two cases it is anticipated that the active compound (s) should be released with satisfactory kinetic hydrolysis reaction (Silva *et al*., 2005). In this study the carrier prodrug approach was contemplated with the cationic half sandwich organometallic fragment envisaged as an inactive non-toxic carrier group (Jean *et al*., 2012).

2.3.2 Molecular Modification by Incorporation of Metals

One way of restoring the activity of organic drugs for which resistance has emerged is to modify the structure to contain a metal either to form coordination metal complexes or organometallic derivatives (Obaleye *et al*., 2009; Mjos and Orvig, 2014; Regiel-Futyra *et al*., 2017). These two approaches are discussed in the following subsections.

2.3.2.1 Transition Metal Complexes as Potential Chemotherapeutic Agents

The use and application of metals and metal complexes as therapeutics is of increasing clinical and commercial importance as can be attested to by the numerous monographs, major reviews, and dedicated volumes on this aspect of chemistry (Violette *et al*., 1995; Sanchez-Delgado *et al*., 1993; Sanchez-Delgado *et al*., 1996; Navarro *et al*., 1997; Sanchez-Delgado *et al*., 1998; Guo and Sadler, 1999; Orvig and Abrams, 1999; Özdemir *et al*., 2004; Melaiye, and Youngs, 2005; Navarro *et al*., 2004; Gianferrara *et al*., 2009; Navarro *et al*., 2010; Özdemir *et al*., 2010; Navarro *et al*., 2011a, b; Barry and Sadler, 2013). Medicinal inorganic compounds can be roughly divided into two, namely, drugs acting as ligands targeting metal ions in some form, whether free or protein-bound and metal-based drugs and imaging agents where the central metal ion or atom plays a key role in the mechanism of action of the drug (Reynolds, 1996; Ming, 2003; Ho, 2005; Mjos and Orvig, 2014**)**.

Coordination and organometallic complexes present an expansive variety of coordination spheres, oxidation states, ligand designs, and redox potentials, hence

presenting the ability to systematically alter the kinetic and thermodynamic properties of the complexes toward biological receptors. It should be noted, however, that the use of inorganic compounds containing transition metals in medicine is hampered by heavy metal toxicity and poor water solubility, and hence poor bioavailability. However, the therapeutic opportunities are rigorously defined to minimize such side effects. For example, bioinorganic chemists have directed their efforts towards nanoformulations. These systems are designed to solubilize the metallodrugs, to increase the metallodrugs overall stability in physiological media, and to selectively deliver the cargo to the target site (Nardon and Fregona, 2018). Generally, the usefulness of any drug whether organic, inorganic or organometallic is a balance between its toxicity and activity (Farrell, 1989).

The modification of the structures of purely organic drugs so as to contain a metal, offers numerous advantages arising from the fact that transition metals have unique features, such as variable oxidation states, redox potentials, coordination numbers and geometries. Thus, metals not only offer prototypes for synthesis, but they also present functionalities that enhance drug delivery routes. For example, the activity of most organic drugs requires the interaction of the drugs with metals either at their target site or during their metabolism or sometimes drugs even disturb the balance of metal ion uptake and distribution in cells and tissues. Therefore, the distinctive properties of metal complexes offer advantages in the discovery and development of new therapeutics (Biot *et al*., 1999a; Ming, 2003; Ho, 2005; Chhan and Supuran, 2006; Blackie *et al*., 2007). Furthermore, in coordination and organometallic complexes, the metal centres are

capable of organizing surrounding atoms to achieve unique pharmacophore geometries that are not easily achieved by other chemical entities. Therefore, a massive diversity of structural scaffolds can be achieved with metal complexes. The effects of metal atom/ions can be highly specific and can be modulated by recruiting cellular processes that recognize specific types of metal-macromolecules interactions (Ho, 2005).

It is also known that the nature of the target to be attacked by any drug usually depends on the mechanism of action of the drug. For example, various cytotoxic metal complexes target DNA due to its importance in replication and cell viability. Organometallic and coordination compounds offer many binding modes to polynucleotides, including outer-sphere noncovalent binding, metal coordination to nucleobase and phosphate backbone sites, as well as strand cleavage induced by oxidation using redox-active metal centres. Transition metals such as Fe, Cu, Co, Ru, Mn, and so forth exhibit multiple or variable oxidation states, which might allow for redox chemistry resulting in DNA strand breakage (Claussen and Long, 1999).

Coordinate bonds are usually much-weaker than the normal covalent bonds. Therefore, ligand substitution reactions can take place in biological media. Most metallodrugs are therefore by default, pro-drugs. They can undergo ligand substitution and redox reactions before reaching the target site. Moreover, a displaced ligand may itself attack a target site and controlled ligand release can play a role in the mechanism of action of the metallodrug (Farrell, 1989). Moreover, metal complexes provide a rich platform for the design of novel chemotherapeutics. One can choose to focus on the metal itself and

its oxidation state, the numbers and types of coordinated ligands or the coordination geometry of the metal complexes (Mjos and Orvig, 2014).

The ligands in metallodrugs can not only regulate the reactivity of the metal, but also play a key role in determining the nature of secondary coordination sphere interactions involved in the recognition of biological target sites such as DNA, enzymes and protein receptors. The ligands themselves can sometimes undergo biologically-important redox reactions or other modifications for instance hydrolysis *in vivo* mediated by the metal. All these variables provide an immense diversity for the structural design of metallodrugs (Farrell, 1989).

2.3.2.2 Organometallic Derivatization of Organic Active Pharmaceutical Agents

This section describes in brief the advances made so far in the development of organometallic compounds as novel classes of therapeutics with potential for clinical use to treat various types of diseases.

Organometallic derivatization of existing purely organic drugs is an attractive strategy to overcome the drug resistance menace (Fouda *et al*., 2007). This approach may perhaps offer a metal-specific mode of action which is not available for the purely organic therapeutic drug molecules. It is postulated that there is a difficulty in general for microorganisms to develop resistance against drugs with multiple targets, especially, if the resistance is associated with target modification. A case in point is the inability of

bacteria to develop resistance against silver-based antimicrobials currently in use. This has enabled such antibiotics to survive for long in the market (Klasen, 2000; Chopra, 2007).

The use of the ferrocenyl moiety in structure modification of organic drugs has become quite popular due to the promising results it has afforded (Van Staveren and Metzler-Nolte, 2004; Gasser, and Metzler-Nolte, 2011; Gasser *et al*., 2011; Hillard and Jaouen, 2011; Patra *et al*., 2010; Patra *et al*., 2011; Gasser and Metzler-Nolte, 2012; Patra *et al*., 2012b; Patra and Gasser, 2012; Gasser, 2015). Using a rational drug design approach, Edwards *et al*. (1975) published a series of articles in the 1970s describing the synthesis of ferrocenyl analogues of commercially available antibiotics the Penicillins and Cephalosporins as sodium salts. Figure 2.1 shows selected examples from their studies. Biological tests of these compounds showed that the compounds had *in vitro* antibacterial activity against various strains of bacteria including strains of *Staphylococcus aureus.* In addition, the ferrocenyl derivatives also acted as β-lactamase inhibitors. The degree of β-lactamase inhibition increased with the increase in substitution at the α-ferrocenyl carbon atom (Edwards *et al*., 1975; Edwards *et al*., 1976a; Edwards *et al*., 1976b; Edwards *et al*., 1979).

In general, the introduction of the ferrocenyl moiety into these purely organic molecules had three outcomes. First it modified their two and three dimensional profiles, secondly it introduced or enhanced some aromaticity via the cyclopentadienyl fragments and finally it introduced a metal in the form of iron. The overall effect was seen in the form

of changes in the antibiotic activities of the molecules. It is important to note that no more detailed information on the mechanism of action of the ferrocenyl analogues was given. Thus, it is still unclear whether the ferrocenyl derivatives could help to overcome resistance against penicillin-resistant microbes.

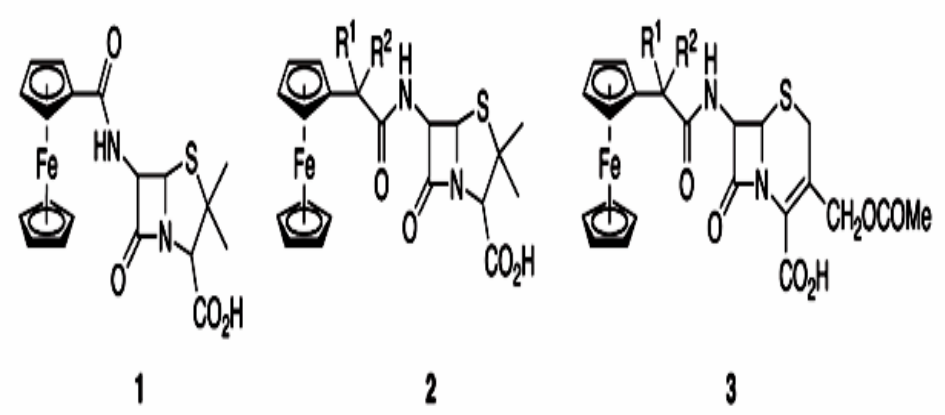

Figure 2.1: Ferrocenoyl-Penicillin (1), Ferrocenyl- Penicillin (2) and Ferrocenyl-Cephalosporin (3)

Use of ferrocene has also been directed towards the fight against malaria drug resistance (Biot *et al*., 1997; Biot *et al*., 1999a, b; Biot *et al*., 2000; Blackie *et al*., 2007; Blackie and Chibale, 2008; Hartinger and Dyson, 2009; Biot *et al*., 2011;) For example, in one study Biot and co-workers inserted the full sandwich ferrocene into the molecular structure of the organic antimalarial drug chloroquine producing the hybrid compound ferroquine (Fig. 2.2). Ferroquine is a push–pull compound to the malarial parasites since it combines a poison chloroquine and a bait iron. The parasite requires iron for its development inside the red blood cells. The structural change of chloroquine using ferrocene was found to circumvent chloroquine resistance. Biological tests showed that the hybrid chloroquine-ferrocene molecule was much more potent in mice than the

parent compound chloroquine. The hybrid compound was active against chloroquine sensitive parasites and chloroquine resistant strains of *Plasmodium.* It was safe and effective in mice, and was non-mutagenic and is currently undergoing clinical trials (Biot *et al.,* 1999a and b; Pradines, 2001; Supan *et al*., 2012; Held *et al*., 2015). Biot and co-workers also used the same strategy to incorporate ferrocene into the antimalarial mefloquine to produce a mefloquine-ferrocene hybrid (Figure 2.2) (Biot *et al*., 2000).

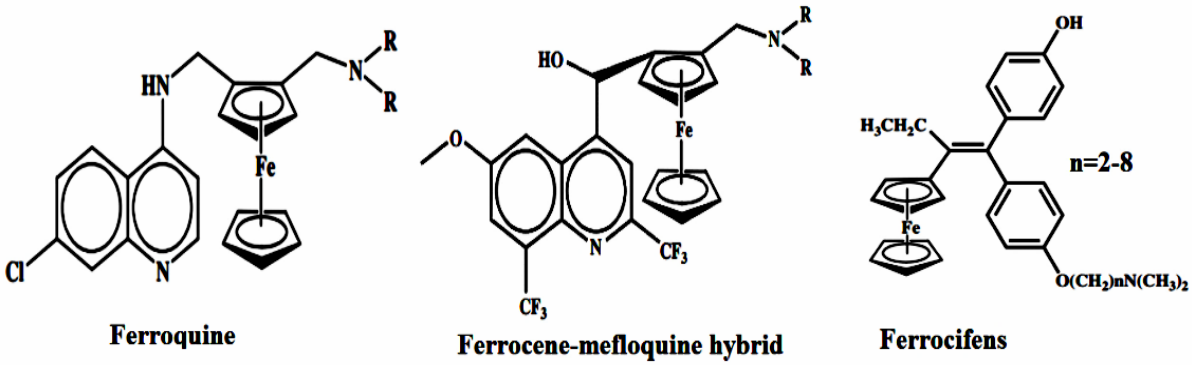

Figure 2.2: Ferrocene Derivatized Chloroquine, Mefloquine and Tamoxifen

Another example that shows the versatility of ferrocene in derivatisation of organic drugs was the synthesis of artemisinin ferrocenic complexes. Delhaes *et al*. 2000 synthesized novel ferrocenic artemisinin derivatives and studied their antimalarial activity and affinity towards Ferritoporphyrin (IX). Here all the compounds isolated and tested showed the ability to bind to Ferritoporphyrin (IX) and their activities as antimalarials were higher than the parent molecules (Held *et al*., 2015).

Tamoxifen, trans-1-(4-***b***-dimethylaminoethoxyphenyl)-1,2-diphenylbut-1-ene, a member of the selective oestrogen receptor modulators (SERMs) is the drug most frequently used for the treatment of estrogen receptor positive breast cancer (Shagufta and Ahmad, 2018). However, tamoxifen suffers several disadvantages including the fact that it is only effective in 60% of cases, and that resistance can develop when the drug is used for longer periods (Jaouen *et al*., 2004). In addition, tamoxifen is associated with the increase in the risks of endometrial or uterine cancer and blood clotting in the lungs **(**Shagufta and Ahmad, 2018). To overcome these shortcomings and with the initial idea of enhancing the efficacy of tamoxifen, by modifying the structure through the incorporation of an organometallic moiety possessing novel properties Jaouen *et al*. (2004) inserted ferrocene into the molecular structure of tamoxifen to form hybrid compounds, the ferrocifens (Figure 2.2). This initial study sparked an interest in the area and numerous workers have joined the bandwagon (Hillard *et al*., 2006; Jaouen; 2006; Nguyen *et al*., 2007; Jaouen and Metzler-Nolte, 2010; Cázares-Marinero *et al*., 2013; Cázares-Marinero *et al*., 2014; Jaouen *et al*., 2015; Wang *et al*., 2015).

Other metallocenes and metallocene dichlorides such as the Titanocene dichloride ($TiCl_2Cp_2$) have also been proposed as potential candidates for cancer treatment. Titanocene dichloride demonstrates general anti-proliferation activity and is effective against five types of cancer cells (Köpf-Maier and Köpf, 1984; Köpf-Maier, 1985; Köpf-Maier and Gerlach, 1986; Köpf-Maier *et al*., 1988a, b; Köpf-Maier, 1989; Ward *et al*., 1989; Köpf-Maier and Klapotke, 1992; Köpf-Maier and Köpf, 1994; Zhang and Sadler, 2017).

Metal arene complexes have also been proposed as potential anticancer agents (Dougan *et al*., 2006; Peacock *et al*., 2007; Peacock and Sadler, 2008; Van Rijt and Sadler, 2009; Filak *et al*., 2013; Filak *et al*., 2014; Riedl *et al*., 2016). Organometallic half-sandwich iridium, osmium, chromium and ruthenium complexes have also been reported as potential antibacterial and anticancer agents (Chen *et al*., 2002; Hanif *et al*., 2010; Liu *et al*., 2011; Henke *et al*., 2012; Patra *et al*., 2012a and b).

In a separate study Chen *et al*. (2004) reported the first example of antibacterial organometallic tungsten (W) complex $[W(H_2O)(CO)_3(H\text{-}Norf)]\cdot(H\text{-}Norf)\cdot H_2O$ with the antibiotic Norfloxacin as ligand. Figure 2.3 shows the single crystal structure of the compound.

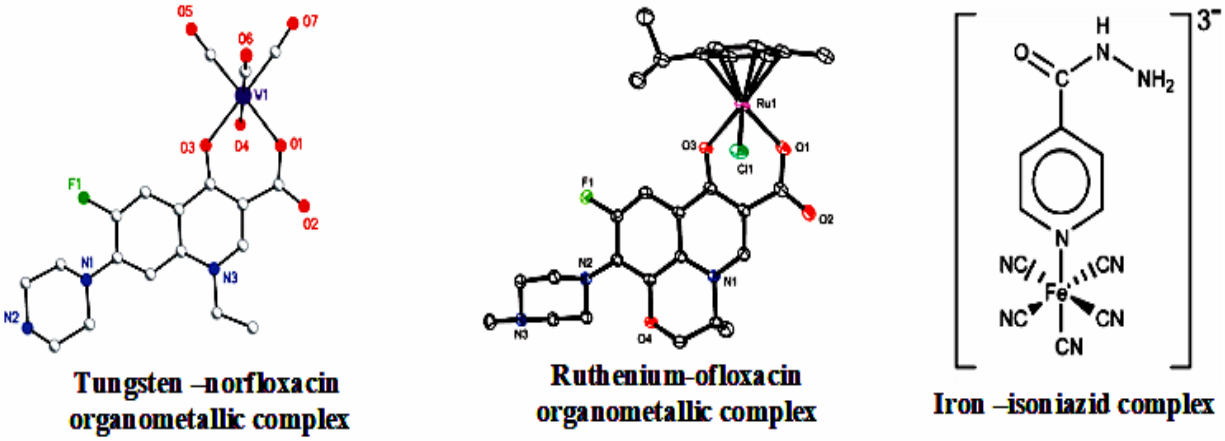

Figure 2.3: Organometallic Complexes of Norfloxacin, Ofloxacin and Isoniazid

In this compound the tungsten atom coordinates to three carbon atoms of the carbonyl ligands, one oxygen atom from water (H_2O) and two oxygen atoms from Norfloxacin one from the quinoline ring and the other from the carboxylate group, forming a slightly distorted octahedral geometry around the tungsten metal (W) centre. The antibacterial effect of the compound was tested *in vitro* against gram negative bacteria *Escheria coli* and *Bacillus dysenteriae* and gram positive bacteria *Staphylococcus aureus*. The results obtained showed that the activity of the complex against the tested organisms was significantly superior to that of the free ligand (H-Norf). Thus, the coordination of the metal tungsten (W) to the purely organic free ligand possibly resulted in some synergetic effect (Chen *et al*., 2004).

Using a similar reaction like that of Chen and co-workers, Turel *et al*. (2010) reported the isolation of the first ruthenium organometallic complex of the antibacterial drug ofloxacin. Furthermore, the interactions of the complex with DNA were also studied. Here also like in the norfloxacin-tungsten complex, the crystallographic data showed that ofloxacin is coordinated to the metal through the quinoline ring carbonyl oxygen and another oxygen atom from one of the carboxylic groups (Fig. 2.3). The compound exhibited good antibacterial activity and also showed a, direct interaction with double-stranded DNA in solution (Turel *et al*., 2010).

Isoniazid also known as isonicotinic acid hydrazide or simply INH was first reported to be active and effective in the treatment of tuberculosis (TB) in the year 1952 (Bernstein *et al*., 1952). However, soon after *Mycobacterium tuberculosis* developed resistance to

the drug and INH resistant strains of *Mycobacterium tuberculosis* were reported (Middlebrook, 1952). In their contribution towards the fight against TB drug resistance Oliveira *et al*. (2004) reported the isolation of an INH iron organometallic complex $[Fe^{II}(CN)_5(INH)]^{3-}$ that inhibits wild-type and an INH-resistant mutant 2-trans-enoyl-ACP (CoA) reductase from *Mycobacterium tuberculosis*. In this complex, iron coordinates to INH through the pyridyl nitrogen atom (Figure 2.3). An investigation on the biological activity of the complex showed that the complex had minimum inhibitory concentration (MIC) of 0.2 mg ml^{-1} in comparison to the free INH MIC of 0.02–0.2 mg ml^{-1}. Thus, the complex $[Fe^{II}(CN)_5(INH)]^{3-}$ seems to be a good contender for further development as an antitubercular drug and/or as a lead compound to a new class of antituberculars (Oliveira *et al*., 2004).

Other organometallic complexes with biological molecules such as diorganotin (IV)-chloramphenicol and cycloserine derivatives and half sandwich chromium complexes of Platensimycin have also been reported (Pellerito *et al*., 1998, Yin *et al*., 2005; Patra *et al*., 2012a and b; Rehman *et al*., 2014).

It is clear from the foregoing examples therefore, that the derivatization of organic drug molecules with organometallic fragments has the potential of enhancing their performance as drugs. Furthermore, most of the studies have concentrated on the use of the full sandwich ferrocene and a few other metallocenes in structure modification of the organic drug molecules and with little exploration of the half sandwich organometallic fragments in general and the cationic half sandwich in particular. It is in

this backdrop that this study pursued the use of the cationic iron half sandwich organometallic fragment, $(\eta^5\text{-}C_5R_5(CO)_2Fe]^+$ in the modification of existing purely organic active pharmaceutical agents (APA). The coordination of the purely organic drugs to the Lewis acid iron half sandwich organometallic fragment may have three effects. First is introducing aromaticity in the form of the cyclopentadienyl ring where there was none or enhancing it where it was present. Aromatic rings are very powerful motifs in drug activity, they offer several unique and strong modes of interaction with target proteins, such as the classical arene-arene (p stacking) interaction and arene--H bonding (edge-to-face interactions) and the recently identified interactions, p-cation stabilisation and sulphur-arene interactions (Meyer *et al* ., 2003). Currently, majority of the marketed drugs contain at least one aromatic ring (Ward and Beswick, 2014)). The second effect is the modification the shape of the drug in its 2D or 3D profiles and lastly introducing a metal centre in the drug molecule in the form of iron that may participate in biochemical reactions.

2.4 Quantum-Chemical Calculations

The motivation for the computational study was to gain insight into the theoretical framework in which to recognize the relationships between electronic structure and the ligation properties of the active pharmaceutical agents as ligands towards the cationic iron half sandwich and predict the molecular and spectroscopic properties of the organometallic salts arising from the active pharmaceutical agents and the cationic half sandwich. Density functional theory (DFT) computations were thus performed to model the electronic structures.

2.4.1 Density Functional Theory (DFT)

The basis of DFT is that the energy of a system composed of fixed nuclei and mobile electrons can be expressed as a functional $E(\rho)$ of the electron density function (Dreitzler and Gross, 1990). This differs from the traditional electronic structure theory in which the central construct is the electronic wave function (Ψ), which hinges on the coordinates of all the electrons (3N variables). The electronic density function ρ is a function of three variables (x,y,z) and is therefore (relatively) easy to visualise. (Cramer and Truhlar, 2009; Peverati and Truhlar, 2014).

Density functional theory (DFT) is currently the ideal method for the determination of electronic structures of complex chemical systems, partly because its cost scales more favourably with system size than does the cost of correlated wave function theory (WFT), with accuracy similar to WFT (Politzer and Abu-Awwad, 1998; Zhao *et al*., 2004; Siegbahn, 2006; Malik and Michalska, 2014). This is true for both organic compounds and chemical systems involving metals. However, the advantages of DFT are actually greater for metals systems, particularly transition metal systems (Zhao and Truhlar, 2008). This added advantage can be attributed to the static electron correlation (Sinanoğlu, 1961; Tuan and Sinanoğlu, 1964; Grant, 1994; Quiney, 1991; Schmidt and Gordon, 1998; Sinanoğlu, 2007a and b). Thus, the application of DFT to transition metal systems has become a well- known methodology (Zhao and Truhlar, 2008; Cramer and Truhlar, 2009).

In the area of organometallic chemistry, computational chemistry is growing in importance like it has done in organic chemistry. Computational organometallic chemistry has passed the stage of qualitative orbital diagrams and is now making semi-quantitative predictions of great importance to experimental work. This growth has led to a massive change in the field of theoretical transition metal chemistry. DFT calculations have become an established means for analysing structure, bonding, reactivity and properties of transition metal complexes (Eichkorn *et al*., 1997; Diaz-Acosta *et al*., 2003; Mitin *et al*., 2003). Literature has many reports on applications of DFT to problems in molecular transition metal chemistry which supports the fact that DFT is sufficiently accurate for such studies (Sosa *et al*., 1992; Chan and Au-Yeung, 1997; Görling *et al*., 1999; Neese, 2001; Padilla-Campos and Fuentealba, 2003; Vallet *et al*., 2003; Neese, 2006; Schinzel *et al*., 2006; Petrenko *et al*., 2006; Zein and Neese, 2008; Zein *et al*., 2008; Ramírez-Ramírez *et al*., 2010; Baldenebro-Lopez *et al*., 2013; Fizer *et al*., 2017). Most workers attempt to reproduce either one or more known experimental observations, and then make novel predictions based on information sometimes leading to further computations (Korth *et al*., 2002 Neese, 2006; Kirchner *et al*., 2007; Kokatam *et al*., 2007; Kossmann *et al*., 2007; Bühl *et al*., 2008; Baldenebro-Lopez *et al*., 2013; Blomberg *et al*., 2014).

It is worth noting however, that all functionals currently used in DFT studies are still liable to yield very inaccurate results, especially for energetic quantities. This type of problem occurs more often for transition metal compounds than for other species. As a consequence, all computational projects should include comparison of the results from

the chosen method with experimental data. Where this is not possible or ambiguous, comparison between several different functionals is also useful (Eriksson *et al*., 1995; Mitin *et al*., 2003; Neugebauer and Hess, 2003; Neese, 2009).

In a situation where the structural data of a new transition metal complex or novel compound as determined by a single crystal X-ray diffraction analysis is unavailable the calculations of the molecular geometry and vibrational spectra by quantum chemistry methods, combined with experimental studies of the Raman and IR spectra of such a complex play a crucial part in the elucidation of its structure. Furthermore, the calculations of vibrational frequencies and IR/Raman intensities accompanied by normal coordinate analysis is key in producing the reliable assignments of the experimental vibrational spectra (Montgomery *et al*., 1999; Malik and Michalska, 2014). In general, DFT appears reliable for geometries, vibrational frequencies, and total energies, having an edge over wavefunction based methods the advantage being quick convergence to the basis set limit (Kohn *et al*., 1996; Karpagam *et al*., 2010). DFT is quite successful in the prediction of molecular properties such as vibrational spectra. For instance, a good number of spectroscopic properties of interest to the bioinorganic community can be predicted with good accuracy using DFT. Hybrid functionals are in most cases better performers than the wavefunction based methods and the pure DFT functionals (Parr and Yang 1989; Fitzgerald and Andzelm, 1991; Stephens *et al*., 1994; Parr and Yang 1995; Chermette, 1998; Martínez-Araya *et al*., 2013; Pribram-Jones *et al*., 2015)

Density functional theory (DFT) consists of a large set of diverse functionals (Zhao *et al*., 2004). In other words, there exist a vast number of approximations available in the average DFT code. The order of these approximations is local-density approximations (LDA), generalized gradient approximations (GGA) and the hybrid functionals.

$$XC \sim XC^{unif}(\rho) \quad (LDA)$$

$$\sim XC^{GGA}(\rho, |\nabla|) \quad (GGA),$$

$$\sim a(X - X^{GGA}) + XC^{GGA} \quad (hybrid).$$

The Local-density approximations (LDA) are a class of approximations to the exchange–correlation (XC) energy functional that depend solely upon the value of the electronic density at each point in space (and not, for example, derivatives of the density or the Kohn–Sham orbitals). The most successful local approximations are those that have been derived from the homogeneous electron gas (HEG) model. Within the framework of LDA the density is assumed to be the same everywhere. As such therefore, the LDA has a tendency to underestimate the exchange energy and over-estimate the correlation energy (Becke, 2014). To correct for this tendency, it is common to expand in terms of the gradient of the density in order to account for the non-homogeneity of the true electron density. Thus, allowing for corrections based on the changes in density away from the coordinate. These expansions are known as generalized gradient approximations (GGA) (Langreth and Mehl, 1983; Becke, 1988; Perdue *et al*., 1992).

Very good results for molecular geometries and ground-state energies can be obtained using the GGA. The meta-GGA functionals, a natural development after the GGA are more accurate Meta-GGA DFT functional includes the second derivative of the electron density (the Laplacian) whereas GGA includes only the density and its first derivative in the exchange–correlation potential. Difficulties in expressing the exchange part of the energy in GGA and Meta-GGA is relieved by including a component of the exact exchange energy calculated from Hartree–Fock theory, giving rise to hybrid functionals.

Hybrid functionals are now very widely used in chemical applications with the B3LYP functional being the most notable (Lee *et al*., 1988). Computed binding energies, geometries and frequencies are systematically more reliable than the best GGA functionals. The hybrid-exchange functionals reduce the binding energies errors to 3-5 kcal/mol and 2-3%. This is close to the accuracy required for predictive simulations of thermochemical properties (Sholl and Steckel, 2009).

It should be noted that the PBE GGA is the most popular non-empirical approximation, whereas the most popular empirical functional approximation is the B3LYP hybrid. Both models have been incredibly successful, as revealed by their large followings among developers and users. However, no single approximation works well enough for every property of every material of interest. Many users sit squarely and pragmatically in the middle of the two divisions, taking what is best from both of their accomplishments and insights. Often, empiricists and non-empiricists find themselves

with similar end products, a good clue that something valuable has been created with the strengths of both (Szabo and Ostlund, 1982; Pribram-Jones *et al*., 2015).

It should be noted that despite the numerous approximations available, most calculations rely on only a few of the most popular approximations (Pribram-Jones *et al*., 2015). In this study the hybrid functional B3LYP and its variation CAM-B3LYP and the pure DFT functional PBEPBE were employed. It should be noted that the PBE GGA is the most popular non-empirical approximation, whereas the most popular empirical functional approximation is the B3LYP hybrid. Both models have been incredibly successful, as revealed by their large followings among developers and users. However, no single approximation works well enough for every property of every material of interest. Many users sit squarely and pragmatically in the middle of the two divisions, taking what is best from both of their accomplishments and insights. Often, empiricists and non-empiricists find themselves with similar end products, a good clue that something valuable has been created with the strengths of both (Szabo and Ostlund, 1982; Pribram-Jones *et al*., 2015).

To date if measured by the number of publications on density functional theory (DFT), as it is implemented for computational chemistry, the hybrid functional B3LYP seems to provide the highest contribution (Becke, 1993; Stephens *et al*., 1994). The Becke3LYP or simply B3LYP functional is a hybrid of several components, whose relative weights are selected by reference to experimental thermochemical data (Stephens *et al*., 1994). It is a hybrid of exact (Hartree-Fock) exchange with local and

gradient-corrected exchange and correlation terms, (Becke, 1993). B3LYP is the widely used three-parameter hybrid GGA functional (Becke, 1993; Lee *et al*., 1988; Stephens *et al*., 1994a and b). In other words, of the plethora of diverse DFT functionals, B3LYP is one of the most popular and widely employed DFT methodology. This is informed by the fact that it is a very good compromise between accuracy and computational cost. Furthermore, B3LYP has shown to be one of the best performer in the prediction of properties of transition metal compounds (Cramer and Truhlar, 2009).

In the recent past, a lot of progress has been made in the formulation of new DFT functionals or methods, which have been implemented into existing quantum chemical computational programs/ softwares. Among the new functionals is the long-range corrected hybrid model, the Coulomb attenuating method-version of B3LYP known simply as CAM-B3LYP. CAM–B3LYP is a new hybrid long-range corrected exchange–correlation DFT functional version of B3LYP. Calculations show that the functional predicts energetic quantities with the same accuracy as the B3LYP functional. Furthermore, the implementation of CAM-B3LYP does not add a further additional computational cost other than that required for the B3LYP functional. This functional is simply a hybrid functional with superior long-range properties (Yanai *et al*., 2004). In an evaluation of new DFT functionals for calculating the vibrational spectra and structure of cisplatin and by extension platinum(II) complexes, the long-range corrected functional CAM-B3LYP alongside LC- ωPBE and, ωB97XD displayed good performances in predicting the vibrational frequencies of Pt-ligand vibrations (Malik and Michalska, 2014). Therefore, CAM-B3LYP alongside the mentioned

functional are promising new DFT tools for theoretical study of novel compounds especially transition metal complexes (Cramer and Truhlar, 2009).

2.5 Global Molecular Chemical Reactivity Descriptors

Global properties are characteristics of a molecule or a subsystem as a whole (Orozco-Valencia *et al*., 2017). Generally, the chemical properties of molecules can be correlated with quantum chemical parameters (Oguzie *et al*., 2014; Eddy *et al*., 2015; Njoku *et al*., 2017). In the chemical reactivity theory, the parameters like electronegativity, hardness and softness have proved to be very useful quantities in determining the general reactivity of molecules towards electrophiles or nucleophiles (Fuentealba, 1995; Savin *et al*., 1998; Fuentealba and Savin, 2000; Pérez *et al*., 2000; Pérez-Méndez and Contreras, 2015). Currently, the treatment of chemical reactivity is generally implemented in the setting of conceptual density functional theory (DFT) developed and advanced by several workers (Pearson, 1963; Pearson and Songstad, 1967; Perdew and Zunger, 1981;Perdew *et al*, 1982; Langreth and Mehl, 1983; Parr and Pearson, 1983; Pearson, 1985; Pearson, 1988; Pearson, 1989; Pearson, 1990; Chattaraj and Schleyer, 1994; Pearson,, 1994; Parr *et al*., 1995; Pearson, 1995; Parr *et al*., 1999; Chattaraj *et al*., 1999; Chamorro *et al*., 2000; Chattaraj *et al*., 2000; Chamorro *et al*., 2001;Chattaraj *et al*., 2001; Chattaraj *et al*., 2003; Kümmel and Perdew, 2003; Pearson,, 2005; Padmanabhan *et al*., 2007; Kümmel and Kronik, 2008; Stein *et al*., 2010; Kronik *et al*., 2012; Kumar *et al*., 2019a). This reactivity model has transformed classical chemical concepts such as electronegativity, hardness, and softness into figures or numbers, such that, atoms, molecules, and charged systems can be classified into

quantitative scales of reactivity (Domingo, 2000; Domingo *et al*., 2002a; Domingo and Picher, 2004; Nguyen *et al*., 2004; Toro-Labbé, 2007; Cervantes-Navarro and Glossman-Mitnik, 2013; Cerda-Monje *et al*., 2014; Ormazábal-Toledo and Contreras, 2014; Miranda-Quintana, 2017; Manachou *et al*., 2019). The key leading to the quantitative description of electronegativity, hardness, and softness, is based on the concept of the electronic chemical potential (μ) and its derivatives (Parr and Yang, 1984; Mendez and Gazquez, 1994; Melin *et al*., 2003; Meneses *et al*., 2004; Meneses *et al*., 2006; Merouani *et al*., 2013).

2.5.1 Chemical Potential, μ

Within this DFT conceptual framework, the chemical potential μ, which measures the escaping tendency of electrons from equilibrium, is defined as (Parr and Yang, 1989):

$$\mu = \left(\frac{\partial E}{\partial N}\right)_{v(r)} \approx -\frac{IP - EA}{2} = -\chi \qquad eqn\ 1$$

Where, μ is the electronic chemical potential, E is the total energy, N is the number of electrons, ν(r) is the external potential of the system, χ is the electronegativity, IP is the vertical ionization potential, and EA is vertical electron affinity.

Equation (1) links the electronic chemical potential of DFT with the first derivative of the energy with respect to the number of electrons, and therefore with the negative of the Mulliken electronegativity χ at constant external potential v(r) (Geerlings *et al*., 2003). Hence it is commonly used to describe the direction of the electronic flux in a chemical interaction. In general terms, the electronic chemical potential (μ) has been

proposed as a quantity that measures the tendency of electrons to escape from a given chemical system (Parr *et al*., 1999). The beauty of this approach is that, it enables one to carry out an initial assessment of the global electron donating or electron accepting relationship of an interacting pair of chemical species such as atoms or molecules. For example, if the chemical potential (μ) of a species X, is greater than the chemical potential (μ) of its partner Y, then the electronic flux will take place from the chemical species X to the chemical species Y until an equilibrium is established. This signifies that, during their interaction species X will act as nucleophile while species Y will act as an electrophile (Domingo *et al*., 2003a, b; Ormazábal-Toledo *et al*., 2011; Domingo *et al*., 2013; Ormazábal-Toledo and Contreras, 2014). For practical computational purposes a useful definition of the electronic chemical potential is obtained from the Koopmans's theorem (Koopmans, 1934). This theorem defines the chemical potential on the basis of one-electron energy levels of the frontier molecular orbitals which includes the highest occupied molecular orbital (the HOMO) and the lowest unoccupied molecular orbital (the LUMO) as illustrated by equation 2.

$$\mu \approx -\frac{1}{2}(IP + EA) \approx -\frac{1}{2}(E_{LUMO} + E_{HOMO}) \qquad eqn\ 2$$

2.5.2 Electronegativity

According to Pauling, electronegativity is the tendency of an atom in a molecule to attract electrons to itself. Pauling's definition of electronegativity was based on thermodynamic arguments in relation to bond energies (Pauling, 1932). Later on Mulliken defined electronegativity as the arithmetic average of the ionization energy or

potential (IP) and electron affinity (EA) as shown in equation 3 (Mulliken, 1934; Mulliken, 1935; Mulliken, 1955).

$$\chi = \frac{IP + EA}{2} \qquad eqn\ 3$$

The Mulliken expression of electronegativity is obtainable in a natural way within the DFT framework, through the identification that electronegativity (χ) is equal to the negative chemical potential (μ) as shown in equation 1 (Parr, 1980; Parr, 2001; Parr *et al*., 2005). It is rationally expectated that reliable electronegativities should stem directly from the electronic density of the molecule. This is where DFT becomes very useful since it provides a simple way to do exactly that through equation 1. Indeed, this equation has been used widely, but almost uniquely through its finite difference approximation, namely Mulliken's definition in equation 3. This is indeed not sufficiently accurate for the purpose of obtaining an absolute value for electronegativity. However, it provides a powerful means for relative comparisons. In practice, most studies of electronegativities nowadays use Mulliken's approximation (Pearson, 1963; Chermette, 1999). In general, the electronegativity of the nucleophiles or Lewis bases is lower than that of the Lewis acids or electrophiles. Hence, electrons will move from the molecules with lower electronegativity towards the molecule with higher electronegativity until equilibrium in chemical potential is reached (Miranda-Quintana *et al*., 2016).

2.5.3 Chemical Hardness (η) and Softness (S)

Hardness (η) has been defined within the DFT theory as the second derivative of the total energy with respect to total number of electrons N at v(r) (equation 4). It is a property which measures both the stability and reactivity of a given molecule and can be seen as the resistance to charge transfer (Parr and Pearson, 1983; Parr and Gazquez, 1993; Liu *et al*., 1997; Senet, 1997a, b; Mineva *et al*., 1998; Miranda-Quintana *et al*., 2018a, b).

$$\eta = \left(\frac{\partial^2 E}{\partial N^2}\right)_{v(r)} \qquad eqn\ 4$$

Considering the variation in energy when one electron is added to or removed from the system and using the finite difference approximation and assuming the validity of Koopmans'theorem (Koopmans, 1934; Young, 2001; Lewars, 2003; Cramer, 2004; Jensen, 2007), equation 4 can be written as follows:

$$\eta \approx \frac{1}{2}(IP - EA) \approx \frac{1}{2}(E_{LUMO} - E_{HOMO}) \qquad eqn\ 4a$$

Or simply,

$$\eta = \frac{IP - EA}{2} = \frac{1}{2}(E_{LUMO} - E_{HOMO}) \qquad eqn\ 4b$$

Where, E_{HOMO} and E_{LUMO} are the energies of the highest occupied molecular orbital (HOMO) and the lowest unoccupied molecular orbital, (LUMO), respectively.

Within the context of density functional theory (DFT), the expression in equation 4 is justified in light of the work of Perdew and co-workers, where they observed the significance of the highest occupied Kohn–Sham eigenvalue, and proved the ionization

potential theorems for the exact Kohn–Sham density functional theory of a many–electron system (Perdew and Levy, 1983; Perdew and Levy, 1997).

Furthermore, the use of the energies of frontier molecular orbitals (FMO) as an approximation to obtain ionisation potential (IP) and electron affinity (EA) is also supported by the Janak's Theorem (Janak, 1978; Gonis, 2014). In particular, the negative of Hartree–Fock and Kohn–Sham HOMO orbital has been found to define upper and lower limits, respectively, for the experimental values of the first ionization potential (Zevallos and Toro-Labbé, 2003). Thus, validating the use of energies of Kohn–Sham frontier molecular orbitals to calculate reactivity descriptors coming from conceptual DFT (Glossman-Mitnik, 2013).

The global softness (S) is simply equal to the inverse of hardness given in equation 5 (Vela and Gazquez, 1990):

$$S = \frac{1}{\eta} = \frac{2}{IP - EA} \qquad eqn\ 5$$

2.5.4 Ionization Potential (IP) and Electron Affinity (EA)

Ligand-binding phenomena are of great interest in coordination and organometallic chemistry. Although many kinds of interactions are involved in such processes, in many cases partial charge transfer through covalent bonding or dative bonding occur. The capability of a Lewis acid or electron deficient species to receive precisely one electron from a ligand (Lewis base or electron rich species) is measured by its electron affinity

(EA). Accordingly, the ionization potential (IP) and electron affinity (EA) are related to the energies of the frontier orbitals E_{HOMO} and E_{LUMO} through equations 6a and 7a assuming the validity of Koopmans' theorem (Koopmans, 1934; Duke and O'Leary, 1995; Plakhutin *et al*., 2006; Salzner and Baer, 2009; Davidson, and Plakhutin, 2010; Putz, 2013).

$$IP = E_{HOMO} \qquad eqn\ 6a$$

$$EA = E_{LUMO} \qquad eqn\ 7a$$

Koopmans' theorem has been used in many studies because in most cases it has been found to reproduce the expected trends. However, in order to check the inadequacy of the Koopmans' approximation on the ionisation potential (IP) and electron affinity (EA) values, it is customary to calculate the vertical electron affinity (EA) and vertical ionisation potential (IP) using equations 6b and 7b, respectively (Levy *et al*., 1984; Lemierre *et al*., 2005; Shankar *et al*., 2009). It is instructive to note that such comparisons are useful only when made at the same level of theory, method and basis set (Mendoza-Huizar, 2018).

$$IP = E_{(N-1)} - E_{(N)} \qquad eqn\ 6b$$

$$EA = E_{(N)} - E_{(N+1)} \qquad eqn\ 7b$$

In equation 6b the ionization potential (IP) is defined as the difference in energy of neutral atom and its cation in gas phase, while electron affinity (EA) as defined by equation 7b is the difference in energy of a neutral atom and its anion in gas phase.

2.5.5 Global Electrophilicity Index (ω)

The global electrophilicity index (ω) represents the stabilization energy of a system when it gets saturated by electrons coming from the surroundings (Chamorro *et al*., 2003; Pérez *et al*., 2003;Chattaraj *et al*., 2006; Chattaraj *et al*., 2009; Soto-Delgado *et al*., 2011). In other words it is the stabilization in energy that an electron accepting species (molecule or atom) undergoes, when it is embedded in an electron bath at constant electronic chemical potential (Domingo *et al*., 2002b, c; Domingo *et al*., 2004). The electrophilicity index (ω) measures the susceptibility of chemical species to accept electrons (Parthasarathi *et al*., 2004). The electrophilicity index (ω) as defined by Parr *et al*. (1999) is a measure of the energy change of an electrophile when it becomes saturated with electrons. For this reason, they considered a chemical species immersed in an idealized bath of electrons, with zero chemical potential. Such a chemical species will accept electrons until the point at which its chemical potential becomes equal to that of the bath (Ormazábal-Toledo *et al*., 2011; Ormazábal-Toledo *et al*., 2013a, b; Frau and Glossman-Mitnik, 2018a and b; Frau *et al*., 2018; Robles *et al*., 2018). Mathematically, this index is defined as shown in equation 8.

$$\omega = \frac{\mu^2}{2\eta} \approx \frac{(IP + EA)^2}{2(IP - EA)} \approx \frac{(E_{LUMO} + E_{HOMO})^2}{2(E_{LUMO} - E_{HOMO})} \qquad eqn\ 8$$

According to this definition, low values of ω indicates a good nucleophile while higher values suggest that the species is a good electrophile. Equation 8 simplifies to equation 9

$$\omega = \frac{\mu^2}{2\eta} = \frac{\mu^2}{2} S \qquad eqn\ 9$$

From equation 9 we deduce that the best electrophile is the species that displays a high value of the electronic chemical Potential (μ) and a low value of chemical hardness (η) or high electronegativity (χ) and high softness (S) otherwise a high polarizability. The global electrophilicity index in the form of reactivity scales has been implemented for a series of classical reactions in organic chemistry including nucleophilic reactions (Ormazábal-Toledo *et al*., 2011; Ormazábal-Toledo *et al*., 2013; Ormazábal-Toledo and Contreras, 2014). Generally, the global electrophilicity index (ω) measures the propensity of chemical species to accept electrons. A good, more reactive, nucleophile is characterized by lower value of ω while a good electrophile is characterized by a high value of ω.

2.5.6 Electron Donating (ω^-) and Electron Accepting (ω^+) Powers

. The electron donating (ω^-) and electron accepting (ω^+) powers of molecules have been defined as shown in equations 10 and 11 (Gázquez *et al*., 2007; Gázquez, 2008; Morell *et al*., 2014; Mendoza-Huizar, 2017)

$$\omega^- = \frac{(\mu^-)^2}{2\eta} = \frac{(3IP + EA)^2}{16(IP - EA)} \qquad eqn10$$

$$\omega^+ = \frac{(\mu^+)^2}{2\eta} = \frac{(IP + 3EA)^2}{16(IP - EA)} \qquad eqn11$$

Where,

$$\mu^- = -\frac{1}{4}(3IP - EA) \qquad eqn\ 12a$$

$$\mu^+ = -\frac{1}{4}(IP + 3EA) \qquad eqn\ 12b$$

It is instructive to note that, the electron donating (ω^-) and the electron accepting (ω^+) powers display a similar behaviour to that of the first ionization potential and the electron affinity, respectively, even though in the case of IP and EA what is measured is the capability of a chemical system to donate or to accept one electron. In the case of electron donating (ω^-) and the electron accepting (ω^+) powers, what is measured is the capability of a chemical system to donate or to accept a small fractional amount of charge (Gázquez, 2008). A larger ω^+ value corresponds to a better capability of accepting charge, whereas while a larger ω^- value of a system makes it a better electron donor. Moreover, in order to compare ω^+ with ω^-, that is, the electron accepting power relative towith the electron donating power, a definition of net electrophilicity as expressed in equation 13 was proposed (Chattaraj et *al*., 2009):

$$\Delta\omega^{\pm} = \omega^{+} - (-\omega^{-}) = \omega^{+} + \omega^{-} \qquad eqn\ 13$$

2.5.7 Global Nucleophilicity Index (N)

The global nucleophilicity index or simple nucleophilicity cannot be derived within the conceptual DFT using the same model as applied for global electrophilicity. However, despite this handicap, several schemes for obtaining the nucleophilicity index are currently available. The most common one is based on tetracyanoethylene (TCE) as a reference and relates the nucleophilicity N of a molecule with the highest occupied molecular orbital (HOMO) energy of tetracyanoethylene (TCE) within the framework of DFT (Roy *et al*., 2006).

$$N = E_{HOMO(Nu)} - E_{HOMo(TCE)} \qquad eqn\ 14$$

In addition to this method three other methods are also available for use to obtain the nucleophilicity of the molecules under a given study (Muir and Baker, 2005; Pratihar and Roy, 2010; Soto-Delgado *et al.*, 2011). These methods are depicted by equations 15, 16, 18 and 20.

$$N' = \frac{1}{\omega}\ x\ 10 \qquad eqn\ 15$$

Where, ω is the global electrophilicity index defined in equations 8 and 9

$$N'' = \frac{1}{\omega^-} x\ 10 \qquad eqn\ 16$$

Where, $\omega^- = \frac{(IP)^2}{2(IP-EA)}$ $eqn\ 17$

$$N''' = \frac{1}{\omega^-} \qquad eqn\ 18$$

Where,

$$\omega^- = \frac{(3IP+EA)^2}{16(IP-EA)} \qquad eqn\ 19$$

And lastly; $N'''' = -IP \approx \in_{HOMO}$ $eqn\ 20$

2.5.8 Frontier Orbitals and the HOMO-LUMO Energy Gap (ΔE)

Generally, the chemical properties of molecules can be correlated with quantum chemical parameters such as the energy of the Highest Occupied Molecular Orbital (HOMO), Lowest Unoccupied Molecular Orbital (LUMO) and the energy gap between the LUMO and HOMO defined by equation 21 (Chamorro *et al*., 2005; Oguzie *et al*., 2011; Oguzie *et al*., 2014; Eddy *et al*., 2015; Njoku *et al*., 2017). Each ligand has a

filled orbital that acts as a σ-donor and an empty orbital. These orbitals are almost always the highest occupied molecular orbitals (HOMO) and the lowest unoccupied molecular orbitals (LUMO) of the ligand (L), respectively. The HOMO of the ligand (L) is the donor to the LUMO of the metal which is normally a d- orbital. The HOMO and LUMO of each fragment also known as the frontier orbitals dominate the bonding most of the time. Usually, the LUMO of the metal fragment (M) is usually closest in energy to the HOMO of the partner fragment- the ligand (L) than to any other vacant orbital of the partner. Strong bonding is therefore expected if the HOMO-LUMO gap of both partners is small. When the HOMO of one molecule interacts favourably with the LUMO of another molecule then the two molecules should readily combine in a rigorous way to form a product (Karthick *et al*., 2011; Stein *et al*., 2012; Karaca *et al*., 2015).

A small HOMO-LUMO gap within a molecule usually makes a ligand soft. The so called "frontier orbitals" (the LUMO and HOMO) often provide the key to understanding chemical reactivity (Woodward and Hoffmann, 1970; Chattaraj *et al*., 2000). The LUMO shows which regions of a molecule are most electron deficient and hence most susceptible to nucleophilic attack.

$$\Delta E = E_{LUMO} - E_{HOMO} \qquad eqn\ 21$$

High HOMO values are associated with the capacity of a molecule to donate an electron to an appropriate acceptor with an empty molecular orbital, which facilitates the nucleophile-electrophile interaction process and therefore indicates better performance

of a substance as a nucleophile or Lewis base. To date the orbital arguments can easily be extended to three-dimensional systems thanks to modern computer graphics.

2.5.9 Electronic Back-Donation ($\Delta E_{Back\text{-}donation}$)

According to the simple charge transfer model for donation and back-donation of charges, an electronic back-donation process can occur between a Lewis base and a Lewis acid (Comas-Vives and Harvey, 2011; Madkour and Elshamy, 2016). This concept establishes that if the two processes namely, charge transfer to the molecule and back-donation from the molecule occur, the energy change is directly proportional to the hardness of the molecule, (η), as indicated by equation 22.

$$\Delta E_{Back-donation} = -\frac{\eta}{4} \qquad eqn\ 22$$

This implies that when $\eta > 0$ and $\Delta E_{Back\text{-}donation} < 0$ the charge transfer to a molecule, followed by a back donation from the molecule, is energetically favoured. Hence, it is possible to compare the stabilization that occurs among several Lewis bases (ligands) if they interact with one or the same Lewis acid (Madkour and Elshamy, 2016).

2.5.10 Number of Electrons Transferred (ΔN)

The number of electrons transferred (ΔN) is another global reactivity index that measures the stabilization in energy when a system acquires an additional electronic charge ΔN from the environment (Madkour and Elshamy, 2016). For a reaction of two systems with different electronegativities such as a Lewis acid and Lewis base, an electronic flow will take place from the molecule with the lower electronegativity value towards the species with a higher value, until the chemical potentials are the same. The

number of electrons transferred (ΔN) from the Lewis base to the Lewis acid can be calculated using the equation 23 (Madkour and Elshamy, 2016);

$$\Delta N = \frac{\chi_{LA} - \chi_{LB}}{[2(\eta_{LA} + \eta_{LB})]} \qquad eqn\ 23$$

Where. χ_{LA} and χ_{LB} denote the absolute electronegativity of the Lewis acid and Lewis base, respectively. η_{LA} and η_{LB} denote the absolute hardness of the Lewis acid and Lewis base respectively.

2.6 Local Reactivity Indices

Local properties may vary from point to point in space and are one-point (r) functions (Cioslowski *et al*., 1993; Contreras *et al*., 1999; Cárdenas *et al*., 2011). Local properties are highly desirable in the establishment of a reactivity focused description of molecular systems (Ponti *et al*., 2000; Sablon *et al*., 2009; Sánchez-Márquez *et al*., 2018; Sánchez-Márquez, 2019).

2.6.1 Fukui Functions

The Fukui function for a molecule, f(r), represents the changes in electron density at a point r with respect to the variation of the number of electrons N at a fixed external potential v(r). Also known as the frontier function, f(r), is defined using the Maxwell relations, analogous to the functional derivative of the chemical potential with respect to a change in the external potential, equation 24 (Yang *et al*., 1984; Tiznado, *et al*., 2005; Szarek *et al*., 2010; Chamorro *et al*., 2013)

$$f(r) = \left(\frac{\partial \rho(r)}{\partial N}\right)_{v(r)} \qquad eqn\ 24$$

Electron density distribution is basic for the understanding of chemical reactivity. Furthermore, electrophilic or nucleophilic attacks can be rationalized on the basis of electrostatic interactions (Santos *et al*., 2002; Santos *et al*., 2004a and b). Therefore, the change in electron density in a species under the influence of an approaching reagent is of considerable importance. It was Fukui who first recognized the importance of frontier orbitals as principal factors governing the ease of chemical reactions and the stereoselective path (Yonezawa *et al*., 1954; Fukui, 1982). Later Parr and Yang demonstrated that frontier orbital theory could be rationalized from DFT. The Fukui function of a molecule is the change in the electron density driven by a change in the number of electrons.

The Fukui function measures the sensitivity of a system's chemical potential to an external perturbation at a particular point. As opposed to hardness (η) and/ or electronegativity (χ), which are global molecular properties, the Fukui functions are local descriptors and reflect the properties of the different regions within a molecule. The derivative of equation 24 for molecular or atomic system is discontinuous and difficult to evaluate (Perdew *et al*., 1982). As a result of this discontinuity, Yang and Parr proposed a set of three equations which gave a numeric definition of the Fukui functions (Parr *et al*., 1984)

$$f^{+}(r) = \left(\frac{\partial \rho(r)}{\partial N}\right)^{+}_{v(r)} \qquad eqn\ 25a$$

$$f^{-}(r) = \left(\frac{\partial \rho(r)}{\partial N}\right)^{-}_{v(r)} \qquad eqn\ 25b$$

$$f^{o}(r) = \left(\frac{\partial \rho(r)}{\partial N}\right)^{o}_{v(r)} \qquad eqn\ 25c$$

Equations 25a-c govern nucleophilic attack (that is the system increases its number of electrons), electrophilic attack (that is, the system decreases its number of electrons) and radical attack, respectively. Using the same finite difference approximation approach employed for the global molecular descriptors electronegativity (χ) and hardness (η), the Fukui functions, f(r), can be calculated from differences in density (Chermette, 1999).

2.6.2 The Condensed Fukui Function

Condensed Fukui functions are integers or numbers obtained by approximate integrations of the Fukui function over atomic regions (Yang and Mortier, 1986). The condensed Fukui functions are usually calculated by means of a finite difference (FD) methodology considering discrete numbers of electrons (Fuentealba *et al*., 2000a). In practice calculations are performed for the neutral molecule and for the cationic and anionic species with the same molecular geometry. In finite difference (FD) calculations, there are three types of condensed Fukui functions, depending on the species involved (Kolandaivel *et al*., 2005). In general terms these condensed Fukui functions are depicted by equations 26a, 26b and 26c for nucleophilic, electrophilic and radical attack, respectively.

$$f_k^{+} = q_{k_{(N)}} - q_{k_{(N+\Delta N)}} \qquad (ucleophilic\ attack) \qquad eqn\ 26a$$

$$f_k^- = q_{k_{(N-\Delta N)}} - q_{k_{(N)}} \qquad (Electrophilic\ attack) \qquad eqn\ 26b$$

$$f_k^o = \frac{1}{2}\left(q_{k_{(N-\Delta N)}} - q_{k_{(N+\Delta N)}}\right) \qquad (Radical\ attack) \qquad eqn\ 26c$$

For ΔN = 1 electron we have equations 27a, 27b and 27c for nucleophilic, electrophilic and radical attack, respectively (Bultinck *et al*., 2003).

$$f_k^+ = q_{k_{(N)}} - q_{k_{(N+1)}} \qquad (Nucleophilic\ attack) \qquad eqn\ 27a$$

$$f_k^- = q_{k_{(N-1)}} - q_{k_{(N)}} \qquad (\ Electrophilic\ attack) \qquad eqn\ 27b$$

$$f_k^o = \frac{1}{2}\left(q_{k_{(N-1)}} - q_{k_{(N+1)}}\right) \qquad (Radical\ attack) \qquad eqn\ 27c$$

A frequently cited difficulty with Fukui functions and condensed Fukui functions is that of negative values. A negative Fukui function value implies that when adding an electron to the molecule, in some positions the electron density is lowered, then again when removing an electron from the molecule, in some sites or regions the electron density increases (Echegaray *et al*., 2014). This is a counterintuitive observation. Whether negative Fukui and condensed Fukui functions are physically plausible is not easy to show, and the only firm condition is that their sum should be equal to one, that is, Fukui functions should be normalized. For condensed atom Fukui functions, this condition means that they should be governed by equation 28 (Bultinck *et al*., 2003).

$$\langle|f\rangle\rangle = \sum_{k=1}^{N} f_k = 1 \qquad eqn\ 28$$

In general, the condensed Fukui functions depend on the approximation used in the definition of the atomic region. Furthermore, functions are sensitive to the various parameters employed in the calculation such as level of theory, method and basis sets

(Arumozhiraja and Kolandaivel, 1997). In fact, it is recognized that the choice of the Mulliken population analysis scheme to define the atomic charges is mainly responsible for the dispersion of values. This is not surprising, because atomic charges, unlike the electron density, are not quantum-mechanically observable, and the weakness of Mulliken population analyses in the calculation of charges in polar molecules is well known (Sannigrahi *et al*, 1993). Indeed, any property based on population analyses grounded on Hilbert space partitioning should show some unreliability (Cioslowski *et al*., 1990; Murray *et al*. 1992; Nath *et al*., 1993; Nath *et al*., 1994; Geerlings *et al*., 1996; Senet, 1996; Saha *et al*., 2009).

2.6.3 Local Softness

The local softness is defined as shown in equation 29 (Mendez and Gazquez, 1994; Roy *et al*., 1998)

$$s(r) = \left(\frac{\partial \rho(r)}{\partial \mu}\right)_{v(r)} \qquad eqn\ 29$$

Since the global softness is given by equation 30a;

$$S = \frac{1}{\eta} = \left(\frac{\partial N}{\partial \mu}\right)_{v(r)} \qquad eqn\ 30a$$

Then one has,

$$S = \int s(r)dr \qquad eqn\ 30b$$

And as such the local softness is obtained as shown in equation 31;

$$s(r) = \left(\frac{\partial \rho(r)}{\partial \mu}\right)_{v(r)} = \left(\frac{\partial \rho(r)}{\partial N}\right)_{v(r)} \left(\frac{\partial N}{\partial \mu}\right)_{v(r)} = f(r).S \qquad qn\ 31$$

From equation 31, it can be clearly seen that the local softness s(r) and the Fukui function f(r) are closely related, and they should play a significant role in the field of chemical reactivity. Indeed, the local softness s(r) combines the site reactivity index, f(r), with the global softness measure (S). Therefore, the local softness s(r) can be considered as a distribution of global softness (S) weighted by the Fukui function f(r) over the molecule, thus it may be considered as a softness density. Consequently, the local softness is the natural DFT concept for the characterization of a site (Harbola *et al*., 1991; Nguyen *et al*., 2003). It should be noted that the Fukui function may be obtained from the local softness from equations 30b and 31 but the reverse is not true (Chermette, 1999).

2.6.4 Local Hardness

Local hardness or hardness density, η(r), can be defined in a similar manner to local softness; that is, analogous to equation 29 as illustrated by equation 32a (Mendez and Gazquez, 1994; Roy *et al*., 1998);

$$\eta(r) = \left(\frac{\partial \mu}{\partial \rho(r)}\right)_{v(r)} \qquad eqn\ 32a$$

Or by analogy to equation 30b as depicted by equation 32b.

$$\eta = \int \eta(r) dr \qquad eqn\ 32b$$

The definition of local hardness as given by equation 32b can be combined with equation 24, such that local hardness and the Fukui functions are related through equation 32c.

$$\eta = \int \eta(r) f(r) dr \qquad eqn\ 32c$$

An inverse relation is obtained with the local softness (equation 30b) to obtain equation 33. However, this inverse equation holds globally, but not locally (Chermette, 1999).

$$\int \eta(r)(s(r) dr = 1 \qquad eqn\ 33$$

2.6.5 The Dual Descriptor

Literature reports have cited that the dual descriptor, $f^2(r)$, shown in equation 34 is a more accurate tool than nucleophilic and electrophilic Fukui functions in predicting local or regional reactivity and that the dual descriptor is able to reveal unambiguously the truly nucleophilic and electrophilic sites in a molecule (Mendoza-Huizar *et al*., 2016; Franco-Pérez *et al*., 2017; Mendoza-Huizar *et al*., 2017). From the dual descriptor the most preferable sites for nucleophilic attacks are obtained when ($f^2(r) > 0$) while the preferable sites for electrophilic attacks are obtained when ($f^2(r) < 0$). Hence, the reactive sites for electrophilic and nucleophilic attack can be obtained simultaneously over the system at point r when the dual descriptor is employed (Morell *et al*., 2005; Morell *et al*., 2006; Morell *et al*., 2008a and b; Pino-Rios *et al*., 2017).

$$f^2(r) \approx f^+(r) - f^-(r) = \rho_{N+1}(r) - 2\rho_N(r) + \rho_{N-1}(r) \qquad eqn\ 34$$

CHAPTER THREE

MATERIALS AND METHODS

3.1 Research Design

The study used a two pronged approach: theoretical/computational studies based on Density Functional Theory (DFT) and experimental studies involving, organometallic synthesis, characterization and bioassay of cationic iron half sandwich organometallic complexes of selected active pharmaceutical agents(APAs) on selected strains of gram-negative and gram-positive bacteria.

3.2 Materials for Synthetic Work

All the chemicals used were of analytical grade. The cyclopentadienyliron dicarbonyl dimer (Fp_2), silver tetrafluoroborate ($AgBF_4$), Terizidone (TZD), 3-Aminosalicylic acid (3-ASA), 4-Aminosalicylic acid (4-ASA), 5-Aminosalicylic acid (5-ASA), Linezolid (LZD), Ethionamide (ETH) and Prothionamide (PTH) were obtained from Sigma Aldrich, USA through DLD Scientific, South Africa. Iodine, benzophenone, the organic solvents (tetrahydrofuran (THF), dichloromethane (DCM), hexane, diethylether (Et_2O), and Petroleum ether), and the salts anhydrous sodium sulphite, sodium thiosulphate, anhydrous calcium chloride were obtained from Sigma Aldrich, USA through Kobian Kenya.

3.3 Experimental Methods

3.3.1 General

All experimental operations in the wet chemistry laboratory were carried out under an inert atmosphere of nitrogen using standard Schlenk line procedures. Analytical grade

THF, hexane and Et_2O were freshly distilled from sodium-benzophenone ketyl before use. DCM (CH_2Cl_2) was distilled from phosphorus (V) oxide and used immediately. Elemental analyses were performed on a LECO CHNS-932 elemental analyzer. Infrared spectra were recorded using a Shimadzu IR Tracer-100, either as KBr pellets for solid samples and solutions of the complex salts in the mother liquor (reaction solvent) in the range of 4500-500 cm^{-1}. ^{1}H and ^{13}C NMR spectra were recorded using Bruker topspin 400 MHz and 600 MHz spectrometers and chemical shifts are recorded in ppm.

3.3.2 Synthesis of Cyclopentadienyliron(II)dicarbonyl iodide (FpI)

The organometallic complex $[\eta^5\text{-}C_5H_5)Fe(CO)_2I]$ was prepared by a slight variation of literature methods (King and Stone 1963; King *et al*., 2007). A mixture of 25.0 g (0.0705 mol) of cyclopentadienyliron dicarbonyl dimer (Fp_2) and 25.0 g (0.0985 mol) of iodine (I_2), in 125.0 ml of DCM was refluxed in a 250.0 ml flask for about 45 minutes, in a dry nitrogen inert atmosphere. After cooling to room temperature, the mixture was then washed with several portions of a solution of sodium thiosulfate pentahydrate (100.0 g/400.0 ml water) in a separatory funnel to remove excess iodine. The solution was then dried using anhydrous sodium sulphate. The volume of the green DCM solution was then reduced using a rotatory evaporator to 10.0 ml and shiny black microcrystals of $[\eta^5\text{-}C_5H_5Fe(CO)_2I]$ were obtained by precipitation with petroleum ether. The product was then air dried to yield 41.76 g (89%) of solid. FTIR (KBr) $\upsilon(C{\equiv}O)$ 2037, 1978 cm^{-1}, melting point 116.12 $^{\circ}C$.

3.3.3 Synthesis of $[(\eta^5\text{-}C_5H_5)(CO)_2Fe(terizidone)]BF_4$

A pre-weighed Schleck tube was charged with a mixture of $[(\eta^5\text{-}C_5H_5)Fe(CO)_2(THF)]BF_4$ (0.4000 g, 1.1880 mmol), terizidone (0.3992 g, 1.3200 mmol) and 20.0 ml of CH_2Cl_2. The mixture was stirred for 16 hours at 40 °C with the progress of the reaction periodically monitored by FTIR spectroscopy. An orange solid precipitated out of the solution. The mother liquor was syringed off and the solid dried under vacuum. Yield 0.6196 g, 92% FTIR (KBr): υ(C≡O) 2124 and 2068 cm^{-1} and υ(B-F) 1054, υ(C=N) 1704 cm^{-1} υ(C=O) 1659, 1637 and 1608 cm^{-1}.

3.3.4 Synthesis of $[(\eta^5\text{-}C_5H_5)(CO)_2Fe(linezolid)]BF_4$

A mixture of the iodo complex, $[\eta^5\text{-}C_5H_5)Fe(CO)_2I]$ (1.00 g, 3.290 mmol) and $AgBF_4$ (0.7 g, 3.630 mmol) was stirred in DCM (20 ml) for 45 minutes at 40 °C. The mixture was then filtered using filter aid. The ligand linezolid (1.15 g, 3.409 mmol) was added to the filtrate and the solution was stirred for 16 hours. When the reaction was deemed complete (FTIR) diethyl ether was added dropwise to the reaction mixture forming an orange-yellow precipitate. The mother liquor was removed and the solid dried under reduced pressure. Yield 1.9815 g, 94%. FTIR(DCM): υ(C≡O) 2032 cm^{-1}, 1985, υ(C=O) 1744 cm^{-1}, υ(C=C) 1658 cm^{-1}, δ(NH_2) 1514 cm^{-1}, υ(BF) 1048 cm^{-1} υ(NH) 3366 cm^{-1}, FTIR (KBr): υ(C≡O) 2036, 1979 cm^{-1} υ(B-F) 1077 cm^{-1}. ^{1}HNMR (500 MHz, DMSO-d_6) δ 8.23-8.25 (*t*, 1H, *J* = 5.8 Hz, ArH), 7.47-7.51 (dd. 1H, *J* =15.0 Hz, J=2.6 Hz, ArH), 7.17-7.19 (*dd*. 1H, *J*=8.8 Hz, J=2.3 Hz, ArH), 7.04- 7.09 (*t*, 1H, *J*=9.5 Hz, NH), 4.69-4.72 (*m*, 1H, OCH), 4.06-4.10 (*t*, 1H. *J* = 9.0 Hz, $ArNCH_2$), 3.70-3.73 (*t*, 4H, *J*=4.5 Hz, OCH_2), 3.68 (*dd*, 1H, *J* = 10.6 Hz, 6.4 Hz, $ArNCH_2$), 3.44 (*t*, 1H, *J* = 5.5 Hz, $NHCH_2$),

2.96 (*t*, 4H, *J* = 4.6 Hz, NCH_2), 1.83 (*s*.3H, $N(O)CH_3$), 5.36 (*s* 3H, Cp), 5.01 (*s*, 2H, Cp)}; ^{13}C NMR (126 MHz, DMSO-d_6): δ = 214.49, 170.89, 156.21 (*d*, *J* =246.7 Hz), 153.59-154.52, 136.1 (d, *J* = 8.8 Hz), 133.77 (*d*, *J* = 10.4 Hz), 119.74 (*d*, *J* = 4.2 Hz), 114.32 (*d*, *J* = 3.4 Hz), 107.22, 89.08, 85.73(*d*, *J* = 26.4 Hz), 71.72, 66.61, 50.93 (*d*, *J* = 3.2 Hz), 47.55, 41.40, 22.62 ppm.

3.3.5 Synthesis of $[(\eta^5\text{-}C_5H_5)Fe(CO)_2$(4-aminosalicylic acid)$]BF_4$

A mixture of the iodo complex $[\eta^5\text{-}C_5H_5)Fe(CO)_2I]$ (1.00g, 3.290 mmol) and $AgBF_4$ (0. 7g, 3.630 mmol) was stirred in DCM (15 ml) for 45 minutes at 40°C. The mixture was t hen filtered using filter aid. A 20 ml THF solution of 4-ASA (0.5054 g, 3.300 mmol) wa s added to the filtrate and the mixture stirred for 18 hours, with the progress of the reacti on was monitored periodically using FTIR spectroscopy. A deep red solution was forme d. The solvent was removed at reduced pressure to leave a deep red solid. Yield 0.8987 g, 67% FTIR (KBr): υ(C≡O) 2036, 1978, υ(C=O) 1632, δ(NH_2) 1602, υ(B-F) 1044 cm^{-1} .

3.3.6 Synthesis of $[(\eta^5\text{-}C_5H_5)Fe(CO)_2$(3-Aminosalicylic acid)$]BF_4$

A mixture of the iodo complex $[\eta^5\text{-}C_5H_5)Fe(CO)_2I]$ (1.00g, 3.290 mmol) and $AgBF_4$ (0.7g, 3.630 mmol) was stirred in DCM (15 ml) for 45 minutes at 40°C. The mixture was then filtered using filtering aid. The 3-aminosalicylic acid (3-ASA) ligand (0.5054 g, 3.300 mmol) was added to the filtrate and the solution was stirred for 16 hours. A maroon sold precipitated out of solution. The mother liquor was removed and solid

dried under vacuum. Yield 1.2619 g, 94%, FTIR (KBr): υ(C≡O) 2036,1977 cm^{-1}, υ(B-F) 1082-1039 cm^{-1}.

3.3.7 Synthesis of $[(\eta^5\text{-}C_5H_5)Fe(CO)_2(5\text{-aminosalicylic acid})]BF_4$

A mixture of the iodo complex $[\eta^5\text{-}C_5H_5)Fe(CO)_2I]$ (1.00g, 3.290 mmol) and $AgBF_4$ (0.7g, 3.630 mmol) was stirred in DCM (15 ml) for 45 minutes at 40°C. The mixture was then filtered using filter aid. The ligand (0.5054 g, 3.300 mmol) was added to the filtrate and the solution was stirred for 16 hours. A maroon sold precipitated out of solution. The mother liquor was removed and solid dried under vacuum. Yield 1.240 g, 92%, FTIR (KBr): υ(C≡O) 2037, 1976 cm^{-1}, υ(B-F) 1083-1036 cm^{-1}.

3.3.8 Synthesis of $[(\eta^5\text{-}C_5H_5)Fe(CO)_2(\text{ethionamide})]BF_4$

A mixture of the iodo complex $[\eta^5\text{-}C_5H_5)Fe(CO)_2I]$ (1.00g, 3.290 mmol) and $AgBF_4$ (0.7 g, 3.630 mmol) was stirred in DCM (15 ml) for 45 minutes at 40°C. The resultant mixture was then filtered using a filter aid. The ethionamide ligand (0.5486 g, 3.300 mmol) in 20 ml of freshly distilled THF was added to the filtrate and the solution was stirred for 21 hours. The progress of the reaction was monitored periodically by FTIR spectroscopy. A yellow solution was formed which gave a yellow precipitate on addition of diethyl ether. The solvent was removed under vacuum and the yellow solid was then vacuum dried. Yield 1.1492 g, 83% FTIR (KBr): υ(NH_2) 3468 cm^{-1}, υ(C≡O) 2035, 1979 cm^{-1}, υ(B-F) 1050 cm^{-1}.

3.3.9 Synthesis of $[(\eta^5\text{-}C_5H_5)Fe(CO)_2(\text{prothionamide})]BF_4$

A mixture of the iodo complex $[\eta^5\text{-}C_5H_5)Fe(CO)_2I]$ (1.00 g, 3.290 mmol) and $AgBF_4$ (0.7 g, 3.630 mmol) was stirred in DCM (15 ml) for 45 minutes at 40° C. The mixture was then filtered using a filter aid. The prothionamide ligand (0.5949 g, 3.300 mmol) solution in 20 ml THF of was added to the filtrate and the mixture was stirred for 21 hours. The progress of the reaction was monitored periodically by FTIR spectroscopy. A yellow solution was formed which gave a yellow precipitate on addition of diethyl ether. The yellow solid was then isolated by filtration using filter and dried under vacuum. Yield 1.1589 g, 81%. FTIR (DCM): υ(C≡O) 2031, 1982, υ(C=C) 1626, δ(NH_2) 1599, υ(B-F) 1056 cm^{-1}; FTIR (KBr): υ(C≡O) 2034, 1988, υ(C=C) 1687, 1632, δ(NH_2) 1549, υ(B-F) 1040 cm^{-1}

3.4 Evaluation of Antibacterial Activity (Zones of Inhibition)

The antibacterial activity of the synthesized complexes was tested *in vitro* by agar disc diffusion method against gram negative bacteria (*Staphylococcus aureus*, *Bacillus subtilis* and *Enterococcus faecalis* and the gram positive strains (*Escherichia coli, Salmonella typhi* and *Pseudomonas aeruginosa*. Mueller Hinton agar was prepared according to the manufacturer's instructions. A 0.5 McFarland standard was prepared by diluting a 24-hour bacterial culture using a normal saline salt solution (Wilkins and Thiel, 1973). The microbial suspension (0.1 ml) was inoculated into the Petri dishes. Filter paper discs (6 mm) were soaked into the test compound solution (made by dissolving 5.0 µg of the compound in 1 ml of 0.1% DMSO) and placed on the inoculated Petri dishes at reasonable distances. The plates were then incubated at 37 ºC

for 24 hours. This was replicated three times for each test bacteria. Zones of inhibition were measured using a ruler (Dickert *et al.*, 1981). Discs soaked in 0.1% DMSO were used as a negative control whereas the pure APA, terizidone, ethionamide, prothionamide, 3-aminosalicylic acid, 4-aminosalicylic acid, 5-aminosalicylic acid and linezolid were used as positive controls for the respective complexes. The synthesized organometallic compounds were screened for bioactivity against three strains of gram negative bacteria namely, *Escherichia coli, Salmonella typhi, Pseudomonas aeruginosa*, and three gram positive bacteria *Staphylococcus aureus, Bacillus subtilis and Enterococcus faecalis*. The bacterial responses to the synthesized compounds were evaluated as follows: diameter of inhibition, 10 mm and below-resistant, 11-15 mm - intermediate and 16 mm or more - susceptible (Johnson and Case, 1995)

3.5 Computational Methods

The calculations were performed in a CHPC cluster in South Africa using Gaussian 16, version B.01 and Hp workstations at Kenyatta University using the Gaussian 09 version E01 (Frisch *et al*., 2009; Frisch *et al*., 2016). All properties of interest were calculated in ground state using DFT functionals CAM-B3LYP, B3LYP, and PBEPBE (Lee *et al*., 1988; Becke, 1988; Becke, 1993; Perdew *et al*., 1996; Perdew *et al*., 1998a and b; Adamo and Barone, 1999; Yanai *et al*., 2004). The basis sets used were 6-311G(d,p), 6-311G(2d,p) and LANL2DZ for C, H, N, F ,Cl, S and O for neutral molecules, 6-311++G(d,p), 6-311++G(2d,p) for ionic species and LANL2DZ for Fe. The parameters calculated included $E_{HOMO,}$ E_{LUMO}, ΔE- Energy gap, ionization potential (IP), electron affinity (EA), electronegativity (χ), global hardness (η), global softness (S), chemical

potential (μ), dipole moment, Fukui indices, bond parameter (lengths and angles) spectroscopic properties such as IR, Raman, and NMR. Global minima searches were performed and different possible spin states calculated were investigated. Calculations were performed in different phases including gas or and in different solvent systems (THF, DCM, DMSO, Et_2O) using the CPCM model.

The optimized geometries or structures were then checked to be real global minima by vibrational frequencies analysis at the same level of theory and basis set. For the ligands the vertical ionization potential and electron affinity (IP_v/EA_v) values were computed in single-point calculations from the energies of systems with N and N±1 electrons, using geometries of the N-electron systems. The adiabatic IPs and EAs (IP_{ad}/EA_{ad}) were also obtained from the energies of the systems with N and N±1 electrons, calculated using optimized geometries of the N±1 electron species. For a system of N electrons, independent calculations were carried out using the Mulliken, NBO and Hirshfeld charge partitioning schemes on N–1, N and N+1 –electronic systems with the same molecular geometry to get the charges $q_k(N–1)$, $q_k(N)$ and $q_k(N+1)$ for all atoms k and these values were substituted in equations 27a-c and the corresponding condensed to atom Fukui indices for nucleophilic (f_k^+), electrophilic (f_k^-) and radical attack (f_k^0) were then obtained. All calculations were implemented in the Gaussian 09 and Gaussian 16 while the molecular orbitals and structures were visualized using GaussView 5.0.9, Mercury 3.10.1 and Avogadro visualization software.

3.6 Validation of Computational Results

In general, the theoretical results obtained were compared with experimental and computational results of compounds similar in structure to the systems of interest. Furthermore, three different functionals were used (B3LYP, CAM-B3LYP and PBEPBE) together with a diverse range of basis sets (6-31G(d,p), 6-311++G(d,p), 6-311G(2d,p), 6-311++G(2d p) and LANL2DZ.

CHAPTER FOUR

RESULTS AND DISCUSSION

The goal of this study was to modify the molecular structures of selected active pharmaceutical agents with the cationic iron half sandwich organometallic fragment, $[\eta^5\text{-}C_5H_5Fe(CO)_2]^+$, (also referred to as Fp), and assess the bioactivities of the resultant organometallic complex salts in comparison to the free ligands (in this case the active pharmaceutical agents). A two pronged approach involving theoretical or computational studies based on Density Functional Theory (DFT) and actual synthesis, characterization and bioassay studies of the synthesized compounds was employed. The computational studies were important for two major reasons; first, to determine the ligation behaviour of the ligands towards the Fp organometallic fragment based on global and regional reactivity descriptors and second, to predict the molecular and spectroscopic properties of the new organometallic complex salts. Global reactivity indices were computed so as to characterize the Fp-APA interaction while regional reactivity indices were determined so as to identify the most nucleophilic coordination sites in the ligand molecules given that the active pharmaceutical agents (APAs) studied were mixed donor ligands with multiple potential coordination sites. The results from the two approaches are presented and discussed separately or jointly where appropriate.

4.1 Ligation Properties of the APAs Based on the Global Reactivity Descriptors

Density Functional Theory (DFT) studies were conducted on the selected active pharmaceutical agents namely 3-aminosalicylic acid (3-ASA), 4-aminosalicylic acid (4-ASA), 5-aminosalicylic acid (5-ASA), terizidone (TZD), ethionamide (ETH),

prothionamide (PTH) and linezolid (LZD) and the Fp organometallic fragment Figure 4.1. First, the molecular structures of the APAs and the Fp organometallic fragment were optimized and the lowest energy conformers in the neutral, cationic and anionic states obtained.

The starting geometry of linezolid was the crystal structure of the linezolid polymorph II (Maccaroni *et al*., 2008) while for the other ligands the starting geometries were the most stable conformers. The optimized structures were checked for imaginary frequencies and when it was established that there were no imaginary frequencies, the molecules were then subjected to further studies to determine the global and regional reactivities, bond parameters and spectroscopic properties. The calculated global reactivity parameters included electronegativity (χ), hardness (η), softness (S), electrophilicity (ω), nucleophilicity (N), ionisation potential (IP), electron affinity (EA), the energy gap between the HOMO and LUMO (ΔE) and the electronic chemical potential (μ). The results are presented in Table 4.1 based on the validity of the Koopmans' theorem. To check on the validity of Koopmans' approximation on the calculated parameters, the values of the adiabatic electron affinity (EA) and adiabatic ionisation potential (IP) were calculated using equations 6b and 7b. Results of this approach are summarised in Table 4.2.

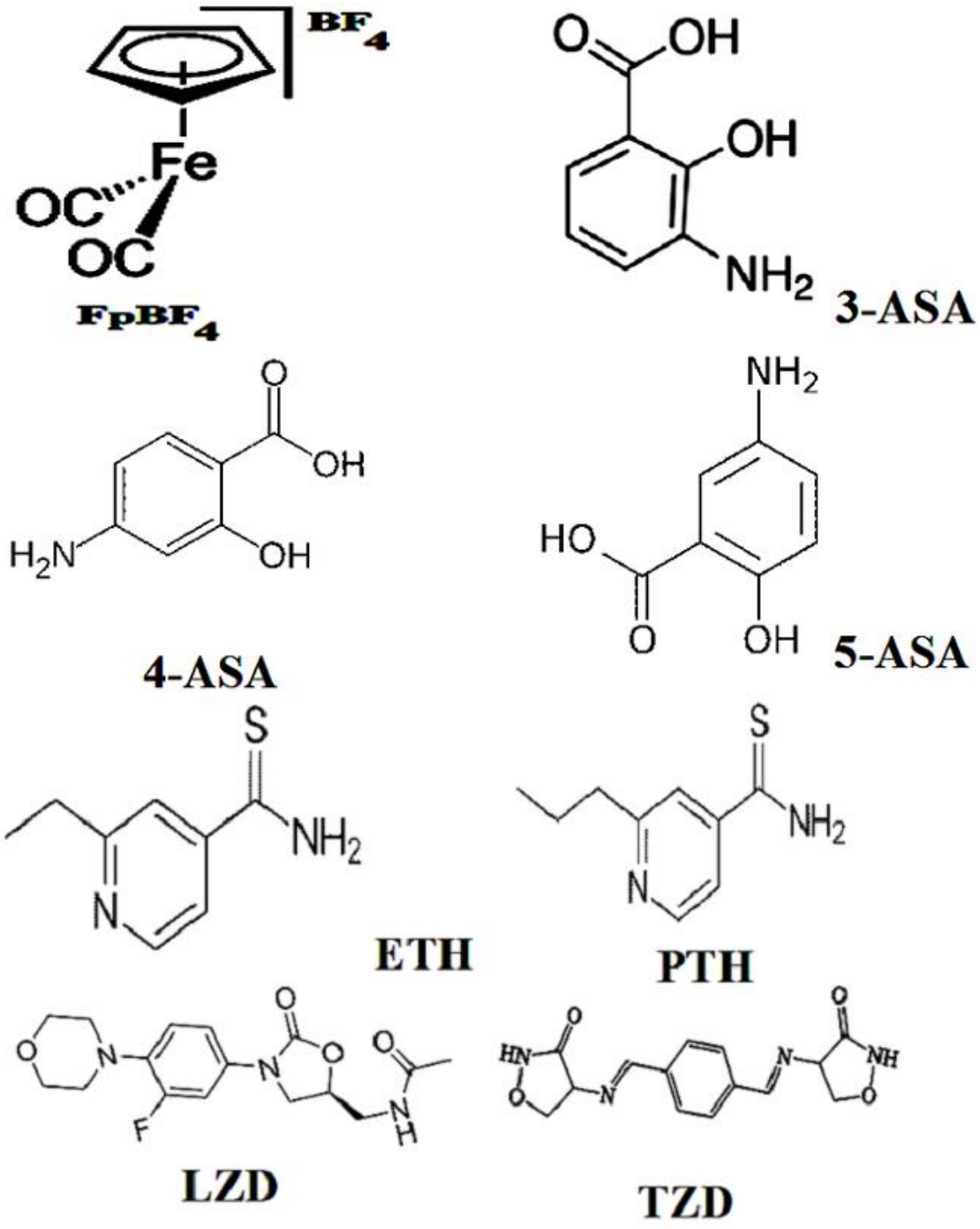

Figure 4.1: Structures of the $[\eta^5\text{-}C_5H_5)Fe(CO)_2]BF_4$ fragment and the selected APAs used in this study

Table 4.1: Global Molecular Reactivity Properties Calculated at CAM-B3LYP (eV)

Species	**Phase**	**E_{HOMO}**	**E_{LUMO}**	**ΔE**	**IP**	**EA**	**χ**	**μ**	**H**	**S**	**ω**	**N'**	**N'''**
3-ASA	Vacuo	-5.610	-1.374	4.235	5.610	1.374	3.492	-3.492	2.118	0.472	2.879	3.473	2.045
	THF	-5.698	-1.466	4.232	5.698	1.466	3.582	-3.582	2.116	0.473	3.033	3.298	1.965
4-ASA	Vacuo	-6.013	-1.139	4.875	6.013	1.139	3.576	-3.576	2.437	0.410	2.623	3.812	2.121
	THF	-6.037	-1.239	4.797	6.037	1.239	3.638	-3.638	2.399	0.417	2.759	3.624	2.050
5-ASA	Vacuo	-5.487	-1.540	3.946	5.487	1.540	3.514	-3.514	1.973	0.507	3.128	3.197	1.949
	THF	-5.554	-1.625	3.929	5.554	1.625	3.590	-3.590	1.964	0.509	3.280	3.049	1.880
ETH	Vacuo	-7.608	-0.873	6.735	7.608	0.873	4.240	-4.240	3.367	0.297	2.670	3.746	1.919
	THF	-7.837	-0.882	6.956	7.837	0.882	4.360	-4.360	3.478	0.288	2.733	3.659	1.870
PTH	Vacuo	-7.604	-0.871	6.733	7.604	0.871	4.237	-4.237	3.366	0.297	2.667	3.750	1.921
	THF	-7.836	-0.886	6.950	7.836	0.886	4.361	-4.361	3.475	0.288	2.736	3.654	1.869
LZD	Vacuo	-7.084	-0.096	6.988	7.084	0.096	3.590	-3.590	3.494	0.286	1.844	5.422	2.453
	THF	-7.177	-0.309	6.868	7.177	0.309	3.743	-3.743	3.434	0.291	2.040	4.902	2.304
TZD	Vacuo	-7.915	-1.050	6.865	7.915	1.050	4.482	-4.482	3.432	0.291	2.927	3.417	1.787
	THF	-7.976	-1.063	6.914	7.976	1.063	4.520	-4.520	3.457	0.289	2.954	3.385	1.771
Fp	Vacuo	-12.150	-8.415	3.735	12.150	8.415	10.283	-10.283	1.868	0.535	28.306	0.353	0.297
	THF	-8.431	-4.459	3.973	8.431	4.459	6.445	-6.445	1.986	0.503	10.456	0.956	0.718

Table 4.2: Global Reactivity Parameters Based on Adiabatic IP and EA Calculated at CAM-B3LYP *In Vacuo* (eV)

Species	**$E_{(N)}$**	**$E_{(N+1)}$**	**$E_{(N-1)}$**	**IP**	**EA**	**χ**	**μ**	**η**	**S**	**ω**	**N'**	**N'''**
3ASA	-15002.456	-15003.062	-14995.468	6.988	0.606	3.797	-3.797	3.191	0.313	2.259	4.427	2.195
4ASA	-15002.795	-15003.179	-14995.328	7.467	0.384	3.926	-3.926	3.542	0.282	2.176	4.596	2.183
5ASA	-15002.539	-15003.265	-14995.711	6.828	0.726	3.777	-3.777	3.051	0.328	2.338	4.277	2.170
ETH	-22272.094	-22273.365	-22264.114	7.980	1.271	4.626	-4.626	3.354	0.298	3.189	3.136	1.689
PTH	-23341.511	-23342.791	-23333.547	7.964	1.280	4.622	-4.622	3.342	0.299	3.196	3.129	1.688
LZD	-32288.824	-32288.453	-32281.884	6.941	-0.372	3.285	-3.285	3.656	0.274	1.475	6.778	2.797
TZD	-28885.293	-28886.143	-28876.746	8.547	0.850	4.699	-4.699	3.848	0.260	2.868	3.486	1.755
Fp	-14782.583	-14789.583	-14769.181	13.403	6.999	10.201	-10.201	3.202	0.312	16.250	0.615	0.460

4.1.1 Chemical Potential (μ)

From Tables 4.1 and 4.2 it can be seen that *in vacuo* as well as in the solvent systems all the studied seven ligands have higher chemical potential values than the Fp organometallic fragment, $[\eta^5\text{-}C_5H_5(CO)_2Fe]^+$ suggesting that the electronic flux will take place from the ligands to the organometallic fragment. Therefore, the results obtained signify that during the interaction, the APAs will act as nucleophiles while the Lewis acid the Fp will act as an electrophile.

4.1.2 Electronegativity (χ)

From the Table 4-1 and Table 4-2 the computed electronegativities of the ligands are lower than that of the Fp organometallic fragment in all the phases studied. For instance, in THF the values are 4–ASA (3.638 eV), TZD (4.520 eV), ETH (4.360 eV), PTH (4.361 eV), LZD (3.743 eV) and Fp (6.445 eV). Furthermore, the electronegativity of the organometallic fragment $[\eta^5\text{-}C_5H_5(CO)_2Fe]^+$ was almost double that of 4-ASA and LZD. This means that electrons will flow from the molecule with lower electronegativity (the APAs) towards that of the species with higher electronegativity, the Fp organometallic fragment until equilibrium in chemical potential is attained.

4.1.3 Electron Affinity (EA) and Ionization Potential (IP)

From Tables 4.1 and 4.2 it can be seen that both the vertical and adiabatic electron affinities (EA) of the electron deficient Fp organometallic moiety are significantly higher than those of each of the ligands studied. For example, the vertical electron affinity of the ligand LZD is 0.31 eV while that of the Fp organometallic fragment in the same solvent

system (THF) is 4.46 eV. Generally, the Fp-Ligand binding phenomena can be viewed as partial charge transfer resulting to the formation of a covalent bond or precisely a dative bond. The ability of a Lewis acid or the electrophile to receive precisely one electron from a ligand (Lewis base or electron rich species) is measured by its electron affinity (EA). Electrophilic species usually have higher values of EA than their nucleophilic counterparts. Thus the results obtained here demonstrate that the Fp organometallic fragment will act as an electrophile while the active pharmaceutical agents will act as nucleophiles.

An examination of the ionisation potential (IP) values reveals a similar trend of lower ionisation potentials in the ligands relative to the Fp organometallic fragment. In terms of the seven ligands studied 5-ASA has the lowest vertical and adiabatic ionisation potentials while TZD has the highest values. The structural analogues ETH and PTH have the same values of ionisation potential of 7.84 eV in THF. It should be noted that in checking for the inadequacy of the Koopmans' approximation the ionisation potential (IP) and electron affinity (EA) values were calculated at the same level of theory, method and basis set as it is the norm (Fuentealba *et al*., 2000b).

4.1.4 Chemical Hardness (η) and Chemical Softness (S)

From Table 4.1 and 4.2 the computed hardness of the Fp organometallic fragment is comparable to that of 5-ASA both *in vacuo* and in THF. These two species have the least hardness as compared to all the species studied. The results also show that the ASA series of ligands are the least hard of the studied ligands. The structural analogues ETH and

PTH have basically the same calculated hardness suggesting that the extra methyl group on PTH has no effect on the hardness of the resultant compound.

4.1.5 Global Electrophilicity Index (ω) and Global Nucleophilicity Index (N)

From Tables 4.1 and 4.2 the Fp organometallic fragment has the highest electrophilicity index in all phases as expected for such an electron deficient system. The global electrophilicity index (ω) represents the stabilization energy of a system in this case the Fp when it gets saturated by electrons coming from the surroundings (or in this case the ligands). The nucleophilicity of LZD is the highest of all seven ligands studied with values of N'=5.422 eV and N'''=2.453 eV in Table 4.1 and N'=6.778 eV and N'''=2.797 eV in Table 4.2, respectively. The results also show that the 16 electron organometallic fragment, $[\eta^5\text{-}C_5H_5(CO)_2Fe]^+$, has much lower nucleophilicity than the electron rich ligands as expected. In addition, a closer examination of the nucleophilicity values reveals that the ligands ethionamide and prothionamide have comparatively similar nucleophilicity values. Finally, it should be noted that the nucleophilicity values as denoted by N' give higher values than that of N''' but similar trends are observed in both the schemes.

4.2 3-Aminosalycylic acid (3-ASA) and its Complex salt $[\eta^5\text{-}C_5H_5(CO)_2Fe(3\text{-ASA})]BF_4$

In this section the results on the local reactivity, molecular and spectroscopic properties of the free 3-aminosalicylic acid (3-ASA), and its organometallic complex salt are presented and discussed in their respective subsections.

4.2.1 Regional Reactivity Indices/ Functions of 3-ASA

In 3-Aminosalicylic acid (3-ASA) and its structural analogues 4-aminosalicylic acid (4-ASA) and 5-aminosalicylic acid (5-ASA) (Figure 4.2), **t**he benzene π system, carboxyl group, hydroxyl group and amino groups are potential binding sites. Thus, the three ASA ligands have been shown to bind to metals by numerous coordination modes: monodentate/ unidentate via O or N donor atoms, bridging, or by two different chelation modes, either the O,O-chelate or the N,O-chelate resulting in the formation of six-membered and five membered chelate-rings **(**Quintal *et al*., 2006).

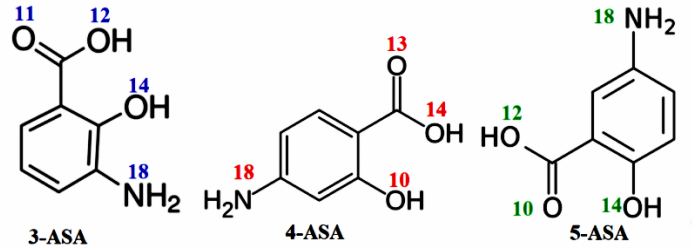

Figure 4.2: The three ASAS (Highlighting the O and N Donor Atoms)

Having satisfactorily answered theoretically the question as to whether 3-ASA can bind to the organometallic fragment through the global reactivity indices and knowing that 3-ASA is a mixed donor ligand, the next task was to determine most nucleophilic atom in 3-ASA is the most nucleophilic and hence will favour coordination to the electron deficient organometallic fragment. Computationally, two approaches were used, that is determination of the nucleophilicity of each atom in the ligand molecule using the so called regional/local/site reactivity indices as implemented in DFT and coordination of the Fp organometallic fragment to each potential donor atom in the ligand followed by

optimization of the resultant structures to find the structure with the lowest global energy. The results of these two approaches are presented and discussed in the same order.

In calculating the Fukui functions the interaction between the Fp organometallic fragment (Lewis acid) and the APA ligands (Lewis bases) was considered as an electrophile-nucleophile interaction. The calculations were carried out in order to predict the sites or atoms in the ligand molecules that would be most susceptible to electrophilic attack. The condensed-to-atoms Fukui functions of 3-ASA were computed in different phases namely *in vacuo* and in solvent systems (THF, diethyl ether and DCM) using the three DFT functionals and three charge partitioning schemes, namely, Mulliken, Hirshfeld and NBO as implemented in G09 and G16. The results of the condensed-to-atoms Fukui indices for 3-ASA in DCM (the solvent that was also used in the synthesis of the complex) are presented in Table 4.3. The results show that the condensed-to-atoms Fukui functions as obtained from the NBO and Hirshfeld charge partitioning schemes identify the N18 of the amino group (Fig 4.2) to be the most nucleophilic hence the site most likely to perform nucleophilic attack.

The nucleophilicity For the heteroatoms in the ASA ligand series was found to vary in the order N18 > O14 > O11 > O12. The results of the condensed-to-atoms Fukui indices obtained suggest that if coordination was to take place on one of the heteroatoms in the 3-ASA molecule in a unidentate fashion then the interaction will involve the iron metal centre and the amine nitrogen to form a Fe–N bond. This is in agreement with literature reports that in reactions of the Lewis acids, $[(\eta^5\text{-}C_5R_5)(CO)_2Fe]^+$ (R=H or CH_3) with

mixed donor ligands such as amino propanol and 4-methoxybenzalyamine, coordination only took place at the amino functionality (M'thiruaine *et al.*, 2012g).

Table 4.3: Condensed-to-atoms Fukui Function for 3-ASA in DCM based on NBO and Hirshfeld charges

	CAM-B3LYP/6-311(2D,P)						**B3LYP/6-311(2D,P)**					
	NBO			**HPA**			**NBO**			**HPA**		
	f_k^+	f_k^-	f_k^o	f_k^+	f_k^-	f_k^o	f_k^+	f_k^-	f_k^o	f_k^+	f_k^-	f_k^o
C1	0.09	0.08	0.08	0.06	0.07	0.06	0.07	0.07	0.07	0.05	0.07	0.06
C2	0.03	0.01	0.02	0.05	0.04	0.04	0.03	0.02	0.02	0.04	0.04	0.04
C3	0.09	0.16	0.12	0.10	0.15	0.12	0.07	0.15	0.11	0.08	0.15	0.12
C4	0.01	0.06	0.04	0.08	0.12	0.10	0.02	0.07	0.04	0.08	0.12	0.10
C5	0.16	0.05	0.10	0.15	0.10	0.12	0.12	0.05	0.08	0.15	0.10	0.12
C6	0.05	0.06	0.05	0.05	0.08	0.06	0.04	0.06	0.05	0.04	0.07	0.06
C10	0.16	-0.03	0.07	0.12	0.01	0.07	0.13	-0.03	0.05	0.09	0.02	0.05
O11	0.15	0.06	0.11	0.13	0.05	0.09	0.12	0.06	0.09	0.11	0.05	0.08
O12	0.05	0.01	0.03	0.10	0.04	0.07	0.03	0.01	0.02	0.08	0.04	0.06
O14	0.05	0.07	0.06	0.07	0.09	0.08	0.03	0.08	0.06	0.06	0.10	0.08
N18	0.04	0.20	0.12	0.10	0.25	0.17	0.05	0.20	0.12	0.22	0.25	0.23

4.2.2 Optimized Structures [Fp(3-ASA)]BF_4 With Fp Coordinated at the Various Donor Sites

In the 3-ASA ligand, the benzene π system, the carboxyl group, the hydroxyl and the amino group are potential binding sites allowing the molecule to exhibit numerous coordination modes (Quintal *et al*., 2006). The organometallic fragment, Fp, was coordinated to each of the donor sites and the resultant salts separately optimized and used for the calculation of the various parameters of interest. The results in Table 4.4 and Figure 4.3 show that the structure with the lowest global optimization energy is the one in which the central metal atom in the organometallic fragment is coordinated to the 3-ASA ligand via the amine nitrogen atom. This suggests that thermodynamics are likely to

favour the formation of Fp complexes in which the 3-ASA ligand is coordinated to the central iron atom in Fp in a unidentate fashion via the amino nitrogen in agreement with the results obtained from the condensed to atom Fukui indices. All the other calculations for all the desired properties of the Fp(3-ASA)BF_4 complex salt were carried out on this structure.

Table 4.4: Global Energies of [Fp(3-ASA)]BF_4 Structures at the Various Donor Sites

[(η^5-C_5H_5)Fe$(CO)_2$(3-ASA)]BF_4 structures	**Energy (kcal/mol)**	**Relative Energy**
Fp coordinated to L through amino N (atom 18)	-953431.7089	0.000
Fp coordinated to L through phenolic OH (O atom 14)	-953409.0055	22.703
Fp coordinated to L through carboxylic OH, O (atom 12)	-953423.4444	8.265
Fp coordinated to L through carbonyl O (atom 11)	-953408.5679	23.141

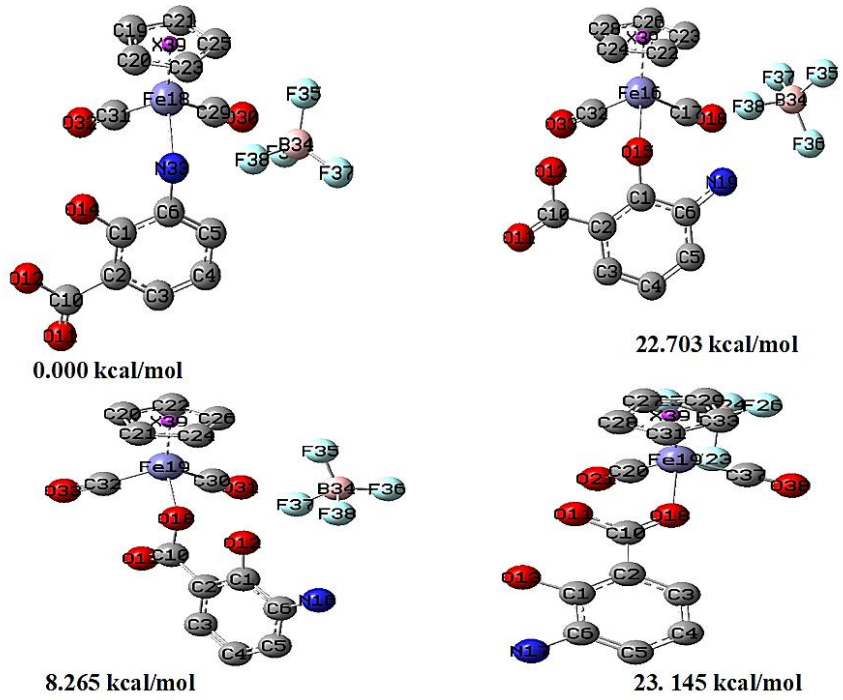

Figure 4.3: Optimized [Fp(3-ASA)]BF_4 at the Various Donor Sites (Hydrogen Atoms Omitted for Clarity)

4.2.3 Geometries of Free 3-ASA and [Fp(3-ASA)]BF_4 and Their Selected Bond Parameters

Three-dimensional rendering of the calculated equilibrium geometries of the most stable structures of 3-ASA and its complex are shown in Figure 4.4 while selected geometric parameters are presented in Table 4.5. The bond lengths of interest obtained in gas phase using the pure and hybrid DFT functionals, PBEPBE (CAM-B3LYP) are Fe-$C_{(CO)}${1.763(1.813)}, Fe-$C_{(Cp)}$ {2.0811 (2.091)}, C-O {1.155 (1.127)}, Fe-$Cp_{(centroid)}$ {1.728 (1.738)}, $(C\text{-}C)_{Cp}${1.430(1.415)}. These values are in close greement with the average literature values based on a large number of cyclopentadienyl carbonyl iron complexes are Fe-$C_{(CO)}$ = 1.78(3), C-O = 1.14(2), Fe-$C_{(Cp)}$ = 2.08(3), Fe-$Cp_{(centroid)}$ = 1.71(4), $(C\text{-}C)_{Cp}$ = 1.40(3) (Orpen *et al*., 1989; Mackie and Baird, 1992; Zeng and Li, 2011; M'thiruaine *et al*., 2012a, b, c, d, e, f).

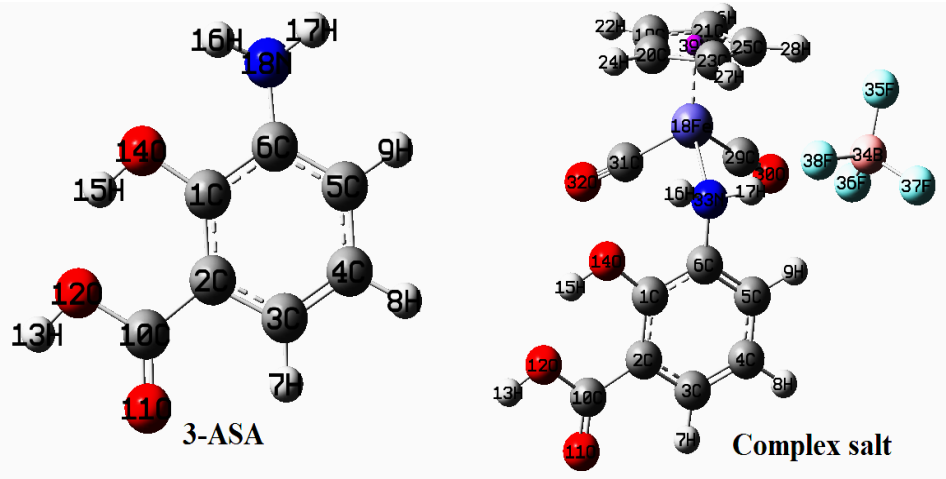

Figure 4.4: Geometries of 3-ASA and [Fp (3-ASA)]BF_4 Showing the Atom Numbering Scheme

Another characteristic bond in such complexes is the Fe-N bond. Here the calculated Fe-N bond length was found to be 2.037 and 2.052 Å for CAM-B3LYP and PBEPBE,

respectively. This is within the range of reported values for similar complexes (M'thiruaine *et al*., 2012a, b, c, d, e, and f). Around the coordinated 3-ASA fragment an elongation of the N-C bond of the amine nitrogen coordinated to the iron metal centre is observed. For example, N-C bond in coordinated 3-ASA was found to be 1.437 and 1.435 Å for CAM-B3LYP and PBEPBE, respectively. The corresponding values in the free optimized ligand using the two functionals are 1.390 and 1.394 Å, respectively.

Table 4.5: Selected Bond Lengths and Angles of the Optimized 3-ASA and its Complex Salt

3-ASA				$[Fp(3\text{-}ASA)]BF_4$			
Bond R(Å)	**CAM-B3LYP**	**B3LYP**	**PBEPBE**	**Bond R(Å)**	**CAM-B3LYP**	**B3LYP**	**PBEPBE**
R(C1,C2)	1.395	1.404	1.412	$(C\text{-}C)_{Cp}$	1.419	1.427	1.427
R(C1,C6)	1.406	1.413	1.421	$(C\text{-}C)_{Cp}$	1.419	1.423	1.420
R(C1,O14)	1.353	1.358	1.362	$(C\text{-}C)_{Cp}$	1.401	1.408	1.440
R(C2,C3)	1.400	1.407	1.413	$(C\text{-}C)_{Cp}$	1.430	1.434	1.425
R(C2,C10)	1.473	1.475	1.474	$(C\text{-}C)_{Cp}$	1.408	1.414	1.439
RC3,C4)	1.371	1.377	1.384	Cp-Fe	1.738	1.767	1.728
R(C4,C5)	1.391	1.396	1.402	$Fe\text{-}C_{C\equiv O}$	1.822	1.816	1.766
R(C5,C6)	1.382	1.389	1.398	$Fe\text{-}C_{C\equiv O}$	1.803	1.799	1.760
R(C6,N18)	1.390	1.394	1.394	C-O	1.125	1.132	1.156
R(C10,O11)	1.198	1.204	1.215	C-O	1.130	1.137	1.154
R(C10,O12)	1.368	1.379	1.393	Fe-N	2.037	2.061	2.052
Bond A (◦)				N-C	1.437	1.441	1.435
A(C2,C1,C6)	120.00	120.06	120.05	**Bond A (◦)**			
A(C2,C1,O14)	125.28	125.24	125.23	$(C\text{-}C\text{-}C)_{Cp}$	107.376	107.379	107.415
A(C6,C1,O14)	114.72	114.70	114.72	$(C\text{-}C\text{-}C)_{Cp}$	108.625	108.707	108.882
A(C1,C2,C3)	119.77	119.60	119.65	$(C\text{-}C\text{-}C)_{Cp}$	107.870	107.760	107.613
A(C1,C2,C10)	123.95	124.08	123.94	$(C\text{-}C\text{-}C)_{Cp}$	107.703	107.829	107.997
AC3,C2,C10)	116.28	116.32	116.42	$(C\text{-}C\text{-}C)_{Cp}$	108.370	108.277	108.076
A(C2,C3,C4)	120.18	120.24	120.19	$Cp\text{-}Fe\text{-}C_{CO}$	121.558	121.512	122.314
AC3,C4,C5)	119.96	120.05	120.13	$Cp\text{-}Fe\text{-}C_{CO}$	123.391	123.244	123.625
A(C4,C5,C6)	121.29	121.29	121.31	$Fe\text{-}C\text{-}O_{CO}$	175.163	175.016	176.264
A(C1,C6,C5)	118.80	118.75	118.67	$Fe\text{-}C\text{-}O_{CO}$	175.746	175.626	175.809
A(C1,C6,N18)	118.45	118.63	118.38	C-Fe-C	94.962	94.905	94.133
A(C5,C6,N18)	122.71	122.56	122.87	Cp-Fe-N	122.055	121.549	121.324
A(C2,C10,O11)	126.03	126.26	126.75	$N\text{-}Fe\text{-}C_{CO}$	93.156	93.647	92.500
A(C2,C10,O12)	114.03	113.88	113.45	$N\text{-}Fe\text{-}C_{CO}$	94.025	94.544	95.119
A(O11,C10,O12)	119.94	119.87	119.80	Fe-N-C	119.832	120.558	119.486

[a]Cp is centroid of cyclopentadienyl ring, CO is the carbonyl functionality

4.2.4 FTIR Spectra of 3-ASA and its Organometallic Complex Salt

The FTIR, spectra of the 3-ASA ligand and its complex salt were recorded and analysed. From the spectral data the most significant bands of the free ligand and its organometallic complex salt were selected. The bands include those associated with the ligand (such as NH_2, OH and the carboxyl group), those associated with the Fp organometallic fragment (the cyclopentadienyl ring, the carbonyl groups) and those associated with the BF_4^- counter ion. Figure 4.5 and Table 4.6 summarises the most important bands in the spectra. The assignment of the observed bands was aided by comparison with the theoretically determined frequencies as well as literature reports of FTIR spectra of salicylic acids (SAs), aminosalicylic acids (ASAs) and their derivatives (Khadikar *et al*., 1985; Borowski and Cole-Hamilton, 1993; Nogueira, 1998; Philip *et al*., 2001; Panicker *et al*., 2002; Akkaya and Akyuz, 2006; Quintal *et al*., 2006; Varghese *et al*., 2007; Soliman and Mohamed, 2013; Zheng and Ma, 2016).

Table 4.6: FTIR Data (cm^{-1}) for 3-Aminosalicylic and its Complex Salt

	Compound	
Mode	**3-ASA**	**[Fp(3-ASA)]BF_4**
υ(OH)	3483 mb	3480 mb
υ(NH_2)	3077 mb	3187 mb
υ(C=O)	1650 vs	1660 vs
$\upsilon(C{=}C)_{Benzene}$	1628 vs	1643 vs
δ(NH_2)	1568 vs	1591 vs
$\upsilon(C\text{-}O)_C$	1391 vs	1391 s
$\upsilon(C{\equiv}O)_{Asymmetric}$	-	2036 vs
$\upsilon(C{\equiv}O)_{Symmetric}$	-	1977 vs
υ(B-F)	-	1082-1017sb

vs= very strong; s=- strong; m= medium; b= broad

In the FTIR spectrum of the complex salt, two very strong bands characteristic of the Fp organometallic fragment were observed at 2035.61 cm^{-1} and 1976.90 cm^{-1}. These bands were assigned to the asymmetric and symmetric vibration modes of the carbonyl groups of the organometallic fragment, respectively. The presence of the BF_4^- counter ion in the complex salt was confirmed by the presence of the broad band in the region of 1081.65-1017.40 cm^{-1} assignable to υ(B-F) stretching vibration modes. It is important to note that the scissoring vibrational frequency of the NH_2 group, δ(NH_2), observed at 1568.00 cm^{-1} in the free 3-aminosalicylic acid (3-ASA) molecule was observed at 1590.92 cm^{-1} in the complex representing, a blue shift by ≈ 23 cm^{-1} upon coordination of the 3-ASA. This is an indication that the amino group may be involved in the coordination to the central metal atom in the organometallic fragment. The two strong bands observed at 1650.00 cm^{-1} and 1623.00 cm^{-1} assigned to the υ(C=O) and υ(C=C) of the carboxyl group and benzene ring, respectively in the free 3-Asa molecule are blue shifted to 1660.00 cm^{-1} and 1643.00 cm^{-1}, respectively in the spectrum of the complex.

The stretching C–O frequency of the phenolic group, $\upsilon(C–O)_{OH}$, was observed at 1319.00 cm^{-1} in the free 3-ASA molecule and undergoes a slight shift to 1319.7 cm^{-1} in the complex. The stretching C–O frequency of the carboxylic group $\upsilon(C–O)_C$ was observed at 1391.00 cm^{-1} in the free 3-ASA molecule and also undergoes a slight shift to 1391.7 cm^{-1} in the complex. The shift in wave numbers associated to the υ(OH) stretching modes is <1 cm^{-1} while that of the C=O stretching mode in the carboxyl group is ≈10 cm^{-1} slightly lower than half the shift in the δ(NH_2). This possibly shows that the oxygen atoms in 3ASA are not involved in the coordination process. The C–NH_2 stretch

frequency, $\upsilon(C–NH_2)$, shifts from 1262.00 cm^{-1} in the free ligand to 1265.00 cm^{-1} upon coordination. Thus, the results described suggest that although 3-ASA may assume several coordination modes, in this complex 3-ASA adopted unidentate coordination via the N atom of the amine group.

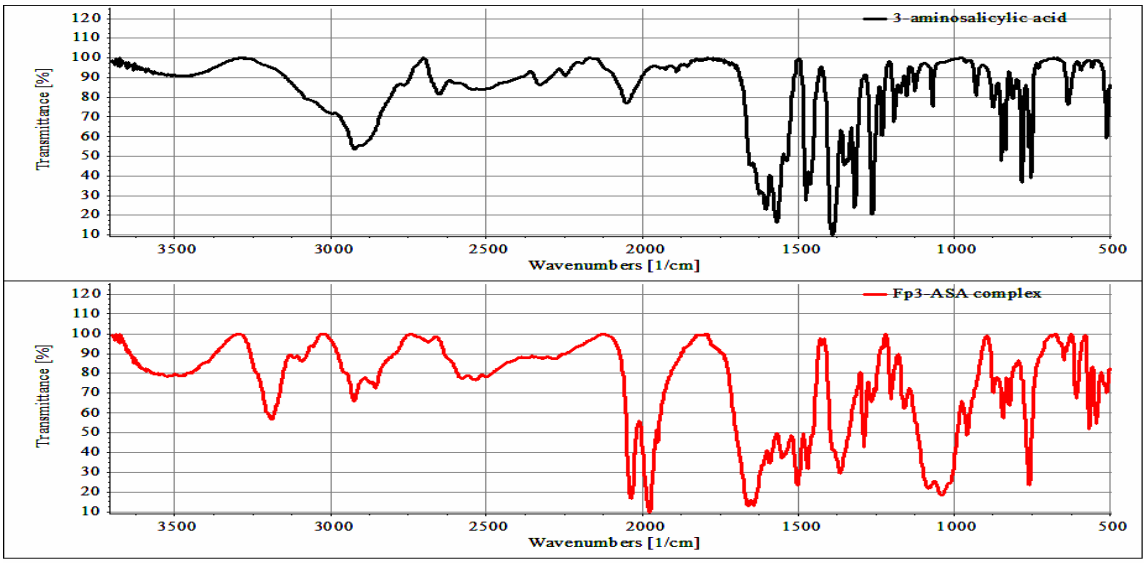

Figure 4.5: FTIR Spectra of 3-aminosalicylic its Organometallic Complex Salt

4.3 4-aminosalicylic Acid (4-ASA) and its Complex Salt [Fp (4-ASA)]BF_4

In this section the results on the local reactivity properties, the molecular and spectroscopic properties of the free 4-aminosalicylic acid (4-ASA) molecule (Fig 4.2) and the molecular and spectroscopic properties of its organometallic complex salt are presented and discussed.

4.3.1 Regional or Local Reactivity Indices/ Functions of 4-ASA

The results on the local reactivity of 4-ASA based on the condensed to atom Fukui indices/ functions are summarized in Table 4.7. The results show that N18 of the amino

group (Figure 4.2) is the most nucleophilic atom in the 4-ASA molecule hence the most susceptible to undergo electrophilic attack. Furthermore, optimization of the 4-ASA complexes with the Fp organometallic fragment coordinated to the ligand at various coordination sites also showed that the complex with the Fp coordinated at the N18 is the most energetically stable (Table 4.8).

Table 4.7: Condensed to atoms Fukui Indices of 4-ASA in THF Using Hirshfeld Charges

	CAM-B3LYP			B3LYP			PBEPBE		
Atom	f_k^+	f_k^-	f_k^o	f_k^+	f_k^-	f_k^o	f_k^+	f_k^-	f_k^o
C1	0.088	0.064	0.076	0.084	0.063	0.073	0.088	0.064	0.076
C2	0.051	0.122	0.087	0.046	0.117	0.081	0.051	0.122	0.087
C3	0.079	0.090	0.085	0.078	0.091	0.085	0.079	0.090	0.085
C4	0.075	0.158	0.116	0.075	0.157	0.116	0.075	0.158	0.116
C5	0.136	0.070	0.103	0.132	0.077	0.105	0.136	0.070	0.103
C6	0.052	0.040	0.046	0.050	0.042	0.046	0.052	0.040	0.046
O10	0.063	0.060	0.061	0.070	0.059	0.065	0.063	0.060	0.061
C12	0.126	0.037	0.082	0.125	0.039	0.082	0.126	0.037	0.082
O13	0.116	0.062	0.089	0.120	0.062	0.091	0.116	0.062	0.089
O14	0.098	0.050	0.074	0.100	0.053	0.077	0.098	0.050	0.074
N18	0.114	0.249	0.181	0.120	0.240	0.180	0.114	0.249	0.181

4.3.2 Optimized Structures [Fp(4-ASA)]BF_4 with Fp Coordinated at the Various Donor Sites

In this ligand the benzene π system, the carboxyl group, the hydroxyl and the amino group are potential binding sites. In all the ASAs studied in this work, coordination via the benzene π system was not contemplated and the ASAs were considered strictly as O, N donor ligands. The results of the optimization of the molecular structures of the 4-ASA Fp complex salts with Fp organometallic fragment coordinated at the various donor atoms in 4-ASA are summarised in Table 4.8 and Figure 4.6. The results presented in

Table 4.8 and Figure 4.6 show that a Fe-N coordinate bond is the most thermodynamically favoured bond in the contemplated complex. Hence, further analysis and computations were carried out on this structure.

Table 4.8: Energies of Optimized Structures [Fp(4-ASA)]BF_4 at the Various Donor Sites

[Fp(4-ASA)]BF_4 structures	**Energy (kcal/mol)**	**Relative Energy**
Fp coordinated to L through amino N atom 18	-953434.409	0.000
Fp coordinated to L through phenolic OH, O atom 10	-953406.362	28.047
Fp coordinated to L through carboxylic OH, O atom 14	-953394.757	39.652
Fp coordinated to L through carbonyl O atom 13	-953429.654	4.755

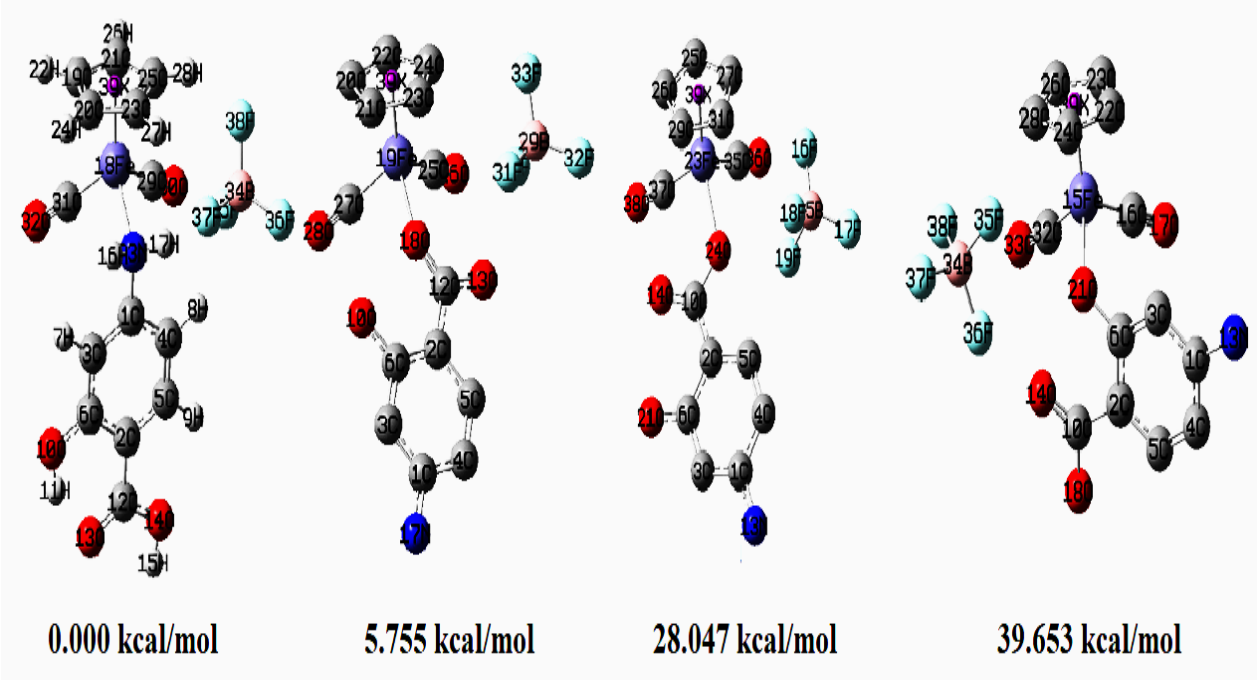

Figure 4.6: Optimized [Fp(4-ASA)]BF_4 at the Potential Donor Atoms (Hydrogen Atoms Omitted for Clarity)

4.3.3 Equilibrium Geometries of 4-ASA and [Fp(4-ASA)]BF_4 and Their Selected Bond Parameters

The 3-D rendering of the optimized geometries of the free 4-ASA and the most stable [Fp(PAS)]BF_4 structure are shown in Figure 4.7 and their geometric parameters are presented in Table 4.9.

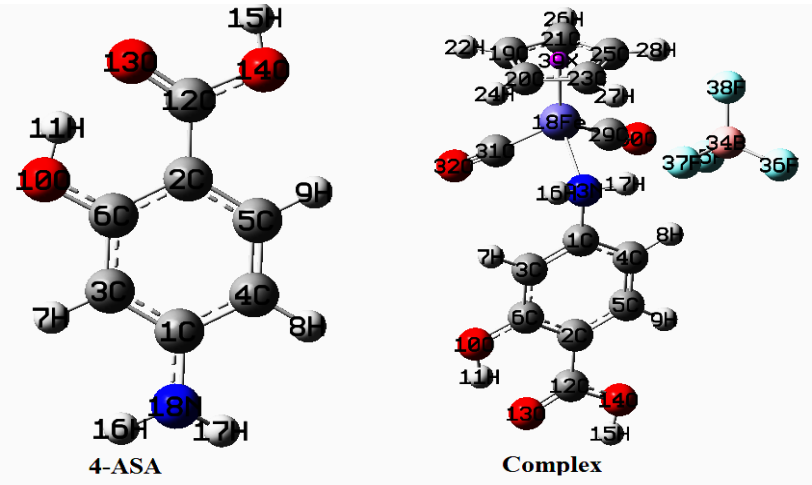

Figure 4.7: Geometries of 4-ASA and its complex showing atom numbering adopted

From Table 4.9, the calculated average C-C bond lengths in the Cyclopentadienyl ring were 1.415 Å and 1.430 Å for CAM-B3LYP and PBEPBE, respectively. The distance between the centroid of the Cp ring and the iron metal centre was 1.738 Å and 1.729 Å for CAM-B3LYP and PBEPBE, respectively. The average C-O bond length for the Fp carbonyl group was found to be 1.127 Å (CAM-B3LYP) and 1.154 Å for (PBEPBE), respectively. These results are within the range of experimentally observed values of cationic iron half sandwich organometallic compounds (Mackie and Baird, 1992; Zeng and Li, 2011; M'thiruaine *et al*., 2012a, b, c, d, e and f).

Table 4.9: Selected Bond Parameters of the Optimized 4-ASA and its Fp Complex

4-ASA				[Fp(4-ASA)]BF_4			
Bond{R(Å), A(◦)}	**CAM-B3LYP**	**B3LYP**	**PBEPBE**	**bond R(Å)**	**CAM-B3LYP**	**B3LYP**	**PBEPBE**
R(C1,C3)	1.388	1.394	1.401	$(C\text{-}C)_{Cp}$	1.420	1.427	1.437
R(C1,C4)	1.407	1.413	1.420	$(C\text{-}C)_{Cp}$	1.420	1.423	1.430
R(C1,N18)	1.376	1.381	1.384	$(C\text{-}C)_{Cp}$	1.401	1.407	1.418
R(C2,C5)	1.399	1.405	1.411	$(C\text{-}C)_{Cp}$	1.430	1.434	1.440
R(C2,C6)	1.410	1.419	1.429	$(C\text{-}C)_{Cp}$	1.408	1.413	1.426
R(C2,C12)	1.449	1.451	1.450	Cp-Fe	1.738	1.767	1.729
R(C3,C6)	1.386	1.391	1.398	$Fe\text{-}C_{C\equiv O}$	1.825	1.820	1.773
R(C4,C5)	1.367	1.373	1.380	$Fe\text{-}C_{C\equiv O}$	1.804	1.800	1.760
R(C6,O10)	1.334	1.340	1.343	C-O	1.125	1.132	1.151
R(C12,O13)	1.222	1.229	1.244	C-O	1.129	1.137	1.157
R(C12,O14)	1.342	1.351	1.360	Fe-N	2.044	2.067	2.055
Bond A(◦)				N-C	1.437	1.442	1.443
A(C3,C1,C4)	119.58	119.45	119.52	**Bond A(◦)**			
A(C3,C1,N18)	120.56	120.57	120.60	$(C\text{-}C\text{-}C)_{Cp}$	107.371	107.381	107.328
A(C4,C1,N18)	119.83	119.92	119.82	$(C\text{-}C\text{-}C)_{Cp}$	108.633	108.706	108.923
A(C5,C2,C6)	118.54	118.36	118.53	$(C\text{-}C\text{-}C)_{Cp}$	107.860	107.762	107.620
A(C5,C2,C12)	122.37	122.55	122.97	$(C\text{-}C\text{-}C)_{Cp}$	107.734	107.848	107.983
A(C6,C2,C12)	119.10	119.09	118.50	$(C\text{-}C\text{-}C)_{Cp}$	108.345	108.256	108.130
A(C1,C3,C6)	120.65	120.75	120.74	$Cp\text{-}Fe\text{-}C_{CO}$	121.227	121.219	121.600
A(C1,C4,C5)	119.74	119.84	119.88	$Cp\text{-}Fe\text{-}C_{CO}$	123.298	123.149	123.785
A(C2,C5,C4)	121.56	121.63	121.52	$Fe\text{-}C\text{-}O_{CO}$	174.767	174.703	174.832
A(C2,C6,C3)	119.94	119.97	119.81	$Fe\text{-}C\text{-}O_{CO}$	175.812	175.755	175.649
A(C2,C6,O10)	122.06	122.08	121.68	$C_{CO}\text{-}Fe\text{-}C_{CO}$	95.090	95.077	93.829
A(C3,C6,O10)	118.00	117.95	118.50	Cp-Fe-N	122.254	121.812	121.544
A(C2,C12,O13)	124.76	124.84	124.66	$N\text{-}Fe\text{-}C_{CO}$	93.225	93.660	93.882
A(C2,C12,O14)	115.17	115.12	115.43	$N\text{-}Fe\text{-}C_{CO}$	94.137	94.530	94.550
A(O13,C12,O14)	120.06	120.04	119.91	Fe-N-C	119.298	119.916	118.999

Cp is centroid of cyclopentadienyl ring, CO=carbonyl group

The calculated Fe-N bond length was found to be 2.044 Å (CAM-B3LYP) and 2.055 Å (PBEPBE), respectively. This is within the range of reported experimental values for

similar complexes (M'thiruaine *et al*., 2012a, b, c, d, e and f). Around the coordinated 4-ASA fragment we see an elongation of the N-C bond for the amine nitrogen coordinated to the iron metal centre. For example, N-C bond in coordinated 4-ASA was found to be 1.437 and 1.443 Å for CAM-B3LYP and PBEPBE, respectively. In the optimized free ligand this bond was found to be 1.376 and 1.384 Å in the corresponding methods. In the crystal structure of the free 4-ASA/PAS the N-C bond was reported to be 1.44 Å (Bertinotti *et al*., 1954). Generally, the overall agreement of the computed values with experimentally observed values was good.

4.3.4 FTIR Spectra of 4-aminosalicylic acid (4-ASA) and its complex salt

The FTIR spectra of 4-ASA and its complex salt are shown on Figure 4.8 while important selected bands are summarised in Table 4-10. The assignments of the observed bands was aided by using the theoretically determined frequencies and their intensities as well as data from published reports on, salicylic acids (SAs), aminosalicylic acids (ASAs) and their derivatives (Khadikar *et al*., 1985; Borowski and Cole-Hamilton, 1993; Nogueira , 1998; Philip *et al*., 2001; Panicker *et al*., 2002; Akkaya and Akyuz, 2006; Quintal *et al*., 2006; Varghese *et al*., 2007; Soliman and Mohamed, 2013; Zheng and Ma, 2016).

Table 4.10: Selected FTIR Bands of 4-ASA and its Organometallic Complex salt (cm^{-1})

	Compound	
Mode	**4-ASA**	**$[Fp(4\text{-}ASA)]BF_4$**
$\upsilon(OH)$	3496 vs	3496 mb
$\upsilon(NH_2)$	3219 mb	3226 mb
$\upsilon(C=O)$	1631vs	1632 vs
$\delta(NH_2)$	1600 vs	1606 s
$\upsilon(C\text{-}O)_C$	1384 m	1383 vs
$\upsilon(C\equiv O)_{Asymmetric}$	-	2036 vs
$\upsilon(C\equiv O)_{Symmetric}$	-	1978 vs
$\upsilon(B\text{-}F)$	-	1102-1034sb

vs. very strong; s. strong; m. medium; b. broad

The broad IR bands observed in the region of 3219.61-3496.17 cm^{-1} in the free ligand and 3226.08 -3495.83 cm^{-1} in the complex salt are assigned to the stretching modes of OH and NH_2 groups. These bands were observed at 3200–3500 cm^{-1} in 4-aminosalicylic acid sodium salt dehydrate (Panicker *et al*., 2002). The strong FTIR band observed at 1631.24 cm^{-1} and 1631.87 cm^{-1} in the free ligand and complex salt respectively are assigned to the $\upsilon(C=O)$ of the carboxyl group. The scissoring mode of vibration of the NH_2 group was observed at 1599.90 cm^{-1} in the free ligand and 1605.98 cm^{-1} in the complex salt. The strong bands observed at 2036.00 cm^{-1} and 1978.00 cm^{-1} are assigned to the asymmetric and symmetric modes of vibration of the carbonyl group. These are in the region of typical bands of the terminal -C≡O. The broad weak bands observed at 2871.45, 2927.02 and 2968.60 cm^{-1} are absent in the FTIR spectrum of the free ligand (Fig. 4.8) and are assigned to the $\upsilon(CH)$ vibration mode of the cyclopentadienyl ring. The bands observed at 608.59 cm^{-1}, 566.03 cm^{-1} and 545.59 cm^{-1} observed in the FTIR spectrum of the complex salt are associated to the deformation of the cyclopentadienyl (Cp) ring and the

Fe -C≡O bonds. These bands are conspicuously absent in the spectrum of the ligand. Another indicator of the complex salt formation is the appearance of a broad band in the region of 1102.02-1035.81 cm^{-1} assigned to the υ(B-F) stretching mode of the BF_4^- counter ion.

The υ(OH) stretching modes are observed at 3388.60 cm^{-1} and 3496.19 cm^{-1} in the free ligand and 3387.72 cm^{-1} and 3495.83 cm^{-1} in the complex salt while the υ(NH_2) stretching mode is observed at 3219.61 cm^{-1} and 3226.08 cm^{-1} in the free ligand and in the complex salt, respectively. From these results it can be seen that moving from the free ligand to the coordinated ligand the shift in stretching frequency of the OH and C=O groups is marginal (<1 cm^{-1}) while the shift in δ(NH_2) and υ(NH_2) is >6 cm^{-1}. This therefore points to a unidentate coordination of the 4-ASA molecule to the central iron atom via the N atom of the amino functionality.

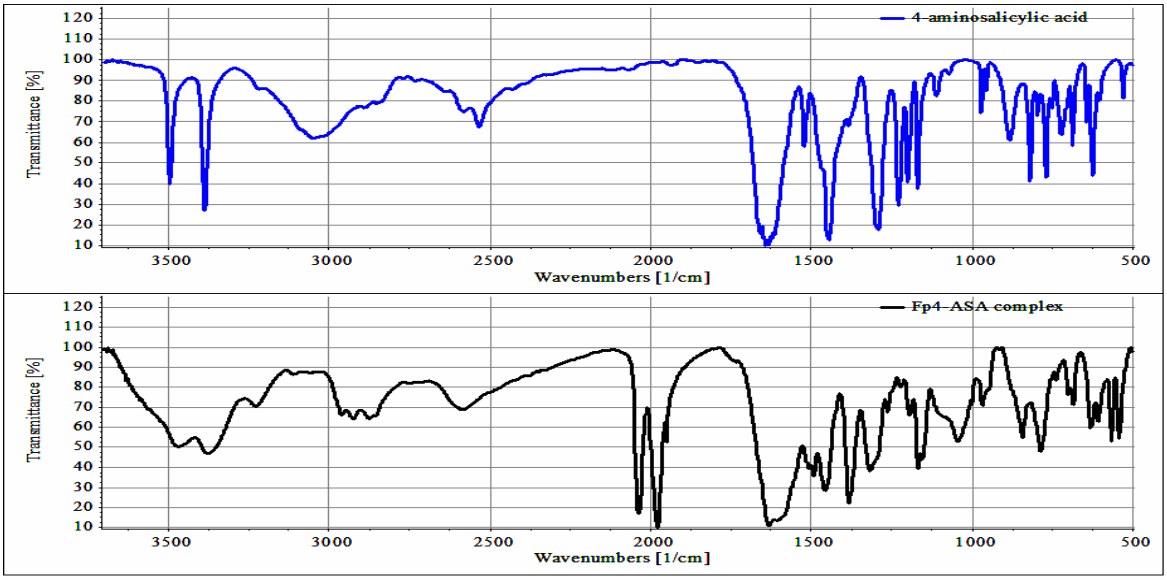

Figure 4.8: FTIR Spectra of 4-ASA and its Organometallic Complex Salt

4.4 5-aminosalycylic acid (5-ASA) and its Complex Salt [Fp(5-ASA)]BF_4

In this section the results on the local reactivity properties of the free 5-aminosalicylic acid (5-ASA) molecule, the molecular and spectroscopic properties of the of 5-ASA and its organometallic complex salt are presented and discussed in their respective subsections sections

4.4.1 Regional or Local Reactivity Indices/ Functions of 5-ASA

The calculated local reactivity indices for the free ligand 5-ASA are summarised in Table 4.11. It can be seen from the f_k^- values that like its structural analogues 3-ASA and 4-ASA the most nucleophilic atom in 5-ASA is the nitrogen atom of the amino group (N18) (Figure 4.2) and hence the preferred site for coordination with the electron deficient organometallic fragment $[Cp(CO)_2Fe]^+$.

Table 4.11: 5-ASA Condensed to Atom Fukui Indices in DCM Using Hirshfeld Charges

	CAM-B3LYP			**B3LYP**			**PBEPBE**		
	f_k^+	f_k^-	f_k^o	f_k^+	f_k^-	f_k^o	f_k^+	f_k^-	f_k^o
C1	0.04	0.09	0.06	0.04	0.08	0.06	0.05	0.08	0.06
C2	0.05	0.08	0.07	0.05	0.08	0.07	0.05	0.08	0.06
C3	0.12	0.13	0.12	0.12	0.13	0.12	0.12	0.12	0.12
C4	0.15	0.09	0.12	0.15	0.10	0.12	0.14	0.10	0.12
C5	0.10	0.10	0.10	0.10	0.10	0.10	0.10	0.10	0.10
C6	0.06	0.05	0.05	0.06	0.05	0.06	0.06	0.06	0.06
C10	0.12	0.02	0.07	0.12	0.02	0.07	0.11	0.03	0.07
O11	0.12	0.03	0.08	0.12	0.03	0.08	0.11	0.04	0.08
O12	0.10	0.03	0.07	0.10	0.03	0.07	0.10	0.04	0.07
O14	0.07	0.11	0.09	0.07	0.11	0.09	0.08	0.12	0.10
N18	0.06	0.25	0.16	0.07	0.25	0.16	0.07	0.24	0.16

4.4.2 Optimized Structures [Fp(5-ASA)]BF_4 with Fp Coordinated at the Various Donor Sites

The results presented in Table 4.12 and Figure 4.9 show that a Fe-N coordinate bond is the most thermodynamically favoured bond in the contemplated complex. Hence further analysis and computations were carried out on this structure.

Table 4.12: Energies of Optimized Structures [Fp(5-ASA)]BF_4 at the Various Donor Sites

[Fp(5-ASA)]BF_4 structures	Energy (kcal/mol)	Relative Energy
Fp coordinated at amino N atom 18	-953432.479	0.000
Fp coordinated at phenolic OH, O atom 14	-953411.053	21.427
Fp coordinated at carboxylic OH, O atom 12	-953415.698	16.781
Fp coordinated at carbonyl O atom 11	-953423.645	8.834

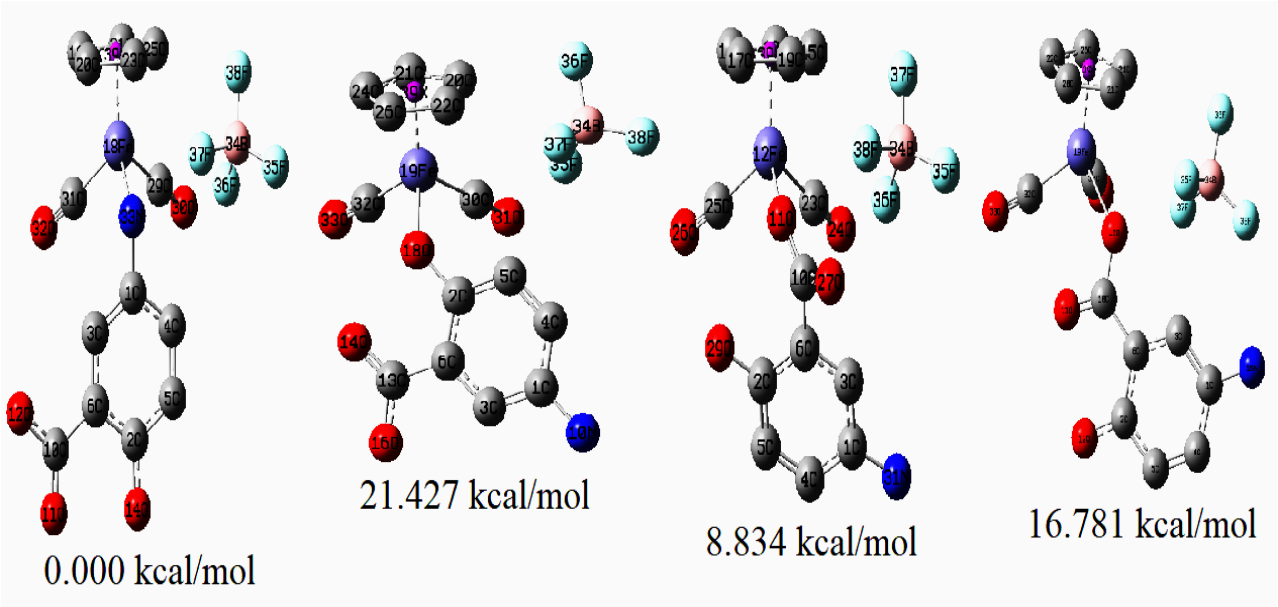

Figure 4.9: Optimized [Fp(5-ASA)]BF_4 at the Potential Donor Atoms (Hydrogen Atoms Omitted for Clarity)

4.4.3 Equilibrium Geometries of 5-ASA and [Fp(5-ASA)]BF_4 and their Selected Bond Parameters

The three-dimensional rendering of the equilibrium geometries of the most stable structures 5-ASA and its complex are shown in Figure 4.10 while the selected geometric parameters are presented in Table 4.13. The values of the most characteristic bonds for cationic iron half sandwich complexes have been isolated for the two DFT functionals PBEPBE and CAM-B3LYP functionals. Fe-$C_{(CO)}$ =1.762 and 1.812, Fe-$C_{(Cp)}$ = 2.0811 and 2.091, C-O =1.156 and 1.127, Fe-$Cp_{(centroid)}$ = 1.732 and 1.739 and $(C\text{-}C)_{Cp}$ = 1.430 and 1.415 for PBEPBE and CAM-B3LYP respectively. These values agree with literature values (Orpen *et al*., 1989; Mackie and Baird, 1992; Zeng and Li, 2011; M'thiruaine *et al*., 2012a, b, c, d, e, f). Another distinctive bond in such complexes is the Fe-N bond. Here the calculated Fe-N bond length was found to be 2.035 and 2.049 Å for CAM-B3LYP and PBEPBE respectively. This is within the range of reported values for similar complexes (M'thiruaine *et al*., 2012a, b, c, d, e and f).

Around the coordinated 5-ASA fragment we see an elongation of the N-C bond for the amine nitrogen coordinated to the iron metal centre. For example, the N-C bond in coordinated 5-ASA was found to be 1.446 and 1.442 Å for CAM-B3LYP and PBEPBE, respectively. The corresponding values in the free optimized ligand are 1.403 and 1.407 Å. Generally, the bond parameters of the free and coordinated 5-ASA ligand compare favourably with crystallographic data of 5-ASA derivatives (Dobson and Gerkin, 1998; Bourque *et al*., 2005). The overall agreement of the computed values with experimental values here is also good.

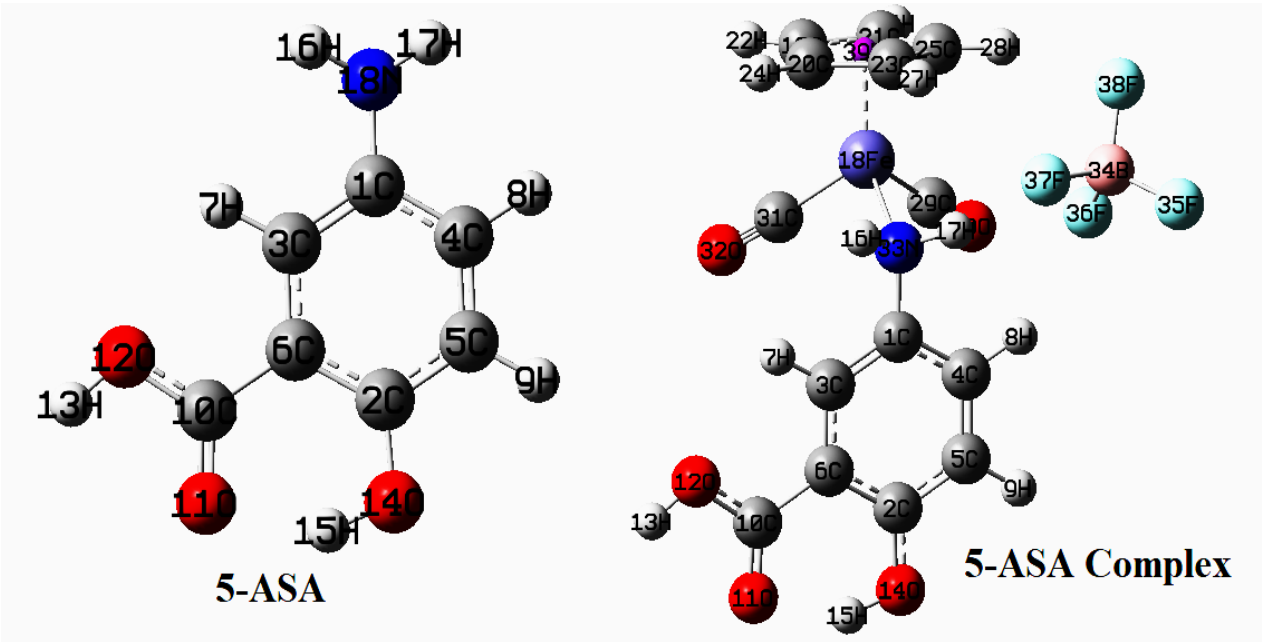

Figure 4.10: Optimized 5-ASA and its Complex Salt Showing the Atom Numbering

Table 4.13: Selected Bond Lengths and Angles of 5-ASA and its Complex

5-aminosalicylic acid (5-ASA)				[Fp(5-ASA)]BF_4			
Bond{R(Å), A(◦)}	**CAM-B3LYP**	**B3LYP**	**PBEPBE**	**Bond R(Å)**	**CAM-B3LYP**	**B3LYP**	**PBEPBE**
R(C1,C3)	1.378	1.385	1.394	$(C\text{-}C)_{Cp}$	1.421	1.428	1.442
R(C1,C4)	1.401	1.406	1.414	$(C\text{-}C)_{Cp}$	1.419	1.423	1.424
R(C1,N18)	1.403	1.406	1.407	$(C\text{-}C)_{Cp}$	1.401	1.408	1.423
R(C2,C5)	1.394	1.398	1.406	$(C\text{-}C)_{Cp}$	1.430	1.434	1.439
R(C2,C6)	1.400	1.410	1.421	$(C\text{-}C)_{Cp}$	1.407	1.413	1.424
R(C2,O14)	1.341	1.346	1.348	Cp-Fe	1.739	1.768	1.732
R(C3,C6)	1.400	1.405	1.411	$Fe\text{-}C_{C\equiv O}$	1.823	1.818	1.764
R(C4,C5)	1.373	1.379	1.386	$Fe\text{-}C_{C\equiv O}$	1.801	1.797	1.759
R(C6,C10)	1.461	1.463	1.461	C-O	1.125	1.132	1.155
R(C10,O11)	1.218	1.225	1.240	C-O	1.130	1.138	1.157
R(C10,O12)	1.339	1.349	1.358	Fe-N	2.035	2.058	2.049
Bond A(◦)				N-C	1.446	1.449	1.442
A(C3,C1,C4)	117.90	117.90	117.85	**Bond A(◦)**			
A(C3,C1,N18)	121.76	121.69	121.74	$(C\text{-}C\text{-}C)_{Cp}$	107.371	107.383	107.574
A(C4,C1,N18)	120.26	120.31	120.30	$(C\text{-}C\text{-}C)_{Cp}$	108.622	108.695	108.843
A(C5,C2,C6)	118.36	118.41	118.27	$(C\text{-}C\text{-}C)_{Cp}$	107.866	107.764	107.539
A(C5,C2,O14)	118.23	118.21	118.74	$(C\text{-}C\text{-}C)_{Cp}$	107.745	107.864	108.176
A(C6,C2,O14)	123.42	123.39	122.99	$(C\text{-}C\text{-}C)_{Cp}$	108.340	108.249	107.852
A(C1,C3,C6)	121.24	121.34	121.26	$Cp\text{-}Fe\text{-}C_{CO}$	121.364	121.346	122.615
A(C1,C4,C5)	121.63	121.60	121.75	$Cp\text{-}Fe\text{-}C_{CO}$	123.528	123.344	123.192
A(C2,C5,C4)	120.68	120.75	120.71	$Fe\text{-}C\text{-}O_{CO}$	175.266	175.131	176.340
A(C2,C6,C3)	120.19	120.00	120.16	$Fe\text{-}C\text{-}O_{CO}$	176.352	176.260	175.961
A(C2,C6,C10)	118.62	118.60	118.01	C-Fe-C	95.221	95.196	94.243
A(C3,C6,C10)	121.19	121.40	121.83	Cp-Fe-N	122.506	122.040	121.704
A(C6,C10,O11)	124.64	124.72	124.59	$N\text{-}Fe\text{-}C_{CO}$	92.821	93.304	92.427
A(C6,C10,O12)	114.94	114.91	115.17	$N\text{-}Fe\text{-}C_{CO}$	93.561	94.017	94.777
A(O11,C10,O12)	120.42	120.37	120.24	Fe-N-C	120.176	120.841	120.376

Cp is centroid of cyclopentadienyl ring, CO=carbonyl group

4.4.4 FTIR Spectra of 5-aminosalicylic acid (5-ASA) and its complex salt

The FTIR results of the distinctive bands and their assignments are presented in Table 4.14, while the spectra of the free ligand and its complex salt are shown in Figure 4.11. The complex salt spectrum shows the characteristic bands associated with the metal carbonyl υ(C≡O) stretching mode at 2036.86 cm^{-1} and 1976.35 cm^{-1} assignable to the asymmetric and symmetric stretching modes, respectively. The presence of the counter ion in the complex salt is shown by the υ(B-F) stretching mode observed as a strong broad band in the region of 1133.86- 1009.37 cm^{-1}.

The participation of the N atom of the amino group (-NH_2) in bond formation to the metal was confirmed from the larger shift in the position of the υ(N-H) stretching frequency by ≈ 8 cm^{-1} and by ≈ 50 cm^{-1} in the position of the δ(NH_2) scissoring vibrational mode. The shift in position of the υ(C=O) and υ(OH) stretching vibration modes was <5 cm^{-1} . Therefore, from the FTIR spectra it can be concluded that the 5-ASA molecule behaved as unidentate ligand to the organometallic fragment forming a complex having a Fe-N coordinate bond.

Table 4.14: Selected FTIR data (cm^{-1}) and 5-Aminosalicylic Acid and its Complex Salt

	Compound	
Mode	**5-ASA**	**$[Fp(5\text{-}ASA)]BF_4$**
υ(OH)	3475 sb	3480 mb
υ(C=O)	1649 vs	1649 vs
$\upsilon(C=C)_{Benzene}$	1621vs	1631 vs
$\delta(NH_2)$	1538 vs	1583 vs
$\upsilon(C\text{-}O)_C$	1381s	1384 s
$\upsilon(C\equiv O)_{Asymmetric}$	-	2037 vs
$\upsilon(C\equiv O)_{Symmetric}$	-	1976 vs
υ(B-F)	-	1134-1009 sb

Vs=very strong; s=. strong; m=. medium; b=. broad

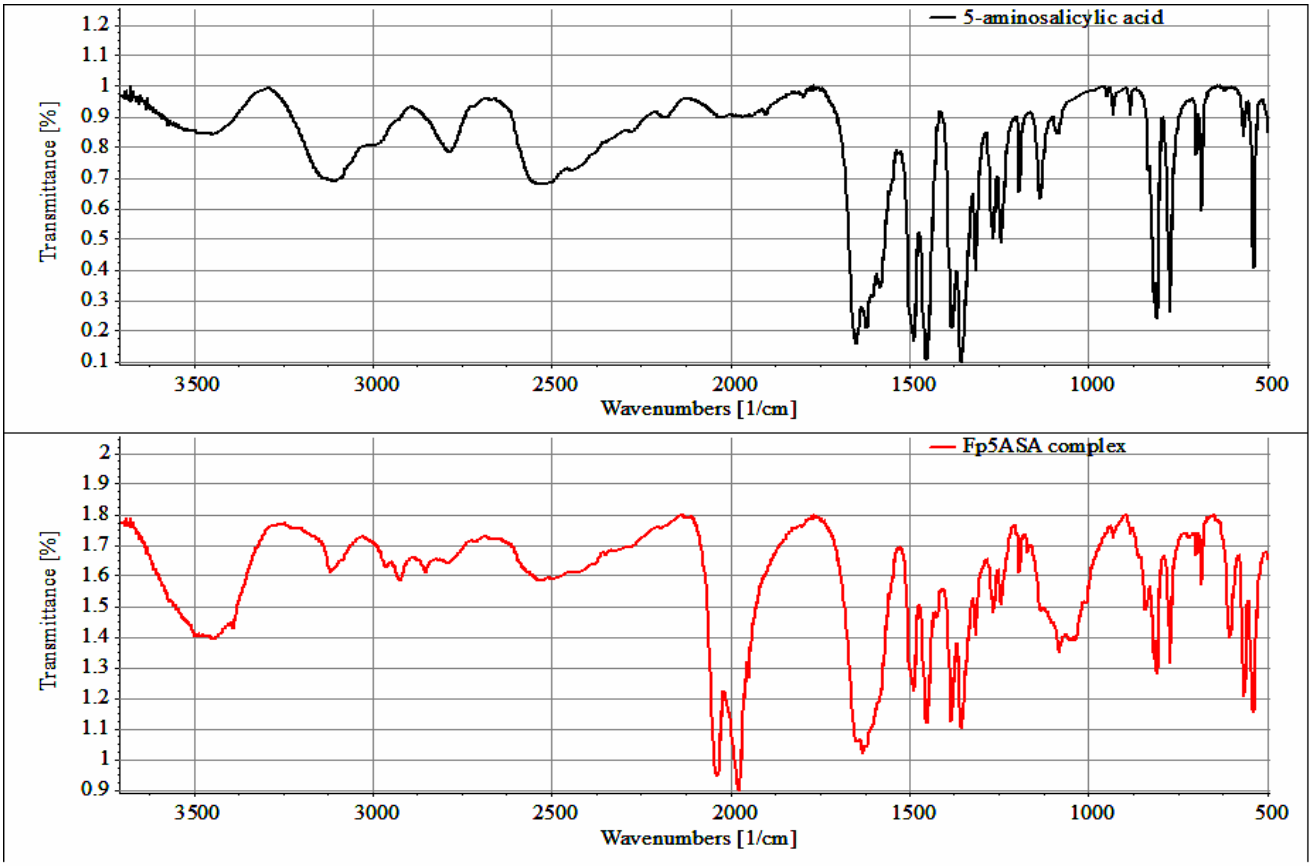

Figure 4.11: FTIR Spectra of 5-ASA and its Organometallic Complex Salt

4.5 Ethionamide (ETH) and its Complex Salt [Fp(ETH)]BF_4

In this section the results on the local reactivity properties of the free ETH molecule, the molecular and spectroscopic properties of ETH and its organometallic complex salt are presented and discussed in their respective subsections.

4.5.1 Regional or Local Reactivity Indices/ Functions of Ethionamide (ETH)

The condensed Fukui functions obtained for ETH are presented in Table 4.15. The atomic numbering scheme adopted is shown in Figure 4.12. Ethionamide (ETH) and its structural analog Prothionamide (PTH) contain multiple donor atoms including the nitrogen atom of the amine functionality, the pyridyl nitrogen and the thiocarbomyl sulphur atom. A close examination of the results in Table 4.15 reveals that the sulphur atom (S17) is the most nucleophilic of all the atoms in the molecule. The nucleophilicity of the three donor atoms follows the order S17>N11>N2.

Table 4.15: ETH Condensed to Atom Fukui Indices Calculated at 6-311G(2d,P) in THF

	CAM-B3LYP						**B3LYP**					
	NBO			**Hirshfeld**			**NBO**			**Hirshfeld**		
	f_k^+	f_k^-	f_k^o	f_k^+	f_k^-	f_k^o	f_k^+	f_k^-	f_k^o	f_k^+	f_k^-	f_k^o
C1	0.04	-0.02	0.01	0.05	0.01	0.03	0.05	-0.02	0.02	0.05	0.01	0.03
N2	0.11	0.04	0.08	0.07	0.03	0.05	0.11	0.05	0.08	0.08	0.03	0.05
C3	0.06	0.03	0.05	0.08	0.03	0.05	0.06	0.03	0.04	0.08	0.03	0.06
C4	0.06	0.02	0.04	0.08	0.04	0.06	0.06	0.03	0.04	0.08	0.05	0.06
C5	0.05	0.00	0.02	0.08	0.03	0.06	0.05	0.00	0.03	0.09	0.04	0.06
C6	0.04	0.00	0.02	0.03	0.02	0.03	0.05	0.00	0.02	0.04	0.02	0.03
C10	0.16	-0.03	0.06	0.11	0.06	0.08	0.14	-0.04	0.05	0.10	0.06	0.08
N11	0.12	0.06	0.09	0.16	0.13	0.15	0.11	0.06	0.09	0.16	0.13	0.14
C14	0.00	-0.01	0.00	0.03	0.01	0.02	0.00	-0.01	0.00	0.04	0.02	0.03
S17	0.27	0.79	0.53	0.27	0.64	0.45	0.26	0.76	0.51	0.26	0.61	0.43
C18	0.01	-0.01	0.00	0.03	0.01	0.02	0.01	-0.01	0.00	0.03	0.02	0.02

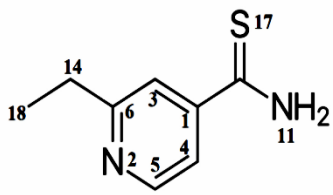

Figure 4.12: Ethionamide (ETH) Showing the Atom Numbering Scheme Adopted

4.5.2 Optimized Structures [Fp(ETH)]BF_4 with Fp Coordinated at the Various Donor Sites

The energies of [Fp(ETH)]BF_4 complexes with the central metal atom coordinated to the three potential coordination sites namely the sulphur atom (S17), the amino nitrogen atom (N11) and the pyridyl nitrogen atom (N2) were computed. The results are presented in Table 4.16 and Figure 4.13. The results show that thermodynamically the coordination of the iron metal centre to the ethionamide (ETH) ligand via the amino nitrogen is favoured. It should be noted that the condensed to atom Fukui indices in the previous section predicted this atom as the second most nucleophilic site. However, conventionally the results of the optimized structures of the systems of interest (products) take precedence over the computational results of the isolated reacting molecules. Hence, all further computations were therefore restricted to the structures in which the organometallic fragment was coordinated to the amino nitrogen.

Table 4.16: Global Energies of [Fp(ETH)]BF_4 Structures at the Various Donor Sites

[(η^5-C_5H_5)Fe$(CO)_2$(ETH)]BF_4 structures	**Energy (kcal/mol)**	**Relative Energy**
Fp coordinated to L through S atom 17	-1121056.737	3.239
Fp coordinated to L through amino N atom 11	-1121059.976	0.000
Fp coordinated to L through pyridyl N atom 2	-1121058.248	1.727

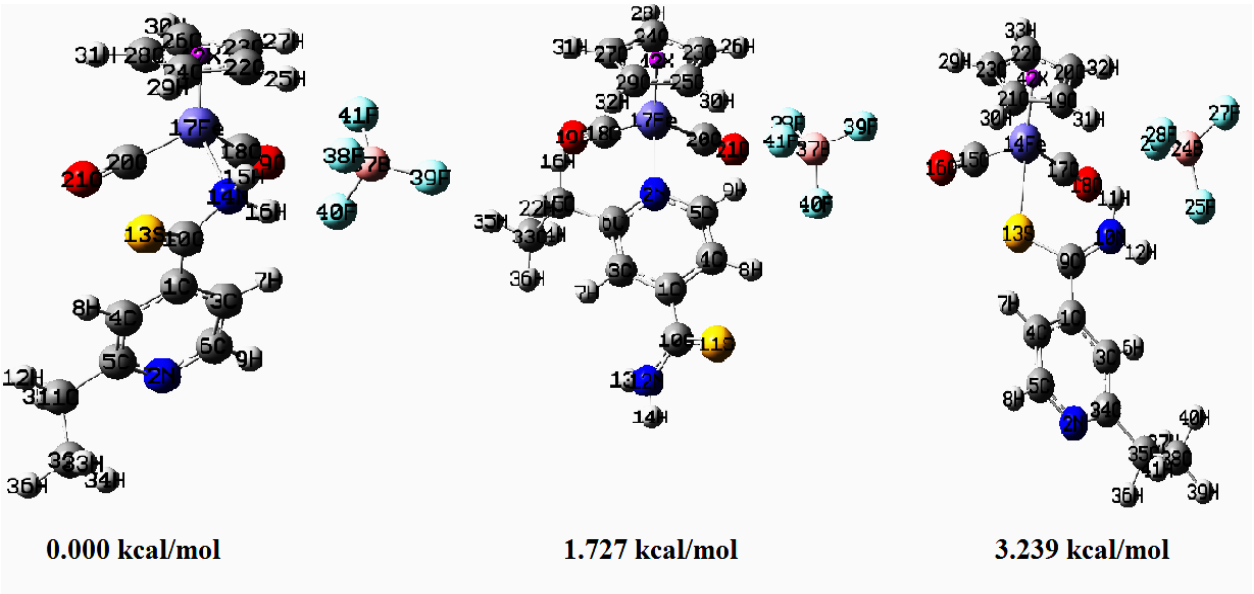

Figure 4.13: Optimized [Fp(ETH)]BF_4 Structures with Fp Coordinated at the Various Coordination Sites

4.5.3 Equilibrium Geometries of ETH and [Fp(ETH)]BF_4 and their Selected Bond Parameters

The equilibrium geometry of ethionamide (ETH) and its complex showing the atom numbering scheme adopted are shown in Figure 4.14. The calculated geometric parameters are presented in Table 4.17. The comparison of the, anisotropic parameters such as bond distance and bond angles of the free ethionamide ligand shows that the calculated values obtained using the three methods, PBEPBE, B3LYP and CAM-B3LYP and the 6-311G(2d,p) basis set are in good agreement with available X-ray crystallographic data (Colleter and Gadret, 1968a and b). Furthermore, the results obtained at the 6-311G(2d,p) basis set in the three methods are much closer to experimental values than those obtained using HF and B3LYP at a basis set of 6-31G(d, p) (Muthu *et al.*, 2012). The slight deviation of theoretical results from experimental values can be attributed to the absence of intermolecular and crystal packing forces in the

gas phase, and due to the fact that the calculations were performed on the neutral ethionamide molecule while the crystal structures were the chloride and bromide hydrates salts of ethionamide (ETH).

The bond length between the central metal iron atom (Fe) and the centroid of the cyclopentadienyl (Cp) ring were found to be in the range of 1.735- 1.764 Å. As observed from the other structures CAM-B3LYP and PBEPBE give values in close agreement with experimentally observed values while B3LYP overestimates this particular bond. The bond distances between the iron metal centre and the carbonyl carbons in the Fp fragment as obtained by PBEPBE are in excellent agreement with results in literature obtained by molecular mechanics and DFT calculations as well as experimental results from available crystallographic data (Mackie and Baird, 1992; Zeng and Li, 2011; M'thiruaine *et al*., 2012a, b, c, d, e and f). The methods CAM-B3LYP and B3LYP slightly overestimate this bond although the values obtained are still within the acceptable limits for values obtained theoretically. Experimentally this bond has been observed in the range of 1.770 - 1.793 Å in similar complexes, while the average values obtained here were 1.815, 1.810 and 1.766Å using CAM-B3LYP, B3LYP and PBEPBE functionals, respectively.

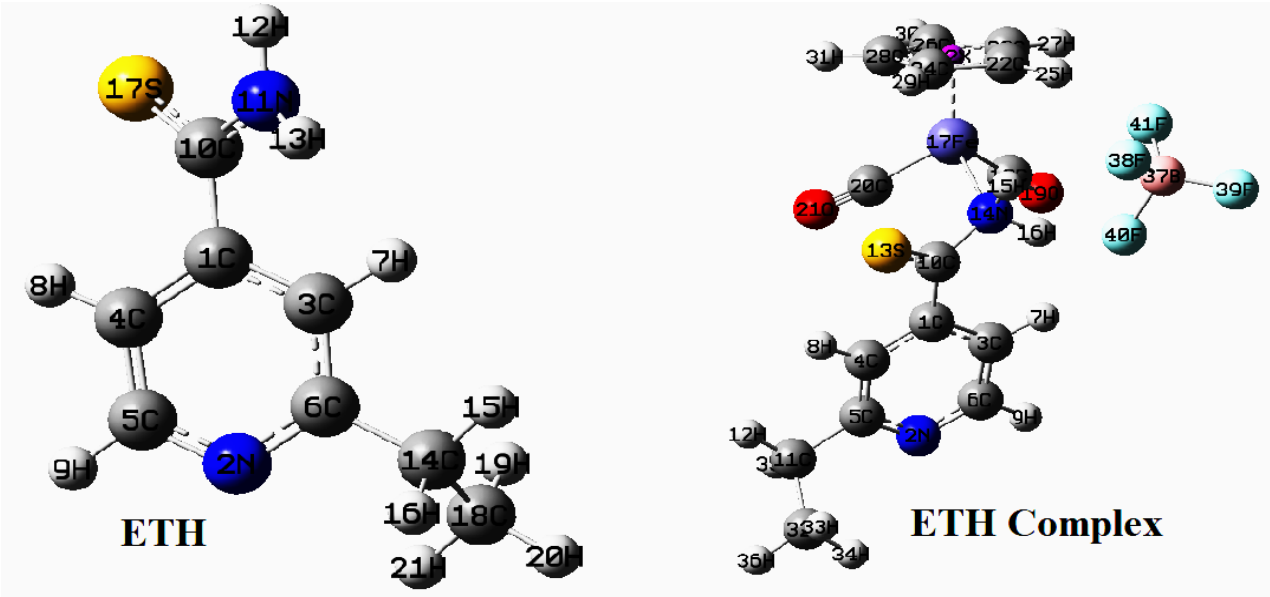

Figure 4.14: Optimized ETH and its Complex Showing the Atom Numbering Scheme

The Fe-N bond distances computed by the CAM-B3LYP and PBEPBE methods are 2.089, and 2.090 Å, respectively. The corresponding value of 2.114 Å obtained by the B3LYP method is marginally higher. However, these values are within the range of literature values (Cotton and Troup, 1974; M'thiruaine *et al*., 2011a and b; M'thiruaine *et al*., 2012a, b, c, d, e and f). In the coordinated ETH ligand, the bond lengths of C10-S13, C10-N14 andC1-C10 at CAM-B3LYP are 1.627, 1.409 and 1.482 Å, respectively. In the uncoordinated ETH ligand the same bonds namely C10-S17, C10-N11 and C1-C10 the values are 1650, 1.339 and 1.488 Å at CAM-B3lYP respectively. This indicates an elongation of these bonds in ETH upon coordination. In the crystal structure of the hydrobromide and hydrochloride forms of ethionamide the corresponding values are 1.69, 1.29 and 1.48 Å, respectively (Colleter and Gadret, 1968a, 1968b).

Table 4.17: Selected Geometric Parameters of the Ethionamide (ETH) and its Complex

ETH			**$[(\eta^5\text{-}C_5H_5)Fe(CO)_2(ETH)]BF_4$**		
Bond length (Å)	**CAM-B3LYP**	**PBEPBE**	**Bond length (Å)**	**CAM-B3LYP**	**PBEPBE**
R(C1,C3)	1.389	1.404	$R(C\text{-}C)_{Cp}$	1.425	1.438
R(C1,C4)	1.385	1.400	$R(C\text{-}C)_{Cp}$	1.402	1.417
R(C1,C10)	1.488	1.490	$R(C\text{-}C)_{Cp}$	1.423	1.437
R(N2,C5)	1.327	1.342	$R(C\text{-}C)_{Cp}$	1.422	1.435
R(N2,C6)	1.332	1.347	$R(C\text{-}C)_{Cp}$	1.406	1.424
R(C3,C6)	1.389	1.401	R(Cp-Fe)	1.735	1.727
R(C4,C5)	1.382	1.394	$R(Fe\text{-}C_{CO})$	1.833	1.775
R(C6,C14)	1.504	1.511	$R(Fe\text{-}C_{CO})$	1.808	1.764
R(C10,N11)	1.339	1.353	R(N-C)	1.409	1.423
R(C10,S17)	1.650	1.667	$R(C\text{-}O)_{CO}$	1.129	1.155
R(C14,C18)	1.527	1.536	$R(C\text{-}O)_{CO}$	1.123	1.151
			R(Fe-N)	2.089	2.090
Bond angle(◦)			**Bond angle(◦)**		
A(C3,C1,C4)	117.971	117.601	$A(C\text{-}C\text{-}C)_{Cp}$	108.041	108.298
A(C3,C1,C10)	121.020	121.490	$A(C\text{-}C\text{-}C)_{Cp}$	108.396	108.190
A(C4,C1,C10)	121.009	120.908	$A(C\text{-}C\text{-}C)_{Cp}$	108.329	108.301
A(C5,N2,C6)	118.245	117.612	$A(C\text{-}C\text{-}C)_{Cp}$	107.890	107.696
A(C1,C3,C6)	119.760	119.926	$A(Cp\text{-}Fe\text{-}C_{CO})$	121.547	121.995
A(C1,C4,C5)	118.286	118.456	$A(Cp\text{-}Fe\text{-}C_{CO)}$	122.452	123.196
A(N2,C5,C4)	123.905	124.278	$A(Fe\text{-}C\text{-}O_{CO})$	174.285	174.515
A(N2,C6,C3)	121.819	122.113	$A(Fe\text{-}C\text{-}O_{CO})$	175.202	174.928
A(N2,C6,C14)	116.461	116.206	$A(C_{CO}\text{-}Fe\text{-}C_{CO})$	94.057	92.578
A(C3,C6,C14)	121.714	121.674	A(Cp-Fe-N)	121.589	120.496
A(C1,C10,N11)	114.580	114.928	$A(N\text{-}Fe\text{-}C_{CO})$	93.329	93.825
A(C1,C10,S17)	122.772	122.705	$A(N\text{-}Fe\text{-}C_{CO})$	96.648	97.496
A(N11,C10,S17)	122.632	122.334	A(Fe-N-C)	116.197	114.783
A(C6,C14,C18)	112.103	112.154			

4.5.4 FTIR Spectra of Ethionamide (ETH) and Its Complex Salt

The FTIR spectra of the synthesized complex salt $[Fp(ETH)]BF_4$ and the free ETH ligand are presented in Fig. 4.15. A summary of the most significant bands is given in Table 4.18. The band assignments were made with the aid of the theoretically observed vibrational frequencies and their intensities as visualized in GaussView 5.0.9 together with the spectroscopic data of similar compounds found in literature (Muthu *et al*., 2012). A strong absorption band appearing at 1596 cm^{-1} in the FTIR spectrum of ETH is assigned to the scissoring vibrational mode of the NH_2 group of the thionamide portion of ETH $\delta(NH_2)$. In the complex salt spectrum this band appears to be blue shifted to 1610 cm^{-1} suggesting that the ligand ETH may have coordinated to the organometallic fragment through the amino nitrogen.

The metal complex also shows new bands at 1095 and 1035 cm^{-1} both of which are assigned to the B-F stretching vibrations of the BF_4^- counter ion (anion). The diagnostic $\nu(CO)$ vibration modes of the carbonyl ligands of the $[Cp(CO)_2Fe]^+$ or simply Fp organometallic fragment can be seen as very strong bands at 2035 and 1976 cm^{-1}. Furthermore, three distinct strong bands are observed at 607, 567 and 543 cm^{-1}. These bands are associated with the C-C stretching frequencies of the cyclopentadienyl ligand and the deformation of the cyclopentadienyl ring and the Fe -C≡O bonds. The broad medium band in the region 3050-3232 cm^{-1} is assignable to the C-H stretching vibration modes of the cyclopentadienyl ring. It should be noted that these bands are conspicuously absent in the spectrum of the free ligand. The bands are characteristic of the

organometallic fragment, $[Cp(CO)_2Fe]^+$ or simply Fp hence are observed only in the FTIR spectrum of complex salt.

Table 4.18: Important FTIR Bands of ETH and its Complex [Fp (ETH)]BF_4 (cm^{-1})

Vibrational Mode	Uncoordinated ETH	$[Cp(CO)_3Fe(ETH)]BF_4$
υ(C≡O)	-	2035 and 1976
υ $(C-H)_{(Cp)}$	-	3050-3232
υ $(C-C)_{(Cp)\ and\ \delta(Fe-C\equiv O)}$	-	607, 567 and 543
υ C-H (pyr ring)	2853, 2879, 2916, 2964	2852, 2877, 2916, 2964
υ(NH_2)	3464	3445
υ(NH)	3266	3266
δ(NH_2)	1595	1610
υ $(C=C)_{(Pyridine\ ring)}$	1631	1631
υ(B-F)	-	1087,1059 and 1035

The NH_2 stretching vibration modes of uncoordinated ethionamide (ETH) molecule were observed at 3464 and 3266 cm^{-1}. These vibration modes are observed at 3438 and 3266 cm^{-1} respectively in coordinated ethionamide molecule in the organometallic complex salt. This suggests that the ETH ligand is coordinated to the metal fragment through the amino nitrogen. The bands assignable to the C-H stretching vibration modes of the pyridine ring in free ETH were observed at 2853, 2879, 2916 and 2964 cm^{-1} while the corresponding values in the coordinated ETH were observed at more or less the same positions of 2852, 2877, 2916 and 2964 cm^{-1}. The υ(C=C) stretching vibration modes in the pyridine ring of uncoordinated ETH and coordinated ETH appear at 1631 cm^{-1}. Thus, ruling out the involvement of the pyridyl nitrogen in the coordination process.

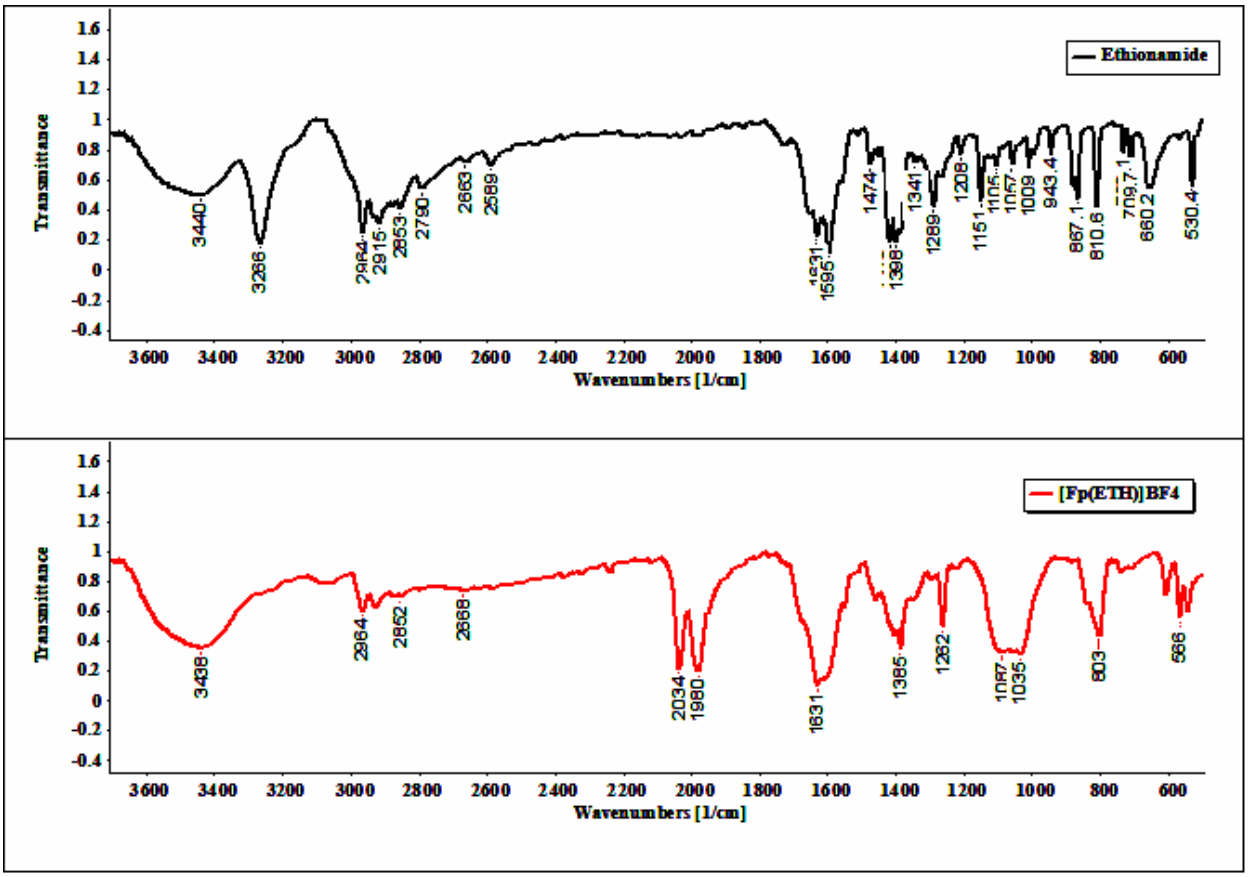

Figure 4.15: FTIR Spectra of ETH and its Fp Complex Salt

4.6 Prothionamide (PTH) and its Complex Salt $[Fp(PTH)]BF_4$

In this section the results on the local reactivity properties of the free PTH molecule, the molecular and spectroscopic properties of PTH and its organometallic complex salt are presented and discussed in their respective subsections.

4.6.1 Regional or Local Reactivity Indices/ Functions of Prothionamide (PTH)

The condensed to atom Fukui functions obtained for PTH are presented in Table 4.19 while the atomic numbering scheme adopted is shown in Figure 4.16. A closer look at

Table 4.19 reveals that the condensed to atom Fukui functions obtained from all charge portioning schemes, phases and methods point to the sulphur atom (S20) as the most nucleophilic site hence the most susceptible to undergo electrophilic attack. The trend is S20>>N11>N2 for the heteroatoms. Furthermore, all the heteroatoms have higher values than the carbon atoms. In this respect Prothionamide behaves like its structural analog Ethionamide.

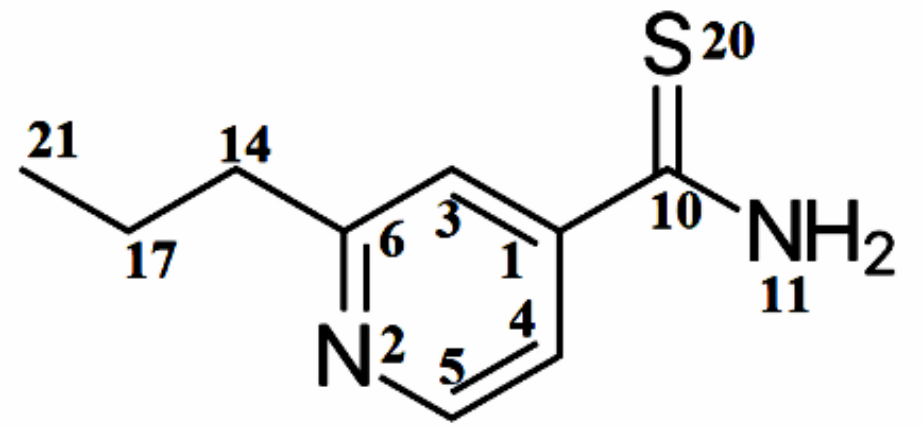

Figure 4.16: Prothionamide (PTH) Showing the Atom Numbering Scheme Adopted

Table 4.19: PTH Condensed to Atom Fukui Indices Calculated at 6-311G(2d,P) in THF

	CAM-B3LYP						B3LYP					
	NBO			Hirshfeld			NBO			Hirshfeld		
	f_k^+	f_k^-	f_k^o	f_k^+	f_k^-	f_k^o	f_k^+	f_k^-	f_k^o	f_k^+	f_k^-	f_k^o
C1	0.04	-0.02	0.01	0.04	0.01	0.03	0.05	-0.02	0.02	0.05	0.01	0.03
N2	0.11	0.04	0.08	-0.16	0.26	0.05	0.11	0.05	0.08	0.08	0.03	0.05
C3	0.06	0.03	0.05	0.09	0.01	0.05	0.06	0.03	0.04	0.08	0.03	0.06
C4	0.06	0.02	0.04	0.08	0.03	0.06	0.06	0.03	0.04	0.08	0.04	0.06
C5	0.05	0.00	0.02	0.19	-0.08	0.06	0.05	0.00	0.03	0.09	0.04	0.06
C6	0.04	-0.01	0.02	0.10	-0.05	0.02	0.05	0.00	0.02	0.04	0.02	0.03
C10	0.16	-0.03	0.06	0.15	0.01	0.08	0.14	-0.04	0.05	0.10	0.05	0.07
N11	0.12	0.06	0.09	0.06	0.23	0.14	0.11	0.06	0.09	0.16	0.12	0.14
C14	-0.01	0.00	0.00	0.06	-0.01	0.02	-0.01	0.00	0.00	0.03	0.02	0.02
C17	0.02	-0.01	0.00	0.02	0.00	0.01	0.02	-0.02	0.00	0.02	0.01	0.01
S20	0.27	0.79	0.53	0.34	0.59	0.46	0.26	0.76	0.51	0.27	0.61	0.44
C21	0.01	-0.01	0.00	0.02	0.01	0.01	0.01	-0.01	0.00	0.02	0.01	0.01

4.6.2 Optimized Structures [Fp(PTH)]BF_4 with Fp Coordinated at Various Donor Sites

The energies of [Fp(PTH)]BF_4 complexes with the central metal atom coordinated to the three potential coordination sites namely the sulphur atom, the amino nitrogen atom and the pyridyl nitrogen atom were computed. The results are presented in Table 4.20 and Figure 4.17. The results show that thermodynamically the coordination of the iron metal centre to the PTH ligand via the amino nitrogen is favoured. All further computations were therefore restricted to the structure in which the organometallic fragment is coordinated to the amino nitrogen.

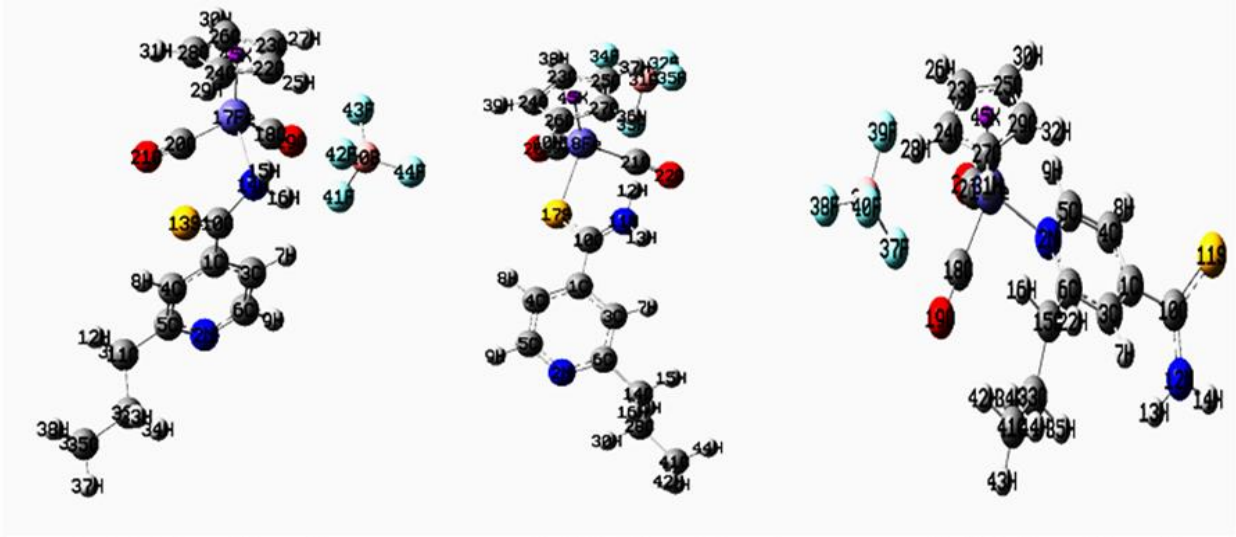

Figure 4.17: Optimized [Fp(PTH)]BF_4 Structures at the Various Coordination Sites

Table 4.20: Global Energies of [Fp(L)]BF4 Structures at Various Donor Sites

[(η^5-C_5H_5)Fe$(CO)_2$(PTH)]BF4 structures	**Energy (kcal/mol)**	**Relative Energy**
Fp coordinated to L through S atom 20	-1145718.183	3.196
Fp coordinated to L through amino N atom 11	-1145721.379	0.000
Fp coordinated to L through pyridyl N atom 2	-1145716.872	4.507

4.6.3 Equilibrium Geometries of PTH and [Fp(PTH)]BF_4 and their Selected Bond Parameters

Figure 4.18 shows the most stable molecular geometry of the complex [Fp(PTH)]BF_4 while Table 4.21 gives the selected bond parameters as computed by the three density functionals CAM-B3LYP, B3LYP and PBEPBE. The optimized geometry of the modelled [Fp(PTH)]BF_4 structure is very similar to that of its analog [Fp(ETH)]BF_4.

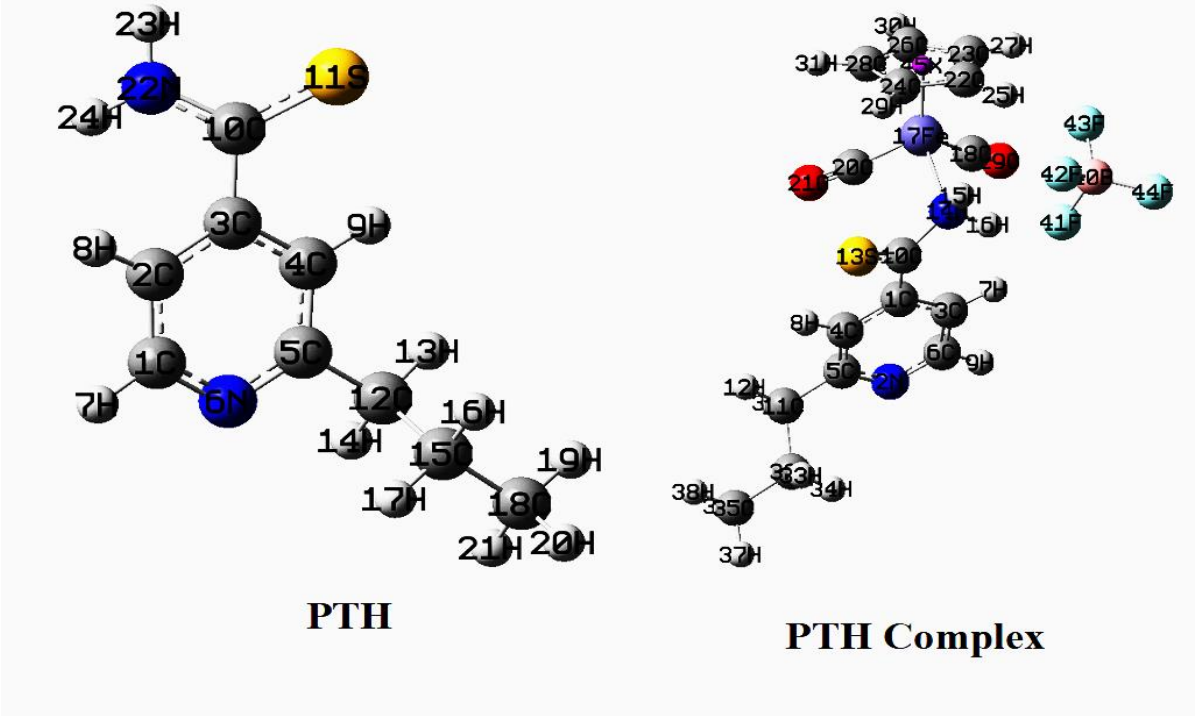

Figure 4.18: Geometries of PTH and [Fp(PTH)]BF_4 Showing the Atom Numbering

The bond lengths between the central metal iron atom (Fe) and the centroid of the cyclopentadienyl (Cp) ring are 1.735 Å and 1.727 Å for CAM-B3LYP and PBEPBE, respectively. Experimentally this bond length is usually observed in the range of 1.71 - 1.72 Å (M'thiruaine *et al*., 2012a, b, c, d, e and f). The average Fe-C_{CO} bond length obtained by PBEPBE at 1.769 Å is in excellent agreement with results in literature obtained by molecular mechanics and DFT calculations as well as experimental results from available crystallographic data (Mackie and Baird, 1992; Zeng and Li, 2011; M'thiruaine *et al*., 2012a, b, c, d, e and f). The method CAM-B3LYP slightly overestimates this bond to give an average value of 1.821 Å. However, these values are still within the acceptable range for values obtained theoretically. Experimentally this bond has been observed in the range of 1.770 - 1.793Å in similar complexes. The iron-

nitrogen bond distances are 2.089 (CAM-B3LYP) and 2.090 Å (PBEPBE), respectively. These values are within the range of values in literature for the Fe – N bond in amine coordinated Fp and iron carbonyl complexes (Cotton and Troup, 1974; M'thiruaine *et al*., 2012a, b, c, d, e and f).

The centroid-Fe-N bond angles are 121.593° and 120.527° for CAM-B3LYP and PBEPBE, respectively. The average N-Fe-C_{CO} was observed at 93.323° and 93.818 for CAM-B3LYP and PBEPBE, respectively. Another characteristic bond angle in such complexes is the C_{CO}-Fe-C_{CO} bond which in this work was observed at 94.061°and 92. 602° for CAM-B3LYP and PBEPBE, respectively. Generally, these values are within the expected range of theoretically obtained values.

Table 4.21: Selected Geometric Parameters of the PTH and its Complex Salt

PTH			**$[(\eta^5\text{-}C_5H_5)Fe(CO)_2(PTH)]BF_4$**		
Bond length (Å)	**CAM-B3LYP**	**PBEPBE**	**Bond length (Å)**	**CAM-B3LYP**	**PBEPBE**
R(C1,C3)	1.389	1.404	$R(C\text{-}C)_{Cp}$	1.425	1.437
R(C1,C4)	1.385	1.400	$R(C\text{-}C)_{Cp}$	1.402	1.417
R(C1,C10)	1.488	1.491	$R(C\text{-}C)_{Cp}$	1.423	1.437
R(N2,C5)	1.327	1.342	$R(C\text{-}C)_{Cp}$	1.422	1.435
R(N2,C6)	1.332	1.348	$R(C\text{-}C)_{Cp}$	1.406	1.424
R(C3,C6)	1.389	1.402	R(Cp-Fe)	1.735	1.727
R(C4,C5)	1.382	1.393	$R(Fe\text{-}C_{CO})$	1.833	1.775
R(C6,C14)	1.503	1.509	$R(Fe\text{-}C_{CO})$	1.808	1.764
R(C10,N11)	1.339	1.353	$R(C\text{-}O)_{CO}$	1.123	1.151
R(C10,C20)	1.650	1.667	$R(C\text{-}O)_{CO}$	1.129	1.155
R(C14,C17)	1.529	1.539	R(Fe-N)	2.089	2.090
R(C17,C21)	1.522	1.529	R(N-C)	1.409	1.423
Bond angle(◦)			**Bond angle(◦)**		
A(C3,C1,C4)	117.954	117.592	$A(C\text{-}C\text{-}C)_{Cp}$	108.039	108.313
A(C3,C1,C10)	121.059	121.520	$A(C\text{-}C\text{-}C)_{Cp}$	108.397	108.182
A(C4,C1,C10)	120.986	120.885	$A(C\text{-}C\text{-}C)_{Cp}$	107.892	108.304
A(C5,N2,C6)	118.242	117.609	$A(C\text{-}C\text{-}C)_{Cp}$	107.328	107.684
A(C1,C3,C6)	119.775	119.928	$A(Cp\text{-}Fe\text{-}C_{CO})$	122.447	121.982
A(C1,C4,C5)	118.302	118.469	$A(Cp\text{-}Fe\text{-}C_{CO)}$	121.551	123.196
A(N2,C5,C4)	123.909	124.284	$A(Fe\text{-}C\text{-}O_{CO})$	174.292	174.511
A(N2,C6,C3)	121.806	122.102	$A(Fe\text{-}C\text{-}O_{CO})$	175.193	174.945
A(N2,C6,C14)	116.445	116.164	$A(C_{CO}\text{-}Fe\text{-}C_{CO})$	94.061	92.602
A(C3,C6,C14)	121.745	121.731	A(Cp-Fe-N)	121.593	120.527
A(C1,C10,N11)	114.622	114.982	$A(N\text{-}Fe\text{-}C_{CO})$	93.323	93.818
A(C1,C10,C20)	122.771	122.709	$A(N\text{-}Fe\text{-}C_{CO})$	96.649	97.455
A(N11,C10,C20)	122.592	122.276	A(Fe-N-C)	116.188	114.814
A(C6,C14,C17)	112.433	112.440			
A(C14,C17,C21)	112.614	112.810			
A(C3,C1,C4)	117.954	117.592			

4.6.4 FTIR Spectra of Prothionamide (PTH) and its Complex Salt

The FTIR spectra of the synthesized complex salt [Fp(PTH)]BF_4 and the free PTH ligand are presented in Fig. 4.19. Like its structural analog ETH the band assignments of the prothionamide Fp complex salt were made by comparison with the spectroscopic data of similar Fp complex salts and those of ETH and its related compounds found in literature and the theoretically computed spectra. The FTIR spectra of PTH and its complex salt show distinct differences confirming the formation of the organometallic complex. A strong absorption band appearing at 1596 cm^{-1} in the FTIR spectrum of the free prothionamide (PTH) molecule is associated to the scissoring vibration of amino group (NH_2) of the thionamide functional group. In the complex salt spectrum this band appears to be blue shifted to 1632 cm^{-1}. This shift of band can be related to the coordination of the amino nitrogen to the central metal atom thus forming a Fe-N coordinate bond**.** Furthermore, we observe the appearance of new bands associated with the BF_4^- counter ion (anion) vibrations.

The spectrum of the complex shows strong broad bands assignable to the B-F stretching vibrations observed at 1084, 1063, 1040 and 1007 cm^{-1}. Additionally, new bands associated with the cyclopentadienyliron(II)dicarbonyl fragment, the C-C and C-H stretching vibration modes from the cyclopentadienyl ring and the CO vibration modes of the carbonyl ligands are also observed. The Fp fragment C≡O symmetric and asymmetric stretching frequencies are observed at 2034 and 1988 cm^{-1} , respectively. The C-C stretching vibration modes of the cyclopentadienyl (Cp) ring appear at 610, 566 and 543 cm^{-1}, while the C-H stretching modes of the Cp ring appear in the region 3180-3065 cm^{-1}. All these bands are conspicously absent in the

FTIR spectrum of the free ligand and hence are diagnostic of the Fp moiety and therefore provide clear evidence for the formation of the desired compound, the complex salt.

The NH_2 vibration modes of prothionamide are observed at 3429 and 3270 cm^{-1} for the asymmetric and symmetric vibration modes respectively. These vibration modes are observed at 3468 and 3232 cm^{-1}, respectively in the complex salt. This observation tentatively points to the involvement of the amino nitrogen of PTH in the coordination process with the central metal atom in Fp. The C-H stretching vibration modes of the pyridine ring in PTH are assigned to four bands 2874, 2901, 2933 and 2960 cm^{-1}. The corresponding values in the Fp complex salts are observed at 2853, 2871, 2930 and 2961 cm^{-1}. The C=C stretching vibration modes in the pyridine ring of uncoordinated PTH and coordinated PTH appear at 1672 and 1686 cm^{-1} respectively. Furthermore, the stretching vibration observed at 1556 cm^{-1} in the FTIR spectrum of prothionamide associated with the C-C and C-N bonds of the pyridine ring is observed at 1612 cm^{-1} in the complex salt. Thus, the three fragments, that is, the Fp organometallic fragment, the PTH ligand and the counter ion all appear to be present in the complex salt as attested by the characteristic FTIR bands of their functional groups.

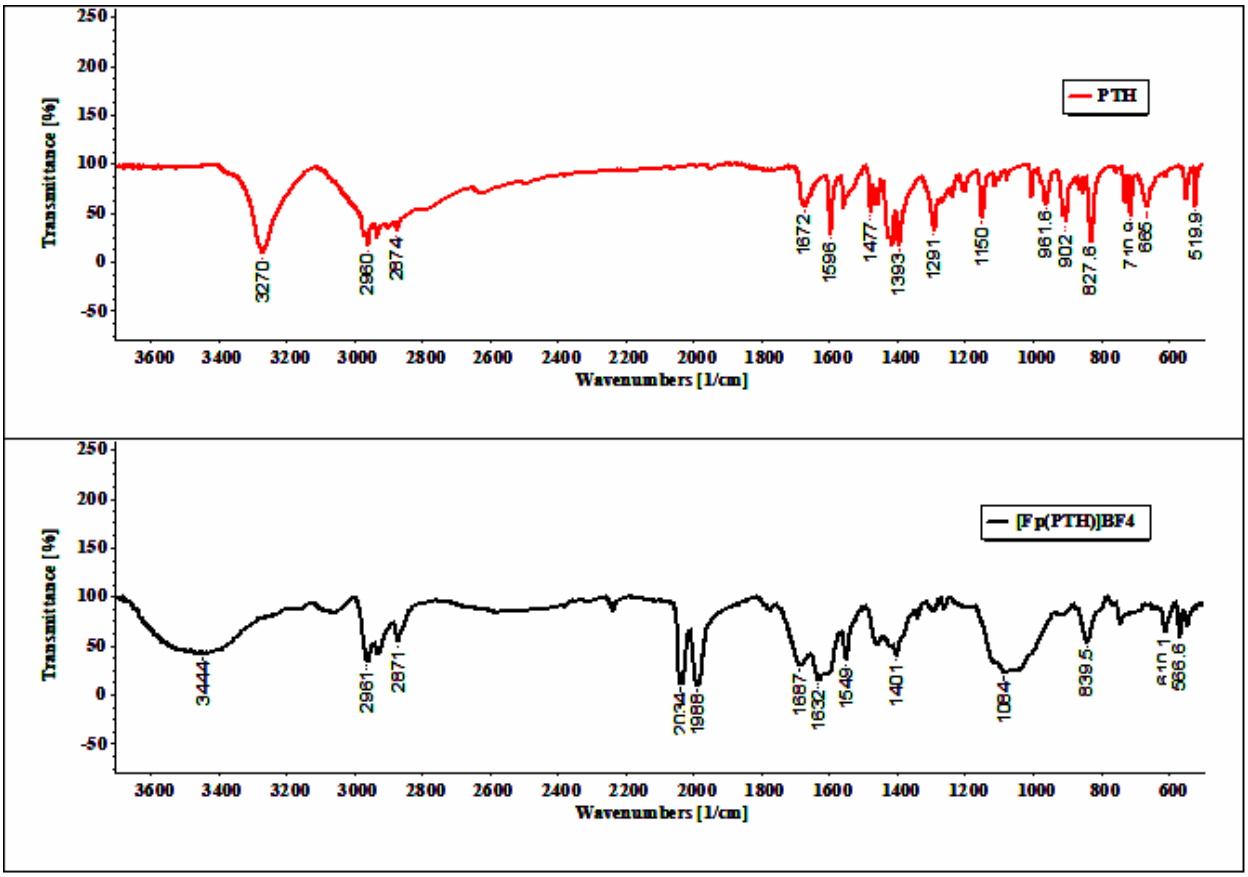

Figure 4.19: FTIR Spectra of Prothionamide and its Fp Complex Salt

4.7 Linezolid (LZD) and its Complex Salt [Fp (LZD)]BF_4

In this section the results on the local reactivity properties of the free LZD molecule, the molecular and spectroscopic properties of the of LZD and its organometallic complex salt are presented and discussed.

4.7.1 Regional or Local Reactivity Indices/ Functions of Linezolid (LZD)

The condensed to atom Fukui functions were calculated in order to determine the most nucleophilic in linezolid (LZD) and the results are presented in Table 4.22. From a chemical

point of view, the molecular structure of LZD can be divided into four entities (Figure 4.20). A morphilinic residue (ring A), a fluorine substituted benzene ring (ring B), a methylene oxazolidinone residue (ring C), and an acetamide fragment (side chain D) (Wielgus *et al*., 2015, Fortuna *et al*. 2013; Fortuna *et al*. 2014). All the fragments except ring B possess nitrogen and oxygen heteroatoms.

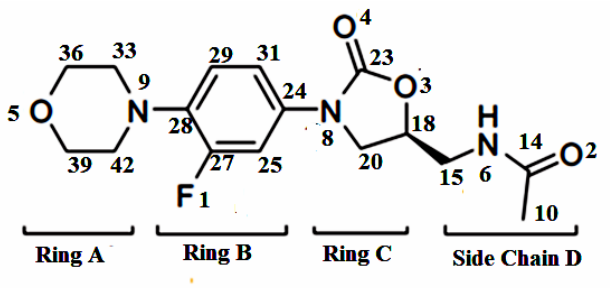

Figure 4.20: Linezolid Showing the Atom Numbering Scheme Adopted

In Table 4.22 the results show that the condensed to atom Fukui functions obtained from all charge portioning schemes, phases and methods point to the morphilinic nitrogen atom (N9) to be the most nucleophilic atom in the linezolid molecule. The dual descriptor ($f^2(r)$ for characterizing the local/site/regional reactivity was also employed. This reactivity descriptor is an extension of the Fukui function. Using the dual descriptor where the most preferable sites for nucleophilic attacks are obtained when ($f^2(r) > 0$) and the preferable sites for electrophilic attacks are obtained when ($f^2(r) < 0$) the morphilinic nitrogen atom N9 was found to be the most preferred site for electrophilic attack overall. Generally, the computation results show that the most reactive sites of the molecule as far as electrophilic attack is concerned are located on the N and O heteroatoms

Table 4.22: Condensed to Atom Fukui Indices for Linezolid

CAM-B3LYP/6-311++G(2D,P), DCM											
	MPA			NBO			Hirshfeld			The Dual descriptor	
	f_k^+	f_k^-	f_k^o	f_k^+	f_k^-	f_k^o	f_k^+	f_k^-	f_k^o	f^2(NBO)	f^2(HPA)
F1	0.00	0.05	0.03	0.00	0.04	0.02	0.02	0.04	0.03	-0.04	-0.02
O2	0.03	0.01	0.02	0.01	0.01	0.01	0.02	0.01	0.02	0.00	0.02
O3	0.01	0.04	0.03	-0.01	0.03	0.01	0.01	0.03	0.02	-0.04	-0.02
O4	0.01	0.05	0.03	0.02	0.04	0.03	0.02	0.04	0.03	-0.03	-0.02
O5	0.01	0.03	0.02	0.00	0.02	0.01	0.01	0.02	0.01	-0.02	-0.01
N6	0.19	0.00	0.10	0.01	-0.01	0.00	0.08	0.00	0.04	0.01	0.08
N8	0.04	0.04	0.04	-0.01	0.05	0.02	0.00	0.04	0.02	-0.06	-0.03
N9	0.01	0.12	0.07	-0.01	0.25	0.12	0.00	0.12	0.06	-0.25	-0.12
C10	-1.95	0.00	-0.97	0.01	0.00	0.00	0.20	0.02	0.11	0.02	0.18
C14	0.99	0.00	0.50	0.00	0.00	0.00	0.03	0.00	0.02	0.00	0.02
C15	-2.23	0.03	-1.10	0.03	0.00	0.01	0.19	0.01	0.10	0.03	0.18
C18	1.48	-0.09	0.70	0.00	0.00	0.00	0.04	0.02	0.03	0.01	0.02
C20	-1.69	-0.01	-0.85	0.02	-0.02	0.00	0.15	0.04	0.10	0.04	0.12
C23	-0.47	0.02	-0.23	0.00	0.00	0.00	0.02	0.02	0.02	0.00	0.00
C24	-2.37	0.05	-1.16	-0.03	0.12	0.04	0.01	0.06	0.03	-0.14	-0.06
C25	0.42	0.02	0.22	0.05	-0.03	0.01	0.06	0.06	0.06	0.08	0.01
C27	1.24	0.08	0.66	-0.01	0.07	0.03	0.02	0.05	0.03	-0.08	-0.03
C28	-0.30	-0.03	-0.17	0.00	0.06	0.03	0.01	0.04	0.03	-0.05	-0.03
C29	0.23	0.03	0.13	0.06	-0.02	0.02	0.02	0.07	0.04	0.08	-0.04
C31	0.12	0.03	0.08	-0.02	0.07	0.03	0.02	0.08	0.05	-0.09	-0.06
C33	-0.04	-0.06	-0.05	0.00	-0.03	-0.02	0.01	0.07	0.04	0.03	-0.06
C36	-0.02	0.01	0.00	0.00	-0.01	0.00	0.02	0.05	0.03	0.01	-0.04
C39	-0.07	0.02	-0.03	0.00	-0.01	0.00	0.02	0.05	0.03	0.01	-0.03
C42	-0.07	-0.08	-0.07	0.00	-0.03	-0.01	0.02	0.07	0.05	0.03	-0.06

4.7.2 Optimized Structures [Fp(LZD)]BF_4 with Fp Coordinated at the various donor sites

According to the results given in Table 4.23 and Figure 4.21, the most stable Fp complex of the linezolid ligand is obtained when the metal centre in Fp coordinates to linezolid through the carbonyl oxygen atom of the oxazolidinone fragment. This structure has a calculated relative energy of 0.000 kcal mol^{-1}. Therefore, thermodynamics, favour the formation of structure (A) Figure 4.24. Hence, calculations for all other properties were carried out on this structure.

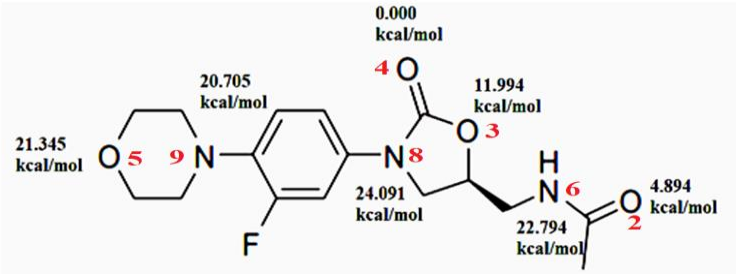

Figure 4.21: Energies of Optimized [Fp(LZD)]BF_4 Structures at the Various Coordination Sites

Table 4.23: Global Energies of [Fp(LZD)]BF4 Structures at the Various Donor Sites

[(η^5-C_5H_5)Fe(CO)$_2$(LZD)]BF_4 structures	**Energy (kcal/mol)**	**Relative Energy**
Fp coordinated to L through morphilinic O atom 5	-1352021.693	21.345
Fp coordinated to L through morphilinic N atom 9	-1352022.333	20.705
Fp coordinated to L through oxazolidinone N atom 8	-1352018.947	24.091
Fp coordinated to L through oxazolidinone carbonyl O atom	-1352043.038	0.000
Fp coordinated to L through oxazolidinone O atom 3	-1352031.044	11.994
Fp coordinated to L through acetamide N atom 6	-1352020.244	22.794
Fp coordinated to L through acetamide carbonyl O atom 2	-1352038.144	4.894

4.7.3 **Optimized Structures of LZD and [Fp(LZD)]BF_4 and their Selected Bond Parameters**

The equilibrium geometry of the most stable structures of the free LZD molecule and its complex [Fp(LZD)]BF_4 are shown on Figure 4.22. Selected bond lengths and angles for the compounds are listed in Table 4.24. A closer examination of the bond parameters obtained from the optimized structures of the free and coordinated linezolid molecule in the three DFT functionals in comparison with the crystal structure of linezolid form II and other compounds containing the oxazolidinone moiety reveals a general agreement. For example, the C23-O4 bond lengths of the uncoordinated LZD obtained by CAM-B3LYP, B3LYP and PBEPBE were 1.197,

1.201 and 1.211 Å, respectively. In compounds with the oxazolidinone moiety this bond has been observed at 1.202(8) (Wang *et al*. 2007), 1.204(2) (Brancatelli *et al*. 2011) and 1.2004(5) (Gaumet *et al*. 2013). In the crystal structure of linezolid form II this bond was observed at 1.201 Å (Maccaroni *et al*., 2008).

In the complex the bonding around the iron centre corresponds to that of a three-legged piano stool arrangement. The iron centre is coordinated to cyclopentadienyl ligand (Cp) in a pentahapto fashion where the Cp ligand occupies three coordination sites. The two carbonyl ligands (CO) and LZD occupy the three remaining coordination sites. The bonds between the iron atom (Fe) and the centroid of the Cp ring averaged 1.723, 1.750 and 1.706 Å for functionals CAM-B3LYP, B3LYP and PBEPBE, respectively.

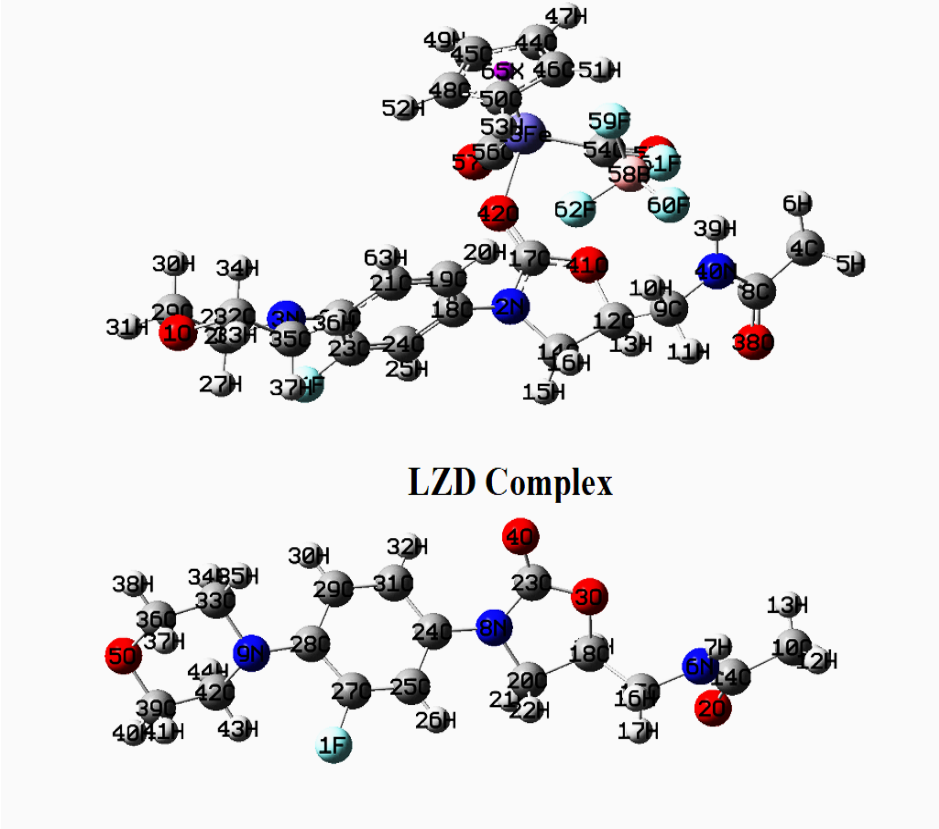

Figure 4.22: Optimized LZD and [Fp(LZD)]BF_4 Showing the Atom Numbering

A typical Cp centroid–Fe bond for similar complexes is usually observed in the range of 1.71 - 1.72 Å (Darensburg *et al.***,** 1981; Akita *et al.***,** 1996**;** M'thiruaine *et al.*, 2012a, b, c, d, e and f). The average Fe-$C_{C\equiv O}$ bond lengths obtained were 1.837Å (CAM-B3LYP), 1.831 Å (B3LYP) and 1.779 Å (PBEPBE) are within the range of experimentally observed data albeit with slight deviation (Mackie and Baird, 1992; Zeng and Li, 2011; M'thiruaine *et al.*, 2011a, b, c, d; M'thiruaine *et al*., 2012a, b, c, d, e and f). Furthermore, around the Cp ring an average C-C bond length of 1.416, 1.422 and 1.432 Å was obtained for CAM-B3LYP, B3LYP and PBEPBE, respectively.

Table 4.24: Selected Geometric Parameters of LZD and its Fp Complex Salt Using the CAM-B3LYP Functional *in vacuo*

LZD				[Fp(LZD)}BF4			
Bond R(Å)		**Bond A (◦)**		**Bond R(Å)**		**Bond A (◦)**	
R(F1,C27)	1.350	A(C18,O3,C23)	110.790	R(O1,C29)	1.414	A(C12,O41,C17)	116.774
R(O2,C14)	1.216	A(C36,O5,C39)	110.858	R(O1,C32)	1.413	A(C17,O42,Fe43)	110.176
R(O3,C18)	1.435	A(C14,N6,C15)	121.088	R(N2,C14)	1.458	A(C54,Fe43,C56)	145.585
R(O3,C23)	1.358	A(C20,N8,C23)	111.190	R(N2,C17)	1.336	A(O42,Fe43,C54)	88.528
R(O4,C23)	1.197	A(C20,N8,C24)	122.311	R(N2,C18)	1.425	A(O42,Fe43,C56)	98.930
R(O5,C36)	1.413	A(C23,N8,C24)	125.723	R(N3,C22)	1.399	$A(C,C,C)_{Cp\ AV}$	123.346
R(O5,C39)	1.415	A(C28,N9,C33)	116.798	R(N3,C26)	1.457	A(F,B,F) AV	112.713
R(N6,C14)	1.361	A(C28,N9,C42)	116.032	R(N3,C35)	1.460	A(Cent,Fe43,O42)	119.854
R(N6,C15)	1.443	A(C33,N9,C42)	110.901	R(C4,C8)	1.508	A(Cent,Fe43,C54)	124.447
R(N8,C20)	1.449	A(O2,C14,N6)	121.836	R(C8,O38)	1.222	A(Cent,Fe43,C56)	121.198
R(N8,C23)	1.375	A(O2,C14,C10)	122.055	R(C8,N40)	1.350	A(C9,C12,O41)	110.048
R(N8,C24)	1.409	A(N6,C14,C10)	116.104	R(C9,C12)	1.518	A(C14,C12,O41)	104.018
R(N9,C28)	1.405	A(N6,C15,C18)	112.720	R(C9,N40)	1.438	A(N2,C14,C12)	102.138
R(N9,C33)	1.454	A(O3,C18,C15)	109.264	R(C12,C14)	1.536	A(N2,C17,O41)	111.844
R(N9,C42)	1.464	A(O3,C18,C20)	104.478	R(C12,O41)	1.459	A(N2,C17,O42)	125.139
R(C10,C14)	1.507	A(C15,C18,C20)	114.178	R(C17,O41)	1.320	A(O41,C17,O42)	122.939
R(C15,C18)	1.513	A(N8,C20,C18)	102.099	R(C17,O42)	1.233	A(N2,C18,C19)	120.374
R(C18,C20)	1.527	A(O3,C23,O4)	122.352	R(C18,C19)	1.387	A(N2,C18,C24)	119.731
R(C24,C25)	1.392	A(O3,C23,N8)	108.830	R(C18,C24)	1.381	A(C19,C18,C24)	119.876
R(C24,C31)	1.390	A(O4,C23,N8)	128.817	R(C19,C21)	1.379	A(C18,C19,C21)	119.456
R(C25,C27)	1.374	A(N8,C24,C25)	118.872	R(C21,C22)	1.400	A(C19,C21,C22)	122.619
R(C27,C28)	1.391	A(N8,C24,C31)	122.725	R(C22,C23)	1.394	A(N3,C22,C21)	119.491
R(C28,C29)	1.393	A(C25,C24,C31)	118.400	R(C23,C24)	1.378	A(N3,C22,C23)	124.886
R(C29,C31)	1.384	A(C24,C25,C27)	119.795	R(C23,F64)	1.351	A(C21,C22,C23)	115.617
R(C33,C36)	1.517	A(F1,C27,C25)	117.121	R(C26,C29)	1.517	A(C22,C23,C24)	123.050
R(C39,C42)	1.515	A(F1,C27,C28)	119.175	R(C32,C35)	1.516	A(C22,C23,F64)	120.105
		A(C25,C27,C28)	123.696	R(O42,Fe43)	1.994	A(C24,C23,F64)	116.841
		A(N9,C28,C27)	120.704	R(Fe43,C54)	1.821	A(C18,C24,C23)	119.343
		A(N9,C28,C29)	124.132	R(Fe43,C56)	1.804	A(N3,C26,C29)	108.747
		A(C27,C28,C29)	115.120	$R(C,C)_{Cp}$ Av	1.415	A(O1,C29,C26)	111.386
		A(C28,C29,C31)	122.847	R(C54,O55)	1.125	A(O1,C32,C35)	111.308
		A(C24,C31,C29)	120.133	R(C56,O57)	1.129	A(N3,C35,C32)	109.741
		A(N9,C33,C36)	109.461	R(B,F) Av	1.402	A(C8,N40,C9)	144.134
		A(O5,C36,C33)	111.488	R(Cent,Fe43)	1.739		

The three methods, CAM-B3LYP, B3LYP and PBEPBE, predict a Fe-O bond length of 1.944, 2.011 and 2.001 Å, respectively. Experimentally the Fe-O bond has been observed at 1.957(2) Å (Darensbourg *et al*. 1981a and b); 1.984(13) and 1.944 (3) Å (Cotton *et al*. 1990) and 1.9686(13) Å (M'thiruaine *et al*. 2011c). Around the oxazolidinone ring the bond C17-O42 was observed at 1.233, 1.239 and 1.252 Å for CAM-B3LYP, B3LYP and PBEPBE, respectively. The corresponding values in the free LZD are 1.197, 1.201 and 1.211 Å for the respective methods while in the crystal structure this bond was obtained at 1.201 Å (Maccaroni *et al*., 2008). Hence upon coordination there is a slight elongation of the C-O bond as expected. Within the limits of theoretically obtained values the bond parameters around the oxazolidinone ring and the coordinated LZD molecule are in general agreement with crystallographic data of compounds with the oxazolidinone fragment and the linezolid polymorph II crystal structure (Maccaroni *et al*., 2008).

4.7.4 FTIR Spectra of Linezolid (LZD) and its Fp Complex Salt

The FTIR spectra of the ligand and its Fp complex salt are shown in Figure 4.23. The assignment of the observed bands in the spectra was aided by comparison with the theoretically determined frequencies and with data from literature on radezolid and tedizolid (Michalska *et al*., 2016; Michalska *et al*., 2017). Generally, the spectrum of the free linezolid molecule and that of the complex are more or less identical except in three distinct regions; around 2000 cm^{-1}, associated with the C≡O stretching band, 3054.30-3213.00 cm^{-1} associated with the stretching vibration mode of the C-H of the cyclopentadienyl ligand and 604.44, 566.50 and 543.70 cm^{-1} all associated with the stretching vibration mode of the C-C of the cyclopentadienyl fragment

In the FTIR spectrum of the complex salt very strong characteristic bands of the carbonyl functionality in the Fp fragment due to the asymmetric and symmetric ν(C≡O) stretches were observed at 2036.00 and 1979 cm^{-1}, respectively. For linezolid and its complex, bands related to the stretching vibration of C–H bonds were observed in the region of 2832-2996 cm^{-1} for the Fluoro-phenyl group and 3054-3213 cm^{-1} for the cyclopentadienyl fragment in the complex salt. The latter bands are absent in the free ligand. A strong band at 1144 cm^{-1} in the free ligand spectrum and 1143 cm^{-1} in the complex salt spectrum correspond to the scissoring vibrations of the C–H bonds in the F-phenyl ring, coupled with some stretching vibration of the C–F bond. Bands corresponding to the vibration of C–H bonds were also observed at 588.4, 829.2, 906.5 and 1183 cm^{-1}.

The bands observed at at 1273 cm^{-1} and 1475 cm^{-1} both in the free ligand and its complex are due to twisting vibrations of the C–H bond in the methyl acetamide fragment, scissoring vibrations of the C–H bonds in the oxazolidinone ring and rocking vibration of the C–H bonds in the Fluoro-phenyl ring. Medium band observed at 1631 cm^{-1} the free LZD spectrum and 1628 cm^{-1} in coordinated LZD spectrum is associated with stretching vibration of the C=C bonds in the Fluoro-phenyl ring. The band observed at 1273 cm^{-1} in both the free linezolid molecule and its complex is assignable to stretching vibration of the C–C bond in the Fluoro-phenyl ring. The band found at 1020 cm^{-1} in the two compounds is assignable to the stretching vibration modes of the C–C bonds in the oxazolidinone ring while the band at 1221 cm^{-1} corresponds to the stretching vibration modes of the C–C bonds. This region is also related with components of the stretching vibration of the C–N bond in the oxazolidinone ring, stretching vibration of the C–F bond and twisting vibration of the C–H bonds in the oxazolidinone ring.

The characteristic peaks in the FTIR spectrum of the free linezolid molecule at 1676 and 1754 cm^{-1} are due to stretching vibrations of the carbonyl (C=O) bonds in the methyl acetamide fragment and oxazolidinone ring, respectively. These bands are observed at 1676 and 1747 cm^{-1} and 1673 and 1748 cm^{-1} in the spectrum of the Fp-LZD complex salts. This shows that while the C=O stretch of the carbonyl in the methyl acetamide remains the same or undergoes a slight change upon coordination, the change in the position of the C=O stretch of the carbonyl group in the oxazolidinone fragment is greater upon coordination. This observation indicates that the metal centre coordinated to the LZD ligand through the oxygen atom of the oxazolidinone carbonyl group. This agrees well with the results obtained from the DFT computations.

The other characteristic stretching vibration modes are those of the C–N bonds. These are observed at 1328.98 and 1376.23 cm^{-1} in the free linezolid and 1328.98 and 1376.20 cm^{-1} in the Fp-LZD complex salt. Bands corresponding to N–H vibrations are also characteristic for linezolid and its related molecules such as radezolid and sutezolid. In this study bands related to this type of stretching vibration mode are observed at 3363.91 cm^{-1} both for the free linezolid molecule and its complex salt thus ruling out coordination via the amino nitrogen. Bands associated with the deformation vibration of the N-H bond were also observed. The bands of deformations in plane bending were assigned 1409.99 and 1445.67 cm^{-1}, and 1409.99 and 1444.71 cm^{-1} in the free linezolid and its complex respectively. The assignments made in this study are also supported by the literature (Michalska *et al.*, 2016***;*** Michalska *et al.*, 2017).

The bands corresponding to the stretching vibrations of the C-O bonds were observed as strong bands at 1220.96, 1115.84, 1102, and 1023.25 cm^{-1} in both the free ligand and the complex salt.

The occurrence of these bands at the same position in both the free molecule and the complex also rules out involvement of the cyclic oxygen atoms in the morphilinic and oxazolidinone rings in coordination the metal fragment. The band at 1220.96 cm^{-1} is also related to the C-H wagging vibration of the aromatic structure in the linezolid molecule. The bands which were observed at 1328.98 cm^{-1} and 1409.99 cm^{-1} correspond to the wagging vibrations of the C-H bonds and bending, stretching vibrations of the C-N-C bonds in the analysed molecules, respectively.

The band associated with (morphilinyl)-Fluoro-phenyl fragment was observed at 1237.00 cm^{-1} and 1237.00 cm^{-1} in the FTIR spectra of free linezolid and its complex. This band corresponds to the C-F bond and the stretching vibrations of the C-N bond from the oxazolidinone fragment. For this fragment, the stretching/wagging vibrations of C-H bonds, were observed at 871.00, 1144.00, 3089, 3130.00, and 3259.00 cm^{-1} in the free ligand and its complex salt.

Based on the analysis of the FTIR spectra of the free ligand and the complex there is no doubt that the Fp organometallic fragment successfully interacted with the active pharmaceutical agent linezolid to form a complex salt and linezolid acted as a monodentate/unidentate ligand with coordination to the central metal atom taking place through the carbonyl oxygen of the oxazolidinone ring to form a monometallic complex salt of the form [Fp(Linezolid)]BF_4.

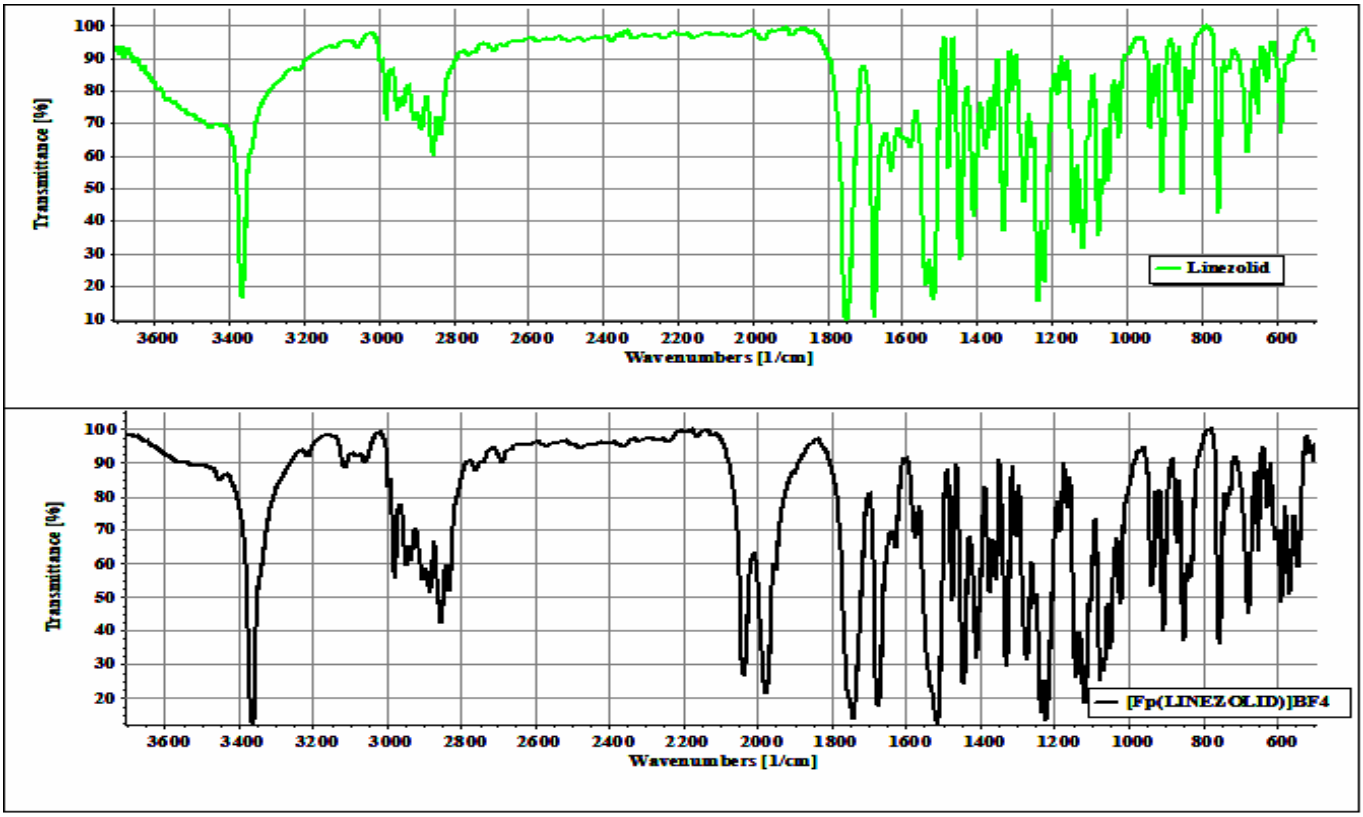

Figure 4.23: FTIR Spectra of Linezolid and its Fp Complex Salt

4.7.5 ^{1}H and ^{13}C NMR Spectra of Linezolid (LZD) and its Complex Salt

The ^{1}H NMR and ^{13}C NMR data of the free linezolid and its Fp complex salt in DMSO-d_6 are presented in Table 4.25. The complete assignments of the chemical shifts is also proposed both in the free ligand and the Fp complex based on the calculated NMR spectra obtained in this study and literature reports (Brickner *et al*., 1996; Yu and Huiyuan, 2002; Madhusudhan *et al*., 2005; Madhusudhan *et al*., 2008; Xu *et al*., 2008; Palumbo Piccionello *et al*., 2012; Greco *et al*., 2014 ; Mahy *et al*., 2014; Wielgus *et al*., 2015; Mahy *et al*., 2016;Taylor *et al*., 2017; Siddaraj *et al*., 2018). It is also important to note that although there are numerous reports of the experimental NMR data for virtually all the known forms of LZD, the the simulated NMR spectrum in DFT

for this compound is reported for the first time. From ^{13}C NMR perspective the largest chemical shift difference (Δδ) between the free linezolid molecule and its Fp complex salt occur at the carbonyl carbon (C23) of the oxazolidinone ring for which $\Delta\delta$ is about 0.48 ppm. This effect suggests that coordination of the central metal atom in Fp to the Linezolid molecule took place at the linezolid carbonyl oxygen of the oxazolidinone ring. This observation is also corroborated by the FTIR results and the results from the computational studies.

The slight difference in the chemical shift (Δδ) of the carbonyl carbon in the acetamide fragment between the free ligand and the complex also rules out the coordination via the oxygen in this portion of the molecule. A closer examination of Table 4-25 also reveals a slight difference in the chemical shift in the proton NMR for hydrogen number 7. This hydrogen atom is bonded to nitrogen in the acetamide portion of linezolid, thus a Fe-N bond is ruled out in the complex formed. From the NMR spectral data obtained the linezolid used was polymorph (II) known as (R) N-3-(3-Fluoro-4-morpholinylphenyl)-2-oxo 5-oxazolidylmethyl) acetamide or simply (R)-Linezolid (McCarthy, 2015).

Table 4.25: ^{1}H and ^{13}C NMR Chemical Shifts (ppm) of LZD and its Fp Complex in DMSO-d6

Chemical Shift, δ (ppm)			Δδ	Chemical shift, δ(ppm)			Δδ
H atom (s)	**LZD**	**[Fp(LZD)]BF_4**		**Carbon atom (s)**	**LZD**	**[Fp(LZD)]BF_4**	
H32	8.22	8.25	0.03	C14	170.80	170.89	0.09
H30	7.51	7.51	0.00	C27	155.90	156.21	0.31
H26	7.19	7.19	0.00	C23	154.04	154.52	0.48
H7	7.06	7.09	0.03	C28	136.34	136.10	-0.24
H19	4.71	4.72	0.01	C24	133.48	133.77	0.29
H21	4.08	4.10	0.02	C29	119.50	119.74	0.24
H22	3.74	3.73	0.00	C31	114.10	114.32	0.22
H(37,38,40,41)	3.65	3.68	0.03	C25	107.17	107.22	0.05
H(16,17)	3.40	3.44	0.04	C18	71.70	71.72	0.02
H(34,35,43,44)	2.96	2.96	0.00	C(36,39)	66.50	66.61	0.11
H(11,12,13)	1.83	1.83	-	C(33,42)	50.71	50.93	0.22
H on Cp	-	5.36	-	C20	47.29	47.55	0.26
H on Cp	-	5.01		C15	41.40	41.45	0.05
				C10	22.42	22.62	0.2
				C of CO in Fp	-	214.49	-
				C of Cp	-	89.08	-
				C of Cp	-	85.73	-

α atom numbering scheme of LZD structure as used in Figure 4.22

4.8 Terizidone (TZD) And Its Complex Salt $[Fp(TZD)]BF_4$

In this section the results on the local reactivity properties of the free terizidone (TZD) molecule, the molecular and spectroscopic properties of the active pharmaceutical agent TZD and its organometallic complex salt are presented and discussed in their respective subsections.

.

4.8.1 Regional or Local Reactivity Indices/ Functions of Terizidone (TZD)

The condensed Fukui functions obtained for TZD are presented in Table 4.7. The atomic numbering scheme adopted is shown in Figure 4.24.

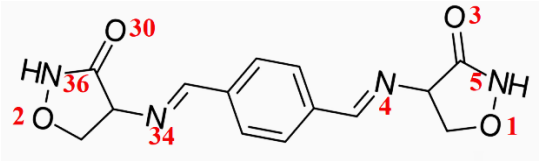

Figure 4.24: Terizidone (TZD) Showing the Numbering of the Heteroatoms

From the outset it should be noted that in the molecular structure of TZD we have two sets of equivalent heteroatoms, with O1, O3, N4 and N5 comprising the first set and O2, O30, N34 and N36 comprising the second set of heteroatoms. O1 is chemically equivalent to O2, while O3 is equivalent to O30, similarly N4 is chemically equivalent to N34 and lastly N5 is chemical equivalent to N36. Since we have two sets of equivalent heteroatoms consideration can be given to any one set of the heteroatoms without loss of generality. The condensed to atom Fukui indices computed using CAM-B3LYP and in the implementation of NBO charge partitioning scheme predicts O3 to be the most nucleophilic centre, followed closely by N4. The trend is O3 (0.066) > N4 (0.064) > O1(0.036) > N5 (0.028). However, in the same method, but using the values obtained from the Hirshfeld charges O3 is ranked a close second to O1. A similar observation is made for the Fukui indices computed using B3LYP. It should be noted here that

the Fukui indices have shown with consistence to chemical theory that chemically equivalent atoms have similar chemical attributes. Various studies have shown that terizidone (TZD) coordinates in monodentate fashion either through the oxygen of the keto group or through the nitrogen of the imino group of the isoxazole ring (Preti and Tosi, 1979; Preti *et al*., 1979; Preti *et al*., 1980; Preti *et al*., 1982; Preti *et al*., 1983).

Table 4.26: Terizidone Condensed to Atom Fukui Indices Calculated at 6-311G(2d,P) in DCM

	CAM-B3LYP/DCM						B3LYP/DCM					
	NBO			Hirshfeld			NBO			Hirshfeld		
	f_k^+	f_k^-	f_k^o	f_k^+	f_k^-	f_k^o	f_k^+	f_k^-	f_k^o	f_k^+	f_k^-	f_k^o
O1	0.015	0.036	0.025	0.009	0.036	0.023	0.017	0.082	0.049	0.015	0.063	0.039
O2	0.015	0.036	0.025	0.009	0.036	0.023	0.017	0.082	0.049	0.015	0.063	0.039
O3	0.031	0.066	0.048	0.036	0.033	0.035	0.042	0.095	0.068	0.026	0.073	0.049
N4	0.078	0.064	0.071	0.113	0.016	0.064	0.065	0.024	0.044	0.069	0.027	0.048
N5	0.021	0.028	0.025	0.052	0.026	0.039	0.015	0.039	0.027	0.037	0.075	0.056
C7	-0.011	0.015	0.002	0.062	0.059	0.061	0.023	0.015	0.019	0.060	0.039	0.049
C9	0.051	0.075	0.063	0.051	0.067	0.059	0.038	0.008	0.023	0.046	0.033	0.040
C10	-0.011	0.015	0.002	0.062	0.059	0.061	0.023	0.015	0.019	0.060	0.039	0.049
C12	0.046	0.002	0.024	0.075	0.070	0.072	0.019	0.005	0.012	0.073	0.040	0.056
C14	0.051	0.075	0.063	0.051	0.067	0.059	0.039	0.008	0.023	0.046	0.033	0.040
C15	0.030	-0.010	0.010	0.076	0.049	0.063	0.020	0.018	0.019	0.090	0.035	0.062
C17	0.030	-0.010	0.010	0.076	0.049	0.063	0.020	0.018	0.019	0.090	0.035	0.062
C19	-0.023	-0.022	-0.023	0.013	0.047	0.030	-0.037	0.003	-0.017	0.032	0.032	0.032
C21	-0.006	-0.012	-0.009	0.025	0.057	0.041	-0.011	-0.038	-0.024	0.039	0.060	0.049
C24	-0.023	-0.022	-0.023	0.013	0.047	0.030	-0.037	0.003	-0.017	0.032	0.032	0.032
C26	-0.006	-0.012	-0.009	0.025	0.057	0.041	-0.011	-0.038	-0.024	0.039	0.060	0.049
C29	-0.012	0.001	-0.005	-0.013	0.038	0.013	0.004	0.017	0.010	0.014	0.025	0.019
O30	0.031	0.066	0.048	0.036	0.033	0.035	0.042	0.095	0.068	0.026	0.073	0.049
C31	0.046	0.002	0.024	0.075	0.070	0.072	0.019	0.005	0.012	0.073	0.040	0.056
C33	-0.012	0.001	-0.005	-0.013	0.038	0.013	0.004	0.017	0.010	0.014	0.025	0.019
N34	0.078	0.064	0.071	0.113	0.016	0.064	0.065	0.024	0.044	0.069	0.027	0.048
N36	0.021	0.028	0.025	0.052	0.026	0.039	0.015	0.039	0.027	0.037	0.075	0.056

4.8.2 Optimized [Fp(TZD)]BF_4 with Fp Coordinated at the Various Donor Sites

From a chemical point of view Terizidone (TZD) is a cycloserine dimer which contains eight potential donor atoms consisting of nitrogen and oxygen heteroatoms. These can be reduced into four pairs of potential donor sites. The computed energies show that the coordination through the carbonyl oxygen atom is thermodynamically favoured with a relative energy of 0.000 kcal/mol Table 4.27 and Figure 4.25. This is followed by the complex in which the organometallic fragment is coordinated to the nitrogen atom bonded to the terephthallic fragment with a relative energy of 1.420 kcal/mol. All further calculations were therefore carried out on the structure in which the ligand is coordinated via the carbonyl oxygen atom.

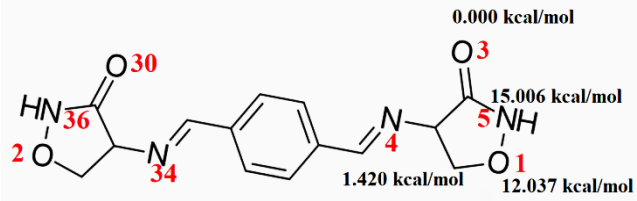

Figure 4.25: Energies of [Fp(TZD)]BF_4 Structures at the Various Coordination Sites

Table 4.27: Energies of [Fp(TZD)]BF_4 Structures at the Various Donor Sites

[(η^5-C_5H_5)Fe$(CO)_2$(TZD)]BF_4 structures	**Energy (kcal/mol)**	**Relative Energy**
Fp coordinated to L through oxazolidinone N atom 5 or 36	-1273538.924	15.006
Fp coordinated to L through carbonyl O 3 or 33	-1273553.930	0.000
Fp coordinated to L through N atom 5 or 36	-1273552.510	1.420
Fp coordinated to L through oxazolidinone O atom 2 or 10	-1273541.893	12.037

4.8.3 **Optimized TZD and [Fp(TZD)]BF_4 and Their Selected Bond Parameters**

The equilibrium geometries of TZD and its complex [Fp(TZD)]BF_4 are shown in Figure 4.26 and the selected bond parameters are presented in Table 4.28. In this study the calculated geometric parameters of the free and coordinated TZD were compared with those of cycloserine monohydrate and cycloserine hydrochloride (Turley and Pepinsky, 1956; Donohue, 1957; Turley and Pepinsky, 1957 and b; Lee *et al*., 1998; Ahmed *et al*., 2014). The bond parameters on the oxazolidinone ring of TZD show an overall agreement with the values of the cited literature taking into account the absence of intermolecular and crystal packing forces in gas phase.

The bonding around the iron centre in the TZD complex corresponds to that of a three-legged piano stool arrangement. The iron centre is coordinated to the cyclopentadienyl ligand (Cp) in a pentahapto fashion where the Cp ligand occupies three coordination sites. The two carbonyl ligands (CO) and the TZD occupy the three remaining coordination sites. The bond lengths between the central metal iron atom (Fe) and the centroid of the cyclopentadienyl (Cp) ring are 1.733, 1.762 and 1.729 Å for CAM-B3LYP, B3LYP and PBEPBE, respectively. A typical Cp centroid–Fe bond for Fe–O bonded Fp complexes is usually observed at a range of 1.71 - 1.72 Å (Darensburg *et al*., 1981; M'thiruaine *et al*. 2011c**).** Hence the results show that the B3LYP method gives a slight overestimation of this particular bond.

The average Fe-$C_{C\equiv O}$ bond lengths obtained were 1.817Å for CAM-B3LYP, 1.809 Å for B3LYP and 1.762 Å for PBEPBE. These distances are within the range of experimentally

observed data (Mackie and Baird, 1992; Zeng and Li, 2011; M'thiruaine *et al*., 2012a, b, c, d, e and f). From the structure we get an average of C-C bond for the Cp ring of 1.415, 1.421 and 1.430 Å for CAM-B3LYP, B3LYP and PBEPBE, respectively. The three methods predict a Fe-O bond length of 1.983, 2.004 and 2.015 Å for CAM-B3LYP, B3LYP and PBEPBE, respectively. Experimentally the Fe-O bond has been observed at 1.957(2) Å, (Darensbourg *et al*. 1981a, b), 1.9844(13) Å and 1.9686(13) Å (M'thiruaine *et al*. 2011c). For the B-F-bond length CAM-B3LYP, B3LYP and PBEPBE gave a range of 1.361-1.428 Å, 1.367-1.429 Å 1.372-1.422 Å, respectively. Experimentally, this bond has been observed at a range of 1.382(3)- 1.397(3) Å (M'thiruaine *et al*., 2012a, b, c, d, e and f).

In terms of bond angles the characteristic O-C-Fe bond normally observed at a range of 176-179° here was obtained at range of 176.049 – 176.634°. The average C-C-C bond of the Cp ring had an average of 122.447° for all the three methods. The C-Fe-C bond was observed at a range of 93.976-95.846°. The F-B-F bond angles obtained were within the range of 107.999-112.580° for CAM-B3LYP, 107.867- 112.971° for B3LYP and 106.643-113.540° for the PBEPBE method. The CAM-B3LYP and B3LYP results for this bond are in excellent agreement with experimentally observed data (M'thiruaine *et al*., 2012a, b, c, d, e and f). Generally, the three methods give a good molecular description of the Fp structure. The slight deviation of the bond parameters of theoretical computed values from experimentally observed data arise from the fact that the calculations were carried out in gas phase while crystallographic data usually emanates from solids where crystal packing forces are in play. It is also good to note that the ligand used here is structurally

different from the ligands in the cited reports the only similarity in the systems being the Fe-O bond in a cationic Fp organometallic complex. It is also important to mention that the theoretical analysis of the molecular and spectroscopic properties of TZD is reported for the first time by this study.

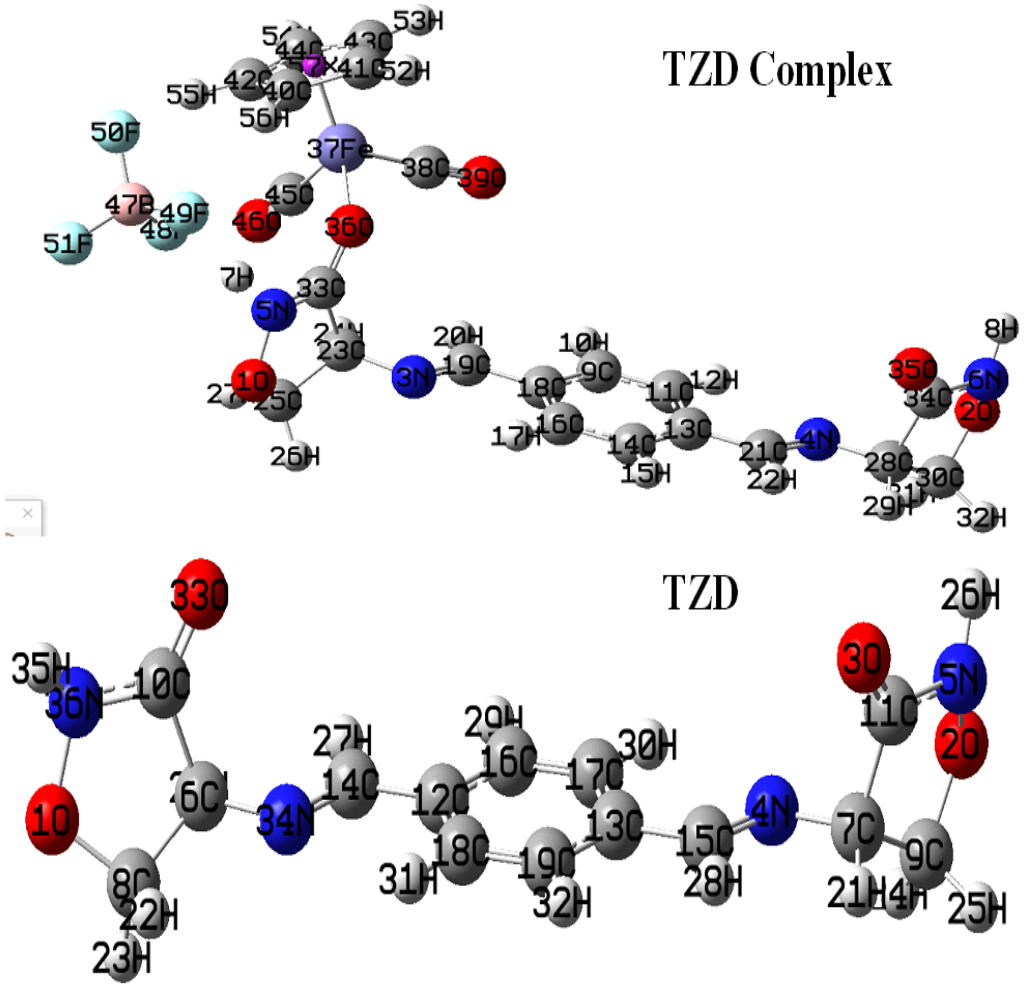

Figure 4.26: Geometries of TZD and [Fp(TZD)]BF_4 Showing the Atom Numbering

Table 4.28: Selected Geometric Parameters of TZD and its Complex

TZD				[Fp(TZD)]BF_4	
Bond Length (Å)		**Bond Angle (◦)**		**Bond Length**	**(Å)**
R(O1,N5)	1.409	A(N5,O1,C21)	103.237	R(C40-C41)	1.423
R(O1,C21)	1.432	A(C26,O2,N36)	103.238	R(C41-C43)	1.407
R(O2,C26)	1.432	A(C15,N4,C19)	117.725	R(C43-C44)	1.42
R(O2,N36)	1.409	A(O1,N5,C33)	111.579	R(C44-C42)	1.426
R(O3,C33)	1.203	A(C14,C7,C31)	120.715	R{$(C\text{-}C)_{Cp}$ Av}	1.401
R(N4,C15)	1.265	A(C10,C9,C17)	119.266	R(Cp-Fe37)	1.733
R(N4,C19)	1.443	A(C10,C9,C31)	119.376	R(Fe37-C38)	1.809
R(N5,C33)	1.368	A(C17,C9,C31)	121.358	R(Fe37-C45)	1.825
R(C7,C14)	1.396	A(C9,C10,C12)	120.715	R(C38-O39)	1.129
R(C7,C31)	1.382	A(C10,C12,C14)	119.909	R(C45-O46)	1.125
R(C9,C10)	1.396	A(C7,C14,C12)	119.376	R(Fe37-O36)	1.983
R(C9,C17)	1.47	A(C7,C14,C15)	119.266	R(O36-C33)	1.235
R(C9,C31)	1.394	A(C12,C14,C15)	121.358	**Bond Angle**	**(◦)**
R(C10,C12)	1.382	A(N4,C15,C14)	122.762	A(C40-C41-C43)	108.015
R(C12,C14)	1.394	A(C9,C17,N34)	122.762	A(C41-C43-C44)	108.271
R(C14,C15)	1.47	A(N4,C19,C21)	112.494	A(C43-C44-C42)	107.224
R(C17,N34)	1.265	A(N4,C19,C33)	108.283	A(C44-C42-C40)	108.38
R(C19,C21)	1.524	A(C21,C19,C33)	101.131	A(C42-C40-C41)	108.015
R(C19,C33)	1.541	A(O1,C21,C19)	105.326	A(Cp-Fe37-C38)	124.434
R(C24,C26)	1.524	A(C26,C24,C29)	101.132	A(Cp-Fe37-C45)	121.113
R(C24,C29)	1.541	A(C26,C24,N34)	112.493	A(Fe37-C38-O39)	177.839
R(C24,N34)	1.443	A(C29,C24,N34)	108.283	A(Fe37-C45-O46)	174.259
R(C29,O30)	1.203	A(O2,C26,C24)	105.327	A(C38-Fe37-C45)	95.539
R(C29,N36)	1.368	A(C24,C29,O30)	127.37	A(Cp-Fe37-O36)	118.153
		A(C24,C29,N36)	106.063	A(O36-Fe37-C38)	93.696
		A(O30,C29,N36)	126.542	A(O36-Fe37-C45)	97.348
				A(Fe37-O36-C33)	140.025

4.8.4 FTIR Spectra of Terizidone (TZD) and its Complex Salt

The reaction of Lewis acid $[Cp(CO)_2Fe]BF_4$ with terizidone gave a dark orange solid tending to brown. The solid was found to be soluble in DCM, acetone, water, DMSO and THF. The infrared spectra of the Terizidone ligand and its Fp complex in the region

4000-500 cm^{-1} are shown in Figure 4.27. Upon coordination of TZD the band associated with the υ(C=O) stretching vibration mode was split into two bands observed at 1637.59 cm^{-1} and 1607.70 cm^{-1}. This behaviour has also been observed in chromium and ruthenium Terizidone complexes (Preti *et al.,* 1982). In the free TZD molecule the band associated with υ(C=O) stretching mode occurs at 1637.00 cm^{-1}. This mode has been observed at 1640 cm^{-1} by other workers (Preti and Tosi, 1980 a and b; Preti *et al*., 1982; Preti *et al*., 1983).

In the coordinated TZD the band observed at 1703.00 cm^{-1} is assignable to the υ(C=N) stretching mode. In the uncoordinated TZD this band was observed at 1706.00 cm^{-1}. The presence of the Fp organometallic fragment in the complex salt was confirmed by the two very strong terminal carbonyl stretching frequencies υ(C≡O) at 2124.00 cm^{-1} and 2068.00 cm^{-1} due to the asymmetric and symmetric stretches, respectively. The presence of the counter ion (anion) BF_4^- in the compound is indicated by a very strong band observed at 1058.00 cm^{-1} associated with the υ(B-F) stretching vibration mode. The coordination of Terizidone to the iron metal centre via the oxygen atom of the keto group of the oxazolidinone ring is also corroborated by the DFT studies carried out on this molecule as shown earlier on.

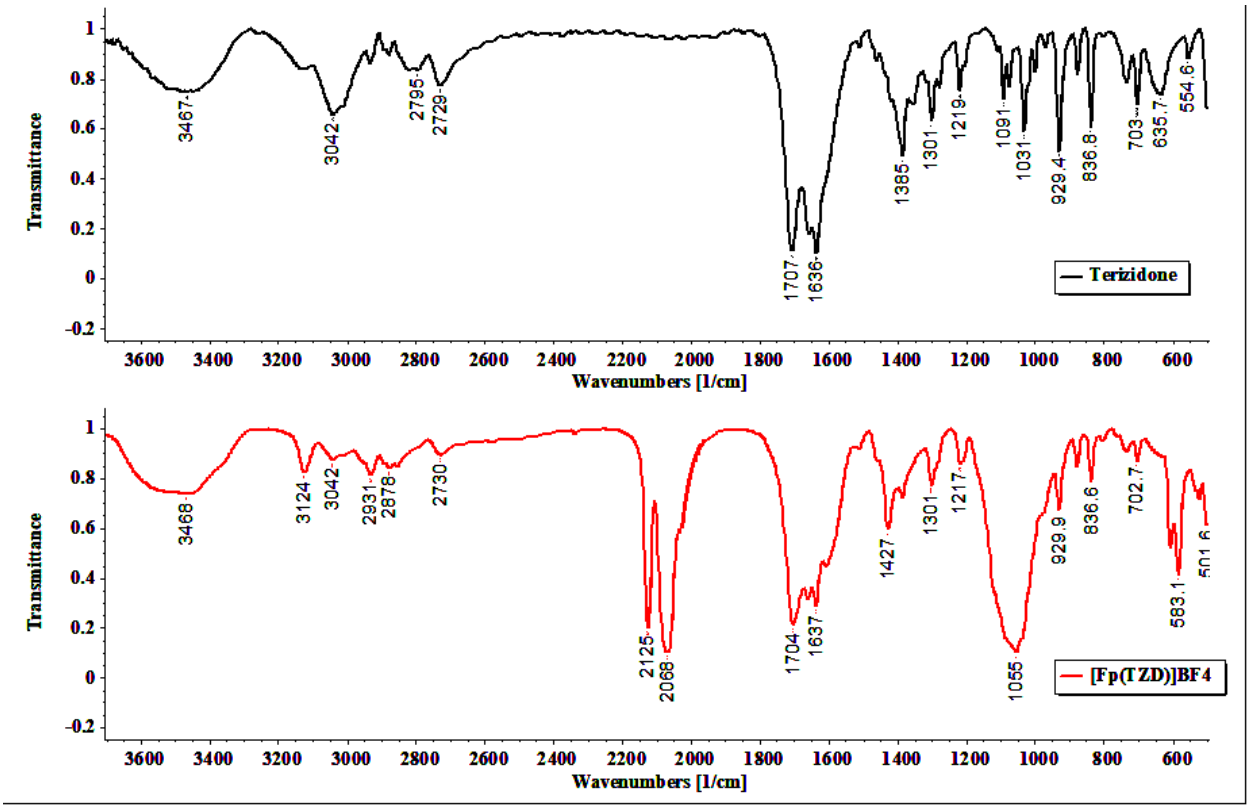

Figure 4.27: FTIR Spectra of Terizidone and its Fp Complex Salt

4.9 Elemental Analysis

The elemental analysis data of the complexes are presented in Table 4.29. All the complexes formed are micro-crystalline solids with moderate to high yields (61% to 87%). Furthermore, the complexes are stable in air and in various solvent systems such as THF, DCM and DMSO. This can be corroborated by the fact that the biological tests and FTIR-ATR and NMR experiments were performed in these solvents without loss of information. The elemental analysis of the complex salts for carbon (C), nitrogen (N), sulphur (S) and hydrogen (H) show that the complexes are monometallic with the APA/API ligands acting as unidentate ligands despite the multiple potential coordination sites.

Table 4.29: Elemental Analysis of the Synthesized Complexes[Ψ]

Compound	Empirical Formula	Elemental Composition Found (Calculated) %							
		C		H		N		S	
[(□^{5}-C_5H_5)$(CO)_2$Fe] (3-ASA)]BF_4	$C_{14}H_{12}BF_4FeNO_5$	40.12	(40.33)	2.89	(2.90)	3.33	(3.36)		
[(□^{5}-C_5H_5)$(CO)_2$Fe] (4-ASA)]BF_4	$C_{14}H_{12}BF_4FeNO_5$	39.53	(40.33)	2.81	(2.90)	3.34	(3.36)		
[(□^{5}-C_5H_5)$(CO)_2$Fe] (5-ASA)]BF_4	$C_{14}H_{12}BF_4FeNO_5$	40.22	(40.33)	2.88	(2.90)	3.32	(3.36)		
[(□^{5}-C_5H_5)$(CO)_2$Fe] (ETH)]BF_4	$C_{15}H_{15}BF_4FeN_2O_2S$	41.48	(41.90)	3.46	(3.52)	6.50	(6.52)	7.44	(7.46)
[(□^{5}-C_5H_5)$(CO)_2$Fe] (PTH)]BF_4	$C_{16}H_{17}BF_4FeN_2O_2S$	42.63	(43.28)	3.81	(3.86)	6.25	(6.31)	7.08	(7.22)
[(□^{5}-C_5H_5)$(CO)_2$Fe] (TZD)]BF_4	$C_{21}H_{19}BF_4FeN_4O_6$	44.34	(44.56)	3.34	(3.38)	9.80	(9.90)		
[(□^{5}-C_5H_5)$(CO)_2$Fe] (LZD)]BF_4	$C_{23}H_{25}BF_5FeN_3O_6$	45.82	(45.96)	4.14	(4.19)	6.92	(6.99)		

[Ψ]The Carbon, Hydrogen, Sulphur and Nitrogen analyses were determined at the ICP-MS Laboratory Central Analytical Facilities Stellenbosch University.

4.10 Antibacterial Tests (Bioassay)

The complex [Fp(TZD)]BF_4 only showed moderate activity against *Escherichia coli* and *Salmonella typhi* as compared to the free molecule, and showed comparable activity against *Enterococcus faecalis.* However, the complex had no activity for *Staphylococcus aureus* and *Bacillus subtilis.* The Fp complex of linezolid showed moderate activity against *Escherichia coli* and had no activity against *Salmonella typhi*. However; the activities of this complex against *Pseudomonas aeruginosa*, *Bacillus subtilis* and *Enterococcus faecalis* were comparable to the free linezolid molecule. Linezolid as a molecule is active against both antibiotic-susceptible and antibiotic-resistant aerobic gram-positive cocci, as well as methicillin-resistant (MRSA) and methicillin-susceptible (MSSA) strains of *Staphylococcus aureus* and is also active against vancomycin-resistant *Enterococcus faecium* (VRE). Moreover, this molecule is the drug of choice for dealing with methicillin resistant *Staphylococcus aureus* (MRSA) (Rathnanand *et al*., 2016). However, cases of resistance to this drug have been reported (Long and Vester. 2011). Thus modifying its structure to include a metal may help in overcoming the resistance.

The free prothionamide (PTH) molecule didn't show any activity against all the bacterial strains investigated. However, on complexation to the Fp, some moderate activity was observed against *P. aeruginosa* and *E. faecalis*. A similar observation was made on its structural analog ethionamide (ETH) where the free molecule showed only limited activity against *Escherichia coli* but upon coordination to the Fp organometallic moiety some moderate activity was observed against *Pseudomonas aeruginosa Staphylococcus aureus*, and *Enterococcus faecalis*.

The free aminosalicylic acid (ASA) ligands showed no activity at all against the tested bacterial strains. However, slight activities against *Staphylococcus aureus, Pseudomonas aeruginosa, Bacillus subtilis* and *Enterococcus faecalis* were observed on the Fp organometallic complex salts of 4-aminosalicylic acid (4-ASA), while the complex salt of 3-ASA showed some activity against *Escherichia coli, Pseudomonas aeruginosa*, and *Enterococcus faecalis* while the Fp complex salt of 5-ASA had some encouraging activity against *Pseudomonas aeruginosa* (Pa), *Staphylococcus aureus, Bacillus subtilis* and *Enterococcus faecalis* with zones of inhibition ≈10 mm. This shows that coordination confers some bioactivity to these ASA molecules against the tested bacterial strains.

Overall, of all the complexes synthesized and tested for bioactivity the Linezolid and Terizidone complex salts had the highest bioactivity with inhibition zones of >20 mm implying that the introduction of a metal did not diminish the activities of the ligands. It should also be noted that INH, ETH, PTH are quite bioactive against the *Mycobacterium tuberculosis* (Mtb) bacteria but show no response to other microbial forms (DeBarber *et al*., 2000). Generally, the structural modifications of 3-ASA, 4-ASA, 5-ASA, ETH and PTH expanded their therapeutic activity to include some Gram-positive and Gram-negative organisms for which the free molecules had no effect on. Furthermore, it is worth noting that that compounds involving metal centres may work via new alternative mechanisms of action which cannot be mimicked by organic drugs. At the molecular level, their vocation is to trigger cellular effects by redox and/or by coordinative processes. Therefore, although the bioactivities of the complexes of LZD and TZD were comparable to the uncoordinated molecules against some organisms, the derivatization of

these purely organic drugs to include a metal in the form of an organometallic fragment may have the potential of optimizing further the performance of these drugs and even overcome drug resistance.

Table 4.30: Screening for Antibacterial Activity of the $[(\eta^5\text{-}C_5H_5)(CO)_2Fe](APA)]BF_4$ Compounds

	Bacteria and Inhibition zone (mm)					
	Gram (-Ve)			**Gram (+Ve)**		
Compound	*E. coli*	*S. typhi*	*P. aeruginosa*	*S. aureus*	*B. subtilis*	*E. faecium*
Prothionamide (PTH)	-	-	-	-	-	-
$[(\eta^5\text{-}C_5H_5)(CO)_2Fe]$ (PTH)]BF_4	-	-	6.5	-	-	7
Terizidone (TZD)	23	24	-	20	22	21
$[(\eta^5\text{-}C_5H_5)(CO)_2Fe]$ (TZD)]BF_4	11	9	-	-	-	23
Linezolid	12	8	-	>32	>32	>32
$[(\eta^5\text{-}C_5H_5)(CO)_2Fe]$ (LZD)]BF_4	7	-	-	>32	>30	28
Ethionamide(ETH)	6.5	-	-	-	-	-
$[(\eta^5\text{-}C_5H_5)(CO)_2Fe]$ (ETH)]BF_4	-	-	-	8	15	7
3-Aminosalicylic acid (3-ASA)	-	-	-	-	-	-
[Fp(3-ASA)]BF_4	8	-	7	-	-	8
4-Aminosalicylic acid (4-ASA)	6.5	-	-	-	-	-
$[(\eta^5\text{-}C_5H_5)(CO)_2Fe$(4-ASA)]$BF_4$	-	-	7	9	7	9
5-Aminosalicylic acid (5-ASA)	-	-	-	-	-	-
$[(\eta^5\text{-}C_5H_5)(CO)_2Fe$ (5-ASA)]BF_4	-	-	6.5	10	8	11
1% DMSO	-	-	-	-	-	-

(-) no bioactivity,

CHAPTER FIVE

CONCLUSIONS AND RECOMMENDATIONS

5.1 Conclusions

i. The ligation properties of the active pharmaceutical agents; ethionamide (ETH), prothionamide (PTH), linezolid (LZD), terizidone (TZD), 3-aminosalicylic acid (3-ASA), 4-aminosalicylic acid (4-ASA) and 5-aminosalicylic acid (5-ASA) were calculated in gas phase and in various solvent systems (to mimic the reaction conditions) based on the global and local reactivity indices. Globally the molecules were shown to be nucleophilic towards the electron deficient iron organometallic fragment $[(\eta^5\text{-}C_5H_5)(CO)_2Fe]^+$ while the regional reactivity descriptors revealed the O, N and S heteroatoms to be the most nucleophilic sites in the molecules.

ii. The geometric and spectroscopic properties of the free ligands and the complexes were calculated using three DFT functionals namely CAM-B3LYP, B3lYP and PBEPBE with mixed basis sets; LANL2DZ, 6-311G(2d,p) and 6-311G(d,p) *in vacuo* and in various solvent systems. The results obtained were found to be consistent with experimentally observed data from this study and from literature.

iii. The molecular structures of the seven active pharmaceutical agents namely; ethionamide (ETH), prothionamide (PTH), linezolid (LZD), terizidone (TZD), 3-aminosalicyli acid (3-ASA), 4-aminosalicylic acid (4-ASA) and 5-aminosalicylic acid (5-ASA) were successfully modified by coordinating each of them to the organometallic fragment $[(\eta^5\text{-}C_5H_5)(CO)_2Fe]^+$. The resultant organometallic complex salts were characterized by FTIR spectroscopy, NMR spectroscopy and

elemental analysis and complexation to the central metal atom in $[Cp(CO)_2Fe]^+$ confirmed. For linezolid and terizidone the coordination occurred via the carbonyl oxygen heteroatom while in 3-aminosalicylic acid, 4-aminosalicylic acid, 5-aminosalicylic acid, ethionamide and prothionamide the coordination occurred via the amine nitrogen atom. Here the experimental results and the computational results complemented one another.

iv. The bacterial bioassays showed that the introduction of the organometallic fragment $[(\eta^5\text{-}C_5H_5)(CO)_2Fe]^+$ in the molecular structures of 3-ASA, 4-ASA, 5-ASA, ETH, PTH conferred the ability to inhibit the growth of some pathogenic bacteria. The free ligands were not active against the studied bacteria. On the other hand the introduction of the metal fragment into the molecular structures of LZD and TZD not only produced compounds with comparable *in vitro* bioactivities against the tested bacteria but with the additional advantage of having a metal in their structural motif hence a potentially different mode of action.

5.2 Recommendations

5.2.1 From this Study

i. Some of the organometallic derivatives synthesized in this study have shown comparable biological activity to the free APA ligands. Some even show biological activity to some bacterial strains that the free APA ligand normally is inactive. Thus, it is recommended that the Fp organometallic could forms a new structure modification strategy in drug development.

ii. Molecular modelling can be used as a tool to reliably predict the properties of yet to be synthesized organometallic compounds and to give useful insights into experimentally observed properties.

5.2.2 For Further Study

i. Minimum inhibitory concentrations studies should be carried out on the compounds reported herein

ii. Further biological tests should be carried out on different microorganisms in particular the ones against which the seven selected pharmaceutical agents are used against.

iii. Mechanism of action of the organometallic salts should be investigated

iv. Effect of different counter ions should be investigated.

v. The effect of change of the metal centre should be investigated

vi. Investigate the effect of using different forms of the cyclopentadienyl ligand

vii. Docking studies should be carried out.

REFERENCES

Adamo, C. and Barone, V. (1999). Toward Reliable Density Functional Methods Without Adjustable Parameters: The PBE0 model. *The Journal of Chemical Physics,* **110**, 6158–6170.

Ahmed, M., Wang, F., Acres, R. G. and Prince, K. C. (2014). Structures of Cycloserine and 2-Oxazolidinone Probed by X-Ray Photoelectron Spectroscopy: Theory and Experiment. *The Journal of Physical Chemistry A,* **118**, 3645–3654.

Akkaya, Y. and Akyuz, S. (2006). Infrared and Raman Spectra, *Ab Initio* Calculations Vibrational Assignment of 4-Aminosalicylic Acid. *Vibrational Spectroscopy*, **42**, 292–301.

Albert, A. (1958). Chemical Aspects of Selective Toxicity. *Nature*, (1958). **4633**, 421-423.

Baldenebro-Lopez, J. Flores-Holguin, N., Castorena-Gonzalez, J., Almaral-Sanchez, J. and Glossman-Mitnik, D. (2013). Theoretical Study of Copper Complexes: Molecular Structure, Properties, and its Application to Solar Cells. *International Journal of Photoenergy*, **2013**, 1–7.

Barry, N. P. E., and Sadler, P. J. (2013). Exploration of the Medical Periodic Table: Towards New Targets. *Chemical Communications*, **49**, 5106-5110.

Basit Wani, A., Singh, J. and Upadhyay, N. (2017). Synthesis and Characterization of Transition Metal Complexes of Para-Aminosalicylic Acid with Evaluation of their Antioxidant Activities. *Oriental Journal of Chemistry*, **33**, 1120–1126.

Becke, A. D. (1988). Density-Functional Exchange-Energy Approximation with Correct Asymptotic Behaviour. *Physical Review A,* **38**, 3098–3100.

Becke, A. D. (1993). Density-Functional Thermochemistry. III. The Role of Exact Exchange. *The Journal of Chemical Physics,* **98**, 5648–5652.

Becke, A. D. (2014). Perspective: Fifty Years of Density-Functional Theory in Chemical Physics. *The Journal of Chemical Physics,* **140**, 18A301-17.

Bertinotti, F., Giacomello, C. and Liquori, A. M. (1954). Crystals and Molecular Structure of p-Amino-Salicylic Acid. *Acta Crystallographica*, **7**, 808–812.

Biot, C., Delhaes, L., Abessolo, H., Domarle, O., Maciejewski, L. ., Mortuaire, M. and Brocard, J. (1999a). Novel Metallocenic Compounds as Antimalarial Agents. Study of the Position of Ferrocene in Chloroquine. *Journal of Organometallic Chemistry*, **589**, 59–65.

Biot, C., Delhaes, L., Maciejewski, L. A., Mortuaire, M., Camus, D., Dive, D. and Brocard, J. S. (2000). Synthetic Ferrocenic Mefloquine and Quinine Analogues as Potential Antimalarial Agents. *European Journal of Medicinal Chemistry*, **35**, 707–714.

Biot, C., Delhaes, L., N'Diaye, C. M., Maciejewski, L. A., Camus, D., Dive, D. and Brocard, J. S. (1999b). Synthesis and Antimalarial Activity *In Vitro* of Potential Metabolites of Ferrochloroquine and Related Compounds. *Bioorganic and Medicinal Chemistry, **7**,* 2843–2847.

Biot, C., Glorian, G., Maciejewski, L. A., Brocard, J. S., Domarle, O., Blampain, G. and Lebibi, J. (1997). Synthesis and Antimalarial Activity *In Vitro* and *In Vivo* of a New Ferrocene−Chloroquine Analogue. *Journal of Medicinal Chemistry,* **40**, 3715–3718.

Biot, C., Nosten, F., Fraisse, L., Ter-Minassian, D., Khalife, J. and Dive, D. (2011). The Antimalarial Ferroquine: From Bench to Clinic. *Parasite*, **18**, 207–214.

Blackie, M. A. L. and Chibale, K. (2008). Metallocene Antimalarials: The Continuing Quest. *Metal-Based Drugs,* **2008**, 1–10.

Blackie, M. A. L., Beagley, P., Croft, S. L., Kendrick, H., Moss, J. R. and Chibale, K. (2007). Metallocene-Based Antimalarials: An Exploration into the Influence of the Ferrocenyl Moiety on *In Vitro* Antimalarial Activity in Chloroquine-Sensitive and Chloroquine-Resistant Strains of *Plasmodium falciparum*. *Bioorganic and Medicinal Chemistry,* **15**, 6510–6516

Blomberg, M. R. A., Borowski, T., Himo, F., Liao, R.-Z. and Siegbahn, P. E. M. (2014). Quantum Chemical Studies of Mechanisms for Metalloenzymes. *Chemical Reviews,* **114**, 3601–3658.

Borowski, A. F. and Cole-Hamilton, D. J. (1993). Structures and Properties of Anthranilato- and N-Phenylanthranilato-Rhodium(I) Complexes Containing Triphenylphosphine Ligands. *Polyhedron*, **12**, 1757–1765.

Boucher, H. W., Talbot, G. H., Bradley, J. S., Edwards, J. E., Gilbert, D., Rice, L. B. and Bartlett, J. (2009). Bad Bugs, No Drugs: No ESKAPE! An Update from the Infectious Diseases Society of America. *Clinical Infectious Diseases*, **48**, 1–12.

Bourque, T. A., Nelles, M. E., Gullon, T. J., Garon, C. N., Ringer, M. K., Leger, L. J. and Westcott, S. A. (2005). Late Metal Salicylaldimine Complexes Derived From 5-Aminosalicylic Acid — Molecular Structure of a Zwitterionic Mono Schiff Base Zinc Complex. *Canadian Journal of Chemistry,* **83**, 1063–1070.

Bradford, P. A., Bratu, S., Urban, C., Visalli, M., Mariano, N., Landman, D. and Quale, J. (2004). Emergence of Carbapenem-Resistant Klebsiella Species Possessing the Class A Carbapenem-Hydrolyzing KPC-2 and Inhibitor-Resistant TEM-30 -Lactamases in New York City. *Clinical Infectious Diseases,* **39**, 55–60.

Brickner, S. J., Hutchinson, D. K., Barbachyn, M. R., Manninen, P. R., Ulanowicz, D. A., Garmon, S. A. and Zurenko, G. E. (1996). Synthesis and Antibacterial Activity of U-100592 and U-100766, two Oxazolidinone Antibacterial Agents for the Potential Treatment of Multidrug-Resistant Gram-Positive Bacterial Infections. *Journal of Medicinal Chemistry*, **39**, 673–679.

Bruijnincx, P. C. and Sadler, P. J. (2008). New Trends for Metal Complexes with Anticancer Activity. *Current Opinion in Chemical Biology*, **12**, 197–206.

Bühl, M., Reimann, C., Pantazis, D. A., Bredow, T., and Neese, F. (2008). Geometries of Third-Row Transition-Metal Complexes from Density-Functional Theory. *Journal of Chemical Theory and Computation*, **4**, 1449–1459.

Cárdenas, C., Tiznado, W., Ayers, P. W. and Fuentealba, P. (2011). The Fukui Potential and the Capacity of Charge and the Global Hardness of Atoms. *The Journal of Physical Chemistry A*, **115**, 2325–2331.

Cázares-Marinero, J. de J., Lapierre, M., Cavaillès, V., Saint-Fort, R., Vessières, A., Top, S. and Jaouen, G. (2013). Efficient New Constructs Against Triple Negative Breast Cancer Cells: Synthesis and Preliminary Biological Study of Ferrocifen–SAHA Hybrids and Related Species. *Dalton Transactions*, **42**, 15489–15501.

Cázares-Marinero, J. de J., Top, S., Vessières, A. and Jaouen, G. (2014). Synthesis and Antiproliferative Activity of Hydroxyferrocifen Hybrids against Triple-Negative Breast Cancer Cells. *Dalton Transactions*, **43**, 817–830.

Cerda-Monje, A., Ormazábal-Toledo, R., Cárdenas, C., Fuentealba, P. and Contreras, R. (2014). Regional Electrophilic and Nucleophilic Fukui Functions Efficiently Highlight the Lewis Acidic/Basic Regions in Ionic Liquids. *The Journal of Physical Chemistry B*, **118**, 3696–3701.

Chamorro, E., Chattaraj, P. K. and Fuentealba, P. (2003). Variation of the Electrophilicity Index along the Reaction Path. *The Journal of Physical Chemistry A*, **107**, 7068–7072.

Chamorro, E., Contreras, R. and Fuentealba, P. (2000). Some Relationships within the Nonlocal (Pair–Site) Chemical Reactivity Formalism Of Density Functional Theory. *The Journal of Chemical Physics*, **113**, 10861–10866.

Chamorro, E., Duque, M., Cárdenas, C., Santos, J., Tiznado, W. and Fuentealba, P. (2005). Condensation Of The Highest Occupied Molecular Orbital within the Electron Localization Function Domains. *Journal of Chemical Sciences*, **117**, 419–424.

Chamorro, E., Fuentealba, P. and Contreras, R. (2001). Higher Order Derivatives for Nuclear Indexes in the Framework of Density Functional Theory. *The Journal of Chemical Physics*, **115**, 6822–6826.

Chamorro, E., Pérez, P. and Domingo, L. R. (2013). On The Nature Of Parr Functions to Predict the Most Reactive Sites Along Organic Polar Reactions. *Chemical Physics Letters*, **582**, 141–143.

Chan, J. C. C. and Au-Yeung, S. C. F. (1997). A Comparative Study of the Calculation of ^{59}Co NMR Shielding Constants of Hexacoordinated Diamagnetic Co(III) Complexes Using DFT-IGLO and DFT-GIAO Methods. *Journal of Molecular Structure: Theochem*, **393**, 93–96.

Chattaraj, P. K. and Schleyer, P. V. R. (1994). An Ab Initio Study Resulting in a Greater Understanding of the HSAB Principle. *Journal of the American Chemical Society,* **116**, 1067–1071.

Chattaraj, P. K., Chakraborty, A. and Giri, S. (2009). Net Electrophilicity. *The Journal of Physical Chemistry A,* **113**, 10068–10074.

Chattaraj, P. K., Chamorro, E. and Fuentealba, P. (1999). Chemical Bonding and Reactivity: A Local Thermodynamic Viewpoint. *Chemical Physics Letters,* **314**, 114–121.

Chattaraj, P. K., Fuentealba, P., Gómez, B. and Contreras, R. (2000). Woodward−Hoffmann Rule in the Light of the Principles of Maximum Hardness and Minimum Polarizability: DFT and *Ab Initio* SCF Studies. *Journal of the American Chemical Society,* **122**, 348–351.

Chattaraj, P. K., Gómez, B., Chamorro, E., Santos, J. and Fuentealba, P. (2001). Scrutiny of the HSAB Principle in Some Representative Acid−Base Reactions. *The Journal of Physical Chemistry A,* **105**, 8815–8820.

Chattaraj, P. K., Maiti, B. and Sarkar, U. (2003). Philicity: A Unified Treatment of Chemical Reactivity and Selectivity. *The Journal of Physical Chemistry A,* **107**, 4973–4975.

Chattaraj, P. K., Sarkar, U. and Roy, D. R. (2006). Electrophilicity Index. *Chemical Reviews,* **106**, 2065–2091.

Chattaraj, P. K., Sarkar, U., Parthasarathi, R. and Subramanian, V. (2005). DFT Study Of Some Aliphatic Amines Using Generalized Philicity Concept. *International Journal of Quantum Chemistry,* **101**, 690–702.

Chen, H., Parkinson, J. A., Parsons, S., Coxall, R. A., Gould, R. O. and Sadler, P. J. (2002). Organometallic Ruthenium (II) Diamine Anticancer Complexes: Arene-Nucleobase Stacking and Stereospecific Hydrogen-Bonding in Guanine Adducts. *Journal of the American Chemical Society,* **124**, 3064–3082.

Chen, X.-B., Ye, Q., Wu, Q., Song, Y.-M., Xiong, R.-G., and You, X.-Z. (2004). The First Organometallic Carbonyl Tungsten Complex of Antibacterial Drug Norfloxacin. *Inorganic Chemistry Communications*, **7**, 1302–1305.

Chermette, H. (1998). Density Functional Theory. *Coordination Chemistry Reviews,* **178**, 699–721.

Chermette, H. (1999). Chemical Reactivity Indexes in Density Functional Theory. *Journal of Computational Chemistry,* **20**, 129–154.

Chohan, Z. H. and Supuran, C. T. (2006). Metalloantibiotics: Synthesis, Characterization and *In-Vitro* Antibacterial Studies on Cobalt (II), Copper (II), Nickel (II) and Zinc (II)

Complexes with Cloxacillin. *Journal of Enzyme Inhibition and Medicinal Chemistry*, **21**, 441–448.

Chopra, I. (2007). The Increasing Use of Silver-Based Products as Antimicrobial Agents: A Useful Development or a Cause for Concern? *Journal of Antimicrobial Chemotherapy*, **59**, 587–590.

Ciol, M. R., Manzano, C. M., Cuin, A., Pavan, F. R., Ribeiro, C. M., Ruiz, A. L. T. G. and Corbi, P. P. (2018). A Silver Complex with Cycloserine: Synthesis, Spectroscopic Characterization, Crystal Structure and *In Vitro* Biological Studies. *Chemistryselect*, **3**, 1719–1726.

Cioslowski, J., Hay, P. J. and Ritchie, J. P. (1990). Charge Distributions and Effective Atomic Charges in Transition-Metal Complexes Using Generalized Atomic Polar Tensors and Topological Analysis. *The Journal of Physical Chemistry*, **94**, 148–151.

Cioslowski, J., Martinov, M. and Mixon, S. T. (1993). Atomic Fukui Indexes from the Topological Theory of Atoms in Molecules Applied to Hartree-Fock and Correlated Electron Densities. *The Journal of Physical Chemistry*, **97**, 10948–10951.

Claussen, C. A., and Long, E. C. (1999). Nucleic Acid Recognition by Metal Complexes of Bleomycin. *Chemical Reviews*, **99**, 2797–2816.

Cohen, M. L. (1992). Epidemiology of Drug Resistance: Implications for a Post--Antimicrobial Era. *Science*, **257**: 1050–1055.

Colleter, J. C. and Gadret, M. (1968). Structure Cristalline De Composés Antituberculeux. I. Structure Cristalline Du Chlorhydrate D'éthionamide. *Acta Crystallographica Section B Structural Crystallography and Crystal Chemistry*, **24**, 513–519.

Colleter, J. C. and Gadret, M. (1968). Structure Cristalline De Composés Antituberculeux. II. Structure Cristalline Du Bromhydrate D'éthionamide. Comparaison Avec Celle Du Chlorhydrate D'éthionamide. *Acta Crystallographica Section B Structural Crystallography and Crystal Chemistry*, **24**, 519–525.

Comas-Vives, A. and Harvey, J. N. (2011). How Important is Backbonding in Metal Complexes Containing N-Heterocyclic Carbenes? Structural and NBO Analysis. *European Journal of Inorganic Chemistry*, **2011**, 5025–5035.

Contreras, R. R., Fuentealba, P., Galván, M. and Pérez, P. (1999). A Direct Evaluation of Regional Fukui Functions in Molecules. *Chemical Physics Letters*, **304**, 405–413.

Cotton, F. A. and Troup, J. M. (1974). Reactivity of Diiron Nonacarbonyl in Tetrahydrofuran. I. Isolation and Characterization of Pyridinetetracarbonyliron and Pyrazinetetracarbonyliron. *Journal of the American Chemical Society*, **96**, 3438–3443.

Cotton, F. A., Luck, R. L. and Son, K. (1990). A Structural Study of Trichloro(Tetrahydrofuran)Iron(III). *Acta Crystallographica Section C Crystal Structure Communications*, **46**, 1424–1426.

Cramer, C. J. and Truhlar, D. G. (2009). Density Functional Theory for Transition Metals and Transition Metal Chemistry. *Physical Chemistry Chemical Physics*, **11**, 10757-10816.

Cuprys, A., Pulicharla, R., Lecka, J., Brar, S. K., Drogui, P. and Surampalli, R. Y. (2018). Ciprofloxacin-Metal Complexes –Stability and Toxicity Tests in the Presence of Humic Substances. *Chemosphere*, **202**, 549–559.

Darensbourg, D. J., Day, C. S. and Fischer, M. B. (1981a). Crystal and Molecular Structure of Dicarbonyl(η5-Cyclopentadienyl)(Formato)Iron(II). *Inorganic Chemistry*, **20**, 3577–3579.

Darensbourg, D. J., Fischer, M. B., Schmidt, R. E. and Baldwin, B. J. (1981b). Formate Ion as a Monodentate Ligand. Synthesis, Structure, and Decarboxylation of (η5-Cyclopentadienyl)Dicarbonyl(Formato)Iron. *Journal of the American Chemical Society*, **103**, 1297–1298.

Davies, J. and Davies, D. (2010). Origins and Evolution of Antibiotic Resistance. *Microbiology and Molecular Biology Reviews*, **74**, 417–433.

De Oliveira, L. P., Carneiro, Z. A., Ribeiro, C. M., Lima, M. F., Paixão, D. A., Pivatto, M. and Guerra, W. (2018). Three New Platinum Complexes Containing Fluoroquinolones and DMSO: Cytotoxicity and Evaluation against Drug-Resistant Tuberculosis. *Journal of Inorganic Biochemistry*, **183**, 77–83.

DeBarber, A. E., Mdluli, K., Bosman, M., Bekker, L.-G. and Barry, C. E. (2000). Ethionamide Activation and Sensitivity in Multidrug-Resistant *Mycobacterium tuberculosis*. *Proceedings of the National Academy of Sciences*, **97**, 9677–9682.

Delhaes, L., Biot, C., Berry, L., Maciejewski, L., Camus, D., Brocard, J.S., Dive, D. (2000). Novel Ferrocenic Artemisinin Derivatives: Synthesis, *In-Vitro* Antimalarial Activity and Affinity of Binding with Ferrophotoporphyrin (IX). *Bioorganic Medicinal Chemistry*, **8**, 2739-2745.

Demoro, B., Sarniguet, C., Sánchez-Delgado, R., Rossi, M., Liebowitz, D., Caruso, F. and Gambino, D. (2012). New Organoruthenium Complexes with Bioactive Thiosemicarbazones as Co-Ligands: Potential Anti-Trypanosomal Agents. *Dalton Transaction*, **41**, 1534–1543.

Diaz-Acosta, I., Baker, J., Hinton, J. F. and Pulay, P. (2003). Calculated and Experimental Geometries and Infrared Spectra of Metal Tris-Acetylacetonates: Vibrational Spectroscopy as a Probe of Molecular Structure for Ionic Complexes. Part II. *Spectrochimica Acta Part A: Molecular and Biomolecular Spectroscopy*, **59**, 363–377.

Dickert, H., Machka, K., and Braveny, I. (1981). The Uses and Limitations of Disc Diffusion in the Antibiotic Sensitivity Testing of Bacteria. *Infection,* **9**, 18–24.

Dive, D. and Biot, C. (2008). Ferrocene Conjugates of Chloroquine and other Antimalarials: the Development of Ferroquine, a New Antimalarial. *Chemistry Medicinal Chemistry,* **3**, 383–391.

Dobson, A. J., and Gerkin, R. E. (1998). 5-Ammoniosalicylic Acid Chloride Monohydrate. *Acta Crystallographica Section C Crystal Structure Communications,* **54**, 1632–1634.

Doern, G. V., Pfaller M.A. and Kugler, K.(1998). Prevalence of Antimicrobial Resistance Among Respiratory Tract Isolates of *Streptococcus pneumoniae* in North America: 1997 Results from the SENTRY Antimicrobial Surveillance Program. *Clinical Infectious Diseases* **27**, 764–768.

Dolezal, M., Cmedlova, P., Palek, L., Vinsova, J., Kunes, J., Buchta, V. and Kralova, K. (2008). Synthesis and Antimycobacterial Evaluation of Substituted Pyrazinecarboxamides. *European Journal of Medicinal Chemistry,* **43**, 1105–1113.

Domingo, L. R. (2000). A Density Functional Theory Study of the Chemoselectivity and Regioselectivity of the Domino Cycloaddition Reactions of Nitroalkenes with Substituted Alkenes. *Theoretical Chemistry Accounts: Theory, Computation, and Modeling (Theoretica Chimica Acta),* **104**, 240–246.

Domingo, L. R. and Picher, M. T. (2004). A DFT Study Of The Huisgen 1,3-Dipolar Cycloaddition Between Hindered Thiocarbonyl Ylides and Tetracyanoethylene. *Tetrahedron,* **60**, 5053–5058.

Domingo, L. R., Arnó, M., Contreras, R. and Pérez, P. (2002a). Density Functional Theory Study for the Cycloaddition of 1,3-Butadienes with Dimethyl Acetylenedicarboxylate. Polar Stepwise vs Concerted Mechanisms. *The Journal of Physical Chemistry A,* **106**, 952–961.

Domingo, L. R., Aurell, M. J., Pérez, P. and Contreras, R. (2002b). Quantitative Characterization of the Local Electrophilicity of Organic Molecules. Understanding the Regioselectivity on Diels−Alder Reactions. *The Journal of Physical Chemistry A,* **106**, 6871–6875.

Domingo, L. R., Aurell, M. J., Pérez, P. and Contreras, R. (2002c). Quantitative Characterization of the Global Electrophilicity Power of Common Diene/Dienophile Pairs in Diels–Alder Reactions. *Tetrahedron,* **58**, 4417–4423.

Domingo, L. R., José Aurell, M., Pérez, P. and Contreras, R. (2003a). Origin of the Synchronicity on the Transition Structures of Polar Diels−Alder Reactions. Are these Reactions [4 + 2] Processes? *The Journal of Organic Chemistry,* **68**, 3884–3890.

Domingo, L. R., Pérez, P. and Contreras, R. (2003b). Electronic Contributions to the σpParameter of the Hammett Equation. *The Journal of Organic Chemistry*, **68**, 6060–6062.

Domingo, L. R., Pérez, P. and Contreras, R. (2004). Reactivity of the Carbon–Carbon Double Bond Towards Nucleophilic Additions. A DFT Analysis. *Tetrahedron*, **60**, 6585–6591.

Domingo, L. R., Pérez, P. and Sáez, J. A. (2013). Understanding the Local Reactivity in Polar Organic Reactions Through Electrophilic And Nucleophilic Parr Functions. *Royal Society of Chemistry Advances*, **3**, 1486–1494.

Donohue, J. (1957). Bifurcated Hydrogen Bonds and the Structure of Cycloserine Hydrochloride. *Acta Crystallographica*, **10**, 383–384.

Dougan, S. J., Melchart, M., Habtemariam, A., Parsons, S. and Sadler, P. J. (2006). Phenylazo-pyridine and Phenylazo-pyrazole Chlorido Ruthenium(II) Arene Complexes: Arene Loss, Aquation, and Cancer Cell Cytotoxicity. *Inorganic Chemistry*, **45**, 10882–10894.

Dreitzler, R.M. and Gross, E. K. U. (1990). Density Functional Theory. Springer Verlag, Berlin, New York.

Dubar, F., Egan, T. J., Pradines, B., Kuter, D., Ncokazi, K. K., Forge, D. and Biot, C. (2011). The Antimalarial Ferroquine: Role of the Metal and Intramolecular Hydrogen Bond in Activity and Resistance. *ACS Chemical Biology*, **6**, 275–287.

Dubar, F., Khalife, J., Brocard, J., Dive, D. and Biot, C. (2008). Ferroquine, an Ingenious Antimalarial Drug –Thoughts on the Mechanism of Action. *Molecules*, **13**, 2900–2907.

Eddy, N. O., Momoh-Yahaya, H. and Oguzie, E. E. (2015). Theoretical And Experimental Studies On The Corrosion Inhibition Potentials of Some Purines for Aluminium in 0.1M HCl. *Journal of Advanced Research*, **6**, 203–217.

Edwards, E. I., Epton, R. and Marr, G. (1975). Organometallic Derivatives of Penicillins and Cephalosporins A New Class of Semi-Synthetic Antibiotics. *Journal of Organometallic Chemistry*, **85**, C23–C25.

Edwards, E. I., Epton, R. and Marr, G. (1976a). 1,1′-Ferrocenyldiacetic Acid Anhydride and Its Use in the Preparation of Heteroannularly Substituted Ferrocenyl-Penicillins and -Cephalosporins. *Journal of Organometallic Chemistry*, **122**, C49–C53.

Edwards, E. I., Epton, R. and Marr, G. (1976b). A New Class of Semi-Synthetic Antibiotics: Ferrocenyl-Penicillins and -Cephalosporins. *Journal of Organometallic Chemistry*, **107**, 351–357.

Edwards, E. I., Epton, R. and Marr, G. (1979). The Synthesis and Reactions of Homonuclear Ferrocene Acid Anhydrides and Their Use in the Preparation of

Ferrocenylpenicillins and -Cephalosporins. *Journal of Organometallic Chemistry*, **168**, 259–272.

Eichkorn, K., Weigend, F., Treutler, O. and Ahlrichs, R. (1997). Auxiliary Basis Sets for Main Row Atoms and Transition Metals and their use to Approximate Coulomb Potentials. Theoretical Chemistry Accounts: *Theory, Computation, and Modeling (Theoretica Chimica Acta),* **97**, 119–124.

Einsiedel, J., Schoerner, C. and Gmeiner, P. (2003). Synthesis of Dihydrooxazole Analogues Derived from Linezolid. *Tetrahedron*, **59**, 3403–3407.

Ellner, J. J. (2008). The Emergence of Extensively Drug-Resistant Tuberculosis: A Global Health Crisis Requiring New Interventions: Part I: The Origins and Nature of the Problem. *Clinical and Translational Science*, **1**, 249–254.

Ellner, J. J. (2009). The Emergence of Extensively Drug-Resistant Tuberculosis: A Global Health Crisis Requiring New Interventions: Part II: Scientific Advances that May Provide Solutions. *Clinical and Translational Science*, **2**, 80–84.

El-Wahed, M. G. A., Refat, M. S. and El-Megharbel, S. M. (2008). Spectroscopic Studies on the Complexation of Some Transition Metals with Chloramphenicol Drug. *Journal of Molecular Structure*, **892**, 402–413.

Eriksson, L. A., Wang, J. and Boyd, R. J. (1995). The Interactions Between Alkali Metals And C2H2. Density Functional Theory as an Analytic Tool. *Chemical Physics Letters*, **235**, 422–429.

Falagas, M. E., & Bliziotis, I. A. (2007). Pandrug-Resistant Gram-Negative Bacteria: The dawn of the post-antibiotic era? *International Journal of Antimicrobial Agents,* **29**, 630–636.

Falagas, M. E., Kasiakou, S. K., & Saravolatz, L. D. (2005). Colistin: The Revival of Polymyxins for the Management of Multidrug-Resistant Gram-Negative Bacterial Infections. *Clinical Infectious Diseases,* **40**, 1333–1341.

Farrell, N. (1989). Transition Metal Complexes as Drugs and Chemotherapeutic Agents Springer, Netherlands.

Ferguson, L. A. and Rhoads, J. (2009). Multidrug-resistant and extensively drug-resistant tuberculosis: The new face of an old disease. *Journal of the American Academy of Nurse Practitioners*, **21**, 603–609.

Filak, L. K., Göschl, S., Heffeter, P., Ghannadzadeh Samper, K., Egger, A. E., Jakupec, M. A. and Arion, V. B. (2013). Metal–Arene Complexes with Indolo[3,2-c]-quinolines: Effects of Ruthenium vs Osmium and Modifications of the Lactam Unit on Intermolecular Interactions, Anticancer Activity, Cell Cycle, and Cellular Accumulation. *Organometallics,* **32**, 903–914.

Filak, L. K., Kalinowski, D. S., Bauer, T. J., Richardson, D. R. and Arion, V. B. (2014). Effect of the Piperazine Unit and Metal-Binding Site Position on the Solubility and Anti-Proliferative Activity of Ruthenium(II)- and Osmium(II)- Arene Complexes of Isomeric Indolo[3,2-c]quinoline—Piperazine Hybrids. *Inorganic Chemistry*, **53**, 6934–6943.

Finch, R. and Hunter, P. A. (2006). Antibiotic Resistance-Action to Promote New Technologies: Report of an EU Intergovernmental Conference Held in Birmingham, UK, 12-13 December 2005. *Journal of Antimicrobial Chemotherapy*, **58**, i3–i22.

Fitzgerald, G. and Andzelm, J. (1991). Chemical Applications Of Density Functional Theory: Comparison To Experiment, Hartree-Fock, And Perturbation Theory. *The Journal of Physical Chemistry*, **95**, 10531–10534.

Fizer, M., Sidey, V., Tupys, A., Ostapiuk, Y., Tymoshuk, O. and Bazel, Y. (2017). On the Structure of Transition Metals Complexes with the New Tridentate Dye of Thiazole Series: Theoretical and Experimental Studies. *Journal of Molecular Structure*, **1149**, 669–682.

Fortuna, C. G., Berardozzi, R., Bonaccorso, C., Caltabiano, G., Di Bari, L., Goracci, L. and Musumeci, R. (2014). New Potent Antibacterials Against Gram-positive Multiresistant Pathogens: Effects of Side Chain Modification and Chirality in Linezolid-like 1,2,4-Oxadiazoles. *Bioorganic and Medicinal Chemistry*, **22**, 6814–6825.

Fortuna, C. G., Bonaccorso, C., Bulbarelli, A., Caltabiano, G., Rizzi, L., Goracci, L. and Musumeci, R. (2013). New Linezolid-Like 1, 2, 4-Oxadiazoles Active against Gram-Positive Multiresistant Pathogens. *European Journal of Medicinal Chemistry*, **65**, 533–545.

Fouda, M. F. R., Abd-Elzaher, M. M., Abdelsamaia, R. A. and Labib, A. A. (2007). On The Medicinal Chemistry Of Ferrocene. *Applied Organometallic Chemistry*, **21**, 613–625.

Franco-Pérez, M., Polanco-Ramírez, C.-A., Ayers, P. W., Gázquez, J. L. and Vela, A. (2017). New Fukui, Dual and Hyper-Dual Kernels as Bond Reactivity Descriptors. *Physical Chemistry Chemical Physics*, **19**, 16095–16104.

Frau, J. and Glossman-Mitnik, D. (2018a). Local Molecular Reactivity of the Coloured Dansylglycine in Water and Dioxane Studied through Conceptual DFT. *Journal of Chemistry*, **2018**, 1–7.

Frau, J. and Glossman-Mitnik, D. (2018b). Conceptual DFT Study of the Local Chemical Reactivity of the Coloured BISARG Melanoidin and Its Protonated Derivative. *Frontiers in Chemistry*, **6**, 1-9.

Frau, J., Flores-Holguín, N. and Glossman-Mitnik, D. (2018) Chemical Reactivity Theory (CRT) Study of the Melanoidin M8: Local Conceptual Density Functional Theory Descriptors. *Computational Molecular Bioscience*, **8**, 80-90.

Frisch, M. J.; Trucks, G. W.; Schlegel, H. B.; Scuseria, G. E.; Robb, M. A.; Cheeseman, J. R.; Scalmani, G.; Barone, V.; Petersson, G. A.; Nakatsuji, H.; Li, X.; Caricato, M.; Marenich, A. V.; Bloino, J.; Janesko, B. G.; Gomperts, R.; Mennucci, B.; Hratchian, H. P.; Ortiz, J. V.; Izmaylov, A. F.; Sonnenberg, J. L.; Williams-Young, D.; Ding, F.; Lipparini, F.; Egidi, F.; Goings, J.; Peng, B.; Petrone, A.; Henderson, T.; Ranasinghe, D.; Zakrzewski, V. G.; Gao, J.; Rega, N.; Zheng, G.; Liang, W.; Hada, M.; Ehara, M.; Toyota, K.; Fukuda, R.; Hasegawa, J.; Ishida, M.; Nakajima, T.; Honda, Y.; Kitao, O.; Nakai, H.; Vreven, T.; Throssell, K.; Montgomery, J. A., Jr.; Peralta, J. E.; Ogliaro, F.; Bearpark, M. J.; Heyd, J. J.; Brothers, E. N.; Kudin, K. N.; Staroverov, V. N.; Keith, T. A.; Kobayashi, R.; Normand, J.; Raghavachari, K.; Rendell, A. P.; Burant, J. C.; Iyengar, S. S.; Tomasi, J.; Cossi, M.; Millam, J. M.; Klene, M.; Adamo, C.; Cammi, R.; Ochterski, J. W.; Martin, R. L.; Morokuma, K.; Farkas, O.; Foresman, J. B.; Fox, D. J. Gaussian, Inc., Wallingford CT, 2016. Gaussian 09, Revision E.01.

Frisch, M. J.; Trucks, G. W.; Schlegel, H. B.; Scuseria, G. E.; Robb, M. A.; Cheeseman, J. R.; Scalmani, G.; Barone, V.; Petersson, G. A.; Nakatsuji, H.; Li, X.; Caricato, M.; Marenich, A. V.; Bloino, J.; Janesko, B. G.; Gomperts, R.; Mennucci, B.; Hratchian, H. P.; Ortiz, J. V.; Izmaylov, A. F.; Sonnenberg, J. L.; Williams-Young, D.; Ding, F.; Lipparini, F.; Egidi, F.; Goings, J.; Peng, B.; Petrone, A.; Henderson, T.; Ranasinghe, D.; Zakrzewski, V. G.; Gao, J.; Rega, N.; Zheng, G.; Liang, W.; Hada, M.; Ehara, M.; Toyota, K.; Fukuda, R.; Hasegawa, J.; Ishida, M.; Nakajima, T.; Honda, Y.; Kitao, O.; Nakai, H.; Vreven, T.; Throssell, K.; Montgomery, J. A., Jr.; Peralta, J. E.; Ogliaro, F.; Bearpark, M. J.; Heyd, J. J.; Brothers, E. N.; Kudin, K. N.; Staroverov, V. N.; Keith, T. A.; Kobayashi, R.; Normand, J.; Raghavachari, K.; Rendell, A. P.; Burant, J. C.; Iyengar, S. S.; Tomasi, J.; Cossi, M.; Millam, J. M.; Klene, M.; Adamo, C.; Cammi, R.; Ochterski, J. W.; Martin, R. L.; Morokuma, K.; Farkas, O.; Foresman, J. B.; Fox, D. J. Gaussian, Inc., Wallingford CT, 2016. Gaussian 16, Revision B.01.

Fuentealba, P. (1995). A Local Model For The Hardness Kernel And Related Reactivity Parameters In Density Functional Theory. *The Journal of Chemical Physics*, **103**, 6571–6575.

Fuentealba, P. and Savin, A. (2000). Electronic Structure and Bonding of the Ground State of Alkaline-Earth-Metal Monoxides and Carbides. *The Journal of Physical Chemistry A*, **104**, 10882–10886.

Fuentealba, P., Pérez, P. and Contreras, R. (2000a). On The Condensed Fukui Function. *The Journal of Chemical Physics*, **113**, 2544–2551.

Fuentealba, P., Simón-Manso, Y., and Chattaraj, P. K. (2000b). Molecular Electronic Excitations and the Minimum Polarizability Principle. *The Journal of Physical Chemistry A*, **104**, 3185–3187.

Fukui, K. (1982). Role of Frontier Orbitals in Chemical Reactions. *Science*, **218**, 747–754.

Gasser, G. (2015). Metal Complexes and Medicine: A Successful Combination. *Chimia International Journal for Chemistry,* **69**, 442–446.

Gasser, G. and Metzler-Nolte, N. (2011). In Bioinorganic Medicinal Chemistry, ed. Alessio, E. Wiley-VCH, Weinheim, 2011, pp. 351–382; and references therein.

Gasser, G. and Metzler-Nolte, N. (2012). The Potential of Organometallic Complexes In Medicinal Chemistry. *Current Opinion in Chemical Biology,* **16**, 84–91.

Gasser, G., Neukamm, M. A., Ewers, A., Brosch, O., Weyhermüller, T. and Metzler-Nolte, N. (2009). Synthesis and Characterization of Dicobalthexacarbonyl-Alkyne Derivatives of Amino Acids, Peptides, and Peptide Nucleic Acid (PNA) Monomers. *Inorganic Chemistry,* **48**, 3157–3166.

Gasser, G., Ott, I. and Metzler-Nolte, N. (2011). Organometallic Anticancer Compounds. *Journal of Medicinal Chemistry*, **54**, 3–25.

Gibaud, S and Jaouen, G. (2010). In Medicinal Organometallic Chemistry, ed. Jaouen, G. and Metzler-Nolte, N. Springer-Verlag, Berlin, Heidelberg, pp. 1–20.

Giske, C. G., Monnet, D. L., Cars, O. and Carmeli, Y. (2007). Clinical and Economic Impact of Common Multidrug-Resistant Gram-Negative Bacilli. *Antimicrobial Agents and Chemotherapy,* **52**, 813–821.

Glossman-Mitnik, D. (2013). Computational Study of the Chemical Reactivity Properties of the Rhodamine B Molecule. *Procedia Computer Science,* **18**, 816–825.

Görling, A., Trickey, S.B., Gisdakis, P. and Rösch, N. (1999). A Critical Assessment of Density Functional Theory with Regard to Applications in Organometallic Chemistry. In: Brown J.M., Hofmann P. (Eds) Organometallic Bonding and Reactivity. Topics in Organometallic Chemistry, Volume 4. Springer, Berlin, Heidelberg

Grant, I. P. (1994). Relativistic Electronic Structure of Atoms and Molecules. *Advances in Atomic, Molecular, and Optical Physics,* 1994, 169–186.

Guo, Z., and Sadler, P. J. (1999). Metals in Medicine. *Angewandte Chemie International Edition,* **38**, 1512–1531.

Hanif, M., Henke, H., Meier, S. M., Martic, S., Labib, M., Kandioller, W. and Hartinger, C. G. (2010). Is the Reactivity of M (II) −Arene Complexes of 3-Hydroxy-2(1H)-pyridones to Biomolecules the Anticancer Activity Determining Parameter? *Inorganic Chemistry*, **49**, 7953–7963.

Harnett, N., Brown, S. and Krishnan, C. (1991). Emergence of quinolone resistance among clinical isolates of methicillin-resistant *Staphylococcus aureus* in Ontario, Canada. *Antimicrobial agents and chemotherapy*, **35**, 1911-3.

Harper, N. J. (1959). Drug latentiation. *Journal Medicinal and Pharmaceutical Chemistry*, **5**, 467-500.

Hartinger, C. G. and Dyson, P. J. (2009). Bioorganometallic Chemistry—From Teaching Paradigms to Medicinal Applications. *Chemical Society Reviews*, **38**, 391–401.

Held, J., Supan, C., Salazar, C. L. O., Tinto, H., Bonkian, L. N., Nahum, A. and Kremsner, P. G. (2015). Ferroquine And Artesunate in African Adults and Children with Plasmodium Falciparum Malaria: A Phase 2, Multicentre, Randomised, Double-Blind, Dose-Ranging, Non-Inferiority Study. *The Lancet Infectious Diseases,* **15**, 1409–1419.

Henke, H., Kandioller, W., Hanif, M., Keppler, B. K. and Hartinger, C. G. (2012). Organometallic Ruthenium and Osmium Compounds of Pyridin-2- and -4-ones as Potential Anticancer Agents. *Chemistry and Biodiversity,* **9**, 1718–1727.

Hillard, E. A. and Jaouen, G. (2011). Bioorganometallics: Future Trends in Drug Discovery, Analytical Chemistry, and Catalysis, *Organometallics,* **30**, 20–27.

Hillard, E., Vessières, A., Le Bideau, F., Plażuk, D., Spera, D., Huché, M., & Jaouen, G. (2006). A Series of Unconjugated Ferrocenyl Phenols: Prospects as Anticancer Agents. *ChemMedChem*, **1**, 551–559.

Ho, P. C. (2005). In Metallotherapeutic Drugs and Metal-based Diagnostic Agents – The Use of Metals in Medicine, ed. Gielen, M. and Tiekink, E. R. T. John Wiley and Sons Ltd, Chichester, West Sussex, England, pp.297–311.

Jaouen, G and Metzler-Nolte, N. (2010). In Topics in Organometallic Chemistry, Springer, Heidelberg, Germany, 1st edn, Volume 32; and references therein

Jaouen, G. (2006). Bioorganometallics: Biomolecules, Labeling, Medicine. Wiley-VCH

Jaouen, G., Top, S., Vessieres, A., Leclercq, G. and McGlinchey, M. (2004). The First Organometallic Selective Estrogen Receptor Modulators (SERMs) and Their Relevance to Breast Cancer. *Current Medicinal Chemistry*, **11**, 2505–2517.

Jaouen, G., Vessières, A. and Top, S. (2015). Ferrocifen type anti cancer drugs. *Chemical Society Reviews,* 44, 8802–8817.

Jean, L. S., Luiz, A. D. Thais, R. M. and Chung, M. C. (2012). New Antitubercular Drugs Designed by Molecular Modification, Understanding Tuberculosis - New Approaches to Fighting Against Drug Resistance, Dr. Pere-Joan Cardona (Ed.), ISBN: 978-953-307-948-6, InTech, Available from: http://www.intechopen.com/books/understanding-tuberculosis-new-approaches-to-fightingagainst-drug-resistance/new-antitubercular-drugs-designed-by-molecular-modification

Johnson, T. and Case, C. (1995). Laboratory Experiments in Microbiology 4th edn. Benjamin/Cummings Publishing Co, Redwood City, CA.

Kamal, A., Swapna, P., Shetti, R. V. C. R. N. C., Shaik, A. B., Narasimha Rao, M. P.and Gupta, S. (2013). Synthesis, Biological Evaluation of New Oxazolidino-Sulfonamides as Potential Antimicrobial Agents. *European Journal of Medicinal Chemistry*, **62**, 661–669.

Kamal, A., Swapna, P., Shetti, R. V. C. R. N. C., Shaik, A. B., Narasimha Rao, M. P., Sultana, F. and Chandrakant, B. (2013). Anti-tubercular Agents. Part 7: A New Class of Diarylpyrrole–Oxazolidinone Conjugates as Antimycobacterial Agents. *European Journal of Medicinal Chemistry*, **64**, 239–251.

Karpagam, J., Sundaraganesan, N., Kalaichelvan, S. and Sebastian, S. (2010). Anharmonic Vibrational Analysis of 3, 4-Diaminopyridine and 3-Aminopyridine by Density Functional Theory Calculations. *Spectrochimica Acta Part A: Molecular and Biomolecular Spectroscopy*, **76**, 502–512.

Karthick, T., Balachandran, V., Perumal, S. and Nataraj, A. (2011). Spectroscopic Studies, HOMO–LUMO and NBO Calculations on Monomer and Dimer Conformer of 5-Nitrosalicylic Acid. *Journal of Molecular Structure*, **1005**, 192–201.

Khadikar, P. V., Ali, S. M., Farooqui, M. A. and Heda, B. D. (1985). IR, TG, DTG and DTA Studies Of Bis-(4-Aminosalicylato)-Diaquo Complexes of VO(II), Cu(II), Ni(II), Co(II), Fe(II) and Mn(II). *Thermochimica Acta*, **91**, 159–171.

King, R. B., Stone, F. G. A., Jolly, W. L., Austin, G., Covey, W., Rabinovich, D. and Tsugawa, R. (2007). Cyclopentadienyl Metal Carbonyls and Some Derivatives. *Inorganic Syntheses*, **7**, 99–115.

King, R. B.; Stone, F. G. A. (1963). Cyclopentadienyl Metal Carbonyls and some Derivatives. *Inorganic Syntheses* **7**, 99-115.

Kirchner, B., Wennmohs, F., Ye, S. and Neese, F. (2007). Theoretical Bioinorganic Chemistry: The Electronic Structure Makes A Difference. *Current Opinion in Chemical Biology*, **11**, 134–141.

Klasen, H. J. (2000). Historical Review of the Use of Silver in the Treatment of Burns. I. Early Uses. *Burns*, **26**, 117–130.

Kohn, W., Becke, A. D. and Parr, R. G. (1996). Density Functional Theory of Electronic Structure. *The Journal of Physical Chemistry*, **100**, 12974–12980.

Kokatam, S., Ray, K., Pap, J., Bill, E., Geiger, W. E., LeSuer, R. J. and Wieghardt, K. (2007). Molecular and Electronic Structure of Square-Planar Gold Complexes Containing Two 1, 2-Di (4-tert-butylphenyl) ethylene-1, 2-dithiolato Ligands: [Au (2L) 2]1+/0/1-/2-. A Combined Experimental and Computational Study. *Inorganic Chemistry*, **46**, 1100–1111.

Kolandaivel, P., Praveena, G. and Selvarengan, P. (2005). Study of Atomic and Condensed Atomic Indices for Reactive Sites Of Molecules. *Journal of Chemical Sciences*, **117**, 591–598.

Koopmans, T. (1934). Über die Zuordnung von Wellenfunktionen und Eigenwerten zu den Einzelnen Elektronen Eines Atoms. *Physica*, **1**, 104–113.

Köpf-Maier, P. (1985). Glucocorticoid Induction of Cleft Palate after Treatment with Titanocene Dichloride? *Toxicology*, **37**, 111–116.

Kopf-Maier, P. (1989). Tumour Inhibition by Titanocene Complexes: Influence On Xenografted Human Adenocarcinomas of the Gastrointestinal Tract. *Cancer Chemotherapy and Pharmacology*, **23**, 225–230.

Köpf-Maier, P. and Köpf H. (1984) The Metallocene Dihalides — A Class of Organometallic Early Transition Metal Complexes as Antitumor Agents. In: Hacker M.P., Douple E.B., Krakoff I.H. (Eds) Platinum Coordination Complexes in Cancer Chemotherapy. Developments in Oncology, Volume 17. Springer, Boston, MA

Kopf-Maier, P. and Gerlach, S. (1986). Pattern of Toxicity by Titanocene Dichloride In Mice. *Journal of Cancer Research and Clinical Oncology*, **111**, 243–247.

Kopf-Maier, P. and Klapotke, T. (1992). Ionic Rhenocene Derivatives With Antitumor Activity. *Cancer Chemotherapy and Pharmacology*, **29**, 361–366.

Köpf-Maier, P. and Köpf H. (1994) Organometallic Titanium, Vanadium, Niobium, Molybdenum and Rhenium Complexes — Early Transition Metal Antitumour Drugs. In: Fricker, S. P. (eds) Metal Compounds in Cancer Therapy. Springer, Dordrecht

Köpf-Maier, P., Brauchle, U. and Henssler, A. (1988a). Organ Distribution and Pharmacokinetics Of Titanium after Treatment with Titanocene Dichloride. *Toxicology*, **51**, 291–298.

Kopf-Maier, P., Janiak, C. and Schumann, H. (1988b). Antitumor Properties Of Organometallic Metallocene Complexes Of Tin and Germanium. *Journal of Cancer Research and Clinical Oncology*, **114**, 502–506.

Korth, H.-G., de Heer, M. I. and Mulder, P. (2002). A DFT Study on Intramolecular Hydrogen Bonding in 2-Substituted Phenols: Conformations, Enthalpies, and Correlation with Solute Parameters. *The Journal of Physical Chemistry A*, **106**, 8779–8789.

Kossmann, S., Kirchner, B. and Neese, F. (2007). Performance Of Modern Density Functional Theory For The Prediction Of Hyperfine Structure: Meta-GGA And Double Hybrid Functionals. *Molecular Physics*, **105**, 2049–2071.

Krivosudský, L. and Rakovský, E. (2014). Catena-Poly[[(Pyrazine-2-Carboxamide-κN4)Copper(I)]-μ3-Iodido]. *Acta Crystallographica Section E Structure Reports Online*, **70**, m267–m268.

Kronik, L., Stein, T., Refaely-Abramson, S. and Baer, R. (2012). Excitation Gaps of Finite-Sized Systems from Optimally Tuned Range-Separated Hybrid Functionals. *Journal of Chemical Theory and Computation*, **8**, 1515–1531.

Kumar, A., Singh, R., and Harbola, M. K. (2019a). Universal Nature of Different Methods of Obtaining The Exact Kohn–Sham Exchange-Correlation Potential for a Given Density. *Journal of Physics B: Atomic, Molecular and Optical Physics,* **52**, 075007-075015.

Kumar, V., Singh, A., Lumb, I.and Mehra, V. (2019b). Ferrocene-Appended Pharmacophores: An Exciting Approach for Modulating Biological Potential of Organic Scaffolds. *Dalton Transactions.***1**, 1-22.

Kümmel, S. and Kronik, L. (2008) Orbital-Dependent Density Functionals: Theory and Applications. *Reviews of Modern Physics*, **80**, 3-60.

Kunin, C. M. (1993). Resistance to Antimicrobial Drugs—A Worldwide Calamity. *Annals of Internal Medicine,* **118**: 557-660.

Kuo, C.Y., Wang, W.H., Huang, C.H., Chen, Y.H., and Lu, P.L. (2018). Resistance to first- and second-line antituberculosis drugs in Southern Taiwan: Implications for empirical treatment. *Journal of Microbiology, Immunology and Infection,* **51**, 88–93.

Kurz, S. G., Furin, J. J. and Bark, C. M. (2016). Drug-Resistant Tuberculosis. *Infectious Disease Clinics of North America,* **30**, 509–522.

Lachowicz, J. I., Nurchi, V. M., Crisponi, G., Cappai, I., Cappai, R., Busato, M. and Aaseth, J. (2018). Para-Aminosalicylic Acid in the Treatment Of Manganese Toxicity. Complexation of Mn^{2+} With 4-Amino-2-Hydroxybenzoic Acid and its N-Acetylated Metabolite. *New Journal of Chemistry*, **42**, 8035–8049.

Langreth, D. C. and Mehl, M. J. (1983). Beyond The Local-Density Approximation in Calculations of Ground-State Electronic Properties. *Physical Review B,* **28**, 1809–1834.

Lee, C. (2008). Therapeutic Challenges in the Era of Antibiotic Resistance. *International Journal of Antimicrobial Agents*, **32**, S197–S199

Lee, C., Yang, W. and Parr, R. G. (1988). Development of the Colle-Salvetti Correlation-Energy Formula into a Functional of the Electron Density. *Physical Review B,* **37**, 785–789.

Lee, H.-H., Takeuchi, N., Senda, H., Kuwae, A. and Hanai, K. (1998). Molecular Structure and Dimerization of d-Cycloserine in the Solid State. *Spectroscopy Letters*, **31**, 1217–1231.

Leeb, M. (2004). Antibiotics: A Shot in the Arm. *Nature*, **431**: 892–893.

Lemierre, V., Chrostowska, A., Dargelos, A. and Chermette, H. (2005). Calculation of Ionization Potentials of Small Molecules: A Comparative Study of Different Methods. *The Journal of Physical Chemistry A,* **109**, 8348–8355.

Levy, M., Perdew, J. P., and Sahni, V. (1984). Exact Differential Equation for the Density and Ionization Energy of a Many-Particle System. *Physical Review A,* **30**, 2745–2748.

Liu, S., De Proft, F. and Parr, R. G. (1997). Simplified Models for Hardness Kernel and Calculations of Global Hardness. *The Journal of Physical Chemistry A,* **101**, 6991–6997.

Liu, Z., Habtemariam, A., Pizarro, A. M., Fletcher, S. A., Kisova, A., Vrana, O. and Sadler, P. J. (2011). Organometallic Half-Sandwich Iridium Anticancer Complexes. *Journal of Medicinal* Chemistry, **54**, 3011–3026.

Locke, J. B., Morales, G., Hilgers, M., G. C., K., Rahawi, S., Jose Picazo, J. and Stein, J. L. (2010). Elevated Linezolid Resistance in Clinical cfr-Positive *Staphylococcus aureus* Isolates Is Associated with Co-Occurring Mutations in Ribosomal Protein L3. *Antimicrobial Agents and Chemotherapy*, **54**, 5352–5355.

Loeffler, J. and Stevens, D. A. (2003). Antifungal Drug Resistance. *Clinical Infectious Diseases,* **36**:S31–S41.

Long, K. S. and Vester, B. (2011). Resistance to Linezolid Caused by Modifications at its Binding Site on the Ribosome. *Antimicrobial Agents and Chemotherapy*, **56**, 603–612.

M'thiruaine, C. M., Friedrich, H. B. and Omondi, B. (2012a). Dicarbonyl(η5-Cyclopentadienyl)(Hexamethylenetetramine-κN1)iron(II) Tetrafluoridoborate. *Acta Crystallographica Section E Structure Reports Online,* **68**, m1077–m1077.

M'thiruaine, C. M., Friedrich, H. B., Changamu, E. O. and Bala, M. D. (2011a). Acetonitriledicarbonyl(η5-Pentamethylcyclopentadienyl)Iron(II) Tetrafluoridoborate. *Acta Crystallographica Section E Structure Reports Online,* **67**, m924–m924.

M'thiruaine, C. M., Friedrich, H. B., Changamu, E. O. and Bala, M. D. (2011b). Synthesis and Characterization of Amine Complexes of the Cyclopentadienyliron Dicarbonyl Complex Cation, $[Cp(CO)_2Fe]^+$. *Inorganica Chimica Acta,* **366**, 105–115.

M'thiruaine, C. M., Friedrich, H. B., Changamu, E. O. and Bala, M. D. (2012b). Reactions of N-Heterocyclic Ligands with Substitutionally Labile Organometallic Complexes, $[(\eta5\text{-}C_5R_5)Fe(CO)_2E]BF_4$. *Inorganica Chimica Acta,* **390**, 83–94.

M'thiruaine, C. M., Friedrich, H. B., Changamu, E. O. and Bala, M. D. (2012c). Synthesis, Characterization and Structural Elucidation of Water-soluble 1-aminoalkane and α,ω-diaminoalkane Complexes of the Pentamethylcyclopentadienyliron Dicarbonyl Cation, $[Cp*(CO)_2Fe]^+$. *Inorganica Chimica Acta,* **382**, 27–34.

M'thiruaine, C. M., Friedrich, H. B., Changamu, E. O. and Fernandes, M. A. (2012d). Dicarbonyl(Hexamethylene-1,3,5,7-Tetramine-κN1)(η5-

Pentamethylcyclopentadienyl)Iron(II) Tetrafluoridoborate. *Acta Crystallographica Section E Structure Reports Online*, **68**, m931–m931.

M'thiruaine, C. M., Friedrich, H. B., Changamu, E. O. and Fernandes, M. A. (2012e). Dicarbonyl(η5-Cyclopentadienyl)(2,3-Dibromopropanamine- κN)Iron(II) Tetrafluoridoborate. *Acta Crystallographica Section E Structure Reports Online*, **68**, m932–m932.

M'thiruaine, C. M., Friedrich, H. B., Changamu, E. O. and Omondi, B. (2011c). (μ-Formato-κ2O:O′)bis[Dicarbonyl(η5-Cyclopentadienyl)Iron(II)] Tetrafluoridoborate. *Acta Crystallographica Section E Structure Reports Online,* **67**, m1252–m1252.

M'thiruaine, C. M., Friedrich, H. B., Changamu, E. O. and Omondi, B. (2011d). (μ-Ethane-1,2-Diamine-κ2N:N′)bis[Dicarbonyl(η5-Cyclopentadienyl)Iron(II)] Bis(Tetrafluoridoborate). *Acta Crystallographica Section E Structure Reports Online*, **67**, m485–m485.

M'thiruaine, C. M., Friedrich, H. B., Changamu, E. O. and Omondi, B. (2012f). Syntheses, Structural Elucidation And Reactions of Allylamino Compounds Of The Type, $[\eta 5\text{-}C_5R_5(CO)_2Fe(NH_2CH_2CHCH_2)]BF_4$. *Polyhedron,* **40**, 81–92.

Maccaroni, E., Alberti, E., Malpezzi, L., Masciocchi, N. and Vladiskovic, C. (2008). Polymorphism of Linezolid: A Combined Single-Crystal, Powder Diffraction and NMR Study. *International Journal of Pharmaceutics,* **351**, 144–151.

Madhusudhan, G., Reddy, G. O., Rajesh, T. Ramanatham, J. and Dubey, P. K. (2008), Stereoselective Synthesis Of Novel (R)- And (S)-5-Azidomethyl-2-Oxazolidinones From (S)-Epichlorohydrin: a Key Precursor for the Oxazolidinone Class of Antibacterial Agents. *Tetrahedron Letters*, **49**, 3060-3062.

Madhusudhan, G., Reddy, G. O., Ramanatham, J. and Dubey, P. K., (2005). A Novel and Short Convergent Approach for N-Aryl-5-Aminomethyl-2-Oxazolidinone Derivatives Linezolid and DUP-721. *Indian Journal of Chemistry***,** **44**, 1236–1238.

Madkour, L. H. and Elshamy, I. H. (2016). Experimental and Computational Studies on the Inhibition Performances of Benzimidazole and its Derivatives for the Corrosion of Copper in Nitric Acid. *International Journal of Industrial Chemistry,* **7**, 195–221.

Mahy, W., Leitch, J. A. and Frost, C. G. (2016). Copper Catalyzed Assembly of n-aryloxazolidinones: Synthesis of Linezolid, Tedizolid, and Rivaroxaban. *European Journal of Organic Chemistry*, **2016**, 1305–1313.

Mahy, W., Plucinski, P. K. and Frost, C. G. (2014). Copper-catalyzed One-pot Synthesis of N-aryl Oxazolidinones from Amino Alcohol Carbamates. *Organic Letters*, **16**, 5020–5023.

Malik, M. and Michalska, D. (2014). Assessment of New DFT Methods for Predicting Vibrational Spectra and Structure of Cisplatin: Which Density Functional Should we

Choose for Studying Platinum(II) Complexes? *Spectrochimica Acta Part A: Molecular and Biomolecular Spectroscopy*, **125**, 431–439.

Martínez, A., Carreon, T., Iniguez, E., Anzellotti, A., Sánchez, A., Tyan, M. and Sánchez-Delgado, R. A. (2012). Searching for New Chemotherapies for Tropical Diseases: Ruthenium–Clotrimazole Complexes Display High *In Vitro* Activity against *Leishmania major* and *Trypanosoma cruzi* and Low Toxicity toward Normal Mammalian Cells. *Journal of Medicinal Chemistry*, **55**, 3867–3877.

Martínez, A., Rajapakse, C. S. K., Jalloh, D., Dautriche, C. and Sánchez-Delgado, R. A. (2009). The Antimalarial Activity Of Ru–Chloroquine Complexes Against Resistant *Plasmodium falciparum* is Related To Lipophilicity, Basicity, and Heme Aggregation Inhibition Ability Near Water/N-Octanol Interfaces. *Journal of Biological Inorganic Chemistry*, **14**, 863–871.

Martínez, A., Rajapakse, C. S. K., Naoulou, B., Kopkalli, Y., Davenport, L. and Sánchez-Delgado, R. A. (2008). The Mechanism of Antimalarial Action of the Ruthenium(II)–Chloroquine Complex $[RuCl_2(CQ)]_2$. *Journal of Biological Inorganic Chemistry*, **13**, 703–712.

Martínez, A., Rajapakse, C. S. K., Sánchez-Delgado, R. A., Varela-Ramirez, A., Lema, C. and Aguilera, R. J. (2010). Arene–Ru(II)–Chloroquine Complexes Interact With DNA, Induce Apoptosis on Human Lymphoid Cell Lines and Display Low Toxicity oo Normal Mammalian Cells. *Journal of Inorganic Biochemistry*, **104**, 967–977.

Martínez, A., Suárez, J., Shand, T., Magliozzo, R. S. and Sánchez-Delgado, R. A. (2011). Interactions Of Arene–Ru(II)–Chloroquine Complexes of Known Antimalarial and Antitumor Activity with Human Serum Albumin (HSA) and Transferrin. *Journal of Inorganic Biochemistry*, **105**, 39–45.

Martínez-Araya, J. I., Salgado-Morán, G. and Glossman-Mitnik, D. (2013). Computational Nutraceutics: Chemical Reactivity Properties of the Flavonoid Naringin by Means of Conceptual DFT. *Journal of Chemistry*, **2013**, 1–8.

Marzano, C., Pellei, M., Tisato, F. and Santini, C. (2009). Copper Complexes as Anticancer Agents. *Anti-Cancer Agents in Medicinal Chemistry*, **9**, 185–211.

McCarthy, J. R. (2015). A Convenient Synthesis of The Antibacterial Agent Linezolid. *Tetrahedron Letters*, **56**, 6846–6847.

Meka, V. G. and Gold, H. S. (2004). Antimicrobial Resistance to Linezolid. *Clinical Infectious Diseases*, **39**: 1010–1015.

Melaiye, A. and Youngs, W. J. (2005). Silver and its Application as an Antimicrobial Agent. *Expert Opinion on Therapeutic Patents*, **15**, 125–130.

Melin, J., Aparicio, F., Galván, M., Fuentealba, P. and Contreras, R. (2003). Chemical Reactivity in the {N,NS,v(r)} Space. *The Journal of Physical Chemistry A*, **107**, 3831–3835.

Mendez, F. and Gazquez, J. L. (1994). Chemical Reactivity of Enolate Ions: The Local Hard and Soft Acids and Bases Principle Viewpoint. *Journal of the American Chemical Society*, **116**, 9298–9301.

Mendoza-Huizar, L. H., Salgado-Morán, G., Ramirez-Tagle, R. and Glossman-Mitnik, D. (2016). A Theoretical Quantum Study of the Intramolecular Interactions and Chemical Reactivity of Polymorphs A And B of Famotidine in the Gas, DMSO, and Aqueous Phases. *Computational and Theoretical Chemistry*, **1075**, 54–62.

Mendozar-Huirar, L., Salgado-Moaran, G., Cardona-Villada, W., Pacheco, A. and Glossman-Mitnik, D. (2017). A DFT Study of the Chemical Reactivity of Cimetidine A, C and D in the Gas Phase and in H_2O, MeOH and ETOH Solvents. *Journal of Serbian Chemical Society*, **82**, 25-37.

Meneses, L., Fuentealba, P. and Contreras, R. (2006). On The Variations Of Electronic Chemical Potential and Chemical Hardness Induced by Solvent Effects. *Chemical Physics Letters*, **433**, 54–57.

Meneses, L., Tiznado, W., Contreras, R. and Fuentealba, P. (2004). A Proposal for a New Local Hardness as Selectivity Index. *Chemical Physics Letters*, **383**, 181–187.

Merouani, H., Morell, C., Ouddai, N. and Chermette, H. (2013). DFT Study of the Stereo-Selectivity of Oxygenated Heterocycles from 10 to 12 Links. *Canadian Journal of Chemistry*, **91**, 811–820.

Michalska, K., Gruba, E., Mizera, M., Lewandowska, K., Bednarek, E., Bocian, W. and Cielecka-Piontek, J. (2017). Application of Spectroscopic Methods (FTIR, Raman, ECD and NMR) in Studies of Identification and Optical Purity of Radezolid. *Spectrochimica Acta Part A*: *Molecular and Biomolecular Spectroscopy*, **183**, 116–122.

Michalska, K., Karpiuk, I., Król, M. and Tyski, S. (2013). Recent Development of Potent Analogues of Oxazolidinone Antibacterial Agents. *Bioorganic and Medicinal Chemistry*, **21**, 577–591.

Michalska, K., Mizera, M., Lewandowska, K. and Cielecka-Piontek, J. (2016). Infrared, Raman And Ultraviolet with Circular Dichroism Analysis and Theoretical Calculations of Tedizolid. *Journal of Molecular Structure*, **1115**, 136–143.

Mineva, T., Sicilia, E. and Russo, N. (1998). Density-Functional Approach to Hardness Evaluation and Its Use in the Study of the Maximum Hardness Principle. *Journal of the American Chemical Society*, **120**, 9053–9058.

Ming, L. J. (2003). Structure and Function of ? Metalloantibiotics? *Medicinal Research Reviews*, **23**, 697–762.

Miranda-Quintana, R. A. (2017). Thermodynamic Electrophilicity. *The Journal of Chemical Physics*, **146**, 214113-214122.

Miranda-Quintana, R. A., and Ayers, P. W. (2018a). Note: Maximum Hardness and Minimum Electrophilicity Principles. *The Journal of Chemical Physics*, **148**, 196101-196110.

Miranda-Quintana, R. A., Franco-Pérez, M., Gázquez, J. L., Ayers, P. W., & Vela, A. (2018b). Chemical Hardness: Temperature Dependent Definitions and Reactivity Principles. *The Journal of Chemical Physics*, **149**, 124110-124119.

Miranda-Quintana, R. A., Martínez González, M. and Ayers, P. W. (2016). Electronegativity and Redox Reactions. *Physical Chemistry Chemical Physics*, **18**, 22235–22243.

Mitin, A. V., Baker, J. and Pulay, P. (2003). An Improved 6-31G* Basis Set for First-Row Transition Metals. *The Journal of Chemical Physics*, **118**, 7775–7782.

Mjos, K. D. and Orvig, C. (2014). Metallodrugs in Medicinal Inorganic Chemistry. *Chemical Reviews*, **114**, 4540–4563.

Moellering, R. C. (1998). Vancomycin-Resistant Enterococci. *Clinical Infectious Diseases*, **26**, 1196–1199.

Montgomery, J. A., Frisch, M. J., Ochterski, J. W. and Petersson, G. A. (1999). A Complete Basis Set Model Chemistry. VI. Use of Density Functional Geometries and Frequencies. *The Journal of Chemical Physics*, **110**, 2822–2827.

Morell, C., Ayers, P. W., Grand, A., Gutiérrez-Oliva, S. and Toro-Labbé, A. (2008a). Rationalization of Diels–Alder Reactions Through the Use of the Dual Reactivity Descriptor Δf(R). *Physical Chemistry Chemical Physics*, **10**, 7239-7246.

Morell, C., Gázquez, J. L., Vela, A., Guégan, F. and Chermette, H. (2014). Revisiting Electroaccepting and Electrodonating Powers: Proposals for Local Electrophilicity and Local Nucleophilicity Descriptors. *Physical Chemistry Chemical Physics*, **16**, 26832–26842.

Morell, C., Grand, A. and Toro-Labbé, A. (2005). New Dual Descriptor for Chemical Reactivity. *The Journal of Physical Chemistry A*, **109**, 205–212.

Morell, C., Grand, A. and Toro-Labbé, A. (2006). Theoretical support for using the Δf(r) descriptor. *Chemical Physics Letters*, **425**, 342–346.

Morell, C., Hocquet, A., Grand, A. and Jamart-Grégoire, B. (2008b) A Conceptual DFT Study of Hydrazino Peptides: Assessment of the Nucleophilicity of the Nitrogen Atoms by Means of the Dual Descriptor . *Journal of Molecular Structure: THEOCHEM*, **849**, 46-51.

Muir, M. and Baker, J. (2005). A Simple Calculational Model for Predicting the Site for Nucleophilic Substitution in Aromatic Perfluorocarbons. *Journal of Fluorine Chemistry*, **126**, 727–738.

Mulliken, R. S. (1934). A New Electroaffinity Scale; Together with Data on Valence States and on Valence Ionization Potentials and Electron Affinities. *The Journal of Chemical Physics*, **2**, 782–793.

Mulliken, R. S. (1935). Electronic Structures of Molecules XI. Electroaffinity, Molecular Orbitals and Dipole Moments. *The Journal of Chemical Physics*, **3**, 573–585.

Mulliken, R. S. (1955). Electronic Population Analysis on LCAO–MO Molecular Wave Functions. I. *The Journal of Chemical Physics*, **23**, 1833–1840.

Murray, C. W., Laming, G. J., Handy, N. C. and Amos, R. D. (1992). Kohn—Sham Bond Lengths and Frequencies Calculated with Accurate Quadrature and Large Basis Sets. *Chemical Physics Letters*, **199**, 551–556.

Muthu, S., Ramachandran, G. and Uma maheswari, J. (2012). Vibrational Spectroscopic Investigation on the Structure of 2-Ethylpyridine-4-Carbothioamide. *Spectrochimica Acta Part A: Molecular and Biomolecular Spectroscopy*, **93**, 214–222.

Muthumariappan, S. (2013). Synthesis and Characterization Of Ciprofloxacin–Zinc (II) Complex and Assay Studies in Pharmaceutical Drugs. *Journal of Pharmacy Research*, **6**, 437–441.

Naresh, A., Venkateswara Rao, M., Kotapalli, S. S., Ummanni, R. and Venkateswara Rao, B. (2014). Oxazolidinone Derivatives: Cytoxazone–Linezolid Hybrids Induces Apoptosis and Senescence in DU145 Prostate Cancer Cells. *European Journal of Medicinal Chemistry*, **80**, 295–307.

Nath, S., Nandi, P. K., Sannigrahi, A. B. and Chattaraj, P. K. (1993). Effect of Basis Sets And Population Analysis Schemes on the Calculation of Group Electronegativity. *Journal of Molecular Structure: THEOCHEM*, **279**, 207–211.

Nath, S., Sannigrahi, A. B. and Chattaraj, P. K. (1994). Effect of Basis Sets on Ab Initio SCF Calculations of Molecular Hardness. *Journal of Molecular Structure: THEOCHEM*, **306**, 87–90.

Nathan, C. (2004). Antibiotics at the Crossroads. *Nature*, **431**, 899–902.

Navarro, M., Castro, W., Higuera-Padilla, A. R., Sierraalta, A., Abad, M. J., Taylor, P. and Sánchez-Delgado, R. A. (2011a). Synthesis, Characterization and Biological Activity of Trans-Platinum(II) Complexes with Chloroquine. *Journal of Inorganic Biochemistry*, **105**, 1684–1691.

Navarro, M., Castro, W., Martínez, A. and Sánchez Delgado, R. A. (2011b). The Mechanism Of Antimalarial Action of $[Au(CQ)(PPh_3)]PF_6$: Structural Effects and

Increased Drug Lipophilicity Enhance Heme Aggregation Inhibition at Lipid/Water Interfaces. *Journal of Inorganic Biochemistry,* **105**, 276–282.

Navarro, M., Cisneros-Fajardo, E. J., Lehmann, T., Sánchez-Delgado, R. A., Atencio, R., Silva, P. and Urbina, J. A. (2001). Toward a Novel Metal-Based Chemotherapy against Tropical Diseases. 6. Synthesis and Characterization of New Copper(II) and Gold(I) Clotrimazole and Ketoconazole Complexes and Evaluation of Their Activity against *Trypanosoma cruzi*. *Inorganic Chemistry,* **40**, 6879–6884.

Navarro, M., Gabbiani, C., Messori, L. and Gambino, D. (2010). Metal-Based Drugs for Malaria, Trypanosomiasis and Leishmaniasis: Recent Achievements and Perspectives. *Drug Discovery* 15: 1070–1078.

Navarro, M., Pérez, H. and Sánchez-Delgado, R. A. (1997). Toward a Novel Metal-Based Chemotherapy Against Tropical Diseases. 3. Synthesis and Antimalarial Activity *In Vitro* and *In Vivo* of the New Gold−Chloroquine Complex [Au(PPh3)(CQ)]PF6. *Journal of Medicinal Chemistry*, **40**, 1937–1939.

Navarro, M., Vásquez, F., Sánchez-Delgado, R. A., Pérez, H., Sinou, V. and Schrével, J. (2004). Toward a Novel Metal-Based Chemotherapy against Tropical Diseases. 7. Synthesis and *In Vitro* Antimalarial Activity of New Gold−Chloroquine Complexes. *Journal of Medicinal Chemistry*, **47**, 5204–5209.

Neese, F. (2001). Prediction of Electron Paramagnetic Resonance G Values Using Coupled Perturbed Hartree–Fock and Kohn–Sham Theory. *The Journal of Chemical Physics,* **115**, 11080–11096.

Neese, F. (2006). A Critical Evaluation Of DFT, Including Time-Dependent DFT, Applied to Bioinorganic Chemistry. *Journal of Biological Inorganic Chemistry,* **11**, 702–711.

Neese, F. (2009). Prediction of Molecular Properties and Molecular Spectroscopy With Density Functional Theory: From Fundamental Theory to Exchange-Coupling. *Coordination Chemistry Reviews,* **253**, 526–563.

Neu, H. C. (1992). The Crisis in Antibiotic Resistance. *Science,* **257**: 1064–1073.

Nguyen, A., Top, S., Vessières, A., Pigeon, P., Huché, M., Hillard, E. A.and Jaouen, G. (2007). Organometallic Analogues of Tamoxifen: Effect of the Amino Side-Chain Replacement by a Carbonyl Ferrocenyl Moiety in Hydroxytamoxifen. *Journal of Organometallic Chemistry,* **692**, 1219–1225.

Nguyen, H. M. T., Peeters, J., Nguyen, M. T. and Chandra, A. K. (2004). Use of DFT-Based Reactivity Descriptors for Rationalizing Radical Reactions: A Critical Analysis. *The Journal of Physical Chemistry A,* **108**, 484–489.

Nguyen, L. T., De Proft, F., Cases Amat, M., Van Lier, G., Fowler, P. W. and Geerlings, P. (2003). Local Softness Versus Local Density of States as Reactivity Index. *The Journal of Physical Chemistry A,* **107**, 6837–6842.

Nikaido, H. (2009). Multidrug Resistance in Bacteria. *Annual Review of Biochemistry*, **78**, 119–146.

Njoku, D. I., Oguzie, E. E. and Li, Y. (2017). Characterization, Electrochemical and Theoretical Study of the Anticorrosion Properties of Moringa Oleifera Extract. *Journal of Molecular Liquids,* **237**, 247–256.

NNIS. (2004). National Nosocomial Infections Surveillance System Report, Data Summary From January 1992 Through June 2004, Issued October 2004. *American Journal of Infection Control,* **32**:470–85.

Nogueira, H. I. . (1998). Surface-Enhanced Raman Scattering (SERS) Of 3-Aminosalicylic and 2-Mercaptonicotinic Acids in Silver Colloids. *Spectrochimica Acta Part A: Molecular and Biomolecular Spectroscopy,* **54**, 1461–1470.

Norrby, S. R., Nord, C. E. and Finch, R. (2005). Lack of Development of New Antimicrobial Drugs: A Potential Serious Threat to Public Health. *The Lancet Infectious Diseases*, **5**: 115–119.

Obaleye, J. A., Adediji, J. F. and Adebayo, M. A. (2011). Synthesis And Biological Activities On Metal Complexes of 2,5-Diamino-1,3,4-Thiadiazole Derived from Semicarbazide Hydrochloride. *Molecules,* **16**, 5861–5874.

Obaleye, J. A., Adeyemi, O. G. and Balogun, E. A. (2001). Some Metal Tetracycline Complexes: Synthesis, Characterization and Their Effects against Malaria Parasites. *International Journal of Chemistry,* **11**, 101-106.

Obaleye, J. A., Caira, M. R. and Tella, A. C. (2009). Synthesis, Characterization And Crystal Structures of the Tetrachlorocuprate and Tetrabromocadmate Salts of the Antimalarial Mefloquine. *Structural Chemistry*, **20**, 859–868.

Ogunniran, K.O., Tella, A. C., Alensela, M. and Yakubu, M. T. (2007). Synthesis, Physical Properties, Antimicrobial Potentials of Some Antibiotics Complexed With Transition Metals and Their Effects on Alkaline Phosphatase Activities of Selected Rat Tissue. *African Journal of biotechnology*, **6**, 1202–1208.

Oguzie, E. E., Njoku, D. I., Chidebere, M. A., Ogukwe, C. E., Onuoha, G. N., Oguzie, K. L. and Ibisi, N. (2014). Characterization and Experimental and Computational Assessment of *Kola nitida* Extract for Corrosion Inhibiting Efficacy. *Industrial and Engineering Chemistry Research*, **53**, 5886–5894.

Oliveira, J. S., Sousa, E. H. S., Basso, L. A., Palaci, M., Dietze, R., Santos, D. S. and Moreira, Icaro S. (2004). An Inorganic Iron Complex That Inhibits Wild-Type and an

Isoniazid-Resistant Mutant 2-Trans-Enoyl-ACP (CoA) Reductase from *Mycobacterium tuberculosis*. *Chemical Communications*, **3**, 312-313.

Ormazábal-Toledo, R. and Contreras, R. (2014). Philicity and Fugality Scales for Organic Reactions. *Advances in Chemistry*, **2014**, 1–13.

Ormazábal-Toledo, R., Campodónico, P. R. and Contreras, R. (2011). Are Electrophilicity and Electrofugality Related Concepts? A Density Functional Theory Study. *Organic Letters,* **13**, 822–824.

Ormazábal-Toledo, R., Contreras, R. and Campodónico, P. R. (2013). Reactivity Indices Profile: A Companion Tool of the Potential Energy Surface for the Analysis of Reaction Mechanisms. Nucleophilic Aromatic Substitution Reactions as Test Case. *The Journal of Organic Chemistry,* **78**, 1091–1097.

Orozco-Valencia, A. U., Gázquez, J. L. and Vela, A. (2017). Global and Local Partitioning of the Charge Transferred in the Parr–Pearson Model. *The Journal of Physical Chemistry A,* **121**, 4019–4029.

Orpen, A. G., Brammer, L., Allen, F. H., Kennard, O., Watson, D. G. and Taylor, R. (1989). Supplement. Tables of Bond Lengths Determined By X-Ray And Neutron Diffraction. Part 2. Organometallic Compounds and Co-Ordination Complexes of the D- And F-Block Metals. *Journal of the Chemical Society, Dalton Transactions*, **12**, S1-S83.

Orvig, C. and Abrams, M. J. (1999). Medicinal Inorganic Chemistry: Introduction. *Chemical Reviews,* **99**, 2201–2204.

Özdemir, İ., Denizci, A., Öztürk, H. T. and Çetinkaya, B. (2004). Synthetic and Antimicrobial Studies On New Gold(I) Complexes of Imidazolidin-2-Ylidenes. *Applied Organometallic Chemistry*, **18**, 318–322.

Özdemir, İ., Temelli, N., Günal, S. and Demir, S. (2010). Gold(I) Complexes of N-Heterocyclic Carbene Ligands Containing Benzimidazole: Synthesis and Antimicrobial Activity. *Molecules*, **15**, 2203–2210.

Padilla-Campos, L. and Fuentealba, P. (2003). Theoretical Study of the Adsorption of Oxygen on a Cu(100) Surface and the Co-adsorption With Alkali Atoms. *Theoretica Chimica Acta,* **110**, 414–420.

Padmanabhan, J., Parthasarathi, R., Elango, M., Subramanian, V., Krishnamoorthy, B. S., Gutierrez-Oliva, S. and Chattaraj, P. K. (2007). Multiphilic Descriptor for Chemical Reactivity and Selectivity. *The Journal of Physical Chemistry A,* **111**, 9130–9138.

Palumbo Piccionello, A., Musumeci, R., Cocuzza, C., Fortuna, C. G., Guarcello, A., Pierro, P. and Pace, A. (2012). Synthesis And Preliminary Antibacterial Evaluation of Linezolid-Like 1,2,4-Oxadiazole Derivatives. *European Journal of Medicinal Chemistry,* **50**, 441–448.

Panicker, C. Y., Varghese, H. T., John, A., Philip, D., Istvan, K. and Keresztury, G. (2002). FTIR, FT-Raman and FT-SERS Spectra of 4-Aminosalicylic Acid Sodium Salt Dihydrate. *Spectrochimica Acta Part A: Molecular and Biomolecular Spectroscopy*, **58**, 281–287.

Panlilio, A. L., Culver, D.H. and Gaynes, R. P. (1992). Methicillin-Resistant *S. aureus* in US Hospitals, 1975–1991. Infectious Control Hospital Epidemiology; **13**, 582–586.

Parker, M. (1970). Methicillin Resistance in *Staphylococcus aureus. The Lancet*, **295**, 800–804.

Parker, M. T. and Jevons, M. P. (1964). A Survey of Methicillin Resistance in *Staphylococcus aureus*. *Postgraduate Medical Journal*, **40**, 170-8.

Parr R.G. (1980) Density Functional Theory of Atoms and Molecules. In: Fukui K., Pullman B. (eds) Horizons of Quantum Chemistry. Académie Internationale Des Sciences Moléculaires Quantiques / International Academy of Quantum Molecular Science, vol 3. Springer, Dordrecht

Parr, R. and Yang, W. (1984). Density Functional Approach to the Frontier-Electron Theory of Chemical Reactivity. *Journal of the American Chemical Society*, **106**, 4049-4050.

Parr, R. G. (2001). Quantum Chemistry: Classic Scientific Papers Quantum Chemistry*: Physics Today*, **54**, 63–64.

Parr, R. G. and Gazquez, J. L. (1993). Hardness Functional. *The Journal of Physical Chemistry*, **97**, 3939–3940.

Parr, R. G. and Parr, J. B. (1999). Kenichi Fukui: Recollections of a Friendship. *Theoretical Chemistry Accounts: Theory, Computation, and Modeling (Theoretica Chimica Acta)*, **102**, 4–6.

Parr, R. G. and Pearson, R. G. (1983). Absolute Hardness: Companion Parameter to Absolute Electronegativity. *Journal of the American Chemical Society*, **105**, 7512–7516.

Parr, R. G. and Yang, W. (1995). Density-Functional Theory of the Electronic Structure of Molecules. *Annual Review of Physical Chemistry*, **46**, 701–728.

Parr, R. G., Ayers, P. W. and Nalewajski, R. F. (2005). What is an Atom in a Molecule? *The Journal of Physical Chemistry A*, **109**, 3957–3959.

Parr, R. G., Szentpály, L. V. and Liu, S. (1999). Electrophilicity Index. *Journal of the American Chemical Society*, **121**, 1922–1924.

Parr, R.G. and Yang, C.Y. (1989). Density Functional Theory of Atoms and Molecules. Oxford University Press, Oxford.

Parr, R.G., Kugler, A.A. and Nagy, A. (1995) Some Identities in Density-Functional Theory. *Physical Review A*, **52**, 969-976.

Parthasarathi, R., Subramanian, V., Roy, D. R. and Chattaraj, P. K. (2004). Electrophilicity Index as a Possible Descriptor of Biological Activity. *Bioorganic and Medicinal Chemistry*, **12**, 5533–5543.

Paterson, D. L. and Doi, Y. (2007). A Step Closer to Extreme Drug Resistance (XDR) in Gram-Negative Bacilli. *Clinical Infectious Diseases*, **45**, 1179–1181.

Patra, M. and Gasser, G. (2012). Organometallic Compounds: An Opportunity for Chemical Biology? *ChemBioChem*, **13**, 1232–1252.

Patra, M., Gasser, G., Pinto, A., Merz, K., Ott, I., Bandow, J. E. and Metzler-Nolte, N. (2009). Synthesis and Biological Evaluation of Chromium Bioorganometallics Based on the Antibiotic Platensimycin Lead Structure. *ChemMedChem*, **4**, 1930–1938.

Patra, M., Gasser, G., Wenzel, M., Merz, K., Bandow, J. E. and Metzler-Nolte, N. (2011). Synthesis of Optically Active Ferrocene-Containing Platensimycin Derivatives with a C6-C7 Substitution Pattern. *European Journal of Inorganic Chemistry*, **2011**, 3295–3302.

Patra, M., Gasser, G., Wenzel, M., Merz, K., Bandow, J. E. and Metzler-Nolte, N. (2010). Synthesis and Biological Evaluation of Ferrocene-Containing Bioorganometallics Inspired by the Antibiotic Platensimycin Lead Structure. *Organometallics*, **29**, 4312–4319.

Patra, M., Gasser, G., Wenzel, M., Merz, K., Bandow, J. E. and Metzler-Nolte, N. (2012a). Sandwich and Half-Sandwich Derivatives of Platensimycin: Synthesis and Biological Evaluation. *Organometallics*, **31**, 5760–5771.

Patra, M., Merz, K. and Metzler-Nolte, N. (2012b). Planar Chiral (η^6-arene)$Cr(CO)_3$ Containing Carboxylic Acid Derivatives: Synthesis And Use In The Preparation Of Organometallic Analogues Of The Antibiotic Platensimycin. *Dalton Transactions*, **41**, 112–117.

Peacock, A. F. A. and Sadler, P. J. (2008). Medicinal Organometallic Chemistry: Designing Metal Arene Complexes as Anticancer Agents. Chemistry - *An Asian Journal*, **3**, 1890–1899.

Peacock, A. F. A., Habtemariam, A., Moggach, S. A., Prescimone, A., Parsons, S. and Sadler, P. J. (2007). Chloro Half-Sandwich Osmium(II) Complexes: Influence of Chelated N,N-Ligands on Hydrolysis, Guanine Binding, and Cytotoxicity. *Inorganic Chemistry*, **46**, 4049–4059.

Pearson, R. G. (1963). Hard and Soft Acids and Bases. *Journal of the American Chemical Society*, **85**, 3533–3539.

Pearson, R. G. (1985). Absolute Electronegativity and Absolute Hardness of Lewis Acids and Bases. *Journal of the American Chemical Society*, **107**, 6801–6806.

Pearson, R. G. (1988). Absolute Electronegativity and Hardness: Application to Inorganic Chemistry. *Inorganic Chemistry,* **27**, 734–740.

Pearson, R. G. (1989). Absolute Electronegativity and Hardness: Applications to Organic Chemistry. *The Journal of Organic Chemistry*, **54**, 1423–1430.

Pearson, R. G. (1990). Hard And Soft Acids and Bases—The Evolution of a Chemical Concept. *Coordination Chemistry Reviews,* **100**, 403–425.

Pearson, R. G. (1994). Principle of Maximum Physical Hardness. *The Journal of Physical Chemistry,* **98**, 1989–1992.

Pearson, R. G. (1995). The HSAB Principle — More Quantitative Aspects. *Inorganica Chimica Acta,* **240**, 93–98.

Pearson, R. G. (2005). Chemical Hardness and Density Functional Theory. *Journal of Chemical Sciences,* **117**, 369–377.

Pearson, R. G. and Songstad, J. (1967). Application of the Principle of Hard and Soft Acids and Bases to Organic Chemistry. *Journal of the American Chemical Society,* **89**, 1827–1836.

Pellerito, A., Fiore, T., Pellerito, C., Fontana, A., Di Stefano, R., Pellerito, L. and Mansueto, C. (1998). Organometallic Complexes with Biological Molecules. XI. Solid State And *In Vivo* Investigations of Some Diorganotin(IV)-Chloramphenicol and Cycloserine Derivatives. *Journal of Inorganic Biochemistry*, **72**, 115–125.

Perdew, J. P. and Levy, M. (1983). Physical Content of the Exact Kohn-Sham Orbital Energies: Band Gaps and Derivative Discontinuities. *Physical Review Letters,* **51**, 1884–1887.

Perdew, J. P. and Levy, M. (1997). Comment on "Significance of the Highest Occupied Kohn-Sham Eigenvalue.*" Physical Review B,* **56**, 16021–16028.

Perdew, J. P., Burke, K. and Ernzerhof, M. (1996). Generalized Gradient Approximation Made Simple. *Physical Review Letters,* **77**, 3865–3868.

Perdew, J. P., Burke, K. and Ernzerhof, M. (1998a). Perdew, Burke, and Ernzerhof Reply*: Physical Review Letters,* **80**, 891–891.

Perdew, J. P., Chevary, J. A., Vosko, S. H., Jackson, K. A., Pederson, M. R., Singh, D. J. and Fiolhais, C. (1992). Atoms, molecules, solids, and surfaces: Applications of the generalized gradient approximation for exchange and correlation. *Physical Review B,* **46,** 6671–6687.

Perdew, J. P., Ernzerhof, M., Zupan, A. and Burke, K. (1998b). Nonlocality Of The Density Functional for Exchange and Correlation: Physical Origins and Chemical Consequences. *The Journal of Chemical Physics,* **108**, 1522–1531.

Perdew, J. P., Parr, R. G., Levy, M. and Balduz, J. L. (1982). Density-Functional Theory for Fractional Particle Number: Derivative Discontinuities of the Energy. *Physical Review Letters,* **49**, 1691–1694.

Perdew, J.P. and Zunger, A. (1981) Self-Interaction Correction to Density-Functional Approximations for Many-Electron Systems. *Physical Review B,* **23**, 5048-5079.

Pérez, P., Domingo, L. R., José Aurell, M. and Contreras, R. (2003). Quantitative Characterization of the Global Electrophilicity Pattern of Some Reagents Involved in 1,3-Dipolar Cycloaddition Reactions. *Tetrahedron,* **59**, 3117–3125.

Pérez, P., Simón-Manso, Y., Aizman, A., Fuentealba, P. and Contreras, R. (2000). Empirical Energy−Density Relationships for the Analysis of Substituent Effects in Chemical Reactivity. *Journal of the American Chemical Society,* **122**, 4756–4762.

Pérez-Méndez, C. and Contreras, R. (2015). Quantitative Characterization of the Global Philicity Patterns of Common Diene/Dienophile Pairs in Cycloaddition Reactions II: The Interacting Pair Model. *Tetrahedron Letters*, **56**, 1767–1770.

Petrenko, T., Ray, K., Wieghardt, K. E. and Neese, F. (2006). Vibrational Markers for the Open-Shell Character of Transition Metal Bis-dithiolenes: An Infrared, Resonance Raman, and Quantum Chemical Study. *Journal of the American Chemical Society,* **128**, 4422–4436.

Peverati, R. and Truhlar, D. G. (2014). Quest For A Universal Density Functional: The Accuracy Of Density Functionals Across a Broad Spectrum of Databases in Chemistry and Physics. *Philosophical Transactions of the Royal Society A: Mathematical, Physical and Engineering Sciences*, **372**, 20120476–20120476.

Philip, D., John, A., Panicker, C. Y. and Varghese, H. T. (2001). FT-Raman, FTIR and Surface Enhanced Raman Scattering Spectra of Sodium Salicylate. *Spectrochimica Acta Part A: Molecular and Biomolecular Spectroscopy,* **57**, 1561–1566.

Pilar, B. M.., María, G. J., Choquesillo-Lazarte, D., Carballo, R., Castiñeiras, A. and Niclós-Gutiérrez, J. (2003). Two Intra-Molecular Inter-Ligand C(Aromatic)–HO(Carboxyl) Interactions Reinforce the Formation of a Single Cu(II)–N4(PZA) Bond in the Molecular Recognition Between Pyrazine-2-Carboxamide (PZA) and the (Iminodiacetato)Copper(II) Chelate. Synthesis, Molecular and Crystal Structure and Properties of $[Cu(IDA)(PZA)(H_2 O)]\cdot H_2O$. *Inorganic Chemistry Communications*, **6**, 270–273.

Pino-Rios, R., Yañez, O., Inostroza, D., Ruiz, L., Cardenas, C., Fuentealba, P. and Tiznado, W. (2017). Proposal of a Simple and Effective Local Reactivity Descriptor

through a Topological Analysis of an Orbital-Weighted Fukui Function. *Journal of Computational Chemistry*, **38**, 481–488.

Politzer, P. and Abu-Awwad, F. (1998). A Comparative Analysis of Hartree-Fock and Kohn-Sham Orbital Energies. *Theoretical Chemistry Accounts: Theory, Computation, and Modeling (Theoretica Chimica Acta)*, **99**, 83–87.

Ponti, A. (2000). DFT-Based Regioselectivity Criteria for Cycloaddition Reactions. *The Journal of Physical Chemistry A*, **104**, 8843–8846.

Pradines, B. (2001). Ferrocene-Chloroquine Analogues as Antimalarial Agents: In Vitro Activity of Ferrochloroquine Against 103 Gabonese Isolates of *Plasmodium falciparum*. *Journal of Antimicrobial Chemotherapy*, **48**, 179–184.

Pratihar, S. and Roy, S. (2010). Nucleophilicity and Site Selectivity of Commonly Used Arenes and Heteroarenes. *The Journal of Organic Chemistry*, **75**, 4957–4963.

Preti, C. and Tosi, G. (1979). Metal Ion Coordination by the Antibiotic Cycloserine. Complexes of Palladium (II), Platinum (II) and Copper (II). *Journal of Coordination Chemistry*, **9**, 125–131.

Preti, C. and Tosi, G. (1980a). The Coordinating Ability of the Antibiotic Cycloserine towards Transition Metal Halides. *Australian Journal of Chemistry*, **33**, 57-68.

Preti, C., and Tosi, G. (1980b). Cycloserine Derivatives as Ligands. Cobalt(II), Nickel(II), Copper(II), Zinc(II) and Cadmium(II) Halide Complexes of N 4,N′ 4-Tereftal-Bis(Cycloserine). Journal of Coordination Chemistry, **10**, 209–216.

Preti, C., Tassi, L., Tosi, G., Zannini, P. and Zanoli, A. (1982). Cycloserine Derivatives as Ligands. The Coordinating Ability of 4,4'-[1,4-Phenylenebis(Methylidynenitrilo)]Bis(Isoxazolidin-3-One) towards Chromium(III), Ruthenium(III) and Rhodium(III) Halides. *Australian Journal of Chemistry*, **35**, 1829-1840.

Preti, C., Tassi, L., Tosi, G., Zannini, P. and Zanoli, A. F. (1983). Coordination Chemistry of Cycloserine Derivatives. Complexes of Iron(II), Iron(III), Manganese(II) and Palladium(II) with N4-N'4-Tereftal-Bis(Cycloserine). *Journal of Coordination Chemistry*, **12**, 177–186.

Preti, C., Tosi, G. and Zannini, P. (1979). Antibiotics as Ligands Coordinating Behaviour of the Cycloserine Towards Cobalt(II), Nickel(II), Zinc(II), Cadmium(II), and Mercury(II) Halides. *Zeitschrift FuR Anorganische Und Allgemeine Chemie*, **453**, 173–184.

Preti, C., Tosi, G. and Zannini, P. (1980). Investigations of Chromium(III), Manganese(III), Tin(II) and Lead(II) Dithiocarbamate Complexes. *Journal of Molecular Structure*, **65**, 283–292.

Pribram-Jones, A., Gross, D. A. and Burke, K. (2015). DFT: A Theory Full of Holes? *Annual Review of Physical Chemistry*, **66**, 283–304.

Putz, M. V. (2013). Koopmans' Analysis of Chemical Hardness with Spectral-Like Resolution. *The Scientific World Journal*, **2013**, 1–14.

Quiney H. M. (1991) High Precision Relativistic Atomic Structure Calculations Using the Finite Basis Set Approximation. In: Wilson, S., Grant, I. P., Gyorffy, B. L. (eds) The Effects of Relativity in Atoms, Molecules, and the Solid State. Springer, Boston, MA

Quintal, S. M. O., Félix, V., Drew, M. G. B. and Nogueira, H. I. S. (2006). Coordination Modes of 3-Aminosalicylic And 3-Hydroxyanthranilic Acids in Palladium(II), Platinum(II) and Rhenium(V) Complexes. The Crystal Structure of Cis-[Pt(HsalNH)(PPh3)2]·0.25C_2H_5OH. *Polyhedron*, **25**, 753–758.

Ramírez-Ramírez, J.-Z., Vargas, R., Garza, J. and Gázquez, J. L. (2010). Simple Charge-Transfer Model for Metallic Complexes. *The Journal of Physical Chemistry A*, **114**, 7945–7951.

Raviglione, M. C. (2008) Facing Extensively Drug-Resistant Tuberculosis a Hope and a Challenge. *New England Journal of Medicine*, **359**, 636-38.

Refat, M. S. and Mohamed, S. F. (2011). Spectroscopic, Thermal And Antitumor Investigations Of Sulfasalazine Drug In Situ Complexation With Alkaline Earth Metal Ions. *Spectrochimica Acta Part A: Molecular and Biomolecular Spectroscopy*, **82**, 108–117.

Regiel-Futyra, A., Dąbrowski, J. M., Mazuryk, O., Śpiewak, K., Kyzioł, A., Pucelik, B. and Stochel, G. (2017). Bioinorganic Antimicrobial Strategies in the Resistance Era. *Coordination Chemistry Reviews*, **351**, 76–117.

Rehman, W., Haq, S., Muhammad, B., Hassan, S. F., Badshah, A., Waseem, M. and Rashid, U. (2014). Organotin (IV) Based Complexes as Promiscuous Antibacterials: Synthesis, *In Vitro*, *In Silico* Pharmacokinetic and Docking Studies. *Journal of Organometallic Chemistry*, **767**, 91–100.

Rice, L. B. (2008). Federal Funding for the Study of Antimicrobial Resistance in Nosocomial Pathogens: No ESKAPE. *The Journal of Infectious Diseases*, **197**, 1079–1081.

Rieder, H. L. (2009). Fourth-Generation Fluoroquinolones in Tuberculosis. *The Lancet*, **373**: 1148–1149.

Riedl, C. A., Flocke, L. S., Hejl, M., Roller, A., Klose, M. H. M., Jakupec, M. A. and Keppler, B. K. (2016). Introducing the 4-Phenyl-1,2,3-Triazole Moiety as a Versatile Scaffold for the Development of Cytotoxic Ruthenium(II) and Osmium(II) Arene Cyclometalates. *Inorganic Chemistry*, **56**, 528–541.

Roca, I., Akova, M., Baquero, F., Carlet, J., Cavaleri, M., Coenen, S. and Vila, J. (2015). The Global Threat of Antimicrobial Resistance: *Science for Intervention. New Microbes and New Infections,* **6**: 22–29.

Roy, D. R., Parthasarathi, R., Padmanabhan, J., Sarkar, U., Subramanian, V. and Chattaraj, P. K. (2006). Careful Scrutiny of the Philicity Concept. *The Journal of Physical Chemistry A,* **110**, 1084–1093.

Roy, R. K., Krishnamurti, S., Geerlings, P. and Pal, S. (1998). Local Softness and Hardness Based Reactivity Descriptors for Predicting Intra- and Intermolecular Reactivity Sequences: Carbonyl Compounds. *The Journal of Physical Chemistry A,* **102**, 3746–3755.

Sablon, N., Proft, F. D. and Geerlings, P. (2009). Molecular Orbital-Averaged Fukui Function for the Reactivity Description of Alkaline Earth Metal Oxide Clusters. *Journal of Chemical Theory and Computation,* **5**, 1245–1253.

Saha, S., Roy, R. K. and Ayers, P. W. (2009). Are the Hirshfeld and Mulliken Population Analysis Schemes Consistent With Chemical Intuition? *International Journal of Quantum Chemistry,* **109**, 1790–1806.

Samuel, M. A. and Justice, K. S. (2016). Copper-Paracetamol Complexes: Promising Lead Antibacterial Drug Candidates. *African Journal of Pure and Applied Chemistry*, **10**, 56–62.

Sanchez-Delgado, R. A., Lazardi, K., Rincon, L., Urbina, J. A., Hubert, A. J. and Noels, A. N. (1993). Toward A Novel Metal-Based Chemotherapy against Tropical Diseases. 1. Enhancement of the Efficacy of Clotrimazole Against *Trypanosoma cruzi* by Complexation to Ruthenium In $RuCl_2(Clotrimazole)_2$. *Journal of Medicinal Chemistry,* **36**, 2041–2043.

Sánchez-Delgado, R. A., Navarro, M., Lazardi, K., Atencio, R., Capparelli, M., Vargas, F. and Masi, D. (1998). Toward a Novel Metal Based Chemotherapy against Tropical Diseases 4. Synthesis And Characterization of New Metal-Clotrimazole Complexes and Evaluation of Their Activity Against *Trypanosoma cruzi. Inorganica Chimica Acta,* **275**, 528–540.

Sánchez-Delgado, R. A., Navarro, M., Pérez, H. and Urbina, J. A. (1996). Toward A Novel Metal-Based Chemotherapy Against Tropical Diseases. 2. Synthesis and Antimalarial Activity *In Vitro a*nd *In Vivo* of New Ruthenium− and Rhodium−Chloroquine Complexes. *Journal of Medicinal Chemistry,* **39**, 1095–1099.

Santos, J. C., Chamorro, E., Contreras, R. and Fuentealba, P. (2004a). Local Reactivity Index as Descriptor of Benzene Adsorption in Cluster Models of Exchanged Zeolite-Y. *Chemical Physics Letters*, **383**, 612–616.

Santos, J. C., Contreras, R., Chamorro, E. and Fuentealba, P. (2002). Local Reactivity Index Defined Through the Density of States Describes the Basicity of Alkaline-Exchanged Zeolites. *The Journal of Chemical Physics,* **116**, 4311–4316.

Santos, J. C., Tiznado, W., Contreras, R. and Fuentealba, P. (2004b). Sigma–Pi Separation of the Electron Localization Function and Aromaticity. *The Journal of Chemical Physics,* **120**, 1670–1673.

Savin, A., Umrigar, C. J. and Gonze, X. (1998). Relationship of Kohn–Sham Eigenvalues to Excitation Energies. *Chemical Physics Letters,* **288**, 391–395.

Schinzel, S., Bindl, M., Visseaux, M. and Chermette, H. (2006). Structural and Electronic Analysis of Lanthanide Complexes: Reactivity May Not Necessarily Be Independent of the Identity of the Lanthanide Atom − A DFT Study. *The Journal of Physical Chemistry A,* **110**, 11324–11331.

Schmidt, M. W. and Gordon, M. S. (1998). The Construction and Interpretation of MCSCF Wavefunctions. *Annual Review of Physical Chemistry,* **49**, 233–266.

Selvakumar, N., Srinivas, D., Khera, M. K., Kumar, M. S., Mamidi, R. N. V. S., Sarnaik, H. and Rajagopalan, R. (2002). Synthesis of Conformationally Constrained Analogues of Linezolid: Structure−Activity Relationship (SAR) Studies on Selected Novel Tricyclic Oxazolidinones. *Journal of Medicinal Chemistry,* **45**: 3953–3962.

Selvakumar, N., Yadi Reddy, B., Sunil Kumar, G., Khera, M. K., Srinivas, D., Sitaram Kumar, M. and Trehan, S. (2006). Synthesis of Novel Tricyclic Oxazolidinones by a Tandem SN2 and SNAr Reaction: SAR Studies on Conformationally Constrained Analogues of Linezolid. *Bioorganic and Medicinal Chemistry Letters*, **16**, 4416–4419.

Senet, P. (1996). Nonlinear Electronic Responses, Fukui Functions and Hardnesses as Functionals of the Ground-State Electronic Density. *The Journal of Chemical Physics,* **105**, 6471–6489.

Senet, P. (1997a). Chemical Hardnesses of Atoms and Molecules from Frontier Orbitals. *Chemical Physics Letters*, **275**, 527–532.

Senet, P. (1997b). Kohn-Sham Orbital Formulation of the Chemical Electronic Responses, Including The Hardness. *The Journal of Chemical Physics*, **107**, 2516–2524.

Shagufta, and Ahmad, I. (2018). Tamoxifen a Pioneering Drug: An Update on the Therapeutic Potential of Tamoxifen Derivatives. *European Journal of Medicinal Chemistry,* **143**, 515–531

Shankar, R., Senthilkumar, K. and Kolandaivel, P. (2009). Calculation of Ionization Potential and Chemical Hardness: A Comparative Study of Different Methods. *International Journal of Quantum Chemistry*, **109**, 764–771.

Shenoi, S.a nd Friedland, G. (2009). Extensively Drug-Resistant Tuberculosis: A New Face to an Old Pathogen. *Annual Review of Medicine*, **60**, 307–320.

Siegbahn, P. E. M. (2006). The Performance of Hybrid DFT for Mechanisms Involving Transition Metal Complexes In Enzymes. *Journal of Biological Inorganic Chemistry*, **11**, 695–701.

Sievert, D. M., Rudrik, J. T., Patel, J. B., McDonald, L. C., Wilkins, M. J. and Hageman, J. C. (2008). Vancomycin-Resistant *Staphylococcus aureus* in the United States, *2002-2006. Clinical Infectious Diseases*, **46**, 668–674.

Sievert, D. M., Rudrik, J. T., Patel, J. B., McDonald, L. C., Wilkins, M. J. and Hageman, J. C. (2008). Vancomycin-Resistant *Staphylococcus aureus* in the United States, 2002-2006. *Clinical Infectious Diseases*, **46**, 668–674.

Silva, A. T. A. Castro, L. F. Guido, R. V. C. Chung, M. C. Ferreira, E.I.(2005). Advances in prodrug design. *Mini-Reviews in Medicinal Chemistry*, **10**, 893–914.

Sinanoğlu, O. (1961). Theory of Electron Correlation in Atoms and Molecules. *Proceedings of the Royal Society A: Mathematical, Physical and Engineering Sciences*, **260**, 379–392.

Sinanoğlu, O. (2007a). Electron Correlation in Atoms and Molecules. *Advances in Chemical Physics*, **2007**, 237–282.

Sinanoğlu, O. (2007b). Many-Electron Theory of Atoms, Molecules and Their Interactions. *Advances in Chemical Physics*, **2007**, 315–412.

Soliman, M. H. and Mohamed, G. G. (2013). Cr(III), Mn(II), Fe(III), Co(II), Ni(II), Cu(II) and Zn(II) New Complexes of 5-Aminosalicylic Acid: Spectroscopic, Thermal Characterization and Biological Activity Studies. *Spectrochimica Acta Part A: Molecular and Biomolecular Spectroscopy*, **107**, 8–15.

Sosa, C., Andzelm, J., Elkin, B. C., Wimmer, E., Dobbs, K. D. and Dixon, D. A. (1992). A Local Density Functional Study of the Structure and Vibrational Frequencies of Molecular Transition-Metal Compounds. *The Journal of Physical Chemistry*, **96**, 6630–6636.

Soto-Delgado, J., Aizman, A., Contreras, R. and R. Domingo, L. (2011). A DFT Study of the Regioselectivity in Intramolecular Diels-Alder Reactions with Formation of a Tricyclodecane Skeleton. *Letters in Organic Chemistry*, **8**, 125–131.

Spellberg, B., Guidos, R., Gilbert, D., Bradley, J., Boucher, H. W. and Scheld, W. M. (2008). The Epidemic of Antibiotic-Resistant Infections: A Call to Action for the Medical Community from the Infectious Diseases Society of America. *Clinical Infectious Diseases*, **46**, 155–164.

Srivastava, B. K., Jain, M. R., Solanki, M., Soni, R., Valani, D., Gupta, S. and Patel, H. (2008). Synthesis and *In Vitro* Antibacterial Activities of Novel Oxazolidinones. *European Journal of Medicinal Chemistry*, **43**, 683–693.

Srivastava, V. and Lee, H. (2015). Chloroquine-Based Hybrid Molecules as Promising Novel Chemotherapeutic Agents. *European Journal of Pharmacology*, **762**, 472–486.

Stephens, P. J., Devlin, F. J., Chabalowski, C. F. and Frisch, M. J. (1994). Ab Initio Calculation of Vibrational Absorption and Circular Dichroism Spectra Using Density Functional Force Fields. *The Journal of Physical Chemistry*, **98**, 11623–11627.

Strasfeld, L. and Chou, S. (2010). Antiviral Drug Resistance: Mechanisms and Clinical Implications. *Infectious Disease Clinics of North America*, **24**, 413–437.

Supan, C., Mombo-Ngoma, G., Dal-Bianco, M. P., Ospina Salazar, C. L., Issifou, S., Mazuir, F. and Lell, B. (2012). Pharmacokinetics of Ferroquine, a Novel 4-Aminoquinoline, in Asymptomatic Carriers of *Plasmodium falciparum* Infections. *Antimicrobial Agents and Chemotherapy*, **56**, 3165–3173.

Suzuki, H., Utsunomiya, I., Shudo, K., Fujimura, T., Tsuji, M., Kato, I. and Iwaki, T. (2013). Potent Oxazolidinone Antibacterials with Heteroaromatic C-Ring Substructure. *ACS Medicinal Chemistry Letters*, **4**, 1074–1078.

Szarek, P., Komorowski, L. and Lipiński, J. (2010). Fukui functions for atoms and ions: Polarizability justified approach. *International Journal of Quantum Chemistry*, **110**, 2315–2319.

Talbot, G. H., Bradley, J., Edwards, J. E., Gilbert, D., Scheld, M. and Bartlett, J. G. (2006). Bad Bugs Need Drugs: An Update on the Development Pipeline from the Antimicrobial Availability Task Force of the Infectious Diseases Society of America. *Clinical Infectious Diseases*, **42**, 657–668.

Tazi, A., Chapron, J., Touak, G., Longo, M., Hubert, D., Collobert, G. and Morand, P. C. (2013). Rapid Emergence of Resistance to Linezolid and Mutator Phenotypes in *Staphylococcus aureus* Isolates from an Adult Cystic Fibrosis Patient. *Antimicrobial Agents and Chemotherapy*, **57**, 5186–5188.

Thakkar, D., Gevriya, B. and Mashru, R. C. (2014). Study on Interaction Between Palladium(II)–Linezolid Chelate with Eosin by Resonance Rayleigh Scattering, Second Order of Scattering and Frequency Doubling Scattering Methods Using Taguchi Orthogonal Array Design. *Spectrochimica Acta Part A: Molecular and Biomolecular Spectroscopy*, **122**, 75–81.

Theuretzbacher, U. (2011). Resistance Drives Antibacterial Drug Development. *Current Opinion in Pharmacology*, **11**, 433–438.

Tiznado, W., Chamorro, E., Contreras, R. and Fuentealba, P. (2005). Comparison among Four Different Ways to Condense the Fukui Function. *The Journal of Physical Chemistry A,* **109**, 3220–3224.

Top, S., Vessières, A., Cabestaing, C., Laios, I., Leclercq, G., Provot, C. and Jaouen, G. (2001). Studies On Organometallic Selective Estrogen Receptor Modulators. (SERMs) Dual Activity in the Hydroxy-Ferrocifen Series. *Journal of Organometallic Chemistry,* **637**, 500–506.

Toro-Labbé, A. (2007). Theoretical Aspects of Chemical Reactivity. Elsevier Science, Amsterdam

Tuan, D. F. and Sinanoğlu, O. (1964). Many-Electron Theory of Atoms and Molecules. IV. Be Atom and Its Ions. *The Journal of Chemical Physics,* **41**, 2677–2688.

Turel, I., Golic, L. and Ramirez, O. L. R. (1999). Crystal Structure and Characterization of a New Copper (II) Cirpofloxacin (CF) Complex $[Cu(CF)H_2O)_3]$ $SO_4.2H_2O$. *Acta Chimica Slovenica*, **46**, 203-211.

Turel, I., Kljun, J., Perdih, F., Morozova, E., Bakulev, V., Kasyanenko, N. and Osheroff, N. (2010). First Ruthenium Organometallic Complex of Antibacterial Agent Ofloxacin. Crystal Structure and Interactions with DNA. *Inorganic Chemistry*, **49**, 10750–10752.

Turley, J. W. and Pepinsky, R. (1956). The Crystal Structure of Cycloserine Hydrochloride. *Acta Crystallographica*, **9**, 948–951.

Turley, J. W. and Pepinsky, R. (1957). Further Refinement of the Crystal Structure of Cycloserine Hydrochloride. *Acta Crystallographica*, **10**, 480–481.

Ullman, B. (1995). Multidrug Resistance and P-glycoproteins in Parasitic Protozoa. *Journal of Bioenergetics and Biomembranes*, **27**, 77–84.

Upadhyay, S. K., Kumar, P. and Arora, V. (2006). Complexes of Quinolone Drugs Norfloxacin and Ciprofloxacin with Alkaline Earth Metal Perchlorates. *Journal of Structural Chemistry*, **47**, 1078–1083.

Urban, C., Bradford, P. A., Tuckman, M., Segal-Maurer, S., Wehbeh, W., Grenner, L. and Rahal, J. J. (2008). Carbapenem-Resistant *Escherichia coli* Harboring *Klebsiella pneumoniae* Carbapenemase β-Lactamases Associated with Long-Term Care Facilities. *Clinical Infectious Diseases,* **46**, e127–e130.

Vallet, V., Wahlgren, U. and Grenthe, I. (2003). Chelate Effect and Thermodynamics of Metal Complex Formation in Solution: A Quantum Chemical Study. *Journal of the American Chemical Society,* **125**, 14941–14950.

Van Rijt, S. H. and Sadler, P. J. (2009). Current Applications and Future Potential for Bioinorganic Chemistry in the Development of Anticancer Drugs. *Drug Discovery Today,* **14**, 1089–1097.

Van Staveren, D. R. and Metzler-Nolte, N. (2004). Bioorganometallic Chemistry of Ferrocene. *Chemical Reviews*, **104**, 5931–5986.

Varghese, H. T., Yohannan Panicker, C., Philip, D., Mannekutla, J. R. and Inamdar, S. R. (2007). IR, Raman and SERS Studies of Methyl Salicylate. *Spectrochimica Acta Part A: Molecular and Biomolecular Spectroscopy*, **66**, 959–963.

Vela, A. and Gazquez, J. L. (1990). A Relationship between the Static Dipole Polarizability, the Global Softness, and the Fukui Function. *Journal of the American Chemical Society*, **112**, 1490–1492.

Volkova, T. V., Blokhina, S. V., Sharapova, A. V., Ol'khovich, M. V. and Perlovich, G. L. (2016). The solubility of Ethionamide and Structural Analogues in Buffer Solutions, Octanol and Hexane at Several Temperatures. *Thermochimica Acta*, **640**, 1–7.

Wang, J., Soisson, S. M,, Young, K., Shoop, W., Kodali, S, Galgoci, A., Painter, R., Parthasarathy, G., Tang, Y. S., Cummings, R., Ha, S., Dorso, K., Motyl, M., Jayasuriya, H., Ondeyka, J., Herath, K., Zhang, C., Hernandez, L., Allocco, J., Basilio, A., Tormo, J. R., Genilloud, O., Vicente, F., Pelaez, F., Colwell, L., Lee, S. H., Michael, B., Felcetto, T., Gill, C., Silver, L. L., Hermes, J. D., Bartizal, K., Barrett, J., Schmatz, D., Becker, J. W., Cully, D. and Singh, S. B. (2007). Discovery of Platencin, A Dual FabF and FabH Inhibitor with *In Vivo* Antibiotic Properties. *Proceedings of the National Academy of Sciences*, **104**, 7612–7616.

Wang, Y., Pigeon, P., Top, S., McGlinchey, M. J. and Jaouen, G. (2015). Organometallic Antitumor Compounds: Ferrocifens as Precursors to Quinone Methides. *Angewandte Chemie International Edition*, **54**, 10230–10233.

Wani, W. A., Jameel, E., Baig, U., Mumtazuddin, S. and Hun, L. T. (2015). Ferroquine and its Derivatives: New Generation of Antimalarial Agents. *European Journal of Medicinal Chemistry*, **101**, 534–551.

War, J. A., Srivastava, S. K. and Srivastava, S. D. (2017). Design, Synthesis and DNA-Binding Study of Some Novel Morpholine Linked Thiazolidinone Derivatives. *Spectrochimica Acta Part A: Molecular and Biomolecular Spectroscopy*, **173**, 270–278.

Ward, S. G., Taylor, R. C., Köpf-Maier, P., Köpf, H., Balzarini, J. and De Clercq, E. (1989). Assessment of the *In Vitro* Broad-Spectrum Antiviral Activity of Some Selected Antitumor Metallocene and Metallocenium Complexes. *Applied Organometallic Chemistry*, **3**, 491–497.

Weaver, J. D., Busch, N. F. and Stammer, C. H. (1974). Cycloserine Carbamates. *Journal of Medicinal Chemistry*, **17**, 1033–1035.

Weidner-Wells, M. A., Boggs, C. M., Foleno, B. D., Melton, J., Bush, K., Goldschmidt, R. M.and Hlasta, D. J. (2002). Novel Piperidinyloxy Oxazolidinone Antibacterial Agents. Diversification of the N -Substituent. *Bioorganic and Medicinal Chemistry*, **10**, 2345–2351.

Wielgus, E., Paluch, P., Frelek, J., Szczepek, W. J. and Potrzebowski, M. J. (2015). Full Characterization of Linezolid and Its Synthetic Precursors by Solid-State Nuclear Magnetic Resonance Spectroscopy and Mass Spectrometry. *Journal of Pharmaceutical Sciences*, **104**, 3883–3892.

Wilkins, T. D. and Thiel, T. (1973). Modified Broth-Disk Method for Testing the Antibiotic Susceptibility of Anaerobic Bacteria. *Antimicrobial Agents and Chemotherapy*, **3**, 350–356.

World Health Organization (WHO). (2018). Global Antimicrobial Resistance Surveillance System (GLASS) Report Early Implementation 2017-18. Geneva: World Health Organization; 2018.

World Health Organization (WHO). (2014).Antimicrobial Resistance Global Report on Surveillance, World Health Organization, Geneva, Switzerland, 2014.

Xu, G., Zhou, Y., Yang, C., and Xie, Y. (2008). A Convenient Synthesis of Oxazolidinone Derivatives Linezolid and Eperezolid from (S)-Glyceraldehyde Acetonide. *Heteroatom Chemistry*, **19**, 316–319.

Yan, S., Miller, M. J., Wencewicz, T. A. and Möllmann, U. (2010). Syntheses and Antibacterial Activity Studies of New Oxazolidinones from Nitroso Diels–Alder Chemistry. *Bioorganic and Medicinal Chemistry Letters*, **20**, 1302–1305.

Yanai, T., Tew, D. P. and Handy, N. C. (2004). A New Hybrid Exchange-Correlation Functional Using the Coulomb-Attenuating Method (CAM-B3LYP). *Chemical Physics Letters*, **393**, 51–57.

Yang, W. and Mortier, W. J. (1986). The Use of Global and Local Molecular Parameters for the Analysis of the Gas-Phase Basicity of Amines. *Journal of the American Chemical Society*, **108**, 5708–5711.

Yang, W., Parr, R. G. and Pucci, R. (1984). Electron Density, Kohn–Sham Frontier Orbitals, and Fukui Functions. *The Journal of Chemical Physics*, **81**, 2862–2863.

Yang, Z., Li, C., Miao, M., Zhang, Z., Sun, X., Meng, H. and Cui, L. (2011). Multidrug-Resistant Genotypes of *Plasmodium falciparum*, Myanmar. *Emerging Infectious Diseases*, **17**, 498–501

Yin, H. D., Hong, M., Li, G. and Wang, D. Q. (2005). Synthesis, Characterization and Structural Studies of Diorganotin (IV) Complexes with Schiff Base Ligand Salicylaldehyde Isonicotinylhydrazone. *Journal of Organometallic Chemistry*, **690**, 3714–3719.

Yu, D. and Huiyuan, G. (2002). Synthesis and Antibacterial Activity of Linezolid Analogues. *Bioorganic and Medicinal Chemistry Letters*, **12**, 857–859.

Zein, S. and Neese, F. (2008). Ab Initio and Coupled-Perturbed Density Functional Theory Estimation of Zero-Field Splittings in Mn (II) Transition Metal Complexes. *The Journal of Physical Chemistry A,* **112**, 7976–7983.

Zein, S., Duboc, C., Lubitz, W., and Neese, F. (2008). A Systematic Density Functional Study of the Zero-Field Splitting in Mn (II) Coordination Compounds. *Inorganic Chemistry*, **47**, 134–142.

Zhai, X., Zhao, Y., Wang, J., Hong, W., Huang, L. and Gong, P. (2006). Synthesis and Antibacterial Activity of Novel Oxazolidinone Analogs Containing Substituted Thiazole/Fused-Bicyclic Groups. *Chemical Research in Chinese Universities*, **22**, 459–464.

Zhang, G.F., Liu, X., Zhang, S., Pan, B. and Liu, M.L. (2018). Ciprofloxacin Derivatives and their Antibacterial Activities. *European Journal of Medicinal Chemistry*, **146,** 599–612.

Zhang, P. and Sadler, P. J. (2017). Advances in the Design of Organometallic Anticancer Complexes. *Journal of Organometallic Chemistry, **839**, 5–14.*

Zhao, Y. and Truhlar, D. G. (2008). Density Functionals with Broad Applicability in Chemistry. *Accounts of Chemical Research,* **41**, 157–167.

Zhao, Y., Pu, J., Lynch, B. J. and Truhlar, D. G. (2004). Tests of Second-Generation and Third-Generation Density Functionals for Thermochemical Kinetics: Mean Errors For Pure and Hybrid DFT Methods. *Physical Chemistry Chemical Physics,* **6**, 673-676.

Zheng, J.-W. and Ma, L. (2016). Metal Complexes of Anthranilic Acid Derivatives: A New Class of Non-competitive α-glucosidase Inhibitors. *Chinese Chemical Letters*, **27**, 627–630.

Zupanicic, M., Turel, I., Bukorec, P., White, A. J. P. and Williams, D. J. (2001). Synthesis and Characterization of Two Novel Zinc (II) Complexes with Ciprofloxacin. Crystal Structure of $(C_{17}H_{19}N_{303}F)_2$. $(ZnCl_4)$. $2H_2O$. *Croatica Chemica Acta*. **74,** 61-74.

APPENDICES

APPENDIX I: NMR Spectra of LZD and its Complex

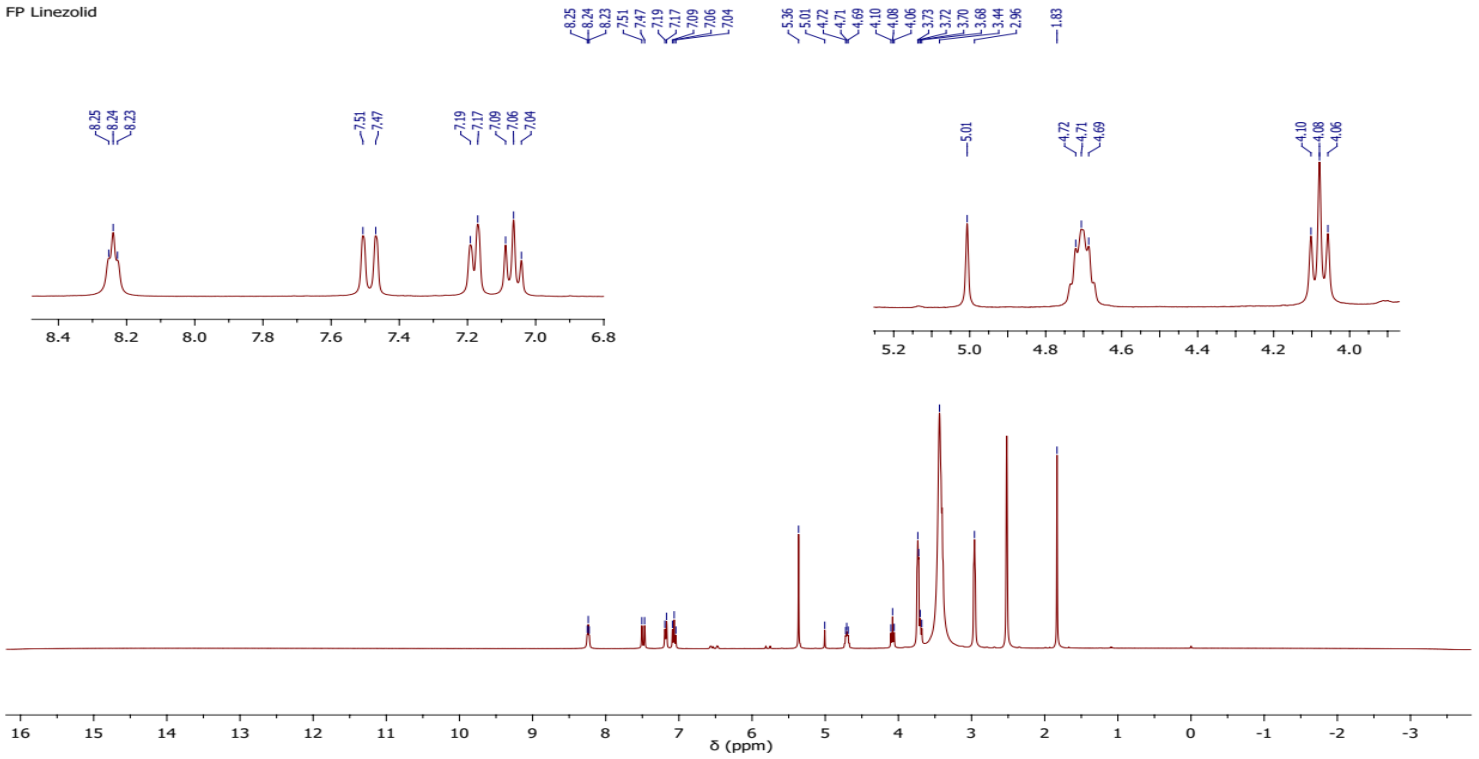

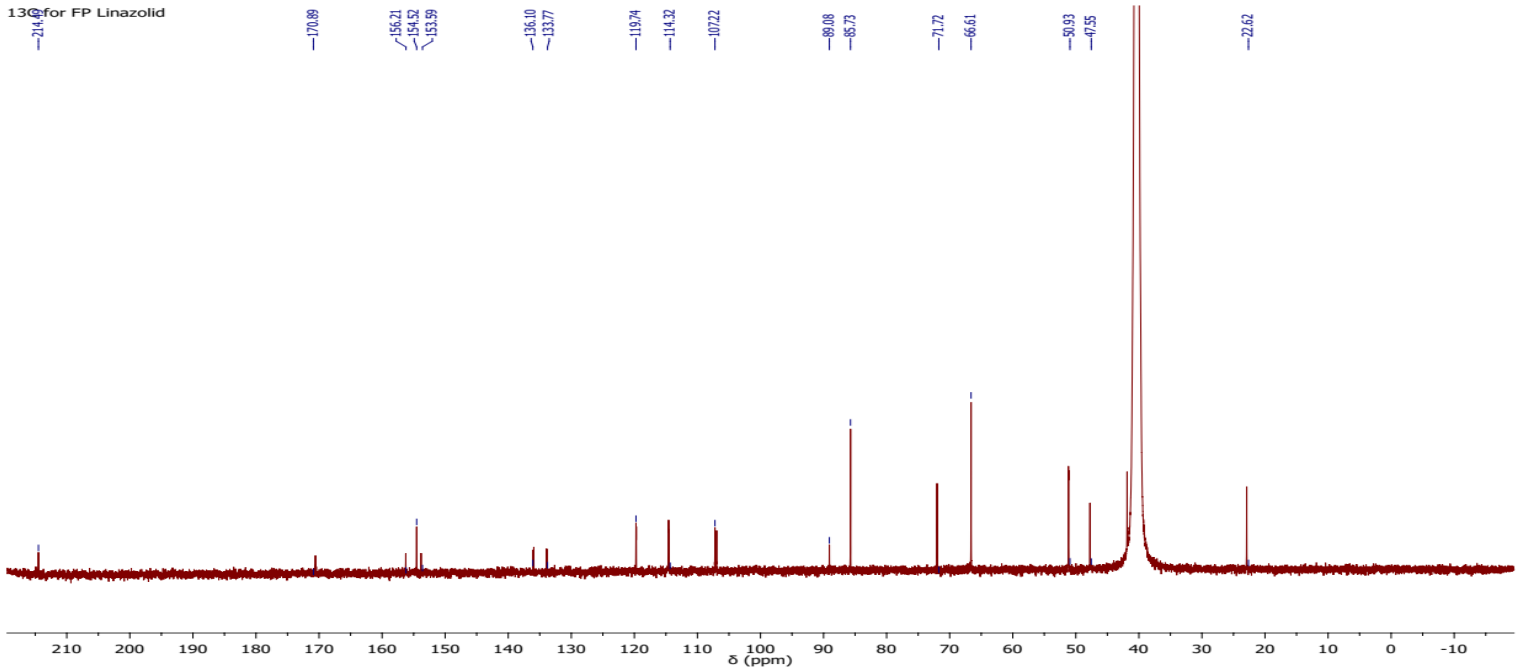
13C for FP Linazolid
214.49
170.89
156.21
154.52
153.99
136.10
133.77
119.74
114.32
107.22
89.08
85.73
71.72
66.61
50.93
47.55
22.62
210 200 190 180 170 160 150 140 130 120 110 100 90 80 70 60 50 40 30 20 10 0 -10
δ (ppm)

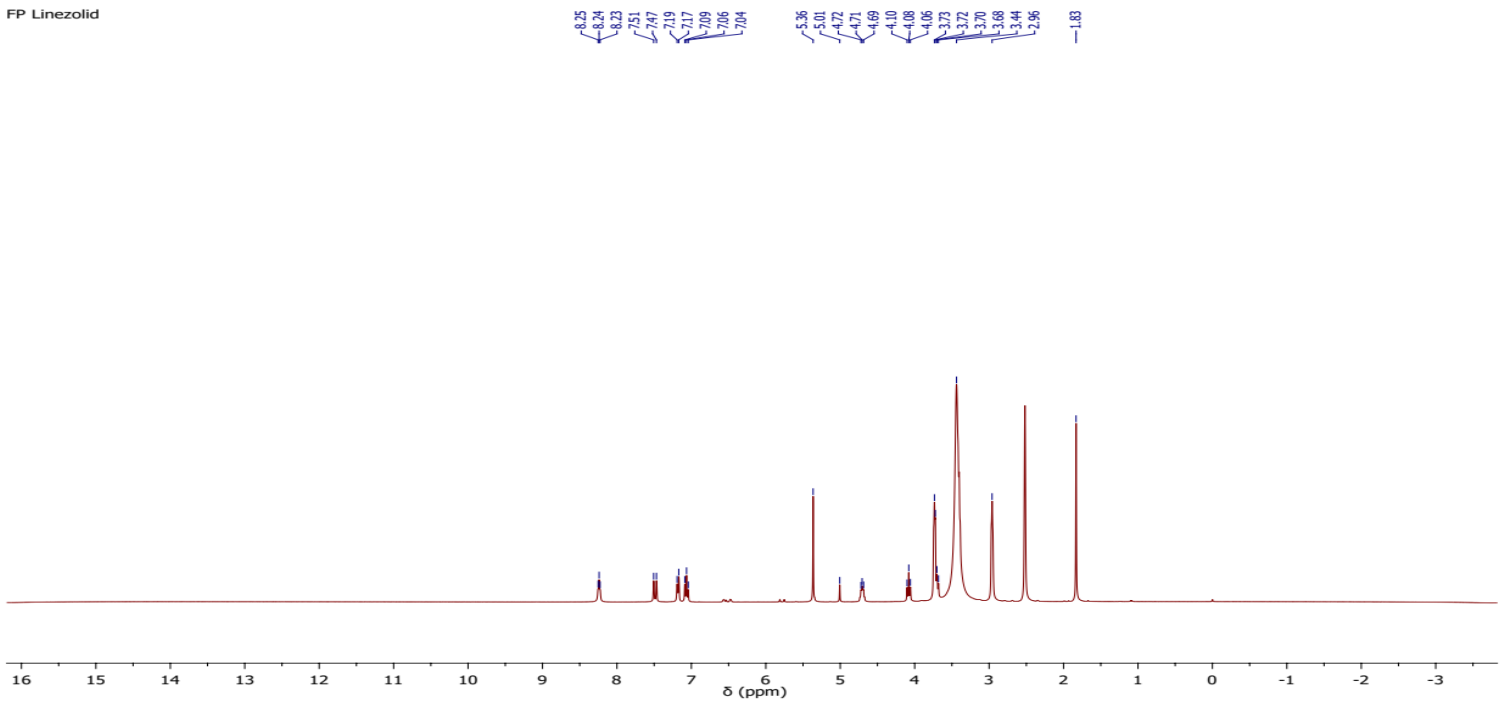
FP Linezolid
8.25
8.24
8.23
7.51
7.47
7.19
7.17
7.09
7.06
7.04
5.36
5.01
4.72
4.71
4.69
4.10
4.08
4.06
3.73
3.72
3.70
3.68
3.44
2.96
1.83
16
15
14
13
12
11
10
9
8
7
6
5
4
3
2
1
0
-1
-2
-3
δ (ppm)